3-Dimensional Reconstruction of the Breast Tumour Microenvironment: Mediation of Tumour Progression by T_{REG} Lymphocytes and NK Cells

TANYA NADINE AUGUSTINE

A thesis submitted in fulfilment of the requirements for the Degree of Doctor of Philosophy

FACULTY OF HEALTH SCIENCES
UNIVERSITY OF THE WITWATERSRAND, JOHANNESBURG
2014

Declaration

I, Tanya Nadine Augustine, declare that this thesis entitled "3-Dimensional Reconstruction of the Breast Tumour Microenvironment: Mediation of Tumour Progression by T_{REG} Lymphocytes and NK Cells" is my own unaided work. It is being submitted for the Degree of Doctor of Philosophy at the University of the Witwatersrand, Johannesburg. It has not been submitted before for any degree or examination at any other University.

_____

Tanya Nadine Augustine

__23rd__ day of ___October___ 2014 at ___Parktown___

Abstract

Breast tumour progression involves complex interactions between malignant cells and the tumour microenvironment. It is increasingly apparent that immunity is a critical determinant for tumour progression. T regulatory (T_{REG}) lymphocytes, which dominate tumour infiltrating lymphocyte populations, are implicated in facilitating tumour immunoediting processes and suppressing Natural Killer (NK) cell anti-tumour function. To investigate such cellular interaction, experimentation traditionally involves using reductionist 2-dimensional culture systems that do not recapitulate the spatial dimensions of the *in vivo* microenvironment. Three-dimensional (3D) culture systems, conversely, recreate these dimensions, allowing tumour cells to assume a phenotype more representative of the tumour microenvironment.

Given that immunity is a critical factor in determining tumour progression, a novel 3D culture system was established to investigate the interactions between T_{REG} lymphocytes, NK cells and hormone-dependent (MCF-7) or hormone-independent (MDA-MB-231) breast cancer cells. Lymphocyte subpopulations were magnetically isolated, with the efficacy of the sorting procedure verified using flow cytometry. To generate 3D cultures, cell populations were resuspended in growth factor-reduced Matrigel and cultured for 72 hours. This culture system proved effective for RNA extraction for downstream applications; for immunolocalisation of selected tumour biomarkers (ER-α, TGF-β, MUC-1 and EGFR) for qualitative analysis; and for acquisition of cytokine data (IL-1β, IL-2, IL-6, TNF-α, IFN-γ, CCL2, CCL4 and CXCL8) for quantitative multivariate statistical analysis.

Immune mediation was shown to induce the disruption of cell-cell associations, altering the expression of biomarkers and secreted cytokine profiles. Collectively, these results reflect tumour cell subversion of NK cell and/or T_{REG} lymphocyte function to promote tumour progression by generating an inflammatory microenvironment. While hormone-dependent and hormone-independent breast cancer cells differed in their specific response to immune mediation, the mechanisms by which they elicited responses resulted in similar

outcomes – that of enhanced evasive and invasive capacity. It is necessary to further elucidate the relationship between the investigated cytokines, biomarkers and immune cells, to understand their interactions and potentially provide more information for therapeutic intervention, given that these factors may contribute to tumours not responding favourably to combined modalities of therapy.

Presentations and Publications Arising from This Thesis

Local Conference – Oral Presentation

The immune-mediated cytokine profile of hormone-dependent and hormone-independent breast cancer cell lines in a 3D *in vitro* system. Tanya Augustine, Raquel Duarte, Geoff Candy. *42nd Meeting of the Surgical Research Society of Southern Africa, Durban June 2014*

Awards

Sceales Antrobus Breast Cancer Research Trust Prize (Best Presentation in the field of Breast Disease/Surgical Oncology at the *42nd Meeting of the Surgical Research Society of Southern Africa*)

International Conference (2015) – Oral Presentation (Invited as Prize Winner by the Society of University Surgeons USA)

The immune-mediated cytokine profile of breast cancer cell lines in a 3D *in vitro* system. Tanya Augustine, Raquel Duarte, Geoff Candy. *10th Annual Academic Surgical Congress, Las Vegas, Nevada, USA February 2015*

Publication under review

The immune-mediated cytokine profile of hormone-dependent and hormone-independent breast cancer cell lines in a 3D *in vitro* system. Tanya Augustine, Raquel Duarte, Geoff Candy. *Cancer Immunology, Immunotherapy*

Acknowledgments

The funders: I thank the following entities for the provision of funds without which this project would not have been possible: Minor equipment grant WHC Dividend *University of the Witwatersrand* (TNA, 2012), University Research Committee Grant *University of the Witwatersrand* (TNA, 2012) and the Carnegie Large Research Grant *Carnegie Corporation Transformation Programme at the University of the Witwatersrand* (TNA, 2012)

The supervisor: My sincere thanks to Geoff Candy – we took the road less travelled and survived Geoff!

The expertise: Annastasia Naidoo and the many nurses at day-ward Charlotte Maxeke Johannesburg Hospital for their phlebotomy assistance; Patti Kay for her assistance on the LSR Fortessa; Raquel Duarte and Thérèse Dix-Peek for their assistance in RNA extraction and cytokine data acquisition – and especially for their encouragement

The stalwarts: Andreas Michael (indomitable and bold!), Kay Augustine, Beverley Kramer Brendon Billings, David Dickinson, Maira du Plessis, Debbie Jones, Hasiena Ali, Kezia Lewins, Monica Gomes, and Wendy van der Spuy

The postgrad students: (In the affectionately, unofficially named 'For Death or Glory Lab') My 2014 BHSc.Hons students - Daniel Klonaros, Daniel Mak, Kyrtania Pather, Ivan Jovanovic, Lindsay Kaberry and Millicent Shayi; and my MSc.Med students - Jacqueline Gil and Nicholas Bacci – for being encouraging, entertaining and for cheering up their supervisor during those particularly rough days! Particular thanks to Kat for her assistance in proofreading and Lindsay for her assistance in cutting sections and ICC.

Dedication

For he who has influenced my life, utterly, profoundly, eternally

Archie Augustine

(1943 – 2009)

"Bodiacos Sunartiu Segos Brigos Anauos"

Helvetios, Eluveitie

List of Abbreviations

2D	Two-dimensional
3D	Three-dimensional
ACT	Adoptive cell therapy
ADCC	Antibody-dependent cellular cytoxicity
AI	Aromatase inhibitor
APC	Allophycocyanin
BC	Breast cancer cells alone control culture group
BPCM	Basal phenotype culture model
BRCA	Breast cancer antigen 1
BSA	Bovine serum albumin
CC	Cophenetic correlation coefficient
CD*	Cluster of differentiation
CTLA-4	Cytotoxic T-lymphocyte antigen-4
DMEM	Dulbecco's Modified Eagles Medium
DMSO	Dimethyl sulfoxide
ECM	Extracellular matrix
EDTA	Ethylenediaminetetraacetic acid
EGFR	Epidermal growth factor receptor
ER-*	Oestrogen receptor
EXP	Experimental culture group
FBS	Foetal bovine serum

Foxp3	Forkhead transcription factor 3
FSC	Forward scatter
g	Relative centrifugal force
GFRM	Growth factor-reduced Matrigel
GITR	Glucocorticoid-induced tumour necrosis family receptor
GM-CSF	Granulocyte/macrophage colony-stimulating factor
h	Hour
HER2/neu	Human epidermal growth factor 2
HLA	Human leukocyte antigen
Hsp	Heat shock protein
ICAM	Intercellular adhesion molecule
ICC	Immunocytochemistry
IFN*	Interferon
IL-*	Interleukin
iNOS	Induced nitric oxide synthase
iTreg	Induced regulatory T lymphocytes
KIR	Killer immunoglobulin-like receptor
LAK	Lymphokine-activated cells
LPCM	Luminal phenotype culture model
mAb(s)	Monoclonal antibody/antibodies
MAP	Mitogen activated protein
MCF-7	Human breast cancer cell line (hormone-dependent, luminal phenotype)

MCP-1	Monocyte chemoattractant protein-1
MDA-MB-231	Human breast cancer cell line (hormone-independent, basal phenotype)
MDS	Multidimensional scaling
MHC	Major histocompatability complex
min	Minute
MICA	MHC class-I-related-protein A
MIQE	Minimum Information for Publication of Quantitative Real–Time PCR Experiments
MMP	Matrix metalloproteinase
MTA1	Metastatic tumour antigen 1
MUC-1	Mucin-1
NCR	Natural cytotoxicity receptors
NK	Natural killer cells
NK-BC	Natural killer cell–breast cancer cell control culture group
NKR	Natural killer cell receptor
nTreg	Natural regulatory T lymphocytes
PBMC	Peripheral blood mononuclear cells
PBS	Phosphate buffered saline
PC*	Principal component
PCA	Principal components analysis
PE	Phycoerythrin
PE-Cy7	Phycoerythrin and cyanine dye 7
PHA	Phytohaemagglutinin

PR	Progesterone receptor
P/S	Penicillin/streptomycin
RT-qPCR	Reverse transcriptase real-time polymerase chain reaction
rpm	Revolutions per minute
RPMI	Roswell Park Memorial Institute culture medium
sec	Second
SERD	Selective oestrogen receptor downregulators
SERM	Selective oestrogen receptor modulators
SSC	Side scatter
STAT	Signal transducer and activator of transcription
TAA	Tumour-associated antigen
TCR	T cell receptor
TGF-β	Transforming growth factor-β
Th3	TGF-β T helper cells
TIL	Tumour infiltrating lymphocytes
TNF-*	Tumour necrosis factor
Tr1	Type I regulatory T cells
T_{REG}	Regulatory T cells
T_{REG}-BC	Regulatory T cells-breast cancer cell control culture group

List of Figures

List of Tables

Table of Contents

CHAPTER I: General Introduction

The incidence of cancer in developing countries is rising, with statistical data indicating that by 2020 the majority of cases will be cancer of the breast (Kruger and Apffelstaedt, 2007). It is estimated that of more than 1 million women per year diagnosed with breast cancer worldwide, 14% will succumb to this disease (Coughlin and Ekwueme, 2009; Youlden *et al*., 2012). Despite advances in surgical procedures and adjuvant treatments, including chemotherapy, hormone therapy and antibody therapy, the median overall survival rate of patients presenting with metastatic breast cancer remains relatively unchanged (Nicolini and Carpi, 2008). Possibly one of the greatest limiting factors to the efficacy of such treatments is the Machiavellian nature of the immune system in its capacity to both prevent and promote tumour formation.

1.1 A brief history of tumour immunology

Rudolf Virchow first documented the relationship between inflammation and neoplasia in 1863 in his identification of tumour-infiltrating lymphocytes (TIL) (Balkwill and Mantovani, 2001). Virchow's proposition that inflammation is a precursor to tumour formation was challenged in subsequent years but later revisited by modern science in the establishment of the relationship between *H. pylori* and gastric cancer, for example (Kim *et al.,* 2011). Conversely, William Coley noted the effects of inflammation on tumour regression as early as 1891, achieving cure rates of approximately 10% using infused streptococcal cultures in sarcoma patients (Coley, 1931; Wiemann and Starnes, 1994; Parish, 2003). Coley's trial, commonly regarded as the first cancer immunotherapy clinical trial, was not widely accepted in clinical practice due to the undefined mechanism of action of successful tumour eradication, low reproducibility and high toxicity levels (Parish, 2003; Ichim, 2005). It was in this climate that Paul Erlich, in 1909, proposed that immunological processes suppressed tumour formation (Ichim, 2005), provoking fierce debate regarding the role of the immune system in tumour prevention, promotion and regression. Despite such contestation, it was

during this period that the forerunner theories to tumour immunology and cancer immunotherapy were established.

Forty years later in 1949, Erlich's contentions were challenged by F. Macfarlane Burnet and Frank Fenner who proposed the theory of acquired immunological tolerance (Parish, 2003), and thus the concept of 'recognition of self'. Burnet and Fenner theorised that lymphocytes which had the capacity to recognise self (-antigens) were eliminated in prenatal life, a concept for which Rupert Billingham, Leslie Brent and Peter Medawar later provided empirical evidence (Billingham *et al.,* 1953; Wood *et al.,* 2010). Since it was presumed that neoplastic transformations exhibited the same molecular phenotype as healthy tissue, it was subsequently proposed that lymphocytes were incapable of recognising and consequently eradicating tumours (Parish, 2003). In the late 1950s, studies showed that upon surgical removal of carcinogen-induced tumours, animals were able to reject a subsequent injection of the same tumour cells, thereby providing evidence for the concept of tumour-associated antigens (TAA) (Parish, 2003). During this period, Lewis Thomas revived Erlich's theories and postulated that in a Darwinian model, an extended life expectancy would necessitate eradication of neoplastic cells to allow for a species level fitness (Dunn *et al*., 2004; Malmberg and Ljunggren, 2006). In light of new evidence, Burnet rejected his earlier assertions and expanded on Thomas' and Erlich's postulations. The theory of immunosurveillance was born (Dunn *et al*., 2004; Ichim, 2005; Malmberg and Ljunggren, 2006;); proposing that thymic-derived lymphocytes monitored the environment for neoplastic cells and that such cells expressed specific antigens which would in turn elicit an immune response (Parish, 2003; Dunn *et al*., 2004).

By the 1970s, Burnet's and Thomas' immunosurveillance concept was challenged in that infections were proposed as a stronger selective pressure for evolution of the immune system than neoplasia. Moreover, with an understanding of T lymphocyte thymic selection emerging, reports of the lack of spontaneous tumour regression, and the lack of increased incidence of tumour formation in immune-privileged sites; support was found for Burnet's initial 1949 hypothesis and the immunosurveillance concept rejected (Parish, 2003; Ichim,

2005). During this period, in 1972, Richmond Prehn proposed the concept of immunostimulation in which he theorised in a remarkably Virchow-esque manner, that spontaneous tumours elicited a mild immune response that could promote tumour growth (Prehn, 1972). In subsequent years, this concept was revisited, with the identification of T regulatory cells (T_{REG}) and consideration of their role in tumour progression (Sakaguchi *et al.,* 1995; Muranski *et al.,* 2006). As ever the field of flux, by the 1980s immunosurveillance had been revived and cancer immunotherapy was reconsidered.

Following the discovery of the inherent genetic instability of transformed cells, a large number of TAA were identified, with research activity peaking in 1991, and a new era of cancer immunotherapy emerged (Parish, 2003). Coupled with the development of hybridoma technology in the 1970s, research into monoclonal antibody (mAb) targeting of TAA was undertaken. While the use of mAbs alone produced poor response rates, when used in conjunction with radiotherapy and chemotherapy, clinical response rates tripled (Kirkwood *et al*., 2012). Active immunisation approaches based on stimulating the adaptive immune system of cancer patients against their own autologous tumours using whole tumour cell, peptide, protein and dendritic cell vaccinations, have resulted in only low response rates (Rosenberg *et al*., 2008; Kirkwood *et al*., 2012).

During this period adoptive cell therapy (ACT), as an immunologic approach to cancer treatment, found recognition. ACT involves the transfer of autologous lymphocytes (commonly lymphokine-activated peripheral blood mononuclear cells (LAK cells), or $CD8^+$ T lymphocytes), activated *in vitro* into irradiated hosts in order to induce tumour regression and prevent the recurrence of cancer (June, 2007). Rosenberg and colleagues, in 1986 published the first account of tumour regression in mouse models treated with *ex vivo* expanded TIL (Rosenberg *et al*., 1986; Rosenberg *et al*., 2008). Muul and colleagues, in 1987, then discovered that TIL could indeed recognise TAA in humans (Muul *et al*., 1987; Rosenberg *et al*., 2008). In 1988, Rosenberg and colleagues published the first account of adoptive cell therapy and non-specific immunomodulation (the use of exogenous cytokines to induce anti-tumour activity) in a clinical setting, where *ex vivo* expanded TIL and

exogenous IL-2 administration induced regression of advanced metastatic melanoma (Rosenberg *et al*., 1988; Rosenberg *et al*., 2008; Kirkwood *et al*., 2012). Irradiation later became an essential component of ACT, depleting the host of T_{REG} lymphocytes. This T lymphocyte subset, identified by Sakaguchi and colleagues (Sakaguchi *et al.,* 1995; Mougiakakos *et al.,* 2010), is not only responsible for maintaining peripheral self-tolerance via suppression of self-reactive conventional T lymphocytes (Beyer and Schultz, 2006) but is also implicated in the maintenance of tumour tolerance (Muranski *et al*., 2006). The T_{REG} lymphocyte compartment has thus been the object of much research to date.

Despite the advances made in ACT through the 20th century, it has yet to be considered as a viable treatment option for cancers. It is now recognised that the relationship between TIL and the tumour itself is far more complex than previously imagined. It was an understanding of the complexity of tumourigenesis that lead to the development of the immunoediting concept in the 21st century, put forth as consisting of three phases: *elimination, equilibrium* and *escape* (Dunn *et al*., 2002; Dunn *et al.,* 2004). The first phase, e*limination*, encompasses the danger theory of immune recognition and immunosurveillance in the early detection and eradication of transformed cells. Danger signals, including cytokine production and the expression of stress-induced signals, elicited by transformed cells and the affected stroma lead to the recruitment of immune cells that in turn may eradicate neoplastic cells (Dunn *et al*., 2002; Dunn *et al.,* 2004; Prestwich *et al*. 2008). However, cancer cells can evade and subvert normal immunosurveillance processes thereby initiating the subclinical phase *equilibrium,* where tumour variants with reduced immunogenicity undergo a Darwinian selection process and may become dormant for a period of years (Dunn *et al*., 2002; Dunn *et al.,* 2004; Prestwich *et al*. 2008). The final phase *escape* occurs when tumour cells circumvent the immune system and become clinically detectable (Dunn *et al*., 2004). The mechanisms by which tumours can escape immunological control include reduction of immunogenicity, resistance to immune-mediated cytotoxicity, and the induction of tolerance in immune cells (Prestwich *et al*., 2008). T_{REG} lymphocytes are implicated in facilitating tumour immunoediting processes by liaising with neoplastic cells to promote reduced

immunogenicity and by actively suppressing anti-tumour functions of cytotoxic T lymphocytes and Natural Killer (NK) cells (Ghiringhelli *et al.,* 2005; Mougiakakos *et al.,* 2010).

An understanding of the concept of immunoediting in light of TIL interaction with transformed cells is essential to effective ACT, considering that ACT is conducted in clinically advanced cancer cases where tumours have already passed the final phase of immunoediting, *escape*. The efficacy of ACT in melanoma has been suggested as being due to the immunogenicity of melanoma itself and the innate anti-tumourigenic capacity of recruited TIL (Zhou and Zhong 2004; Rosenberg *et al*., 2008). However, ACT has had poor results in the treatment of a number of other tumour types including breast cancer, indicative of an incomplete understanding of the tumour microenvironment and the interplay between various cell types in the progression of this disease.

1.2 The tumour microenvironment

The vast majority of cancers are epithelial in origin and are thus classified as adenocarcinomas. While the accumulation of genetic mutations allows for the transformation of normal epithelial cells to a cancerous phenotype; the reciprocal interaction of cancer cells with stromal components including fibroblasts, endothelial cells, immune cells and the extracellular matrix (ECM) has equally important implications for tumour initiation and progression (de Visser and Coussens, 2005; Nyga *et al.,* 2011). A variety of secreted growth factors, cytokines and chemokines form the basis of reciprocal interactions between components of the tumour microenvironment (de Visser and Coussens, 2005). Such secretions allow, either directly or indirectly, for the hallmarks of tumour progression to occur, including invasion and remodelling of the ECM, cellular proliferation, neovascularisation, immune evasion and extravasation into the vascular or lymphatic system for the establishment of distant secondary sites.

Although there exists a considerable amount of research linking the prevalence of TILs or subsets thereof with good prognosis, there is an increasing body of evidence indicating that

tumour cells are not only able to induce tumour tolerance and suppress or evade cytotoxic lymphocyte function, but also to induce TILs to become active participants in tumour progression (Whiteside *et al.,* 1992; Drescher and Lynch 2005; Prestwich *et al.,* 2008; Emens *et al.,* 2012; Cimino-Matthews *et al.,* 2013; West *et al.,* 2013).

1.2.1 The breast tumour microenvironment

Breast cancers are commonly categorised according to their histopathological presentation, the majority being adenocarcinomas. Adenocarcinomas are subdivided into carcinoma *in situ* – where neoplastic proliferation is limited by the basement membrane, or invasive carcinoma – where neoplastic cells have crossed the basement membrane into the surrounding stroma (Lester, 2010). These categorisations historically involve further classifications, ductal or lobular, based on the tumour involvement of both anatomical elements, although there is a fair amount of overlap between the two (Lester, 2010). The degree of morphological differentiation of a tumour is proportional to prognosis and thus impacts on treatment (Walker, 2009) (see Figure 1.1 for seminal contributions to breast cancer management).

The majority of invasive breast tumours present as infiltrating ductal carcinoma (Walker, 2009). Histologically, well-differentiated tumours indicate a better prognosis and present with tubule formation, small nuclei and low numbers of mitotic figures. Poorly differentiated tumours are characterised by nests or sheets of cells, large irregular nuclei with large numbers of mitotic figures and areas of necrosis common (Lester, 2010). In concert with histological presentation, immunohistochemical assays remain the most cost-effective method with which to visually assess receptor expression, oncogene presentation and markers of proliferation (Shyyan *et al*., 2006). This allows for recognition of subtypes of invasive carcinomas. Gene profiling studies have further indicated that most types of invasive breast tumours cluster into several major groups that have important biological and clinical significance (Lester, 2010).

The major subtype of infiltrating ductal carcinoma is the Luminal A phenotype, commonly found in post-menopausal patients. This phenotype is characterised as oestrogen receptor (ER) positive and human epidermal growth factor receptor 2 (HER2/neu) negative (Lester, 2010). Tumours exhibiting a Luminal B phenotype, characterised as ER^{+}, $HER2/neu^{++}$ and progesterone receptor (PR) positive, referred to as triple-positive tumours, are highly proliferative and more likely to undergo lymph node metastases (Lester, 2010). Targeted therapeutics for ER^{+} tumours include third-generation aromatase inhibitors (AI), selective oestrogen receptor modulators (SERM) and selective oestrogen receptor downregulators (SERD), examples of which include Anastrozole, Tamoxifen and Fulvestrant, respectively (Howell *et al.,* 2004). Such targeted therapies are unfortunately not currently available for patients presenting breast tumours of the basal-like tumour phenotype, the incidence of which while lower than that of the luminal subsets, is associated with a poor prognosis. Also known as triple-negative tumours (ER^{-}, PR^{-}, $HER2/neu^{-}$), tumours of the basal-like phenotype have a high grade, proliferative rate and metastatic potential (Lester, 2010). Such tumours often also exhibit the breast cancer antigen 1 *(BRCA1)* mutation and overexpression of epidermal growth factor receptor (EGFR), with increased incidence found in certain ethnic groups and in younger cohorts (Foley *et al.,* 2010; Lester, 2010; Giricz *et al.,* 2012).

Immunophenotypic assessment of breast tumours has demonstrated the presence of a heterogeneous TIL population (Georgiannos *et al*., 2003). An accumulation of T_{REG} cells have been noted in both the TIL population and peripheral blood of breast cancer patients (Bates *et al.,* 2006; Pooi *et al.,* 2006; Bohling and Allison, 2008; Decker *et al.,* 2012). Elevated T_{REG} lymphocyte numbers are associated with poor prognostic significance in ER^{+} invasive ductal carcinoma and $HER2/neu^{+}$ carcinomas (Pooi *et al.,* 2006; Bates *et al.,* 2008). While T_{REG} lymphocytes in triple-negative breast cancers have traditionally been linked with poor overall survival (Bohling and Allison, 2008; Cimino-Matthews *et al.,* 2013), recent data indicates that a dominant T_{REG} lymphocyte infiltrate conversely correlates with good prognosis in triple-negative cancers (West *et al.,* 2013).

T_{REG} lymphocytes are further implicated in the suppression of NK cell function (Ghiringhelli *et al.,* 2005; Mougiakakos *et al.,* 2010). While depletion of the T_{REG} compartment has been found essential for ACT efficacy (Muranski *et al.,* 2006; Mougiakakos *et al.,* 2010), other studies have queried the necessity of such, implicating more complex processes in the suppression of cytotoxic lymphocyte function (Chikileva *et al.,* 2010). Nevertheless, the scarcity of NK cells in TIL populations (Georgiannos *et al.,* 2003; Macchetti *et al.,* 2006), despite an elevated presence in the peripheral blood of breast cancer patients (Mozaffari *et al.,* 2007), may indicate inadequate NK cell homing mechanisms to tumour sites (Albertsson *et al.,* 2003) and possibly the dominance of adaptive immune responses. Tumour cells induce a tolerogenic microenvironment, either by direct suppression or by subversion of normal immunological function. Notably, the cytotoxic function of TIL and peripheral blood NK cells is impaired in breast cancer patients presenting with infiltrating ductal carcinoma, being particularly reduced in HER2/neu^{-} tumours (Dewen *et al.,* 2009; Mamessier *et al.,* 2011). Alterations in NK cell phenotype is notably dependent on tumour stage, with NK cells exhibiting poor cytotoxic capacity dominating NK populations in advanced breast cancer immune infiltrates (Mamessier *et al.,* 2013). The prognostic significance of NK cells in breast cancer has yet to be established (Roberti *et al.,* 2012) but gene expression studies have indicated that signatures associated with NK cells are predicative of relapse-free survival in primary breast cancer patients (Ascierto *et al,* 2013). The scarcity of NK cells and the dominance of T_{REG} lymphocytes in TIL populations may be linked to breast cancer immune evasion and tumour tolerance strategies, where the induction of a local inflammatory response is employed for tumour progression.

It is becoming increasingly apparent that tumour cells subvert inflammatory processes to maintain tumour progression; and that these processes are in turn critical determinants of tumour progression and response to therapy. A number of secreted growth factors, cytokines and enzymes contribute to tumour progression and invasion (Le Bitoux and Stamenkovic, 2008) by mediating the interplay between stromal cellular components, including cells of the innate and adaptive immune system, with malignant cells.

The breast tumour microenvironment and certain breast cancer cell lines frequently express members of the interleukin (IL)-1 cytokine family which transduce pro-inflammatory and anti-inflammatory signals via the mitogen-activated protein (MAP)-kinase pathway (Nicolini *et al.*, 2006; Dinarello, 2008). Members of the IL-1 family induce matrix metalloproteinase (MMP) function as well as the secretion of chemokines including CCL2, CCL4 and CXCL8 which recruit other leukocytes that assist in tissue remodelling (Le Bitoux and Stamenkovic, 2008), resulting in a feedback loop essential for metastasis. Furthermore, IL-1 together with IL-6 and tumour necrosis factor (TNF), functions synergistically as a proinflammatory axis (Ben-Baruch, 2003). Elevated IL-6 serum concentration in breast cancer patients correlates with poor prognosis and in those patients presenting with hormone-dependent invasive tumours, is associated with resistance to hormone therapy (Baumgarten and Frasor, 2012). Heightened expression of TNF-α, also associated with poor prognosis, is linked with endothelial cell activation and may thus play a role, together with transforming growth factor β (TGF-β), in enhancing the metastatic profile of tumour cells (Le Bitoux and Stamenkovic, 2008; Baumgarten and Frasor, 2012).

TGF-β, which is an important link in cytokine production and immune evasion, is implicated in both tumour suppression and tumour progression (Yang *et al.,* 2010). In its role in early tumour suppression, TGF-β inhibits cytokine and chemokine production and induces apoptosis. However, TGF-β is a known pro-oncogenic factor, and in established tumours induces dysregulation of the cell cycle, angiogenesis and immune escape (Yang *et al.,* 2010). TGF-β is also involved in epithelial-mesenchymal transitions, where epithelial tumour cells assume a more invasive phenotype characterised by a loss of apical-basal polarity and cell-cell adhesion (Moustakas and Heldin, 2014). Tumour cells and surrounding stromal components secrete large amounts of TGF-β. In this context, TGF-β is implicated in direct suppression of cytotoxic T lymphocyte and NK cell function, in the recruitment and subversion of T_{REG} lymphocyte function (Park *et al.,* 2009), and in mediation of T_{REG} lymphocyte inhibition of NK cell function (Ghiringhelli *et al.,* 2005; Chikileva *et al.,* 2010). T_{REG} lymphocyte function is also closely associated with the glycoprotein mucin-1 (MUC-1), implicated in playing a dual role in immunoregulation (Konowalchuk and Agrawal, 2012).

MUC-1 has been further linked with breast tumour progression, dependent on phenotype, via signal transduction pathways associated with migration (Walsh *et al.,* 2000; Mukhopadhyay *et al.,* 2011). MUC-1 expression is regulated by Type I cytokines including IL-2, IL-12, interferon-γ (IFN-γ) and TNF-α (Andrianifahanana *et al.,* 2006), reaffirming the importance of the immunoregulatory cytokine axis in tumour progression.

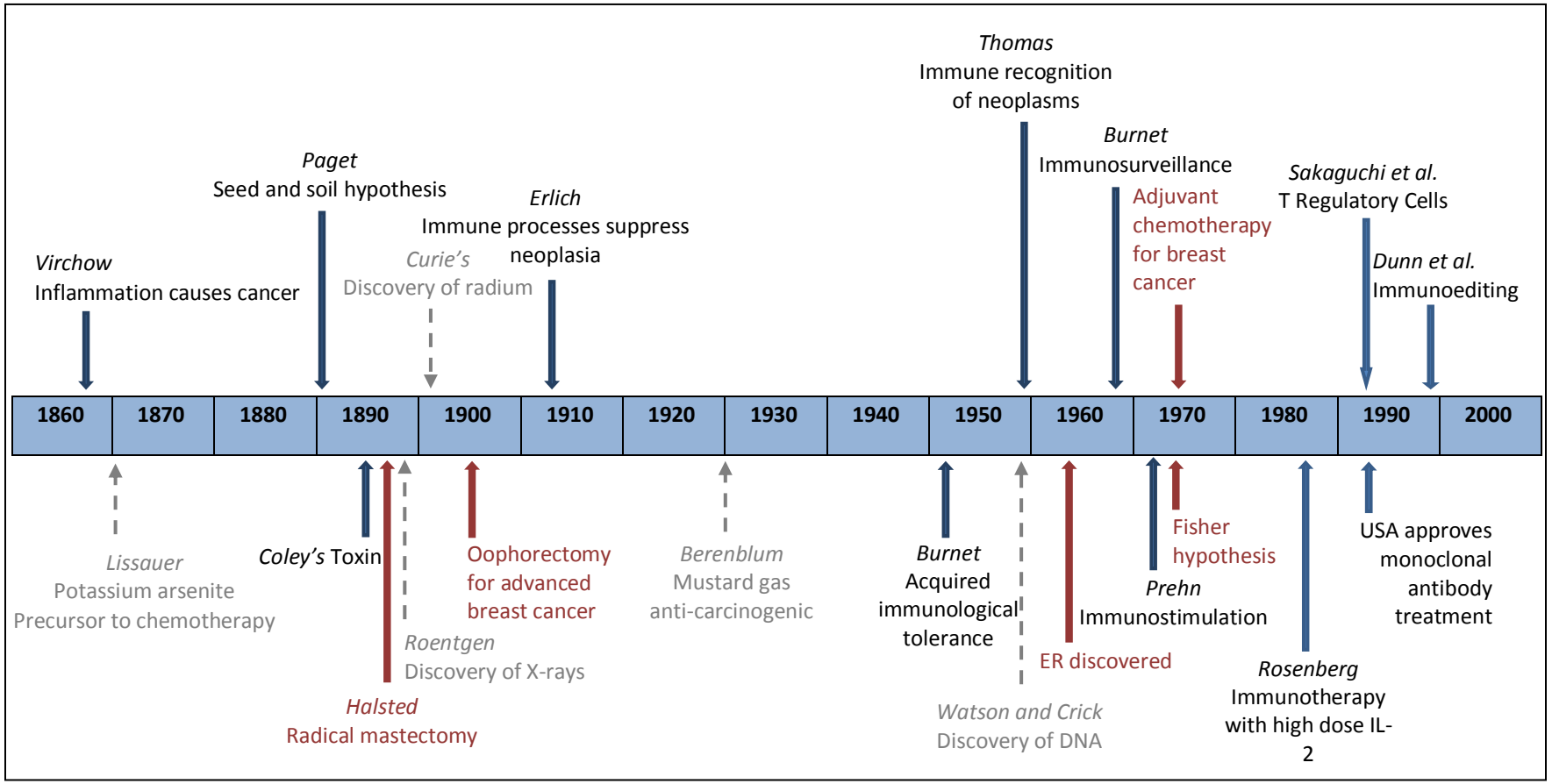

Figure 1.1 Timeline illustrating selected seminal contributions to deciphering the role of the immune system in cancer and breast cancer treatment

Sakaguchi *et al.,* 1995; Papac, 2001; Cotlar *et al.,* 2003; Parish, 2003; Waldman, 2003; Ichim, 2005; Rescigno *et al.,* 2007; Fisher, 2008; Sakorafas and Safioleas, 2010a,b; Devita and Rosenberg, 2012; Kirkwood *et al.,* 2012

1.2.2 Recreating the tumour microenvironment

Ex vivo experimentation has been instrumental in deconstructing the *in vivo* microenvironment, attempting to account for confounding variables in clinicopathological data. The relevance of experimentation conducted on established cell lines to clinical management of cancers is an on-going debate. Primary breast cancer cell lines established from patients is a time-consuming, expensive process (personal observation). Moreover obtaining patient samples on initial presentation and biopsy is essential to ensuring a collection of cells prior to exposure to any therapeutic agents. While established cell lines are prone to genomic instability, molecular profiling indicates that numerous cell lines, including breast cancer cell lines, mimic the genomic heterogeneity and genomic copy number alterations of their primary tumour phenotype, albeit presenting greater complexity (Neve *et al.,* 2006; Kao *et al.,* 2009). Such data thus supports the use of established cell lines in experimental models to gain an understanding of the physiological processes of breast tumourigenesis.

Dominating *in vitro* experimentation are 2-dimensional (2D) culture systems that have provided a plethora of information on tumour cellular processes including differentiation, migration and proliferation. In 2D culture systems, tumour cells are cultured as a monolayer on glass or plastic and typically assume a planar structure with an induced apical-basal polarity (Baker and Chen, 2012). Such polarity is characteristic of an epithelial-like morphology; however, *in vivo,* mesenchymal-like tumours are essentially stellate with no conceivable apical-basal polarity. Cell geometry affects signalling pathways and in turn affects migration and differentiation processes, such that induced polarity in 2D systems may not accurately recapitulate the *in vivo* environment (Weigelt and Bissell, 2014).

In order to compensate for the disadvantages of 2D culture systems, many studies have focused on establishing xenografts or orthotopic grafts in immunocompromised host animals (Walsh *et al.,* 2000; Pegram and Ngo, 2006; Ganapathy *et al.,* 2010). Results obtained from such models generally serve as the translational link between basic science and clinical medicine. Notwithstanding the expense and specialised animal husbandry

services required for the establishment of such *in vivo* models, they too present caveats. Many tumour cell lines (and most primary tumour cells) fail to engraft in immunocompromised hosts, a notable example being HER2/neu^{+} cell lines in athymic mice (Pegram and Ngo, 2006; Nyga *et al.,* 2013). While some studies have overcome this limitation by engineering HER2/neu cell lines able to engraft (Pegram and Ngo, 2006), this in itself adds an additional layer of complexity to the experiment. Furthermore, in drug testing physiological response between host animals and human subjects differ to the extent that by 2010, reports indicated that only 11% of drugs assessed in *in vivo* animal models were successful in clinical trials and approved for therapeutics by the United States of America, Food and Drug Administration (Levitzki and Klein, 2010). Transgenic models are useful for investigating inherited cancers but do not mimic most human cancers and their very transgenic nature implicates a range of responses distinct from normal. Of paramount importance to this study is that the mentioned animal models generally fail to account for the complexity of immune responses involved in tumour progression (Pegram and Ngo, 2006).

Three-dimensional (3D) culture systems are a proposed intermediary between reductionist 2D culture systems and xenograft models (Kim, 2005). By recreating the spatial dimensions associated with the *in vivo* environment, 3D culture systems allow tumour cells to assume a morphology more representative of the *in vivo* tumour environment than those cultured in 2D systems (Kenny *et al.,* 2007; Krause *et al.,* 2010; Pinto *et al.,* 2011). Morphological presentation in 3D culture systems correlates with molecular and genetic phenotypes as per the tumour microenvironment (Han *et al.,* 2010). Thus, 3D culture systems allow for a complex recapitulation of the tumour microenvironment that is cost effective and without the specific limitations presented by animal models (Swamydas *et al.,* 2010; Pinto *et al.,* 2011).

The methodology employed to create 3D cultures predicates on the establishment of cell-cell associations in a geometric space. The establishment of multicellular spheroids has been particularly useful for drug delivery studies (Nyga *et al.,* 2011). Spheroids are characterised

as tumour cell aggregates with actively proliferating cells dominating the periphery, a core of nutrient-deprived and thus potentially necrotic cells, and the ability to secrete ECM components including fibronectin, laminin and collagen (Nyga *et al.,* 2011). The earliest documented establishment of cell spheroids, 'the hanging drop' culture model, followed by the liquid overlay culture method, exploited the spontaneous aggregation of tumour cells in a liquid medium (Kim, 2005). However, the small numbers of spheroids generated for subsequent experimentation are a limiting factor of both techniques.

The gyratory rotation technique used in spinner flask and roller tube culture systems, and the more advanced rotatory cell culture system both generate larger quantities of spheroids. These techniques maintain cells in suspension allowing for spontaneous spheroid formation (Kim, 2005). Some tumour cells however, do not spontaneously aggregate and the addition of microcarrier beads to such culture systems are used to induce cell-cell adhesion (Nyga *et al.,* 2011). Both techniques also present limitations: the gyratory rotation technique produces high shear forces affecting the architecture of cultured spheroids and the rotatory cell culture system, while significantly reducing the shear forces, is an expensive technique for the generation of relatively simple homotypic spheroids (Kim, 2005).

Compared to spheroid cultures, three-dimensional scaffolds allow for the reconstruction of the complex geometry of the tumour microenvironment (Kim, 2005). Bioengineered natural scaffolds include hydrogels that are primarily composed of water; however, their capacity to mimic the tumour microenvironment predicates on the addition of ECM components including collagen type I, hyaluronic acid and laminin (Nyga *et al.,* 2011). Synthetic scaffolds, made from synthetic polymers including polylactide and polyglycolide, are biodegradable and when mixed with ECM components, provide a more biologically relevant culture system. However, their synthetic nature is a limitation to the recapitulation of the tumour microenvironment (Nyga *et al.,* 2011). With increasing evidence that tumour progression requires interaction of ECM components with tumour cells, directing migration and proliferation and further providing a medium for paracrine and autocrine secreted factors, many studies have used cell-secreted ECM scaffolds for the establishment of 3D culture

systems. Cell-secreted ECM scaffolds commonly used include fibroblast-derived ECM (Nyga *et al.,* 2011) and the commercially available Engelbreth-Holm-Swarm tumour-derived ECM (Matrigel) (Kleinman and Martin, 2005). While fibroblast-derived ECM limits the growth of certain breast cancer cell lines (Nyga *et al.,* 2011), Matrigel conversely has been shown to support breast tumour cell behaviour, more reminiscent of the *in vivo* microenvironment (Kenny *et al.,* 2007; Han *et al.,* 2010). Three-dimensional studies have focussed primarily on homotypic cultures investigating breast cancer cell invasion (Poincloux *et al.,* 2011; Chandrasekaran *et al.,* 2012; Yu and Machesky, 2012) or heterotypic cultures investigating breast tumour cell and fibroblast interaction (Olsen *et al.,* 2010) (Table 1.1). Few studies have assessed lymphocyte invasion capacity in 3D cultures (Albertsson *et al.,* 2007; Edsparr *et al.,* 2011) and notably, assessment of the literature to date has yielded no research on the heterotypic interactions between immune and breast cancer cells in such a system.

Table 1.1 Examples of research studies directly comparing 3D scaffold and 2D heterotypic or homotypic breast cancer culture models

Investigation	Cells	3D Culture Conditions	3D versus 2D	Reference
Gene expression profiles / morphology	Breast cancer cell lines - numerous	Homotypic Matrigel model. Sandwich method.	Distinct morphological alterations in 3D. Increased expression of genes involved in signal transduction in 3D	Kenny *et al.,* 2007
Sensitivity to cancer drugs	Mouse breast cancer cells (4TI) and murine embryonic fibroblasts (MEF)	Homotypic and heterotypic 3D spheroids. Variations of Matrigel models. Sandwich method.	3D cultures less sensitive to cytotoxic actions of anti-cancer drug YC-1 (anti-hypoxia inducible factor)	Li and Lu, 2011
Invasive potential / Angiogenic induction potential	Human breast cancer cell line (MCF-7)	Homotypic 3D culture in porous collagen scaffold	3D cultures show increased secretion of bFGF, VEGF and IL-8; and increased expression of MMP-2 and MMP-9	Chen *et al.,* 2012
Invasive potential / morphology	Human breast cancer cell lines (MDA-MB-231, MDA-MB-361) and normal breast epithelium (MCF-10A)	Homotypic 3D aggregates in Matrigel and synthetic polyethylene glycol	In 3D BMP4-induced p21 expression (cell cycle inhibitor) similar to 2D but morphological changes indicate more invasive profile in Matrigel	Ampuja *et al.,* 2013
Migratory and invasive potential	Human breast cancer cell lines (MCF-7, B-20) and normal breast epithelium (MCF-10A)	Homotypic and heterotypic 3D spheroids on polydimethylsiloxane	Increased expression of E-selectin and hypoxia-associated genes in 3D cultures	Chandrasekaran *et al.,* 2013
Invasive potential	Human mammary fibroblasts and breast cancer cells (MCF-10)	Conditioned media. Homotypic and heterotypic collagen I only and collagen I/Matrigel based 3D cultures	Increase in cancer cell invasion in 3D mediated by HGF/c-met interaction	Sung *et al.,* 2013

1.3 Rationale for the study

The failure of ACT in breast cancer reflects an incomplete understanding of the tumour microenvironment. The interaction between cellular components in this microenvironment is difficult to unravel from clinical observations alone. Recapitulation of the *in vivo* tumour microenvironment relies primarily on the manipulation of cell lines in 2D culture systems (Pinto *et al.,* 2011) or the establishment of cancer xenografts in immunocompromised animal hosts (Nyga *et al.,* 2011), with both models presenting advantages and limitations. The reductionist approach of 2D models in unravelling the complexity of the *in vivo* environment, while having provided a plethora of information regarding cancer processes, has been increasingly shown not to be representative of the tumour environment (Nyga *et al.,* 2011; Baker and Chen, 2012). Investigations mimicking the breast tumour environment in 3D culture systems have focussed primarily on the interaction between breast cancer cells and fibroblasts (Kim, 2005; Olsen *et al.,* 2010; Pinto *et al.,* 2011; Li and Lu, 2011). Given that immunity is a critical factor in determining both tumour progression and response to therapy, a niche exists for the development of a 3D culture system in which to investigate the reciprocal interactions between immune cells and breast tumour cells.

1.3.1 Aims

This study thus sought to investigate the reciprocal interactions between T_{REG} lymphocytes, NK cells and breast cancer cells in a 3D culture system. The objectives were as follows:

1. Establishment of a 3D model in which to study the heterotypic actions of T_{REG} lymphocytes, NK cells and hormone-independent and hormone-dependent breast cancer cell lines (Chapter II)
2. Validation of the applicability of the model for RNA extraction for subsequent gene expression assays (Chapter II)

3. Assessment of the effects of NK cell and T_{REG} lymphocyte influence on proinflammatory cytokine and chemokine production in the developed models (Chapter III)
4. Application of exploratory multivariate analysis to ascertain patterns of cytokine and chemokine expression associated with the developed models (Chapter III)
5. Assessment of the effects of NK and T_{REG} influence on the expression of biomarkers (ER-α, MUC-1, EGFR and TGF-β) associated with tumour progression using immunocytochemistry (ICC) (Chapter IV)

CHAPTER II: Establishment of a Heterotypic 3D Culture System: The Interaction between T_{REG} Lymphocytes and NK Cells in Hormone-Dependent and Hormone-Independent Breast Cancer Cell Lines

2.1 Introduction

The breast tumour microenvironment is an intricate network involving multiple cell types, the interactions of which play pivotal roles in cancer progression. *Ex vivo* experimentation has attempted to construct tumour microenvironments in order to better investigate cellular interactions; however the reductionist approach of 2D culture systems fail to recreate the complexity of the *in vivo* microenvironment (Pinto *et al.,* 2011). While 3D culture systems are more successful in this regard, studies of breast tumourigenesis have focussed on metastatic processes, primarily using homotypic cultures to investigate breast cancer cell invasion (Poincloux *et al.,* 2011; Chandrasekaran *et al.,* 2012; Yu and Machesky, 2012) or heterotypic cultures investigating breast tumour cell and stromal cell interaction (Olsen *et al.,* 2010).

Increasing evidence highlights immunity as a fundamental determinant of tumour progression and response to therapy. Tumour infiltrating lymphocyte populations in breast tumours present a paucity of NK cells, which may reflect tumour cell evasion of innate immunity (Georgiannos *et al.,* 2003; Macchetti *et al.,* 2006); and elevated levels of T_{REG} lymphocytes (Pooi *et al.,* 2006; Bates *et al.,* 2008; West *et al.,* 2013), which may reflect the dominance of adaptive immune mechanisms. This stresses the need to investigate the interaction between T_{REG} cells and NK cells in breast cancer in order to shed more light on tumour escape from immunological control, which may or may not be dependent on breast cancer phenotype. This chapter thus presents the establishment of a novel 3D heterotypic culture system in which to investigate the interactions between NK cells, T_{REG} lymphocytes and hormone-dependent and hormone-independent breast cancer cell lines.

2.1.1 Matrigel: Cell-secreted ECM as a scaffold for 3D culture

The development of the now commercially available Matrigel basement membrane extract (Kleinman and Martin, 2005) was a seminal contribution to studies of tumourigenesis. Matrigel is a laminin-rich extract established from Engelbreth-Holm-Swarm tumour cell-secreted basement membrane (Kleinman and Martin, 2005; Nyga *et al.,* 2011). In 3D Matrigel cultures breast tumour cell morphogenesis in linked intrinsically to molecular phenotype and is more reminiscent of the *in vivo* microenvironment than 2D cultures (Kenny *et al.,* 2007; Han *et al.,* 2010). Two-dimensional culture systems force a polarity and monolayer planar structure upon malignant cells, which *in vivo* lose polarity and exhibit disorganised architecture (Kenny *et al.,* 2007). Thus 2D-induced polarity and morphogenesis may directly impinge on signal transduction pathways implicated in tumour progression and give a false impression of the *in vivo* circumstances. Matrigel is regarded as a more biologically relevant scaffold for both normal mammary and cancerous mammary epithelial cell cultures compared to synthetic scaffolds (Ampuja *et al.,* 2013).

For this study, growth factor-reduced Matrigel (GFRM) was used to establish a biomimetic 3D system to assess the interaction between breast tumour cells and lymphocyte subpopulations. In addition to laminin, GFRM contains considerable amounts of collagen IV, heparan sulfate proteoglycans and entactin (BD Biosciences, catalogue number 352430). GFRM, as opposed to complete Matrigel was selected to limit the effects of endogenous growth factors on cultured cells (Table 2.1) (Vaillant *et al.,* 2011).

Table 2.1 Growth factor concentrations in Growth Factor-Reduced Matrigel (GFRM)

Adapted from BD Biosciences, Specification Sheet, catalogue number 354230

Growth Factor	Concentration
TGF-B	1.7 (ng/ml)
IGF	5 (ng/ml)
PDGF	<5 (pg/ml)
EGF	<0.5 (ng/ml)
NGF	<0.2 (ng/ml)
bFGF	0 - 0.1 (pg/ml)

2.1.2 Breast cancer cell lines

The MCF-7 cell line and the MDA-MB-231 cell line, established from pleural effusions of patients presenting with mammary adenocarcinoma, are representative of infiltrating ductal carcinoma (Neve *et al.,* 2006; Prat and Perou, 2010). The MCF-7 cell line exhibits a luminal phenotype (ER^+PR^+); however, whereas primary tumours are subdivided into the luminal A and B phenotypes this is not readily discernible in this cell line (Neve *et al.,* 2006), given variation in HER2/neu expression (Lostumbo *et al.,* 2006). The MDA-MB-231 cell line exhibits a basal-like phenotype, more akin to the pathological basal-like (B) phenotype, presenting with the triple-negative phenotype (ER^-PR^-HER2/neu^-) and expressing progenitor cell markers (Lostumbo *et al.,* 2006; Neve *et al.,* 2006). Moreover, the basal-like phenotype of the MDA-MB-231 cell line is further evidenced in its mesenchymal-like morphology and high invasive potential, unlike the MCF-7 cell line which is more differentiated than basal phenotype cells and develops tight junctions *in vitro* (Neve *et al.,* 2006). Morphology in Matrigel-based 3D cultures is directly linked with phenotype (Kenny *et al.,* 2007). MCF-7 cells fall into the 'mass' morphological category, defined by the formation of a spherical aggregate with disorganised nuclei and robust cell-cell adhesion. MDA-MB-231 cells fall into the 'stellate' morphological category exhibiting disorganised nuclei within elongated cells with notable invasive processes (Kenny *et al.,* 2007).

In order to compare the response of luminal and basal phenotype breast cancer cells to the immune infiltration in a 3D culture model, the MCF-7 and MDA-MB-231 cell lines were thus selected for this study.

2.1.3 Natural Killer cells

NK cells, lymphocytes of the innate arm of the immune system, were first identified by their ability to lyse tumour cells spontaneously (Arnon *et al*., 2006). Constituting between 10-15% of peripheral blood lymphocytes (Farag and Caligiuri, 2006), NK cells can be identified morphologically by their scant cytoplasm, azurophilic cytoplasmic granules and large

indented nucleus. The primary mechanisms of NK cell killing, facilitated by direct contact with stressed, infected or malignant cells, include the activation of death receptors on target cells and the secretion of degradative granules including perforin, a membrane-disrupting protein and granzymes, a family of proteases (Smyth *et al.,* 2005). Both pathways are capable of inducing caspase-dependent apoptosis, although granule-mediated killing of target cells is not entirely contingent on caspase activation. Unlike cells of the adaptive immune system, NK cells do not undergo a selective process in which they are primed to respond to a single antigen with a high degree of specificity, but rather are capable of recognising and destroying a large repertoire of targets (Bottino *et al*., 2000; Arnon *et al*., 2006).

Phenotypic analysis of NK cells has demonstrated that this lymphocyte group is not a homogenous population with identical function, but rather that differential expression of representative markers is associated with variable function. Classical NK cells are characterised by the lack of the T cell receptor (TCR) complex ($CD3^-$), and the presence of the CD56 and CD16 markers (Miller, 2001). The function of CD56 in NK cells remains largely unknown but is postulated to mediate cell-cell interactions or when downregulated, to indicate the acquisition of more specialised function (Miller, 2001; Farag and Caligiuri, 2006). CD16, a low affinity receptor for immunoglobulin G, is proposed to mediate the effects of NK cell antibody-dependent cellular cytotoxicity (ADCC) against antibody-coated target cells (Dewan *et al.,* 2009). The differential expression of these cell surface molecules as demonstrated by flow cytometry analysis has allowed two functionally distinct subsets to be customarily recognized. $CD56^{bright}$ NK cells are the predominant subset in peripheral blood, exhibiting poor cytolytic capacity, high proliferative capacity and capable of secreting a number of immunoregulatory cytokines (Miller, 2001; Farag and Caligiuri, 2006). $CD56^{dim}$ NK cells constitutively express the CD16 marker (Miller, 2001; Farag and Caligiuri, 2006). However, upon stimulation with IL-2 both *in vitro* and *in vivo*, the cytotoxic capacity of the two subtypes are comparable (Farag and Caligiuri, 2006).

NK cell function is mediated by the receipt and interpretation of both stimulatory and inhibitory signals by NK cell receptors (NKRs) and is closely regulated to prevent indiscriminate killing of healthy cells and the induction of autoimmunity, (Bottino *et al*., 2000). Three major superfamilies of NKRs have been identified: the killer immunoglobulin-like receptor (KIR) superfamily that recognise classical major histocompatibility (MHC) class I molecules; the C-type lectin superfamily that recognise non-classical MHC class I or class I-like molecules (Farag and Caligiuri, 2006); and the immunoglobulin-like natural cytotoxicity receptors (NCR) that allow NK cells to exert their cytolytic activity against MHC class I-deficient cells (Bottino *et al*., 2000; Farag and Caligiuri, 2006). Currently, three members of the NCR family have been identified, NKp46, NKp44 and NKp30, the differential expression of which is linked with functional variation (Bottino *et al*., 2000). NKp46 is expressed in both resting and activated NK cells, with high expression in those cells exhibiting greater cytolytic activity (Miller, 2001). Those NK cells expressing an $NKp46^{dim}$ phenotype are associated with reduced cytolytic function and tend to be the minority of isolated NK cells (Bottino *et al*., 2000). The NCRs are postulated to be involved in the identification and elimination of tumour populations.

NK cells further produce a range of cytokines and chemokines that are implicated in controlling tumour progression (Wilk *et al.,* 2008). Based on their cytokine profile, subsets of NK cells have been suggested, including type 1 NK cells, type 2 NK cells and regulatory NK cells (Cooper *et al.,* 2001; Chambers, 2010). However, no consensus has been reached regarding either the phenotype of such subsets or their definitive functions. The cytokines and chemokines produced by NK cells include: IFN-γ, IL-2, IL-8, IL-15, granulocyte/macrophage colony-stimulating factor (GM-CSF), TNF, TGF-β and CCL3, amongst others; which allow for interaction with other cell types including malignant cells and T_{REG} cells of the adaptive immune system (Chambers, 2010).

2.1.4 Regulatory T cells

The identification of CD25 (the IL-2 receptor alpha chain), by Sakaguchi and colleagues, established the phenotype of the T_{REG} population ($CD3^+CD4^+CD25^+$) functionally described as the principal T cell subset responsible for maintenance of self-tolerance (Sakaguchi *et al*., 1995; Beyer and Schultz, 2006; Mougiakakos *et al*., 2010). The $CD4^+CD25^+$ phenotype remains the 'type specimen' of the T_{REG} population; however ensuing studies have identified the existence of functionally distinct subsets.

Natural T_{REG} lymphocytes (nT_{REG}), which form 5-6% of the $CD4^+$ T cell compartment, are named for their thymic-derivation *sans* antigenic stimulus (Wang, 2006). Forkhead transcription factor 3 (Foxp3), an intracellular transcription factor, has been linked to the thymic differentiation of nT_{REG} cells; thus nT_{REG} cells are proposed to have a $CD4^+CD25^{++bright+}Foxp3^+$ phenotype (Mougiakakos *et al*., 2010; Pahwa *et al*., 2010). However, given that Foxp3 is an intracellular molecule, its usefulness remains in characterisation of the T_{REG} population rather than in isolation for subsequent *in vitro* expansion procedures. CD127 has been proposed as a further marker for nT_{REG} cells, by virtue of its expression inversely correlating with that of Foxp3 (Mougiakakos *et al*., 2010). The nT_{REG} subset is further defined by its functional ability to firstly, maintain T lymphocyte tolerance without the secretion of IL-10 and TGF-β; secondly, to maintain the $CD4^+CD25^{++bright+}Foxp3^+$ phenotype, and thirdly to exhibit no differentiation into any of the effector $CD4^+$ subsets or secrete any proinflammatory cytokines (Pahwa *et al*., 2010).

The inducible or adaptive $CD4^+$ T_{REG} (iT_{REG}) population (Whiteside, 2012) has a proposed derivation from circulating naïve $CD4^+$ T lymphocytes (Pahwa *et al.,* 2012) in response to environmental signals (Wang, 2006; Whiteside, 2012). In contrast to the nT_{REG} population, iT_{REG} function is purportedly not contact-dependent but is rather mediated by a number of secreted factors (Jonuleit and Schmitt, 2003). The iT_{REG} subgroups include type I regulatory T cells (Tr1), TGF-β T helper cells (Th3) and nT_{REG}-like cells (Mougiakakos, 2010). Tr1 cells are defined by their ability to produce primarily IL-10, negligible IL-2 and by the expression of low or no Foxp3 and CD25 markers. Th3 cells are defined by their ability to secrete primarily

TGF-β and to a lesser extent, IL-10 and IL-4. nT_{REG}-like cells are considered to have a similar phenotype to nT_{REG} cells, with their derivation rather being dependent on antigen stimulus (Jonuleit and Schmitt, 2003; Bachetta *et al.,* 2005; Mougiakakos, 2010).

Defining the T_{REG} lymphocyte-lineage is however fraught with difficulties. Both cell surface and intracellular molecules initially thought to be T_{REG} cell-specific are able to alter their expression dependent on the environmental milieu in which they exist. There remains no unique suite of cell surface molecules that could be used to delineate T_{REG} lymphocytes from activated effector T lymphocytes. CD25 along with other cell surface molecules proposed as T_{REG} lymphocyte-specific, including glucocorticoid-induced tumour necrosis family receptor (GITR) and cytotoxic T-lymphocyte antigen-4 (CTLA-4), are upregulated on $CD4^+$ effector cells upon activation (Yu and Fu, 2006; Piersma *et al.,* 2008). The expression of chemokine receptors including CD194, CD196 and CD197 also cannot distinguish between T_{REG} lymphocytes and conventional T lymphocytes (Whiteside, 2012). Foxp3 has been shown to be expressed in breast cancer epithelial cells (Droeser *et al.,* 2013), transiently expressed in activated non-regulatory $CD4^+$ T cells (Wang *et al.,* 2006) and to be upregulated in naïve $CD4^+$ T cells in response to TCR and TGF-β stimulation (Tran *et al.,* 2007), notably without inducing functional T_{REG} lymphocyte activity. Furthermore, subsets of T_{REG} cells are capable of downregulating Foxp3 expression (Mougiakakos *et al*., 2010), which in turn would influence the effectiveness of CD127 expression in phenotypic classification of the T_{REG} population. The efficacy of more recently described markers including Helios, a transcription factor, and CD39 remains to be established (Whiteside, 2012).

2.1.5 The interaction between NK cells and T_{REG} lymphocytes

The immunosuppressive action of T_{REG} lymphocytes against effector T lymphocytes and NK cells has been documented in both *in vitro* and *in vivo* studies (Ghiringhelli *et al*., 2005, Ralainirina *et al*., 2007; Salagianni *et al.,* 2011); however, interleukin-activated NK cells have been shown to be resistant to these inhibitory effects (Chikileva *et al*., 2010). T_{REG} lymphocytes are activated via engagement of the TCR that recognises peptides presented by

MHC molecules, and co-stimulatory molecules. TCRs themselves not only recognise peptides but also the MHC molecules (I or II) to which they are bound. In the case of T_{REG} cells, CD4 is a co-receptor that associates with invariant sites on MHC II molecules found primarily on antigen presenting cells. NK cells, while not traditionally regarded as antigen presenting cells, are capable of acting in this regard but require the expression of co-stimulatory molecules to function as such, with expression of these molecules induced by cytokines including IL-2, IL-12 and IL-15 (Chambers, 2010). Resting T_{REG} cells can suppress NK cell cytotoxicity, implying that TCR-mediated activation may not be a prerequisite for T_{REG} cell function in this context (Ghiringhelli *et al*., 2005). The perforin/granzyme pathway mediates NK cytolytic function that occurs in response to cytokines, including IL-2 and IL-15 (Ralainirina et al., 2007). Activated NK cells also release a large repertoire of cytokines; however, the most studied NK cell-released cytokine remains IFN-γ, a proinflammatory cytokine that is able to activate subpopulations of the adaptive immune system and increase expression of MHC class I and class II molecules (Nicolini *et al.,* 2006).

Although the mechanism of T_{REG} lymphocyte suppression of NK cell function has yet to be completely elucidated, it is postulated that soluble factors and/or cell-cell contact is required (Trzonkowski *et al*., 2004; Ralainirina *et al.,* 2007; Mougiakakos *et al.,* 2010). Soluble factors released by T_{REG} lymphocytes include galectin and prostaglandin E2, which may directly suppress NK cell function, or granzyme A and perforin, which may induce NK cell death. T_{REG} lymphocytes are further implicated in modulating surrounding stromal components via cytokine production to aid in NK suppression (Mougiakakos *et al.,* 2010). Membrane-bound TGF-β, as previously mentioned, is implicated in cell-cell contact mechanisms of T_{REG} lymphocyte-mediated suppression of NK cell function (Ghiringhelli *et al*., 2005; Chikileva *et al*., 2010; Mougiakakos *et al.,* 2010). Furthermore, T_{REG} lymphocytes are also able to diminish the functional capacity of antigen presenting cells, of which NK cells are part, via contact dependent mechanisms (Mougiakakos *et al.,* 2010).

Notwithstanding the immunosuppressive effects of T_{REG} lymphocytes on NK cell function, breast tumour cells themselves are capable of inducing a tolerogenic microenvironment and

actively evade NK cell responses (Mamessier *et al.,* 2011). Such research highlights the need to investigate the interaction between T_{REG} cells and NK cells in biomimetic systems of breast cancer, in order to shed more light on tumour escape from immunological control. This chapter thus presents the establishment of a heterotypic 3D culture system with which to explore the interaction between T_{REG} cells and NK cells in hormone-dependent and hormone-independent breast cancer cell lines.

2.2 Materials and Methodology

Human Ethics Clearance was obtained from the Human Ethics Research Committee (Medical), University of the Witwatersrand, Clearance Certificate Numbers M081036 and M140155.

In brief, the luminal phenotype, hormone-dependent MCF-7 cell line (Sigma-Aldrich, St. Louis, USA, 86012803, passage number P11) and the basal phenotype, hormone independent, MDA-MB-231 cell line (Sigma-Aldrich, St. Louis, USA, 92020424, passage number P46) were propagated in monolayer culture to establish a stock of breast cancer cells at appropriate passage numbers for subsequent co-culture with either T_{REG} lymphcoytes and/or NK cells (Fig. 2.1). These lymphocyte subgroups were magnetically isolated from peripheral blood mononuclear cells (PBMCs) obtained from peripheral blood via density gradient centrifugation (Fig. 2.1). Following 48 h activation of T_{REG} lymphocytes and NK cells, cell populations were allocated to co-culture groups for a 72 h incubation period (Table 2.2). Subsequently, these cultures were prepared for RNA extraction for downstream gene expression assays (Chapter II), cytokine analysis (Chapter III) and immunocytochemical localisation of selected biomarkers (Chapter IV).

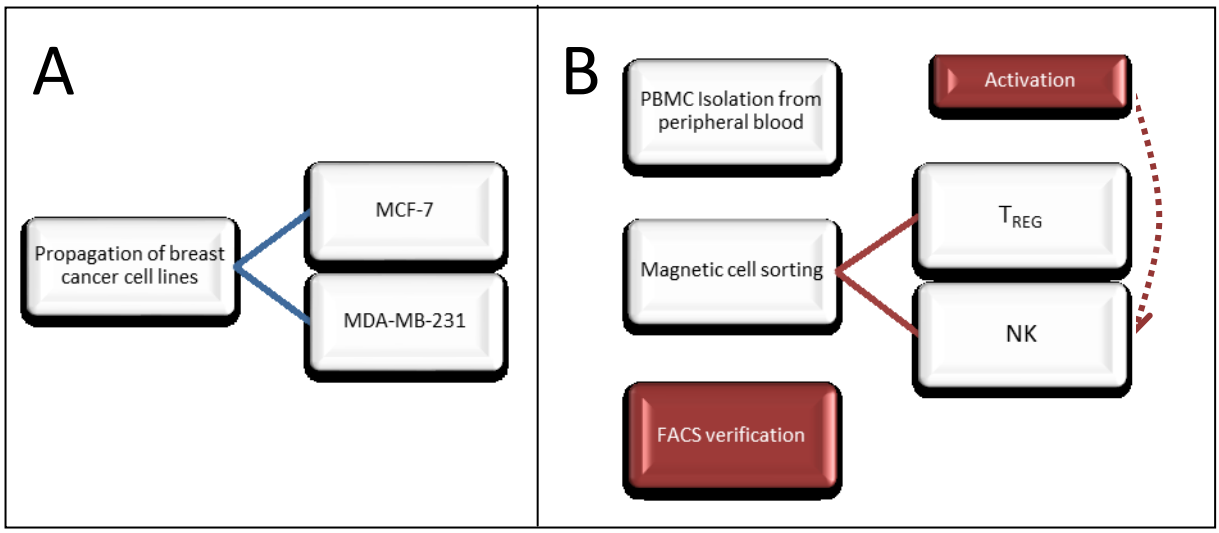

Figure 2.1 Illustration of the methodology employed prior to establishment of 3D heterotypic cultures

A) Propagation of breast cancer cell lines in monolayer for establishment of stock cells. **B)** PMBC isolation from peripheral blood via Ficoll-Hypaque density gradient centrifugation followed by magnetic cell sorting to yield T_{REG} and NK cell populations. Magnetic cell sorting efficacy was verified using flow cytometry. T_{REG} and NK cell populations were activated with IL-2 and phytohaemagglutinin prior to establishment of co-cultures.

2.2.1 Monolayer culture of MCF-7 and MDA-MB-231 cell lines

The MCF-7 and MDA-MB-231 cell lines were cultured in Dulbecco's Modified Eagle's Medium (DMEM) (Lonza, Bloemfontein, South Africa) supplemented with 10% foetal bovine serum (FBS) (Biocom Biotech, Clubview, South Africa, A15101) and 0.1% penicillin/streptomycin (P/S) (Sigma-Aldrich-Aldrich, Aston Manor, South Africa, P3539) at 37°C in 5% CO_2. Cells were subcultured upon approximately 80% confluence by treatment with 0.25% trypsin/ethylenediaminetetraacetic acid (EDTA) (Sigma-Aldrich, T4049) for 5-10 min. The reaction was stopped with the addition of 5ml 1M phosphate buffered saline (PBS) pH 7.4, (See Appendix A) supplemented with 1% FBS. The resulting cell suspension was centrifuged at 400 X *g* for 5 min. The supernatant was discarded and the cell pellet resuspended in 1ml PBS for determination of cell number and viability using the Trypan Blue Exclusion Assay and the Bio-Rad Automated Cell Counter TC-20 (Bio-Rad, Parkwood, South Africa). The cell pellet was obtained by centrifugation at 400 X *g* for 5 min. MCF-7 cells at passage number 14, and MDA-MB-231 cells at passage number 48, were cryopreserved at $1X10^6$cells/ml in 10% dimethyl sulfoxide (DMSO) (Saarchem, Johannesburg, South Africa, 186500) in FBS at -80°C until establishment of 3D cultures.

Images were obtained using an Olympus iX51 Inverted Microscope with CellSens Software. All images were obtained at 20X magnification. Plates were generated using Adobe Photoshop Elements 10.

2.2.2 Isolation of peripheral blood mononuclear cells (PBMC)

Approximately 30ml blood from seemingly healthy female volunteers (n=13) between ages 18-35 years (exclusion criteria included pregnancy, autoimmune diseases, immunodeficiency, cancer and a previous history of cancer) was collected via venipuncture in EDTA-coated Vacutainers (BD Biosciences, Woodmead, South Africa). Anticoagulated blood was diluted (1:1) with PBS followed by density gradient centrifugation to obtain a PBMC fraction. Specifically, the solution was layered 3:2 on to Ficoll-Hypaque ($1.077g/cm^3$)

(GE Healthcare Biosciences AB, Sweden, 17-1440-03) and centrifuged at 400 X *g* for 30 min. The resulting PBMC layer was resuspended in 1ml PBS and centrifuged at 400 X *g* for 5 min at 20°C in order to remove excess Ficoll-Hypaque. The PBMC pellet was resuspended in 1ml PBS and the number of viable cells determined as previously described. The PBMC suspension was thereafter centrifuged at 400 X *g* for 5 min at 20°C and the resulting pellet resuspended in 80µl PBS (pH7.2) supplemented with 0.5% bovine serum albumin (BSA) (Sigma-Aldrich, A9418) and 2mM EDTA, hereafter referred to as sorting buffer, in preparation for magnetic cell sorting.

2.2.3 Magnetic cell sorting

All reagents used in magnetic cell sorting were maintained at a temperature of 8°C. MS separation columns (Miltenyi Biotec, Cologne, Germany, 130-042-201) for positive selection of T_{REG} cells and NK cells were primed by flushing the column attached to the separator with 3ml sorting buffer prior to use.

Isolating the prototypic $CD4^+CD25^+$ T_{REG} cell fraction

The $CD4^+$ Multisort Microbead Kit (Miltenyi Biotec, 130-055-101) was used for positive selection of the $CD4^+$ lymphocyte compartment. Specifically, the PBMC fraction was incubated with 20µl CD4 Multisort Microbeads per $1X10^7$ cells for 15 min at 8°C in the dark. Cells were washed in 1ml sorting buffer by centrifugation at 400 X *g* for 10 min. The cell pellet was resuspended in 1ml sorting buffer and applied to the MS suspension column. Once the reservoir was empty, a further 3ml sorting buffer was applied to the column. This step was conducted three times. All unlabelled PBMC that passed through the column were retained for NK cell sorting. The column was then removed from the separator, placed over a collection tube and the CD4-labelled cells flushed out with 3ml sorting buffer.

For removal of residual magnetically labelled cells and enrichment of the $CD4^+$ population, cells were incubated with 60µl MACS Multisort Release agent (Miltenyi Biotec, 130-055-101) for 10 min at 8°C in the dark. The suspension was then applied to a newly primed MS column

within the separator. When the reservoir was empty, a further 3ml sorting buffer was applied to the column. This step was conducted three times. The unlabelled cells that passed through the column were retained and the column discarded. The cell suspension was centrifuged at 400 X *g* for 5 min and the resulting purified $CD4^+$ cell pellet resuspended in 1ml sorting buffer for viability assessment and cell number determination, conducted as previously mentioned. The cell suspension was thereafter centrifuged at 400 X *g* for 5 min and a cell pellet obtained.

For the removal of Multisort Microbeads and the subsequent magnetic labelling procedure, the cell pellet was incubated with 60µl sorting buffer, 30µl MACS Multisort Stop Reagent (Miltenyi Biotec, 130-055-101) and 10µl CD25 Microbeads (Miltenyi Biotec, 130-092-983) for 15 min at 8°C. Thereafter, the cell suspension was washed in 1ml sorting buffer by centrifugation at 400 X *g* for 10 min. The cell pellet was resuspended in 500µl sorting buffer and applied to a newly primed MS suspension column. Once the reservoir was empty a further 3ml sorting buffer was applied to the column. This step was conducted twice. The column was then removed from the separator, placed over a collection tube and the $CD4^+CD25^+$ cells (prototypic T_{REG} lymphocyte fraction) were flushed out with 3ml sorting buffer. The cell suspension was centrifuged at 400 X *g* for 5 min and resuspended in 1ml PBS for viability assessment and cell number determination.

Isolating the $NKp46^+$ NK cell fraction

For positive isolation of the NK cell population, the unlabelled PBMC fraction that had been previously collected was centrifuged at 400 X *g* for 5 min. The supernatant was aspirated and the cell pellet resuspended in 1ml PBS for cell number and viability determination. The cell suspension was centrifuged for a further 5 min at 400 X *g* and a maximum of $1X10^6$ PBMC were incubated with 20µl Anti-NKp46 conjugated to the fluorochrome, allophycocyanin (APC) (Miltenyi Biotec, 130-092-609), in 80µl PBS supplemented with 10% FBS for 15 min at room temperature in the dark. Thereafter, the cell suspension was washed in 1ml sorting buffer by centrifugation at 400 X *g* for 10 min. The supernatant was aspirated and a further

wash step conducted. The resulting cell pellet was resuspended in 80µl sorting buffer with 20µl Anti-APC Microbeads (Miltenyi Biotec, 130-090-855) and incubated for 15 min at 8°C. The cell suspension was washed in 1ml sorting buffer by centrifugation at 400 X *g* for 10 min. The resulting cell pellet was resuspended in 500µl sorting buffer and applied to a primed MS column. When the reservoir was empty, a further 3ml sorting buffer was applied to the column. This step was conducted twice. The column was then removed from the separator, placed over a collection tube and the $NKp46^+$ cells (NK cell-enriched fraction, henceforth referred to as NK cells) flushed out with 3ml sorting buffer. The cell suspension was centrifuged at 400 X *g* for 5 min and resuspended in 1ml PBS for viability assessment and cell number determination.

2.2.4 Activation and expansion of T_{REG} and NK cell populations

Magnetically isolated T_{REG} and NK cell populations were resuspended at a minimum of $1X10^5$cells/100µl in Roswell Park Memorial Institute (RPMI) medium 1640 (Lonza, Bloemfontein, South Africa) supplemented with 0.1% P/S, 10% FBS, 1µg/ml phytohaemagglutinin (PHA) (Sigma-Aldrich, L1668) and 0.8ng/ml IL-2 (Miltenyi Biotec, 130-093-901) for 18 h (See Appendix A). Subsequently, cell suspensions were harvested, centrifuged at 400 X *g* for 5 min and resuspended in RPMI 1640 supplemented with 0.1% P/S, 10% FBS and 0.8ng/ml IL-2 for a further 30 h, after which the establishment of co-cultures was undertaken (Domaica *et al.,* 2009).

2.2.5 Flow Cytometric Analysis of isolated T_{REG} and NK cell populations

Samples of isolated T_{REG} and NK cell populations were subjected to flow cytometric analysis using an LSR Fortessa (BD Biosciences, South Africa) with 4 laser capacity, to ascertain the efficacy of the magnetic cell sorting technique and the activation procedure. A caveat must be noted in that positive magnetic isolation can result in the downregulation of engaged markers, thus flow cytometric analysis may under-represent the expression of the said markers. Cells were resuspended at a maximum of $1X10^6$ cells/100µl PBS. Magnetically

isolated T_{REG} cells were incubated with 10µl CD4 conjugated to APC (BD Biosciences, Woodmead, South Africa, 555349) and 10µl CD25 conjugated to phycoerythrin (PE) (BD Biosciences, 555432). Magnetically isolated NK cells were incubated with 10µl CD56 conjugated to phycoerythrin and a cyanine dye (PE-Cy7) (BD Biosciences, 557747) and 10µl NKp46 conjugated to APC (BD Biosciences, 558051). Both cell populations were incubated with their respective antibodies for 15 min at room temperature in the dark. Cell suspensions were washed in 1ml PBS and centrifuged at 400 X *g* for 5 min. Supernatants were aspirated and the cell pellets fixed in 1% paraformaldehyde for 10 min at room temperature. The cell suspensions were washed in 1ml PBS by centrifugation at 400 X *g* for 5 min and the supernatants aspirated. The resulting cell pellets were resuspended in 1ml PBS and stored at 4°C in the dark until flow cytometric analysis.

Single bead staining for compensation

Single-stained capture compensation beads (BD Biosciences, 552843) were used to assess fluorescence spill-over across channels to establish the appropriate compensation to be applied prior to data collection. Each fluorescent-conjugated antibody at the concentrations used as above (10µl antibody/100µl PBS) was incubated with compensation beads in the dark for 15 min at room temperature. Negative compensation beads were left unstained, and thus used as a negative control. Suspensions were washed in 2.5ml PBS and centrifuged at 200 X *g* for 10 min followed by fixation in 1% paraformaldehyde for 10 min at room temperature. The suspensions were then washed in 2.5ml PBS and centrifuged at 200 X *g* for 10 min. The supernatant was aspirated and the compensation beads resuspended in 500µl PBS for subsequent flow cytometric analysis on the LSR Fortessa. Data was acquired with BD FACSDiva software v6 and analysed with FlowJo software (Free Trial).

2.2.6 Establishment of heterotypic 3D co-culture models

GFRM (BD Biosciences, BD354230), stored at -20°C, was defrosted at 8°C overnight prior to the establishment of co-cultures. All solutions and pipette tips were placed on ice and plating of cells within the GFRM was conducted on a cooling block.

Luminal-phenotype culture models (LPCM) and basal-phenotype culture models (BPCM) were established by co-culturing MCF-7 cells and MDA-MB-231 cells respectively, with lymphocyte subgroups (Table 2.2). Specifically, cryopreserved MCF-7 (P14) and MDA-MB-231 (P48) cells were thawed at room temperature and washed twice with 1ml PBS at 400 X *g* for 5 min. The cell pellet was resuspended in 1ml RPMI 1640 culture media supplemented with 10% FBS and 0.1% P/S. Activated T_{REG} lymphocyte and NK cell suspensions were aspirated and washed with 1ml PBS at 400 X *g* for 5 min. The resulting cell pellets were resuspended in 1ml RPMI 1640 supplemented with 10% FBS and 0.1% P/S. The number of viable cells within each cell group was determined as previously described.

Thereafter, lymphocyte subgroups (T_{REG} lymphocytes and/or NK cells) were resuspended with breast cancer cells (MCF-7 or MDA-MB-231) at a ratio of 1:1:2 in a volume of 66.5μl RPMI 1640 culture media supplemented with 10% FBS and 0.1% P/S, to yield experimental and control culture groups (Table 2.2). Low effector:target ratios were chosen to mimic the breast tumour microenvironment. The experimental culture groups (EXP) consisted of T_{REG} lymphocytes and NK cells, co-cultured with either MCF-7 cells or MDA-MB-231 cells at a ratio of 1:1:2. The control groups included NK cells cultured with either MCF-7 or MDA-MB-231 cells (NK-BC) at a ratio of 1:2; T_{REG} lymphocytes cultured with either MCF-7 or MDA-MB-231 cells (T_{REG}-BC) at a ratio of 1:2; and MCF-7 or MDA-MB-231 cells cultured alone (BC). As a caveat, two further control groups were considered (NK cells alone and T_{REG} lymphocytes alone); however, given the absence of growth cytokines (IL-2), and the duration of the experiment, the co-culture conditions were deemed insufficient to maintain viability of these mono-cultures.

Cell suspensions for each culture group were mixed with 200µl GFRM and plated in duplicate at ~65µl/well (to yield a minimum $1X10^5$ cell concentration) in two 96-well plates for each downstream application: ICC, RNA extraction and cytokine analysis. The cultures were allowed to solidify at room temperature for 5 min, followed by incubation at 37°C for 30 min. The cultures were then overlaid with 100µl RPMI 1640 culture media supplemented with 10% FBS and 0.1% P/S and incubated at 37°C in 5% CO_2 for 72 h. Culture media levels were checked daily with a further 100µl added over the 72 h period, following which samples were harvested for subsequent assays.

Images were obtained using an Olympus iX51 Inverted Microscope using CellSens Software V10. All images were obtained at 20X or 40X magnification. Adobe Photoshop Elements 10 was used to generate plates.

Table 2.2 Establishment of the Luminal Phenotype Culture Model (LPCM) and the Basal Phenotype Culture Model (BPCM)

Heterotypic 3D culture models based on the MCF-7 (luminal phenotype, hormone-dependent) and MDA-MB-231 (basal phenotype, hormone-independent) breast cancer cell lines were developed. The experimental culture groups (EXP) consisted of T_{REG} lymphocytes and NK cells, co-cultured with either MCF-7 cells or MDA-MB-231 cells at a 1:1:2 ratio in GFRM. The control groups included NK cells cultured with either MCF-7 or MDA-MB-231 cells (NK-BC); T_{REG} lymphocytes cultured with either MCF-7 or MDA-MB-231 cells (T_{REG}-BC) and MCF-7 or MDA-MB-231 cell cultured alone (BC).

Culture Group	Luminal Phenotype Culture Model (LPCM)	Basal Phenotype Culture Model (BPCM)
	MCF-7 cell line	***MDA-MB-231 cell line***
Experimental (EXP)	T_{REG} and NK	T_{REG} and NK
NK-breast cancer cells control (NK-BC)	NK alone	NK alone
T_{REG}-breast cancer cells control (T_{REG}-BC)	T_{REG} alone	T_{REG} alone
Breast cancer cells control (BC)	Control – no lymphocytes	Control – no lymphocytes

2.2.7 Harvesting of heterotypic 3D culture samples

Harvesting of culture supernatants for cytokine analysis

Culture media from each well was aspirated and centrifuged at 400 X *g* for 5 min to pellet any cellular debris. The supernatant was collected, snap frozen in liquid nitrogen and placed at -80°C until use (See Chapter III for further details).

Harvesting and processing of co-cultures for immunocytochemistry

Cultures were rinsed in PBS prior to incubation in 30µl FBS at 37°C for 1 min. Cultures were then incubated with 30µl thrombin (SANBS, Pretoria, South Africa) for approximately 30 sec at 37°C, followed by incubation at room temperature for a further 5 min to ensure clot formation. Samples were fixed in 200µl 4% paraformaldehyde (Sigma-Aldrich, P6148) in PBS for 20 min. The fixative was thereafter drained and eosin applied directly to the wells to allow for visualization of the samples. Samples were removed from the wells and placed into a 0.45µm filter paper envelope for automatic tissue processing. The samples were thereafter embedded in paraffin wax (Merck Millipore, Darmstadt, Germany, 61782320001730) and stored at 4°C until sectioning (See Chapter IV for further details) (Adapted from Graham *et al.,* 2009).

Optimising RNA Extraction Methodology

Various methods of RNA extraction were attempted to determine that which would result in the best yield, purity and integrity of RNA. It was found that the use of the Qiagen RNeasy Mini kit (Qiagen, Hilden, Germany, 74104) with the addition of proteinase K (Qiagen, 19131), was superior to TRIzol (Ambion, Texas, USA, 15596), either used as per protocol or followed subsequently by RNA elution and clean-up using the Qiagen RNeasy Mini kit. Proteinase K digestion of GFRM was found necessary to increase the yield of RNA obtained, and DNA digestion was restricted to off-column digestion only to prevent RNA degradation (See Appendix B for a description of other techniques tested).

Specifically, culture media was removed from wells and samples rinsed in PBS, following which 150µl 0.01% β-mercaptoethanol (Sigma-Aldrich, M6250) in Buffer RLT (Qiagen RNeasy Mini kit) was added to each culture. The resulting lysates were transferred to 1.5ml microcentrifuge tubes for homogenization through a 21-gauge needle. β-Mercaptoethanol was found essential in the prevention of RNA degradation. Samples were snap-frozen with liquid nitrogen and stored at -80°C until RNA extraction.

Samples were thereafter thawed on ice and incubated in 295µl RNAse-free water and 5µl proteinase K at 55°C for 10 min. Samples were centrifuged at 8 000 X *g* for 3 min, following which the supernatant was removed and incubated with 300µl 70% ethanol. Each sample was applied to an RNeasy spin column and centrifuged at 8 000 X *g* for 15 sec. The flow-through was discarded and 350µl Buffer RW1 added to the RNeasy spin column. The column was centrifuged again at 8 000 X *g* for 15 sec and the flow-through discarded.

For RNA elution, 500µl Buffer RPE (concentrate diluted 4X with 100% ethanol) was added to the RNeasy spin column which was centrifuged at 8 000 X *g* for 15 sec. The flow-through was discarded and a further 500µl Buffer RPE added to the RNeasy spin column. Following centrifugation at 8 000 X *g* for 2 min, the column was removed from the collection tube, placed onto a new 2ml collection tube and centrifuged for a further 1 min at 8 000 X *g*. The column was then removed from the collection tube, placed in a new 1.5ml collection tube and 30µl RNAse-free water added to the membrane. The column was centrifuged at 8 000 X *g* for 1min to obtain the RNA elute.

Off-column DNA-digestion was found necessary to increase the yield and purity of the eluted RNA. Thus, 20µl of each RNA elute was incubated with 10µl DNAse I Reaction Buffer (New England Biolabs, Massachusetts, USA, B0303S), 68µl Sabex water (Adcock Ingram, Krugersdorp, South Africa) and 2µl NEB DNAse (New England Biolabs, M0303L) at 37°C on a dry block heater for 10 min. A further 1µl 0.5M EDTA was added to each elution followed by heat-inactivation at 75°C on a dry block heater for 10 min. To conduct RNA clean-up, each sample was adjusted to 100µl with RNase-free water followed by the addition of 350µl

Buffer RLT and 250µl ethanol, mixed by pipetting. Up to 750µl of each sample was placed onto an RNeasy spin column and centrifuged at 8 000 X *g* for 15 sec. The flow-through was discarded and a further 500µl Buffer RPE added to the column which was centrifuged at 8 000 X *g* for 15 sec. The flow-through was again discarded and the column placed in a new 2ml collection tube. This was followed by further centrifugation at 8 000 X *g* for 1 min. The column was again removed from the collection tube and placed into a new 1.5ml collection tube with 30µl RNAse-free water added directly to the column membrane. The column was centrifuged at 8 000 X *g* for 1 min and the flow-through discarded, followed by further centrifugation at 8 000 X *g* for 1 min. Of the resulting solution, 2.5µl was aliquoted for RNA quality control. All aliquots were stored at -80°C until use.

RNA Quality Control

Samples were all analysed individually i.e. samples were not pooled. A NanoDrop Spectrophotometer (Thermo Fisher Scientific, Wilmington, USA) was used to determine the concentration and quality of eluted RNA. In order to blank the NanoDrop, 1µl RNAse-free water was loaded on to the sample pedestal. Thereafter 1µl of the RNA elute was loaded and the ratio of sample absorbance at 260nm and 280nm, and 260nm and 230nm measured. A 260/280 ratio of approximately two, is linked with high RNA purity. Lower ratios are indicative of phenol, protein or other contaminants. The 260/230 ratio is a secondary measure of purity, based on the above principles. Sample concentration at ng/µl was determined based on the absorbance at 260nm.

The Agilent 2100 Bioanalyzer and the RNA 600 Pico LabChip Kit (Agilent technologies, Waldbronn, Germany) were used to further ascertain RNA purity and integrity by determining the ratio of the 18S and 28S ribosomal units. Further analysis yields a RNA Integrity Number (RIN) close to ten (the lowest being one) indicative of intact RNA.

Preparing the RNA ladder

The RNA ladder had previously been heat-denatured at 70°C for 2 min and immediately cooled on ice. Ninety microlitres (90µl) RNase-free water had been added to the ladder and

the suspension mixed. Aliquots that had been stored at -80°C were thawed on ice immediately prior to use.

Preparing the RNA Gel Matrix

The RNA gel matrix was prepared by adding 550µl gel matrix into a spin filter. The spin filter was then placed into a microcentrifuge tube and centrifuged at 1 500 X *g* for 10 min. Aliquots were stored at 4°C till use.

Preparing the gel dye mix

All reagents were allowed to equilibrate at room temperature for 30 min prior to use. The dye concentrate was vortexed for 10 sec and 1µl thereof added to 65µl of the previously mentioned gel matrix. The resulting solution was vortexed to mix, followed by centrifugation at 13 000 X *g* for 10 min.

Loading the chip

The gel-dye mix (9µl) was loaded into indicated wells (as per manufacturers instruction), followed by loading 9µl conditioning solution into the indicated well. Thereafter, 5µl pico marker was loaded into wells designated for the RNA ladder and the samples. One microlitre (1µl) of the diluted RNA ladder was added to the designated well, with 1µl of RNA elute loaded into the remaining sample wells. The chip was thereafter vortexed for 60 sec, after which it was loaded into the Agilent Bioanalyzer for analysis.

2.2.8 Statistical analyses

With regard to the yield of lymphocyte populations, between-subject variability was analysed using the Kruskal-Wallis ANOVA by Ranks method with STATISTICA v12. The Spearman Rank Order Correlation test was used to determine whether correlations exist between lymphocyte populations. For all analyses, $p<0.05$ was regarded as statistically significant.

2.3 Results

2.3.1 Flow cytometry analysis of sorted and activated populations

Flow cytometry analysis confirmed the $CD4^+CD25^+$ profile of magnetically isolated T_{REG} lymphocyte populations, and the $CD56^+/NKp46^+$ profile of NK cells (see Appendix C1 for unstained and compensation controls). Cells exhibited slightly altered scatter properties possibly due to the effects of fixation, thus only those cells which exhibited the traditional side scatter (SSC) properties, associated with lymphocyte granularity or internal complexity and forward scatter (FSC) properties, associated with lymphocyte cell size, were analysed further (Fig. 2.2 – 2.5A).

Post-magnetic cell sorting, two distinct subsets, designated $CD4^{dim}CD25^+$ and $CD4^{bright}CD25^+$ (Fig. 2.2B) were noted, with the latter dominating the total lymphocyte population (See Appendix C2 for illustration of flow cytometric analysis of unfixed T_{REG} lymphocytes from PBMCs using a 2 laser BD FACSCalibur). Further investigations into the CD4 population (Fig. 2.2C) revealed negligible contaminating populations of $CD4^-$ cells (Fig. 2.2D). Both the $CD4^{dim}$ and the $CD4^{bright}$ population (Fig. 2.2C), which collectively comprised 77.6% of the total lymphocyte population, were dominated by $CD25^{dim}$ co-expression (Fig. 2.2E and Fig. 2.2F). Following culture and activation with PHA and IL-2, T_{REG} lymphocytes exhibited apparent alteration of scatter properties. Despite loss of cells outside the prototypic lymphocyte gate (Fig. 2.3A), the presentation of the $CD4^{dim}CD25^+$ and $CD4^{bright}CD25^+$ subsets were maintained (Fig. 2.3B). Further analysis of the CD4 population (Fig. 2.3C) reflected previous observations with a small contaminating population of $CD4^-$ cells (Fig. 2.3D).

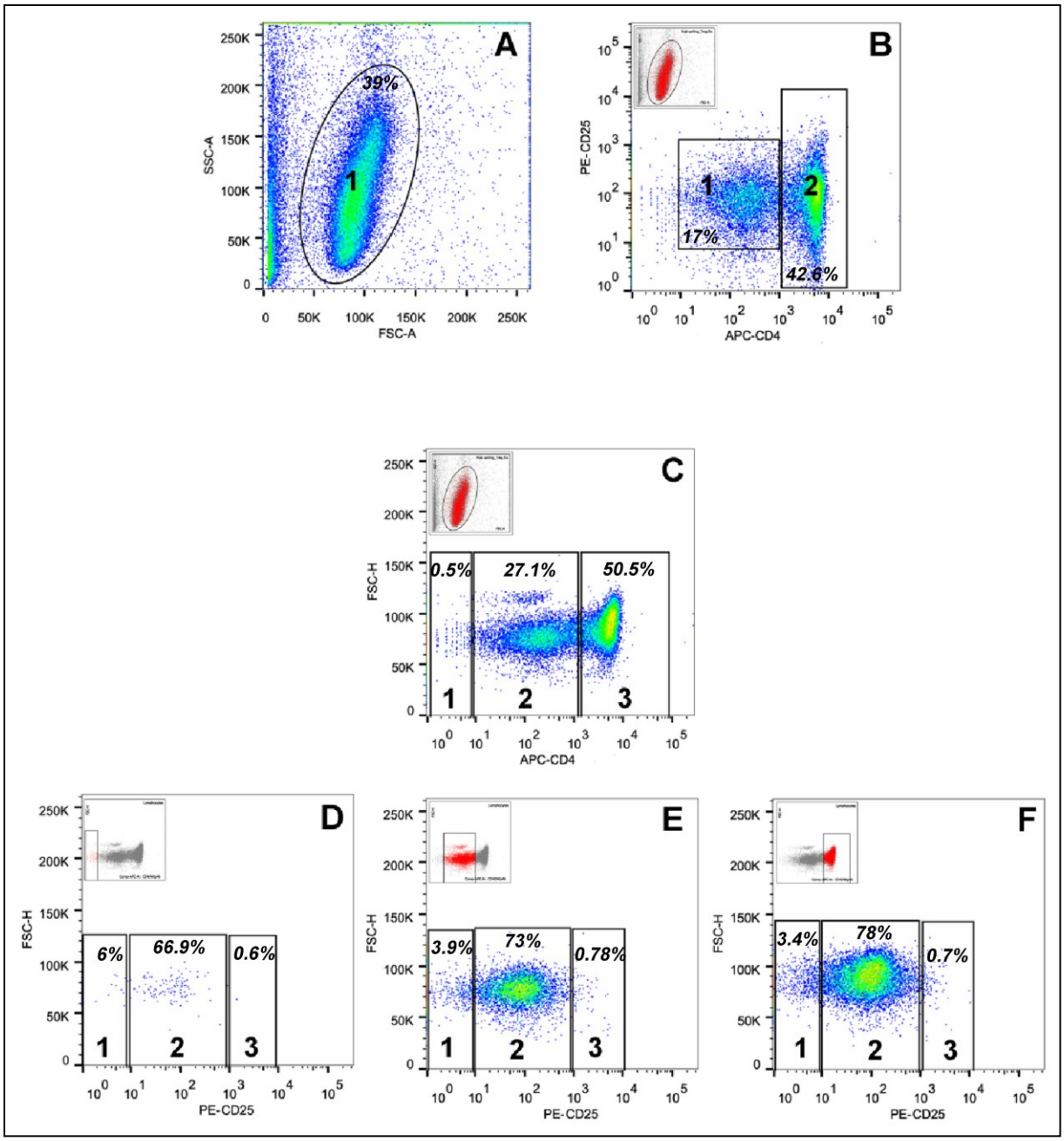

Figure 2.2 Scatterplots illustrating flow cytometric analysis of a T_{REG} cell population following magnetic cell sorting

A) SSC vs FSC showing total T_{REG} cell sorted population. Gate 1 indicates T_{REG} cells exhibiting typical lymphocyte scatter properties. **B)** APC-CD4 vs PE-CD25. Inset shows backgating on ancestral population A1. Note two distinct populations: Gate B1 $CD4^{dim}CD25^{dim}$, Gate B2 $CD4^{bright}CD25^{+}$. **C)** FSC-H versus APC-CD4. Inset shows backgating on ancestral population A1. **D)** FSC-H versus PE-CD25 based on inset parent population C1 ($CD4^{-}$ population). Gate D1 indicates a small population of $CD4^{-}CD25^{-}$ cells. Gates D2 and D3 indicate a slight scatter of contaminating $CD4^{-}CD25^{+}$ cells. **E)** FSC-H versus PE-CD25 based on inset parent population C1 ($CD4^{dim}$population). Gates E1 and E3 reflect small populations of $CD4^{dim}CD25^{-}$ cells and $CD4^{dim}CD25^{bright}$ cells, respectively. Gate E2 shows the dominant proportion of $CD4^{dim}$ cells are $CD25^{dim}$. **F)** FSC-H versus PE-CD25 based on inset parent population C3 ($CD4^{bright}$population). Gate F1 represents a $CD4^{bright}CD25^{-}$ cell population that is marginally larger than the $CD4^{bright}CD25^{bright}$ cell population designated by gate F3. Gate F2 indicates the dominant $CD4^{bright}CD25^{dim}$ population.

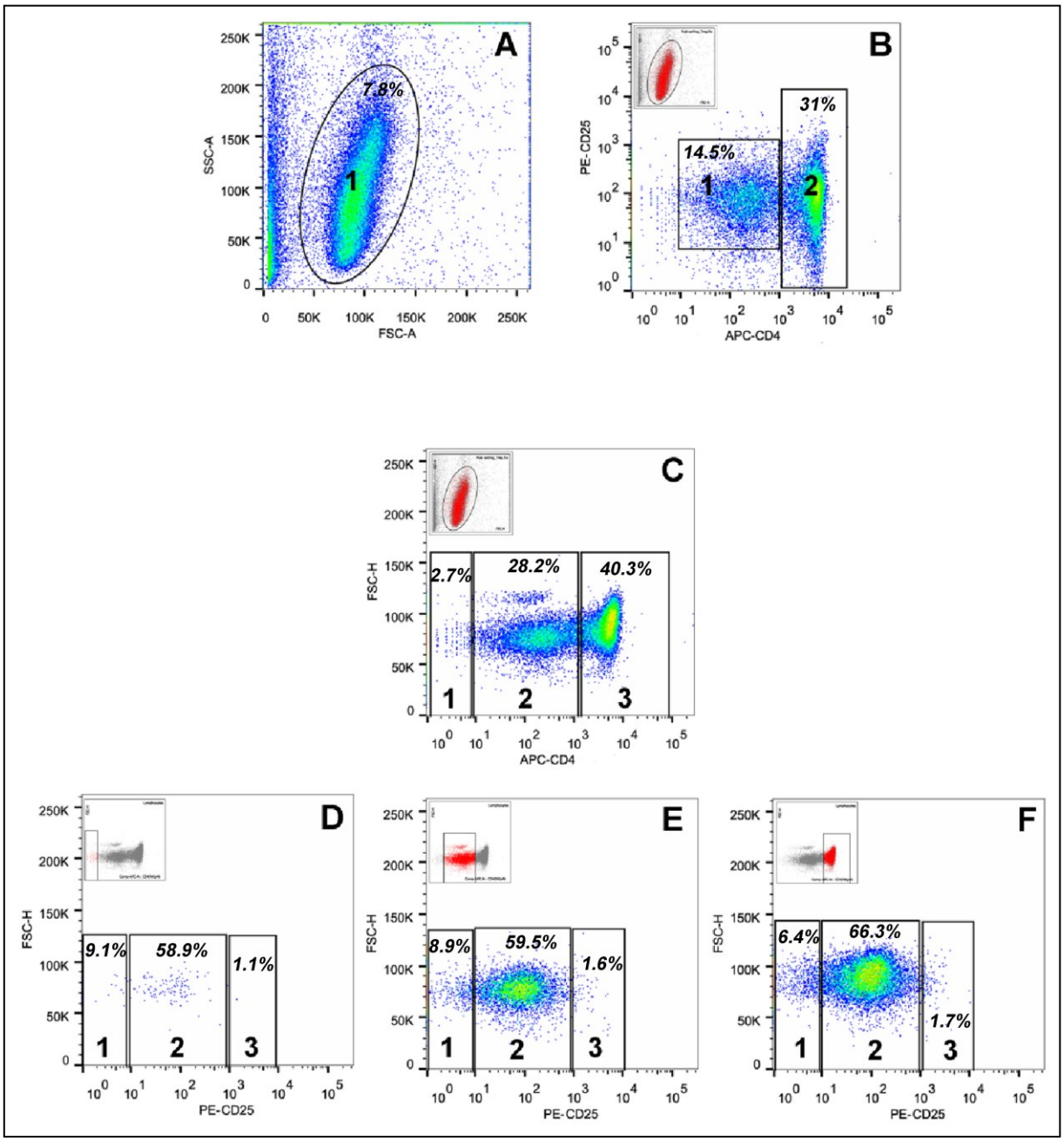

Figure 2.3 Scatterplots illustrating flow cytometric analysis of a T_{REG} cell population following magnetic cell sorting and activation with IL-2 and PHA

A) SSC vs FSC showing total T_{REG} cell population subsequent to sorting and activation. Gate 1 indicates T_{REG} cells exhibiting typical lymphocyte scatter properties. **B)** APC-CD4 vs PE-CD25. Inset shows backgating on ancestral population A1. Two distinct populations are noted: Gate B1 $CD4^{dim}CD25^{dim}$, Gate B2 $CD4^{bright}CD25^{dim}$. **C)** FSC-H versus APC-CD4. Inset shows backgating on ancestral population A1. **D)** FSC-H versus PE-CD25 based on inset parent population C1 ($CD4^{-}$population). Gate D1 indicates a small population of $CD4^{-}CD25^{-}$ cells. Gates D2 and D3 indicate a slight scatter of contaminating $CD4^{-}CD25^{+}$ cells. **E)** FSC-H versus PE-CD25 based on inset parent population C1 ($CD4^{dim}$population). Gates E1 and E3 reflect small populations of $CD4^{dim}CD25^{-}$ cells and $CD4^{dim}CD25^{bright}$ cells, respectively. Gate E2 shows the dominant proportion of $CD4^{dim}$ cells are $CD25^{dim}$. **F)** FSC-H versus PE-CD25 based on inset parent population C3 ($CD4^{bright}$population). Gate F1 represents a $CD4^{bright}CD25^{-}$ cell population that is marginally larger than the $CD4^{bright}CD25^{bright}$ cell population designated by gate F3. Gate F2 indicates the dominant $CD4^{bright}CD25^{dim}$ population.

Following magnetic cell sorting, analysis of the co-expression of CD56 and NKp46 cell surface markers demonstrated four distinct populations based on the total lymphocyte population (Fig. 2.4A) (See Appendix C2 for illustration of flow cytometric analysis of unfixed NK cells from PBMCs using the BD FACSCalibur). These populations were designated $CD56^{bright}NKp46^{bright}$; $CD56^{bright+}NKp46^{bright}$; $CD56^{dim}NKp46^{dim}$ and $CD56^{bright}NKp46^{dim}$ (Fig. 2.4B). Investigations into the $CD56^{+}$ population (Fig. 2.4C) which dominated the total lymphocyte population revealed a small contaminating population of $CD56^{-}$ cells which nevertheless exhibited $NKp46^{dim}$ and $NKp46^{bright}$ expression (Fig. 2.4D). A relationship between CD25 and NKp46 markers was noted. The $CD56^{dim}$ population (Fig. 2.4C), primarily co-expressed $NKp46^{dim}$ (Fig. 2.4E) and the notably large $CD56^{bright}$ population (Fig. 2.4C) expressed comparative levels of $NKp46^{bright}$ and $NKp46^{bright+}$ (Fig. 2.4F). Furthermore, the majority of the $CD56^{bright+}$ subset (Fig. 2.4G) co-expressed $NKp46^{bright}$.

Following *in vitro* activation with PHA and IL-2, NK cells exhibited altered scatter properties (Fig. 2.5A) and only two distinct populations, the $CD56^{dim}NKp46^{bright}$ and $CD56^{dim}NKp46^{dim}$ subsets (Fig. 2.5B). In both the small contaminating $CD56^{-}$ population and the dominant $CD56^{dim}$ population (Fig. 2.5C) the majority of cells co-expressed either $NKp46^{dim}$ or $NKp46^{bright}$ (Fig. 2.5D and 2.5E). There was a noticeable reduction in the presentation of the $CD56^{bright}$ subset (Fig. 2.5C), and corresponding co-expression of NKp46 (Fig. 2.5F).

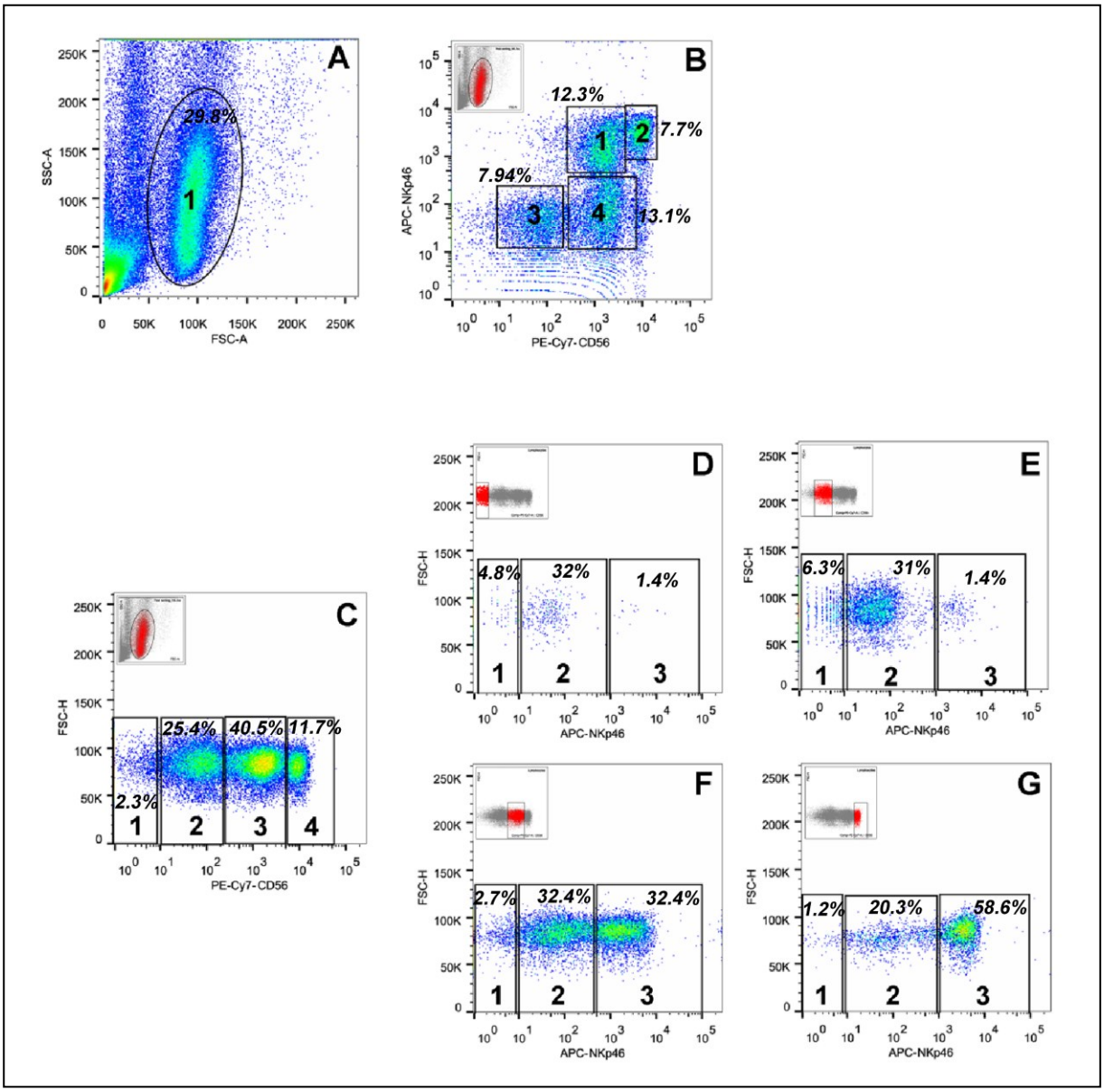

Figure 2.4 Scatterplots illustrating flow cytometric analysis of an NK cell population following magnetic cell sorting

A) SSC vs FSC showing total NK cell sorted population. Gate 1 indicates NK cells exhibiting typical lymphocyte scatter properties. **B)** APC-NKp46 vs PE-Cy7-CD56. Inset shows backgating on ancestral population A1. Four distinct populations are noted: Gate B1 $CD56^{bright}NKp46^{bright}$, Gate B2 $CD56^{bright+}NKp46^{bright}$, Gate B3 $CD56^{dim}NKp46^{dim}$ and Gate B4 $CD56^{bright}NKp46^{dim}$. **C)** FSC-H versus PE-Cy7-CD56. Inset shows backgating on ancestral population A1. **D)** FSC-H versus APC-NKp46 based on inset parent population C1 ($CD56^{-}$ population). Gate D1 shows a small population of $CD56^{-}NKp46^{-}$ cells. Gates D2 and D3 indicate $CD56^{-}NKp46^{dim}$ and $CD56^{-}NKp46^{bright}$ NK cell populations respectively. **E)** FSC-H versus APC-NKp46 based on inset parent population C2 ($CD56^{dim}$ population). Gates E1 and E3 show small populations of $CD56^{dim}NKp46^{-}$ cells and $CD56^{dim}NKp46^{bright}$ cells respectively. $NKp46^{dim}$ NK cells dominate the $CD56^{dim}$ population as indicated by gate E2. **F)** FSC-H versus APC-NKp46 based on inset parent population C3 ($CD56^{bright}$ population). Gate F1 indicates a small $CD56^{bright}NKp46^{-}$ population. Gates F2 and F3 reflect comparable numbers of $CD56^{bright}NKp46^{bright}$ NK cells. **G)** FSC-H versus APC-NKp46 based on inset parent population C4 ($CD56^{bright+}$population). The majority of $CD56^{bright+}$ NK cells express NKp46 as delineated by gate G3.

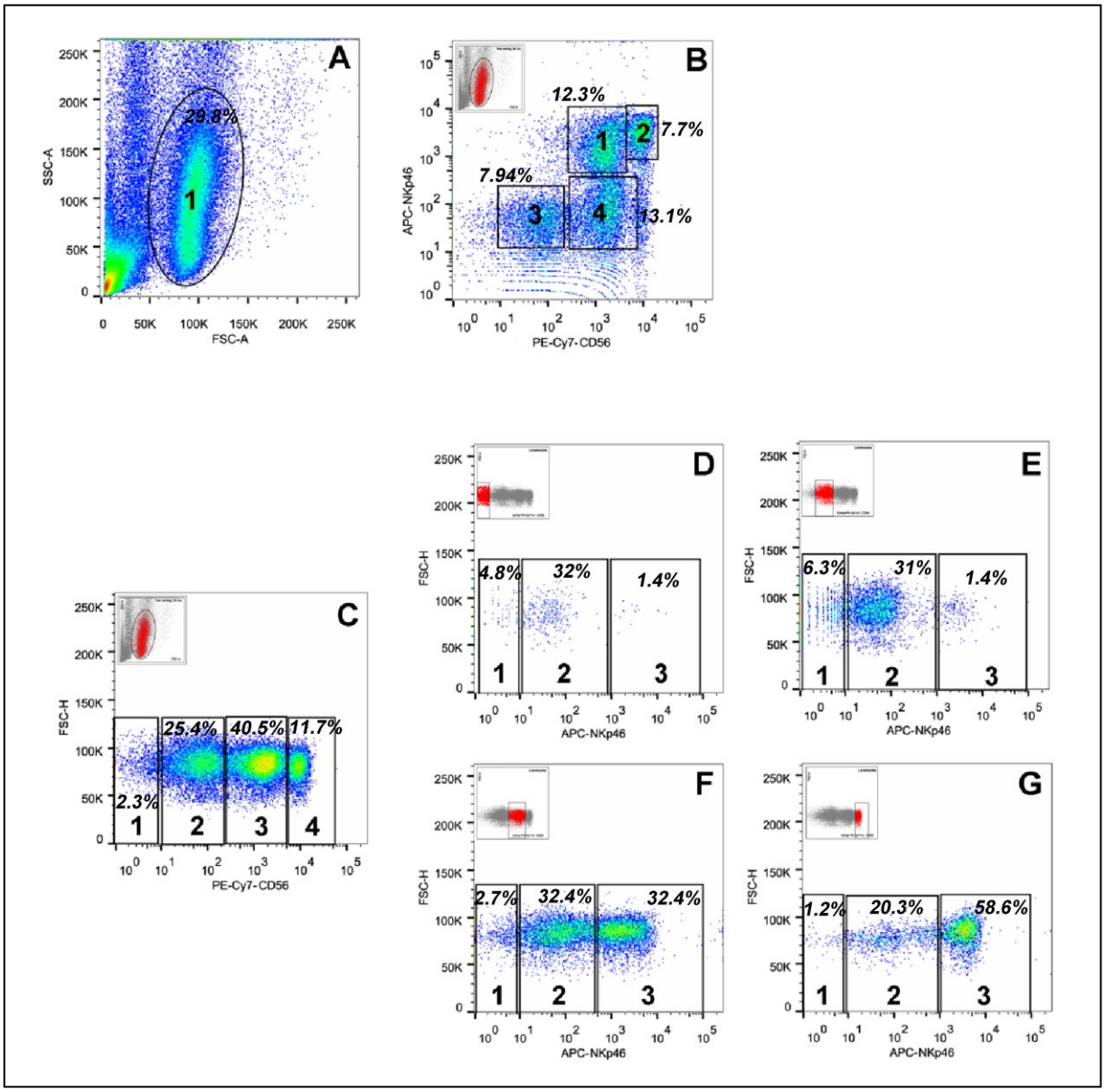

Figure 2.5 Scatterplots illustrating flow cytometric analysis of an NK cell population following magnetic cell sorting and activation with IL-2 and PHA

A) SSC vs FSC showing total NK cell sorted and activated population. Gate 1 indicates NK cells exhibiting typical lymphocyte scatter properties. **B)** APC-NKp46 vs PE-Cy7-CD56. Inset shows backgating on ancestral population A1. Two distinct populations are noted: Gate B1 $CD56^{dim}NKp46^{bright}$, Gate B2 $CD56^{dim}NKp46^{dim}$. **C)** FSC-H versus PE-Cy7-CD56. Inset shows backgating on ancestral population A1. **D)** FSC-H versus APC-NKp46 based on inset parent population C1 ($CD56^{-}$ population). Gate D1 shows a small population of $CD56^{-}NKp46^{-}$ cells. Gates D2 and D3 indicate $CD56^{-}NKp46^{dim}$ and $CD56^{-}NKp46^{bright}$ NK cell populations respectively. **E)** FSC-H versus APC-NKp46 based on inset parent population C2 ($CD56^{dim}$ population). Gates E2 and E3 reflect dominant populations of $CD56^{dim}NKp46^{dim}$ cells and $CD56^{dim}NKp46^{bright}$ cells respectively. Gate E1 shows a small proportion of $CD56^{dim}$ cells which are $NKp46^{-}$. **F)** FSC-H versus APC-NKp46 based on inset parent population C3 ($CD56^{bright}$ population). Gate F1 indicates very few $CD56^{bright}NKp46^{bright}$ NK cells.

2.3.2 Effects of magnetic cell sorting and subsequent activation on T_{REG} lymphocyte and NK cell yield

No statistically significant differences were found with regard to the yields (total and live) of the PBMCs and lymphocyte subgroups following magnetic cell sorting and activation procedures (Fig. 2.6), highlighting the efficacy of technique. Subsequent to magnetic isolation, the median yield of live T_{REG} lymphocytes and NK cells were 1E6 (88.5% viable) and 1.1E6 (83.2% viable) respectively. Following the first 18 h period of activation the average percentage live NK cell count decreased to 68%, and stabilised at 62% over the next 30 h activation period (Fig. 2.7). The average percentage live cell count for T_{REG} lymphocytes post-magnetic cell sorting was 88% and stabilised at 78% during both activation periods. For subsequent co-culture procedures, T_{REG} lymphocytes and NK cells were plated only if the sample percentage viability exceeded 70% and 60% respectively.

The yield of T_{REG} lymphocytes obtained correlated with that of $CD4^+$ lymphocytes post-magnetic cell sorting. However, no correlation was found between these subsets after the first activation procedure, with the T_{REG} subset instead correlating with the PBMCs. Interestingly, following the second activation procedure the yield of the T_{REG} subset correlated with that of the initial post-magnetic cell sorting as well as that of the first activation procedure (see Appendix D). This data may have further value for *in vitro* assays in raising the possibility of predicting the yield of T_{REG} cells post-activation. The yield of the NK cell subset did not correlate with any other subset, including T_{REG} lymphocytes or PBMCs, either prior to or subsequent to activation procedures.

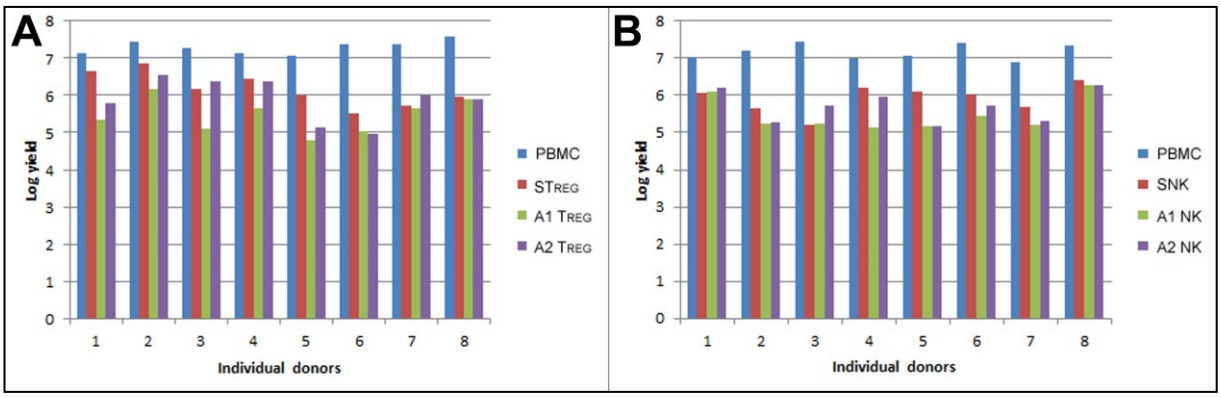

Figure 2.6 Illustration of log yields of PBMC and magnetically isolated lymphocyte subgroups – individual responses

Key: ST_{REG}/SNK – subset yield post-magnetic cell sorting; **A1 T_{REG}/A1 NK** – subset yield following first activation procedure; **$A2T_{REG}$/A2 NK** – subset yield following second activation procedure. **A)** Illustrates T_{REG} lymphocyte yields from PBMC and subsequent alterations in yield post-activation. **B)** Illustrates NK cell yields from PBMC and subsequent alterations in yield post-activation.

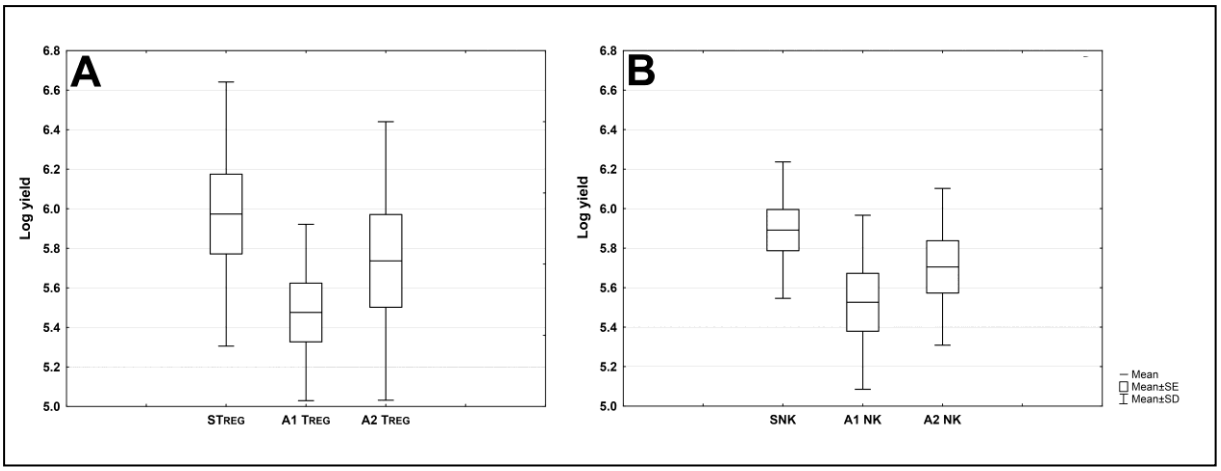

Figure 2.7 Mean log yields of magnetically isolated lymphocyte subgroups and response to IL-2 and PHA

Key: A) Illustrates T_{REG} lymphocyte yields from PBMC. **B)** Illustrates NK yields from PBMC. **X-axis –** ST_{REG}/SNK – subsets post-magnetic cell sorting; A1 T_{REG}/NK – subsets following first activation procedure; $A2T_{REG}$/NK – subsets following second activation procedure. **Y-axis** – log yield. Both T_{REG} lymphocytes and NK cells exhibited a decrease in live cell counts at the first activation period. However, this was compensated for by the end of the second activation period.

2.3.3 Morphological analysis of breast cancer cell lines in monolayer and 3D cultures

Prior to culture in GFRM, MCF-7 and MDA-MB-231 cells were propagated as monolayers in plastic culture dishes to establish stock populations. Under these conditions, MCF-7 cells (Fig. 2.8A) exhibited a characteristic polygonal morphology with vesicular nuclei and prominent nucleoli. Cells evidenced blunt cytoplasmic connections and numerous pseudopodia, forming a cobble stone-like appearance typical of epithelial cells. MDA-MB-231 cells in monolayer (Fig. 2.8B) were primarily spindle-shaped and associated with each other in an irregular, lattice-like manner.

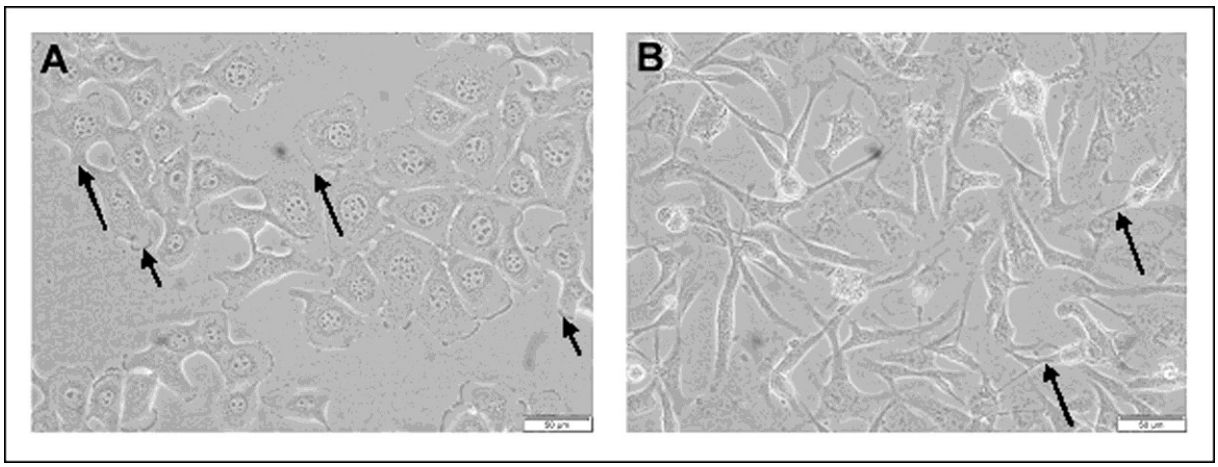

Figure 2.8 Representative photomicrographs of the cellular morphology of MCF-7 cells (A) and MDA-MB-231 cells (B) cultured in monolayer (2D)

A) MCF-7 cells with vesicular nuclei, prominent nucleoli and blunt cytoplasmic projections (long black arrows) allowing for cell-cell connections. Note the cobble stone-like appearance of the cell clusters. Pseudopodia with ruffled edges (short black arrows) are numerous. **B)** MDA-MB-231 cells exhibit a spindle-shaped morphology with long cytoplasmic connections (long black arrows) linking cells in a lattice-like network. Phase contrast microscopy, 20X magnification.

In the 3D culture system, both cell lines required between 24 h and 48 h to attach and spread within the GFRM. In the BC control group in the LPCM (Fig. 2.9D), MCF-7 cells assumed a globular polygonal morphology, noticeably different from that of the monolayer cultures (Fig. 2.8A), with large nuclei and numerous nucleoli, exhibiting connecting cytoplasmic projections by 48 h. With continued culture, MCF-7 cells formed masses (Fig. 2.9). In the BC control group in the BPCM (Fig. 2.10D), MDA-MB-231 cells established

themselves at a slower rate, assuming a stellate morphology with cytoplasmic extensions. With continued culture, MDA-MB-231 cells exhibited an organised lattice-like network of cytoplasmic projections (Fig. 2.10D). Notably both cell lines evince some cells maintaining a rounded morphology (Fig. 2.9D and 2.10D).

2.3.4 The effects of immune mediation on the morphology of breast cancer cell lines in 3D heterotypic cultures

Immune mediation affected the cell-cell associations in both LPCM and BPCM. In the EXP culture groups in which both lymphocyte populations were present, a major disruption in the formation of either MCF-7 cell masses or MDA-MB-231 cell networks was noted (Fig. 2.9A and Fig. 2.10A), as compared to the BC control groups (Fig. 2.9D and Fig 2.10D). Under NK cell influence, there was a marked reduction in the presentation of masses (Fig. 2.9B) in the LPCM and lattice-like networks in the BPCM (Fig. 2.10B). However, both MCF-7 cells and MDA-MB-231 cells under T_{REG} lymphocyte-mediation (Fig. 2.9C and Fig. 2.10C respectively) showed distinct masses and stellate networks, reminiscent of the BC control groups (Fig. 2.9D and Fig. 2.10D respectively). MCF-7 cells also demonstrated the formation of glandular structures, either tubular or acinar in shape, albeit with no lumen formation evident (Fig. 2.9C2-3 and Fig. 2.9D2-3).

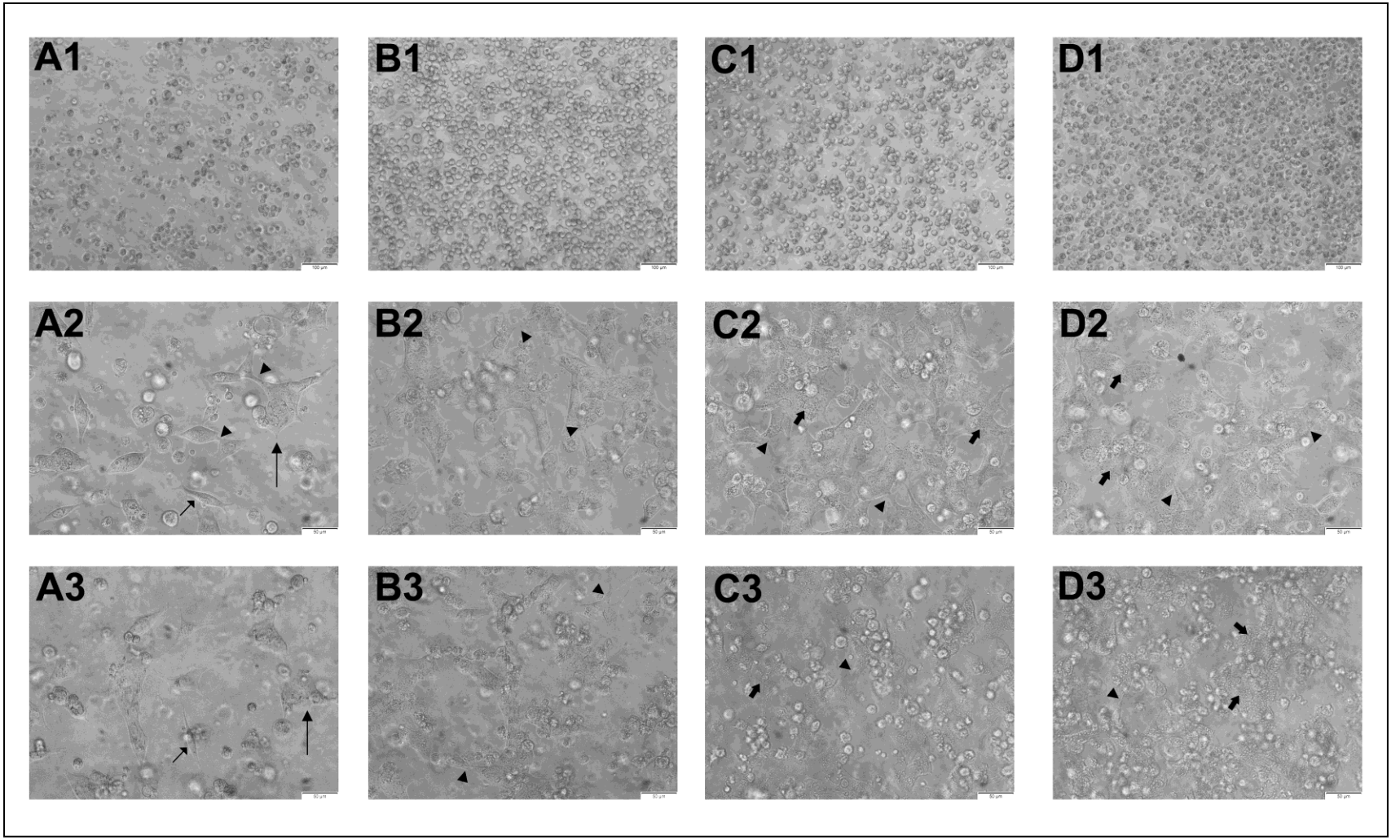

Figure 2.9 Representative photomicrographs illustrating the cellular morphology of culture groups in the LPCM over a 72 h period

Columns: Culture groups **A)** EXP, **B)** NK-BC, **C)** T_{REG}-BC, **D)** BC. **Rows: 1 – 3** are consecutive 24 h culture periods. At 24 h cells are rounded (A1-D1). By 48 h, MCF-7 cells assumed a polygonal (long arrows) or spindle-shaped morphology (short thin arrows), with cytoplasmic projections (arrowheads) linking cell masses. The EXP group showed few cell masses at 48 h and 72 h (A2, A3). The NK-BC group (B2, B3) showed less cell masses than T_{REG}-BC and BC groups (C2, C3, D2, D3). Cells in T_{REG}-BC and BC culture groups (C2, C3, D2, D3) were more granular (short wide arrows) and formed glandular structures with no apparent lumen. Phase contrast microscopy, Row 1 20X magnification, Rows 2 – 3 40X magnification.

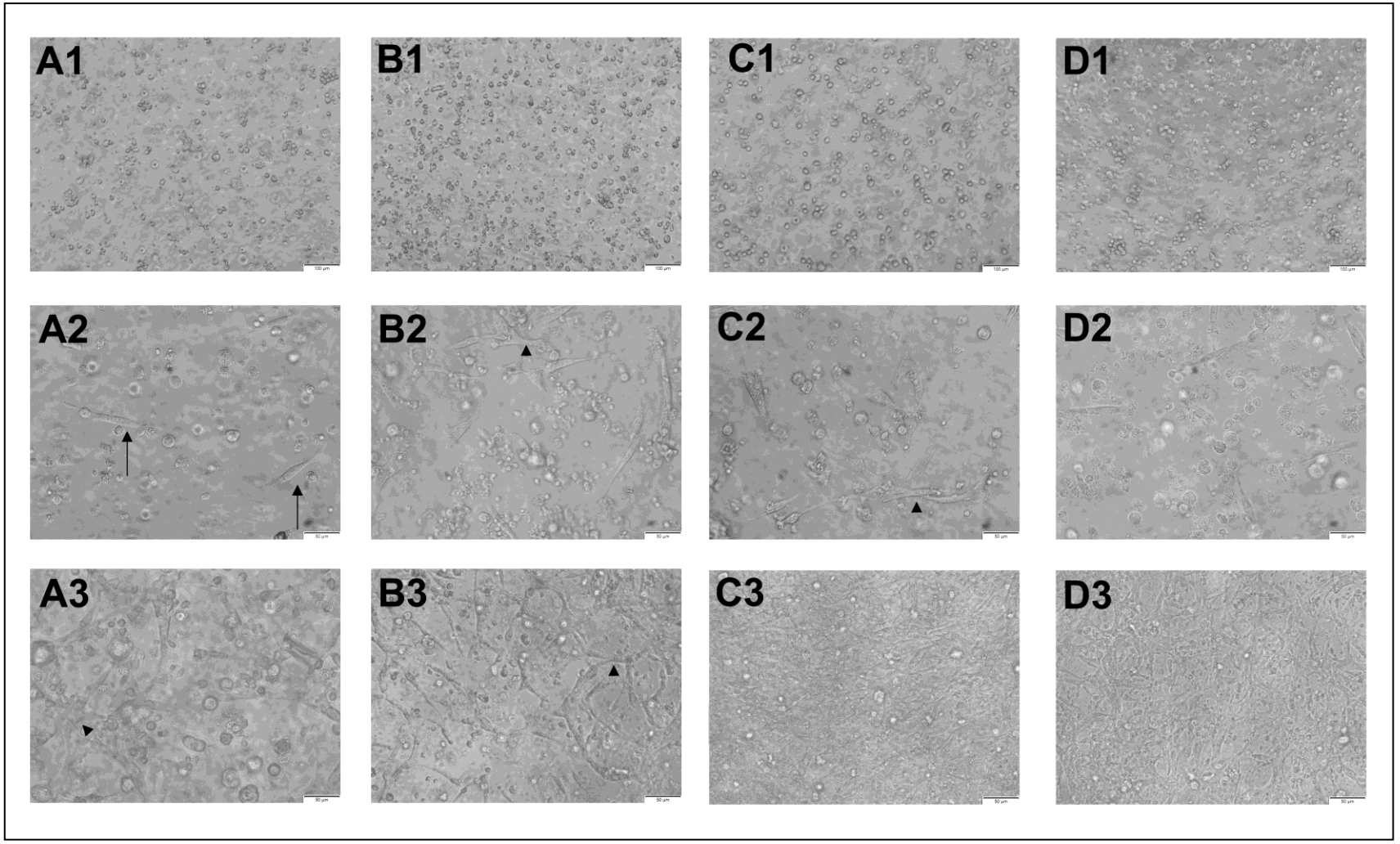

Figure 2.10 Representative photomicrographs illustrating the cellular morphology of culture groups in the BPCM over a 72 h period

Columns: Culture groups **A)** EXP, **B)** NK-BC, **C)** T_{REG}-BC, **D)** BC. **Rows: 1 – 3** are consecutive 24 h culture periods. At 24 h cells are rounded (A1-D1). By 48 h, MDA-MB-231 cells assumed a stellate morphology (long arrows) with cytoplasmic projections (arrowheads). The EXP culture group exhibited poor MDA-MB-231 cell network formation at 48 h and 72 h (A2, A3). The NK-BC group (B2 and B3) exhibited network formation but not to the extent observed in the T_{REG}-BC (C2 and C3) or BC culture groups (D2 and D3). Phase contrast microscopy, Row 1 20X magnification, Rows 2 – 3 40X magnification.

2.3.5 Harvesting of heterotypic cultures for immunocytochemistry

While ICC will be considered in detail in Chapter IV, it is worthwhile to note the following with regard to harvesting of samples for fixation. The samples were all necessarily small, given the limitations of the yield of lymphocyte populations and the expense of GFRM. While this allowed for samples to be run in duplicate for each downstream technique and allowed for both cell lines to be cultured simultaneously, the harvesting of such small samples from microwells proved difficult. Moreover, immune mediation affected the consistency of the GFRM in both LPCM and BPCM. Thus, GFRM in the EXP, NK-BC, and T_{REG}-BC culture groups exhibited reduced viscosity compared to the BC control culture groups.

2.3.6 Harvesting of heterotypic cultures for RNA extraction

A number of techniques were attempted to optimise the yield, purity and integrity of the extracted RNA, and as such, the majority of samples were sacrificed. With time constraints and funding limitations, reverse transcriptase real-time PCR (RT-qPCR), could thus not be conducted for inclusion into this thesis. While the TRIzol method yielded the highest concentration (Fig. 2.11), further analysis showed that RNA integrity was indefinable (Fig. 2.12). Variations to the methodology as per the Qiagen RNeasy Kit demonstrated that proteinase K was necessary for the digestion of residual GFRM (Fig. 2.11). Furthermore, it was noted that lysis in RLT buffer at 55°C followed by both off and on-column DNA digestion, resulted in varying yields of RNA, but no RNA integrity number (Fig. 2.11 and Fig. 2.12). It was thus established that lysis of samples in RLT buffer followed by digestion of residual GFRM with proteinase K and off-column DNA digestion alone presented a fair RNA yield, given the low cell numbers. The value of the primary measure of purity (260/280 ratio), as determined using the NanoDrop, was two, indicative of good purity, with Agilent analysis providing an RNA integrity number of 9.2 (Fig. 2.11 and Fig. 2.12).

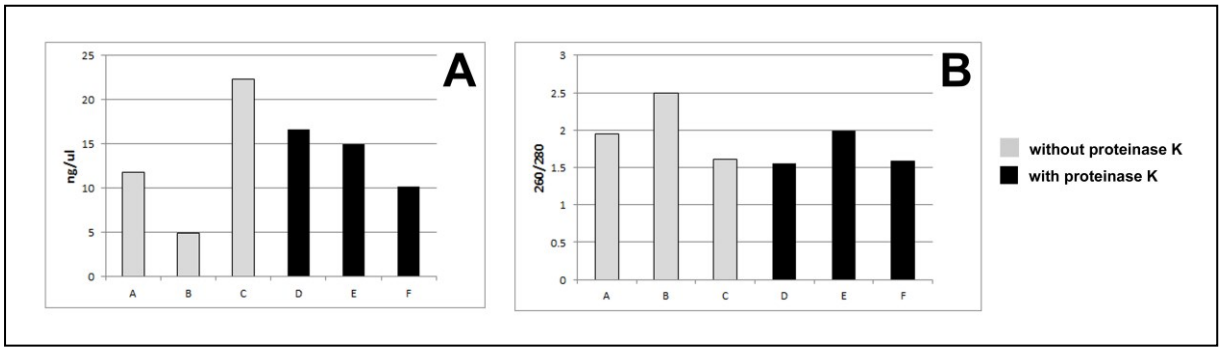

Figure 2.11 Graphs illustrating the average RNA yield (ng/ul) and RNA purity (260/280) based on various extraction methodologies (NanoDrop analysis)

KEY: X-axis labels (A-F) indicate extraction methodology. **Grey columns** indicate omission of proteinase K. **Black columns** indicate inclusion of proteinase K. **A)** Lysis in RLT buffer at 55°C prior to extraction with Qiagen RNEasy Kit. On-column DNA digestion only. **B)** as per A, with the addition of off-column DNA digestion. **C)** TRIzol method. **D)** TRIzol method with off column DNA digestion. **E)** Lysis in RLT buffer prior to extraction with Qiagen RNeasy Kit. Off column digestion only. **F)** As per E, addition of on-column digestion. Method C yielded the highest RNA concentration with methods B and E presenting the highest RNA purity levels.

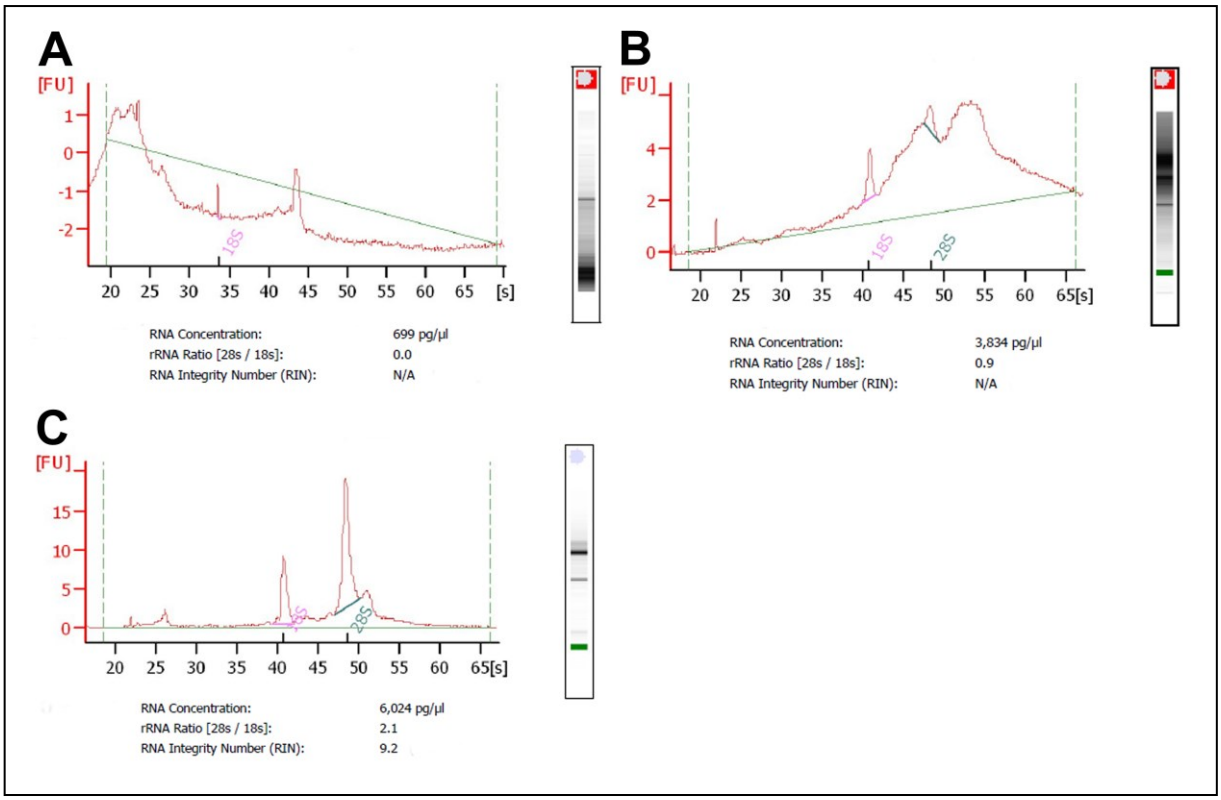

Figure 2.12 Electropherogram summaries of RNA yield, integrity and purity using various extraction methodologies (Agilent Bioanalyzer analysis)

A) Lysis in RLT buffer at 55°C prior to extraction using Qiagen RNEasy Kit. On-column and off-column DNA digestion. **B)** TRIzol method supplemented with off column DNA digestion. **C)** Lysis in RLT buffer prior to extraction using Qiagen RNEasy Kit followed by off-column DNA digestion only. Methods A and C incorporated the use of proteinase K. Only method C yielded acceptable results.

2.4 Discussion

2.4.1 The isolation of T_{REG} lymphocytes and NK cells

The phenotypic characterisation of T_{REG} lymphocytes remains the limiting factor of any study investigating this subset as previously discussed. In this study, the prototypic T_{REG} lymphocyte population ($CD4^+CD25^+$) was obtained using magnetic bead-based technology, the most commonly employed method for lymphocyte isolation for *in vitro* assays (Mandapathil *et al.,* 2009). One of the limiting factors of this isolation method is the inability to ascertain levels of marker expression. While flow cytometry isolation overcomes this problem and allows for increased sample purity, it too is still plagued by arbitrary designations as to what levels constitute high and low expression of selected markers (Whiteside, 2012).

In this study, flow cytometric analysis affirmed the selected profiles of magnetically isolated T_{REG} lymphocytes. It was noted that CD4 expression was clearly delineated into $CD4^{dim}$ and $CD4^{bright}$ subsets. These subsets were found in association with $CD25^{dim}$ and $CD25^+$ (comprising both dim and bright expression), respectively. Following activation with IL-2 and PHA, T_{REG} lymphocytes maintained these phenotypic populations. While upregulation of CD25, the α chain of the IL-2 receptor, is commonly associated with IL-2 signalling (Cheng *et al.,* 2011), CD25 expression has been shown to be reduced following permeabilisation of the cell membrane (Lee *et al*., 2011). While the fixative used in this study does not incorporate a detergent, fixation in paraformaldehyde does to a degree, permeabilise the cell membrane. Furthermore, upregulation of CD25 is also evident on $CD4^+$ effector cells upon activation (Yu and Fu, 2006; Piersma *et al.,* 2008). Thus, studies investigating the T_{REG} subset must take cognizance that without a definitive phenotype, isolated populations may contain contaminating effector cells.

Flow cytometric analysis of magnetically isolated NK cells demonstrated three distinct populations regarding the expression of CD56 alone, and four populations when NKp46 was considered, post-magnetic cell sorting. However, following activation with IL-2 and PHA, cells

presented with either a $CD56^{dim}NKp46^{bright}$ or $CD56^{dim}NKp46^{dim}$ phenotype. NKp46, which functions as a mediator of cytotoxicity against virally or malignantly transformed cells, is expressed in both resting and activated NK cells with proposed high expression in $CD56^{bright}$ cells (Bottino *et al.,* 2000; Miller, 2001; Koch *et al.,* 2013). The results indicate that the $NKp46^{bright}$ phenotype is however, maintained in a $CD56^{dim}$ population as well. $CD56^{bright}$ NK cells are considered to have poor cytolytic capacity, high proliferative capacity and are proposed to be the dominant cytokine-secreting NK subset; however, the downregulation of CD56 is proposed to be indicative of the acquisition of specialised function (Miller, 2001; Moretta, 2011). Other studies have indicated that the $CD56^{dim}$ subset is in fact the major producer of proinflammatory cytokines and chemokines upon target cell recognition, of particular interest to this study (Fauriat *et al.,* 2011; Moretta, 2011).

2.4.2 The establishment of 3D heterotypic culture models

Molecular profiling of the MCF-7 and MDA-MB-231 cell lines has confirmed their representation of infiltrating ductal carcinoma, specifically with reference to their respective luminal and basal phenotypes (Neve *et al.,* 2006; Kao *et al.,* 2009). Furthermore, morphological presentation in 3D culture systems correlates with molecular phenotypes as per the tumour microenvironment (Han *et al.,* 2010). In this study, the majority of MCF-7 cells cultured in the LPCM assumed a globular morphology, associated with their luminal phenotype. In the EXP culture group, in which MCF-7 cells were under both T_{REG} lymphocyte and NK cell-mediation, some cells displayed a spindle-like morphology, commonly associated with a mesenchymal-like phenotype. Mesenchymal-like morphology, reflected by MDA-MB-231 cells in the BPCM, is associated with a more aggressive profile (Zuo *et al.,* 2010). While MCF-7 cells are noted as being relatively weakly invasive (Fox and Kadpal, 2008), these results indicate that under the appropriate spatial and cellular stimuli, selected cells are capable of differentiating into a more invasive phenotype. Epithelial-mesenchymal transitions are linked to metastatic events, which in turn involve considerable interaction

with the surrounding stroma inducing the upregulation of MMPs and cytokine secretion (Krause *et al.,* 2010).

In the BC control group, in which MCF-7 cells were cultured without immune mediation, cells formed putative tubular and acinar glandular structures, indicating a cavitation process despite the lack of definitive lumina (do Amaral *et al.,* 2011); a phenomenon noted in other studies (Krause *et al.,* 2010). The formation of glandular structures, specifically with lumen formation, is indicative of a more well differentiated tumour (Krause *et al.,* 2010) traditionally associated with better prognosis. The more aggressive, MDA-MB-231 cells formed a lattice-like network in the BC control. While this morphological association was distinctly dissimilar to another 3D study in which MDA-MB-231 cells formed stellate clusters (Ampuja *et al.,* 2013); our results do reflect invasion tunnels formed by MDA-MB-231 cells, allowing leading cells to migrate within the tunnel through the GFRM (Yu and Machesky, 2012), a process dependent on upregulation of MMPs.

MMP expression facilitates the migration of IL-2 activated-NK cells through GFRM (Edsparr *et al.,* 2010). In this study, the possibility of MMP induction was highlighted by the reduction in viscosity of GFRM in culture groups under NK cell-mediation (EXP and NK-BC culture groups), and to a lesser extent under T_{REG} lymphocyte mediation, in both the LPCM and BPCM systems. NK cell presence was further associated with the disruption of cell masses (MCF-7 cells) and networks (MDA-MB-231 cells), regardless of T_{REG} lymphocyte presence. While it is tempting to assert that this reflects NK cell cytotoxic function, the complexity of the culture system is suggestive of events that are more complicated. T_{REG} lymphocytes are noted for their ability to suppress NK cell cytotoxic function with or without prior TCR activation, *in vitro* and *in vivo,* in a TGF-β-mediated manner (Ghiringhelli *et al.,* 2005; Ralainirina *et al.,* 2007). Tumour cells themselves, have also been shown to evade NK cell cytotoxicity via TGF-β dowregulation of the MHC class-I-related-protein A (MICA) ligands and their corresponding NK receptors, NKG2D (Park *et al.,* 2009); and by using MMP-9 to cleave the intercellular adhesion molecule (ICAM)-1 which facilitates targeting of transformed cells by NK cells (Fiore *et al.,* 2002). We propose that breast cancer cells subvert both immune cell

subsets to induce tumour tolerance and potentially to facilitate tumour progression. The results presented in Chapter III and Chapter IV, corroborate this assertion; however, further research is required to determine the pro-tumourigenic or anti-tumourigenic profile in the experimental systems.

Initially we planned to use RT-qPCR to identify alterations in gene expression associated with metastasis and cell death. However, the majority of samples were forfeited in optimising the RNA extraction procedure. The vast majority of studies using Matrigel for invasion assays (Pollard *et al.,* 2003; Selander *et al.,* 2004; Jin *et al.,* 2010; Chandrasekaran *et al.,* 2012; Hoover *et al.,* 2012) or to establish xenografts, typically conducted further assessments using immunohistochemistry (Elstner *et al.,* 1998; Pollard *et al.,* 2003; Engelmann *et al.,* 2008; Tate *et al.,* 2012). There is a distinct paucity of studies extracting RNA for further analysis from Matrigel 3D cultures (Table 2.3). With the number of available RNA extraction kits on the market, it is understandable that different research groups use different kits. However, few researchers report in detail, any variation to their extraction methodology or the methods of RNA quality control conducted. The advent of the MIQE (Minimum Information for Publication of Quantitative Real-Time PCR Experiments) guidelines in 2009, aims to ensure the repeatability of experimentation (Bustin *et al.,* 2009). Details essential to reporting nucleic acid extraction methods include modification to extraction procedures or kits and additional DNAse or RNase treatments for example. It is further suggested, that while absorbance ratios as determined using spectrophotometry (NanoDrop) provide an indication of RNA purity, the integrity of the RNA be investigated using microfluidic analysis (Agilent Technologies Bioanalyzer).

This study found that the TRIzol technique, whether used in conjunction with the Qiagen RNeasy Mini Kit or not, did not yield RNA with suitable integrity for further analysis. Some studies have advocated the removal of cell colonies from Matrigel with EDTA (Table 2.3) prior to extraction. However, it was of concern that EDTA treatment would alter gene expression beyond the dictates of the co-culture system. As such, this method was not attempted. The efficacy of sample lysis in RLT buffer followed by extraction using the Qiagen

RNeasy Mini Kit was determined; however, unlike other studies, it was necessary to include proteinase K for digestion of residual GFRM, comparable to the protocol for RNA extraction from fibrous tissue (Table 2.3). Similar to other studies (Table 2.3), it was determined that only one DNA digestion (off-column in this study) was necessary to remove residual DNA but also to ensure no further damage to the integrity of the RNA. A precise method for RNA extraction from GFRM co-cultures incorporating MIQE guidelines, an essential step for downstream gene expression analysis, has thus been determined.

Table 2.3 Examples of references consulted illustrating variability in RNA extraction methodology

Culture Method	Cells	RNA extraction method	RNA purity/integrity method	Reference
Matrigel coated flasks	Human liver stem cells	TRIzol	N/A	Herrera *et al.,* 2006
3D Matrigel culture	Breast epithelial cells	Colonies isolated with PBS/EDTA – 15-30 min for further RNA extraction TRIzol	N/A	Lee *et al.,* 2007 (Methodology article)
3D Matrigel culture	A host of breast cancer cell lines	Colonies isolated with PBS/EDTA Qiagen RNEasy MiniKit with on column DNA digestion	Optical density at 260nm Agarose gel electrophoresis	Kenny *et al.,* 2007
Matrigel coated dishes	Small hepatocytes (rat)	ISOGEN	N/A	Kon *et al.,* 2006
3D Matrigel culture	Normal mammary epithelium	Lyse in lysis buffer. Heat samples to 55°C before homogenization and cryopreservation. Stratagene Absolutely RNA microprep Kit	N/A	Graham *et al.,* 2009 (Methodology article)
3D Matrigel culture	YT cells and freshly isolated NK cells	Qiagen Fibrous Tissue Mini Kit	NanoDrop Spectrophotometer	Edsparr *et al.,* 2010
3D Matrigel culture	A host of breast cancer cell lines	Qiagen RNeasy Mini kit with on column DNA digestion	Agarose gel electrophoresis	Han *et al.,* 2011
3D Matrigel culture	A host of breast cancer cell lines	PBS/EDTA 15 min Qiagen RNEasy MiniKit	N/A	Ampuja *et al.,* 2013

2.5 Conclusion

This study developed a novel heterotypic 3D co-culture system for the investigation of interactions between T_{REG} lymphocytes, NK cells and either hormone-dependent or hormone-independent breast cancer cells. Tumour cells cultured in 3D displayed morphologies and cell-cell associations distinct to that observed in 2D monolayer cultures. It was further evident that immune mediation, primarily NK cell-influence, induced the disruption of cell masses (MCF-7 cells) and networks (MDA-MB-231 cells). It is proposed that the alteration of cell-cell associations reflects an enhanced invasive tumour profile, dependent on breast cancer phenotype, with breast cancer cells subverting immune cell subsets to induce tumour tolerance and potentially to facilitate tumour progression. Previous studies have shown that tumour cells in 3D culture exhibit a molecular phenotype and physiologic behaviour that more accurately reflects the *in vivo* tumour microenvironment. In order to shed light on the mechanisms and results of immune mediation of breast tumours, this study has demonstrated the effectiveness of RNA isolation for subsequent gene expression analysis. The ensuing chapters will illustrate the efficacy of this culture system for analysis of immune-mediated alterations in cytokine profiles (Chapter III) and the expression of selected tumour biomarkers as determined using immunocytochemistry (Chapter IV).

CHAPTER III: The Immune-Mediated Cytokine Profile of Hormone-Dependent and Hormone-Independent Breast Cancer Cell Lines in a 3D *In Vitro* System

3.1 Introduction

The breast tumour environment is an intricate network with tumour progression involving complex cellular interactions mediated by cytokines. Cytokines are proteins that regulate aspects of cell function associated with survival, differentiation and growth, via paracrine or autocrine actions (Leonard, 2008). Most cytokines act as immune mediators implicated in both anti-tumourigenic and pro-tumourigenic functions, acting in an additive, synergistic or antagonistic capacity (Nicolini *et al.*, 2006). While many cytokines are referred to as interleukins (*leuko* – indicating an association with *leuko*cytes), not all interleukins are secreted by leukocytes or for that matter affect leukocytes alone. Stromal components and immune cells also secrete cytokines, exerting their functions on similar cell types (Leonard, 2008). Tumour-secreted cytokines and chemokines ultimately induce a chronic inflammatory environment that is in turn, manipulated to allow for tumour progression (Lorusso and Rüegg, 2008). In such an environment, selective forces favour those tumour cells with reduced immunogenicity, enhanced survival capacity and superior immune evasion/subversion capability (Dunn *et al.,* 2004).

T_{REG} lymphocytes in the tumour microenvironment facilitate immunoediting processes by liaising with tumour cells to promote reduced immunogenicity and actively suppress anti-tumour functions of cytotoxic T lymphocytes and NK cells (DeNardo and Coussens, 2008). The suppression of NK cells by T_{REG} lymphocytes has been postulated to involve cell-cell contact and both bound and soluble TGF-β (Trzonkowski *et al.,* 2004; Ghiringhelli *et al.,* 2005; Ralainirina *et al.,* 2007). While NK cells primarily exert their anti-tumour functions in a direct cell-mediated manner, their ability to produce an array of cytokines allowing for interaction with other cell types, including malignant cells and T_{REG} cells of the adaptive immune system (Chambers, 2010), may in fact be their principal role in controlling tumour progression (Miller, 2001; Wilk *et al.,* 2008).

Of particular interest to this study are IL-2, IL-6 and IL-12; type I cytokines that exhibit a functional homology. High levels of IL-6 are found in breast tumour samples and in breast cancer cell lines (Honma *et al.,* 2002). IL-6 functions via gp-130-mediated activation of signalling pathways, inducing the upregulation of anti-apoptotic and angiogenic proteins within tumour cells. Importantly IL-6 increases oestradiol-17β hydroxysteroid dehydrogenase type I that converts oestrone to oestradiol, thereby inducing hormone-dependent proliferation and metastasis (Purohit *et al.,* 2002). As part of the type I cytokine family, IL-6 exhibits a functional homology with IL-12 and IL-2, both of which are noted for their capacity to activate T lymphocyte subsets and NK cells (Nicolini *et al.,* 2006).

Under cytokine influence, $CD56^{bright}$ NK cells and $CD56^{dim}$ NK cells are capable of altering their phenotype, with $CD56^{bright}$ NK cells acquiring a $CD56^{dim}$ phenotype under IL-2 stimulation, and $CD56^{dim}$ NK cells acquiring a $CD56^{bright}$ phenotype under IL-12 stimulation (Farag and Caligiuri, 2006). NK cells presenting with a $CD56^{bright}$ phenotype have poor cytolytic capacity and a high proliferative capacity. Traditionally regarded as an immunoregulatory subset, $CD56^{bright}$ NK cells produce cytokines and express lymphoid-homing molecules that may indicate interaction with cells of the adaptive immune system (Farag and Caligiuri, 2006). However, other studies have indicated that the $CD56^{dim}$ subset is the major producer of proinflammatory cytokines and chemokines upon target cell recognition (Fauriat *et al.,* 2011; Moretta, 2011). The IL-12-induced activation of NK cells elicits the production of IFN-γ, TNF and other proinflammatory mediators that act to inhibit angiogenesis, amongst other functions (Nicolini *et al.,* 2006). This suggests that immunoregulatory cytokines in disease states may have an important role in manipulating the response of NK cells.

IFN-γ, a type II IFN protein mainly produced by $CD4^+$ cells, $CD8^+$ cells and NK cells, is able to activate subpopulations of the adaptive immune system and increase expression of MHC class I and class II molecules (Nicolini *et al.,* 2006). While exogenous IFN-γ has anti-proliferative effects on breast cancer cell lines, including the MCF-7 cell line, hormone-dependency was shown not to affect its capacity (Nicolini *et al.*, 2006). IFN-γ is further able to induce a cytokine cascade including IL-1β, IL-6, TNF-α and CXCL8. Interleukin-6, IL-

1 and TNF are implicated as a cohort amplifying pro-inflammatory processes (Ben-Baruch, 2003). The breast tumour microenvironment and certain breast cancer cell lines frequently express members of the IL-1 cytokine family that transduce pro-inflammatory and anti-inflammatory signals via the MAP-kinase pathway (Nicolini *et al.*, 2006; Dinarello, 2008). Expression of IL-1α correlates with poor tumour differentiation and decreasing expression of ER-α. High serum concentrations of IL-1β correlate with a high rate of breast cancer relapse and it is proposed that the effects of IL-1β signalling may vary with breast cancer hormone-dependency status (Nicolini *et al.*, 2006). Members of the IL-1 family are further associated with the induction of chemokine secretion (Le Bitoux and Stamenkovic, 2008).

Chemokines are a group of cytokines with leukocyte recruiting and trafficking properties, responding to inflammatory cytokines and promoting inflammation (Ben-Baruch, 2003). In the tumour environment, infiltration of leukocyte subpopulations has implications for tumour progression. Of particular interest to this study are CCL2, also known as monocyte chemoattractant protein-1 (MCP-1), CCL4 and CXCL8 (also known as IL-8). The potent chemoattractant property of CCL2 for monocytes and NK cells is associated with anti-tumour functionality (Conti and Rollins, 2004). However, elevated levels of CCL2 are linked to MMP activity and thus have equally important implications for metastasis. Moreover, CCL2 is associated with poor prognosis in breast cancer patients (Ben-Baruch, 2003; Rollins, 2006; Le Bitoux and Stamenkovic, 2008), with tumour derived-CCL2 shown to reduce the efficacy of T-cell mediated anti-tumour activity (Vitiello *et al.,* 2004). Together with CCL2 and CCL4, CXCL8 shows high efficacy as a pro-angiogenic factor and is implicated in tissue remodelling via MMP induction (Vicari and Caux, 2002; Ben-Baruch, 2003; Mantovani *et al.,* 2010).

Experimental measures taken to deconstruct the tumour microenvironment are dominated by two-dimensional culture systems. However, three-dimensional culture systems are more able to reflect the physiological behaviour of tumour cells (Baker and Chen, 2012). Under the mechanical stresses associated with such culture scenarios, tumour cells create hypoxic hot-spots and are able to suppress cytotoxic T lymphocyte functions in a manner reminiscent of the *in vivo* environment (Feder-Mengus *et al.,*

2008). For this reason, we established a 3D culture system in which to investigate the interactions between lymphocyte subpopulations and breast cancer (Chapter II). This chapter deals with investigations into the cytokine response elicited by the combined interaction of NK cells, prototypic $CD4^{+}CD25^{+}$ T_{REG} lymphocytes and breast cancer cells (either hormone-dependent or hormone-independent) in a 3D culture system. The associations between multiple cytokines were investigated with multivariate exploratory statistical techniques, allowing the unravelling of patterns associated with lymphocyte subpopulations in a recreated breast tumour microenvironment.

3.2 Materials and Methodology

The Bio-Plex Pro cytokine assay (Bio-Rad, Parkwood, South Africa, M50000175D) was used to detect the presence of the following cytokines: IL-1β, IL-2, IL-6, IL-12, IFN-γ, TNF-α, CCL2, CCL4 and CXCL8 (panel designed by author). Data was acquired using the Bio-Plex 200 system and Bio-Plex Manager software (Bio-Rad, Parkwood, South Africa).

3.2.1 Sample preparation

Cryopreserved samples (n=68) were defrosted on ice (Table 3.1). To ensure that no precipitates were present, samples were centrifuged at 10 000 X *g* for 10 min at 4°C and the supernatant retained. Two groups of blank controls consisting of RPMI 1640 culture media supplemented with 10% FBS and 0.1% P/S and GFRM-conditioned RPMI 1640 culture media supplemented with 10% FBS and 0.1% P/S were also prepared. Samples were used undiluted and plated in duplicate. Only one cytokine plate was used.

Table 3.1 Culture groups in the Luminal Phenotype Culture Model (LPCM) and the Basal Phenotype Culture Model (BPCM)

Heterotypic 3D co-culture models based on the MCF-7 (luminal phenotype, hormone-dependent) and MDA-MB-231 (basal phenotype, hormone-independent) breast cancer cell lines were developed. The experimental culture groups consisted of T_{REG} lymphocytes and NK cells, co-cultured with either MCF-7 cells or MDA-MB-231 cells at a 1:1:2 ratio in growth factor reduced Matrigel. The control groups included NK cells cultured with either MCF-7 or MDA-MB-231 cells (NK-BC); T_{REG} lymphocytes cultured with either MCF-7 or MDA-MB-231 cells (T_{REG}-BC) and MCF-7 or MDA-MB-231 cell cultured alone (BC).

Culture Group	Luminal Phenotype Culture Model (LPCM)	Basal Phenotype Culture Model (BPCM)
	MCF-7 cell line	***MDA-MB-231 cell line***
Experimental (EXP)	T_{REG} and NK	T_{REG} and NK
NK-breast cancer cells control (NK-BC)	NK alone	NK alone
T_{REG}-breast cancer cells control (T_{REG}-BC)	T_{REG} alone	T_{REG} alone
Breast cancer cells control (BC)	Control – no lymphocytes	Control – no lymphocytes

3.2.2 Preparation of components for cytokine analysis

Standards preparation

Lyophilized standards were reconstituted in 500µl RPMI 1640 culture supplemented with 10% FBS and 0.1% P/S. The standard solution was thereafter vortexed for 5 sec and incubated on ice for 30 min. A fourfold dilution series of the standard was prepared to allow for the generation of an eight point broad range cytokine standard curve (low photomultiplier tube setting).

Coupled bead preparation

Coupled beads were sonicated for 30 sec prior to use to prevent aggregation. Subsequently, 575µl coupled beads were diluted in 5 175µl Bio-Plex assay buffer (hereafter referred to as assay buffer). The resulting solution was protected from light.

Detection antibody preparation

Detection antibodies were prepared approximately 10 min before use. The stock antibodies were vortexed for 20 sec followed by centrifugation for 30 sec at 10 000 X *g*. Thereafter 300µl of the stock antibodies were diluted in 2 700µl Bio-Plex antibody diluent. The resulting solution was vortexed for 5 sec immediately prior to use.

Streptavidin-PE preparation

The streptavidin-PE solution was prepared approximately 10 min before use. The stock solution was vortexed for 5 sec followed by centrifugation for 30 sec at 10 000 X *g*. Subsequently, 60µl of the stock solution was diluted with 5 940µl assay buffer. The resulting solution was protected from light and vortexed for 5 sec immediately before use.

3.2.3 Cytokine assay

Samples, standards and coupled beads were allowed to equilibrate to room temperature prior to preparation of the filter plate. All wash steps were conducted using vacuum filtration (Bio-Plex Aurum Vacuum Manifold, Bio-Rad, South Africa) followed by blotting

the plate on clean paper towel to remove any excess fluid. All transfers to the plate were conducted using a multichannel pipette, with the exception of the transfer of the standards, blanks and samples.

The filter plate was dampened using 100µl assay buffer. Coupled beads were vortexed for 30 sec and 50µl of the solution transferred to each well. The plate was washed twice with 100µl Bio-Plex wash buffer (hereafter referred to as wash buffer). The standard dilution series, blanks and samples were vortexed briefly and 50µl of each were transferred individually to their designated wells. The filter plate was covered with sealing tape, protected from light with aluminium foil and incubated at room temperature for 30 min on a platform shaker at 300rpm. The plate was washed thrice with 100µl wash buffer followed by a further incubation period with 25µl of detection antibody at room temperature for 30 min on a shaker at 300rpm. The plate was washed three times with 100µl wash buffer. Thereafter, 50µl of the streptavidin-PE working solution was transferred to each well and the plate incubated at room temperature for 10 min on a platform shaker at 300rpm. This was followed by three washes with 100µl wash buffer. Subsequently, 125µl assay buffer was transferred to each well and the plate placed on a platform shaker at 300rpm for 30 sec. Data was acquired using the Bio-Plex 200 System and Bio-Plex Manager software. Assay sensitivity per cytokine was noted as per manufacturer's notation.

3.2.4 Statistical analyses

The data was standardized prior to statistical analysis with STATISTICA v12 and PAST v2.17c. Since normality tests indicated the non-parametric nature of the data, the Kruskal-Wallis ANOVA by Ranks method with Bonferroni adjustment was employed to assess whether culture groups within the LPCM and BPCM were significantly different from each other with regard to cytokine expression. Multiple comparison post-hoc tests (2-tailed with Bonferroni adjustment) were used thereafter to determine which culture groups exhibited the differences found by the Kruskal-Wallis test. Specifically, these statistical tests considered all culture groups including the blank control as comparator

groups for analysis. For all analyses, $p<0.05$ was regarded as statistically significant (See Appendix E1 – E5).

Three exploratory multivariate techniques including cluster analysis, non-metric multidimensional scaling (MDS) and principal component analysis (PCA) were conducted. Given the small initial sample size, the data was first bootstrapped, allowing for the original input data to be resampled (n=1000) (Ballenberger *et al.,* 2012). For cluster analysis, a hierarchical method was conducted to illustrate the association of cytokines within each culture group. The unweighted pair-group average procedure coupled with evaluation of similarities (Euclidean distance) between items was used to generate dendrograms (Saraçli *et al.,* 2013). Since data was resampled, the cophenetic correlation coefficient (CC) was used to indicate the efficacy of the analysis in representing the clustering of the original dataset. Non-metric MDS was used as a complimentary method to cluster analysis. Correlation matrices were generated using Spearman's Rho as a measure of similarity. Scree plots were generated using D-star raw stress values, to determine the optimal number of dimensions to specify for the non-metric MDS (See Appendix F1 – F3).

Principal components analysis with singular value decomposition allowed for the reduction of our multivariate dataset into orthogonal components that account for the majority of the variance in the dataset (Buciński *et al.,* 2007). Eigenvalues were plotted (scree plots) to determine components to be retained.

3.3 Results

For cytokine analysis, GFRM-conditioned culture media and culture media alone were used as blank controls. No significant differences regarding any of the variables were found between these blank controls, thus for subsequent analyses data was combined.

3.3.1 Effects of T_{REG} lymphocytes and NK cells on cytokine secretion in the LPCM

The pro-inflammatory cytokine IL-6 as well as the chemokines CCL2, CCL4 and CXCL8 contributed significantly to the observed differences between culture groups. Subsequent multiple comparison tests demonstrated a significant increase in the secretion of chemokines CCL2, CCL4 and CXCL8 (Fig. 3.1) in both the EXP culture group and the NK-BC control culture group, indicating the impact of NK cell presence regardless of T_{REG} lymphocyte influence. The distribution of the indicated cytokines in the culture groups exhibited greater spread than that of the control groups. The dispersion of the data reflects probable biological variation within groups and the effects of NK cells and T_{REG} cells on cytokine release across groups.

While the chemokines clustered together with the proinflammatory cytokine IL-6 in the absence of T_{REG} cells (Fig. 3.2B), T_{REG} lymphocyte-mediation is noted in both the EXP culture group (Fig. 3.2A) and T_{REG}-BC control (Fig. 3.2C) group, with CCL4 and CCL2 clustering independently of IL-6 and CXCL8. In the BC control culture group in which MCF-7 cells were cultured without lymphocytes, CCL4 clustered independently of CCL2, CXCL8 and IL-6 (Fig. 3.2D). IL-2 and TNF-α cluster consistently across culture groups; however, the separation between this cluster and that associated with IL-12, IFN-γ and IL-1β is small.

Visual representation of non-metric MDS confirmed the association of IL-6 with the chemokines CCL2 and CXCL8 in the EXP culture group (Fig. 3.3A). However, IL-12 associated with CCL4, sharing dimension 1 with IFN-γ and TNF-α in the EXP culture group. Notably, under the influence of NK cells alone, the groupings (bar IFN-γ) demonstrated in the EXP culture group formed a closer association (Fig. 3.3B). The effects of T_{REG} cell-mediation on the cytokine profile of the control culture group T_{REG}-BC, were difficult to

unravel with no clear groupings apparent (Fig. 3.3C). MCF-7 cells cultured without the influence of immune cells in the BC control culture group did however exhibit a profile involving two groups i.e. CCL2-CXCL8 and CCL4-IFN-γ (Fig. 3.3D).

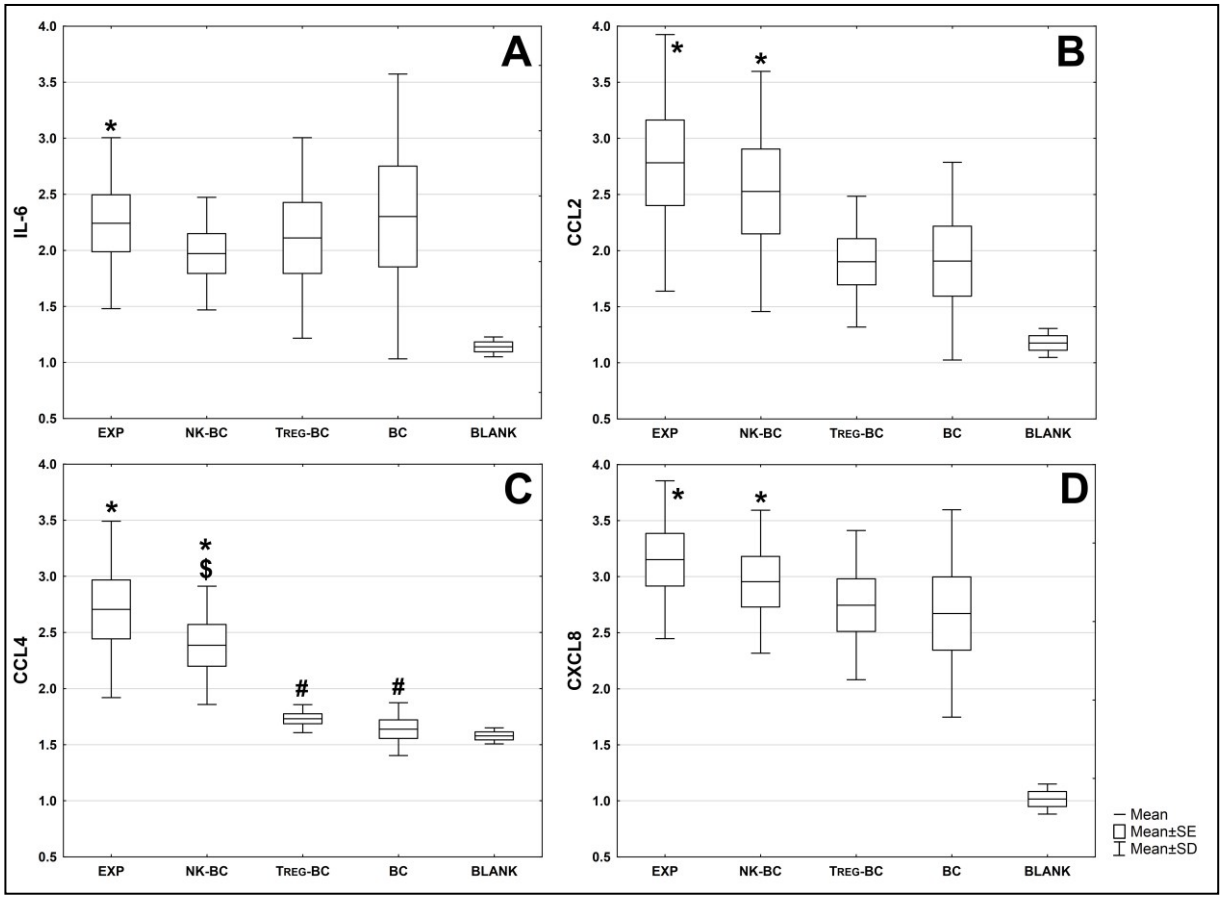

Figure 3.1 Box and whisker plots of cytokines determined to be significantly different ($p<0.05$) within and between multiple culture groups in LPCM.

KEY: X-axis – culture groups; **Y-axis –** log cytokine concentration. **A)** BC control culture group exhibited the greatest dispersion in IL-6 expression. A significant difference in IL-6 expression was found between the EXP culture group and the blank control (*). **B)** The EXP culture group and NK-BC control culture group differed significantly from the blank control (*) with regard to CCL2 expression. **C)** The EXP culture group exhibited the greatest dispersion in CCL4 expression, further proving to be significantly different from the blank control (*) and control culture groups T_{REG}-BC and BC (#). NK-BC control culture group presented with a smaller distribution of data than the EXP culture group, and was significantly different to the blank control (*) and to culture group BC ($). **D)** All groups except the blank control displayed large spreads of data. CXCL8 expression in both culture groups EXP and NK-BC were significantly different to the blank control (*).

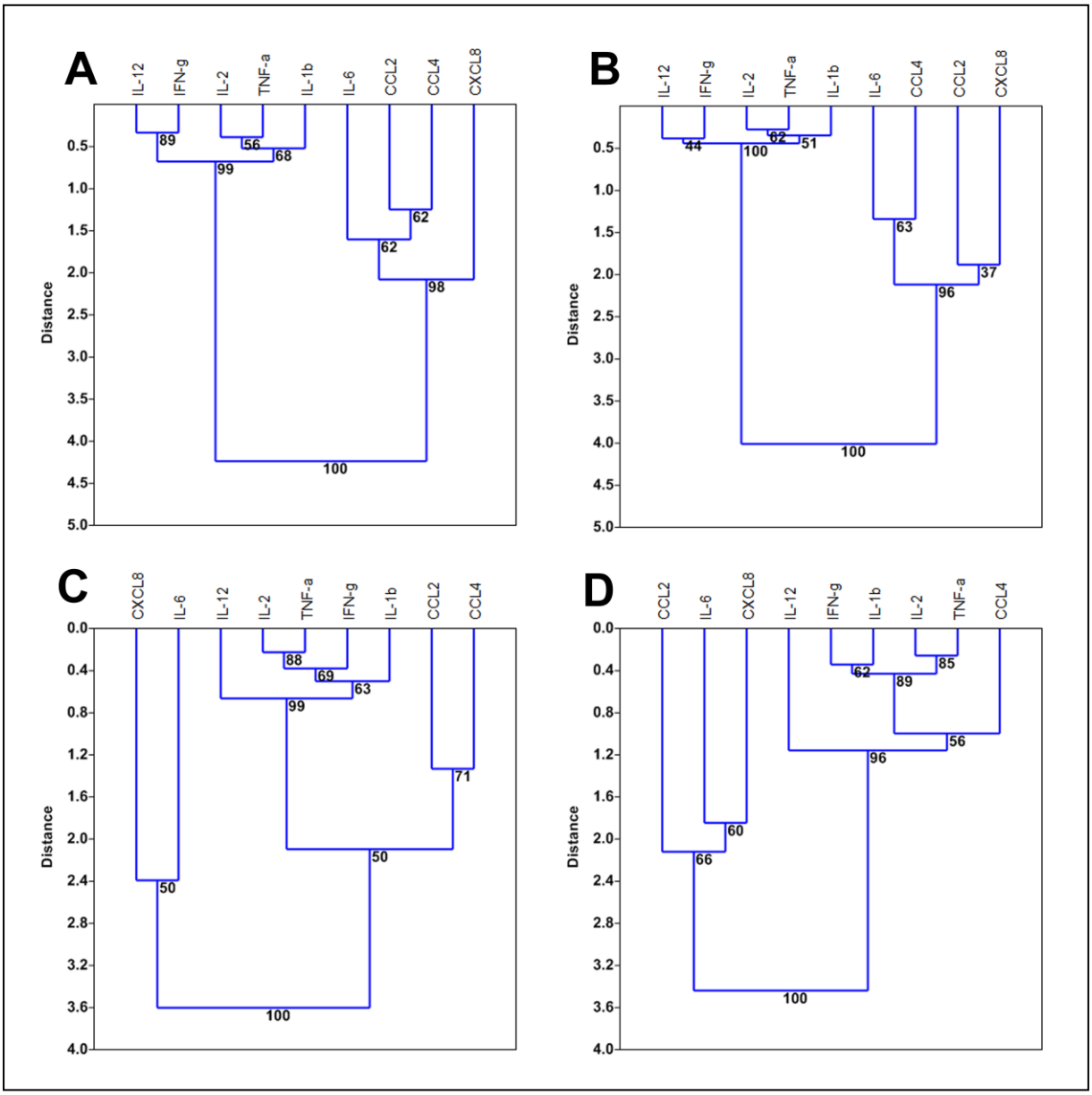

Figure 3.2 Dendrograms indicating cluster analysis of cytokines in each culture group in LPCM.

Culture groups are as follows: **A)** EXP; **B**) NK-BC control; **C)** T_{REG}-BC control; **D)** BC control. Branching points show robustness of bootstrapping in maintaining associations during iterations. The following cophenetic correlation coefficients indicate the high efficiency of the clustering method per culture group **A)** 0.9231, **B)** 0.8933, **C)** 0.8912, **D)** 0.8979.

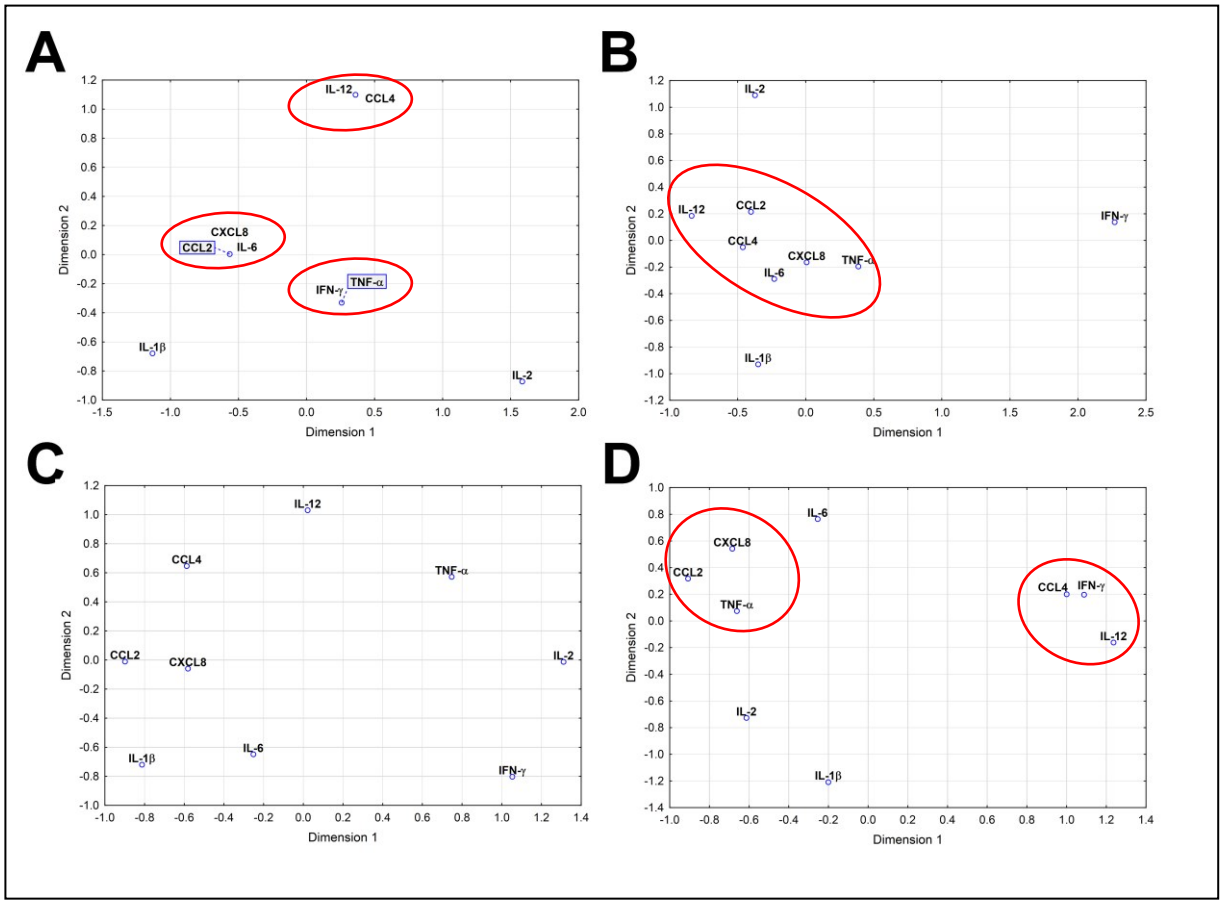

Figure 3.3 Scatterplots illustrating non-metric MDS of cytokines in each culture group in LPCM.

Culture groups are as follows: **A)** EXP; **B)** NK-BC control; **C)** T_{REG}-BC control; **D)** BC control. **A)** In the EXP culture group CCL2, CXCL8 and IL-6 cluster tightly across both dimensions. IL-12 and CCL4 group independently of IFN-γ and TNF-α in dimension 2, while exhibiting an association in dimension 1. **B)** In the NK-BC control culture group, the effects of NK cells alone elicit a distribution involving most of the panel of cytokines, with IFN-γ notably removed in dimension 1. **C**. The T_{REG}-BC control culture group exhibits a distinct lack of groupings in both dimensions, with cytokines rather sharing similarities in one dimension. **D)** In the BC control culture group without the mediation of immune cells, two groupings in both dimensions are noted, CCL2, CXCL8 and TNF-α; and CCL4, IL-12 and IFN-γ.

3.3.2 Effects of T_{REG} lymphocytes and NK cells on cytokine secretion in the BPCM

All cytokines, with the exception of IL-2, contributed significantly to the differences across culture groups. The distribution of cytokines in each culture group exhibited greater spread than that of the control groups, with a number of outliers noted. The dispersion of the data reflects probable biological variation within groups and the effects of NK cells and T_{REG} cells on cytokine release across groups. Subsequent multiple comparison tests (2-tailed) indicated that the combination of T_{REG} and NK cells in the EXP culture group resulted in significant differences in IL-1β, IL-6, TNF-α, CCL4 and CXCL8 abundance compared to MDA-MB-231 cells grown alone (Fig. 3.4.1 and Fig. 3.4.2). The impact of NK cells is noted in the EXP culture group and NK-BC control culture group, with a significant increase in the expression of IL-12 and CCL2.

Cluster analysis demonstrated that IL-6, CXCL8 and CCL2 cluster together in a well-differentiated manner compared to other cytokines in the EXP culture group, and NK-BC and BC control culture groups (Fig. 3.5). This cluster was not maintained in the T_{REG}-BC control culture group, inferring that the function of T_{REG} cells is influenced both by NK cells and by the cell line itself. In the EXP, NK-BC and T_{REG}-BC culture groups, IL-2 and TNF-α clustered closely. This cluster was not well separated from other cytokines with agglomerative clustering indicating the influences of IFN-γ, IL-1β, IL-12 and CCL4 at various branching points. The contribution of NK cells alone resulted in a further cluster with IL-1β, followed by IFN-γ, IL-12 and CCL4 (Fig. 3.5B). While the combined influence of NK cells and T_{REG} lymphocytes (Fig. 3.5A) resulted in the retention of the IL-2-TNF-α cluster, this was soon linked with IFN-γ. This agglomerative cluster associated with the IL-1β-CCL4 cluster, followed by the contribution of IL-12 at a greater distance. This could reflect a heightened T_{REG} lymphocyte influence as per the patterns noted in the T_{REG}-BC culture group (Fig. 3.5C). However, since the clusters were maintained in the BC control culture group (Fig. 3.5D), the cytokine profile of MDA-MB-231 cell line may not be as greatly influenced by immune mediation as the MCF-7 cell line.

Scatterplots illustrating non-metric MDS indicated that IL-1β, IL-2, CCL2 and CXCL8 formed a close association in the EXP culture group (Fig. 3.6A). The NK-BC and BC controls, with only NK cell influence and no immune influence respectively, did not elicit

distinct groupings (Fig. 3.6B and Fig. 3.6D). However, the T_{REG} culture group, with MDA-MB-231 cell cytokine secretion mediated by T_{REG} cells, showed a distinctive cluster of all cytokines with the exception of IL-6 and CCL4.

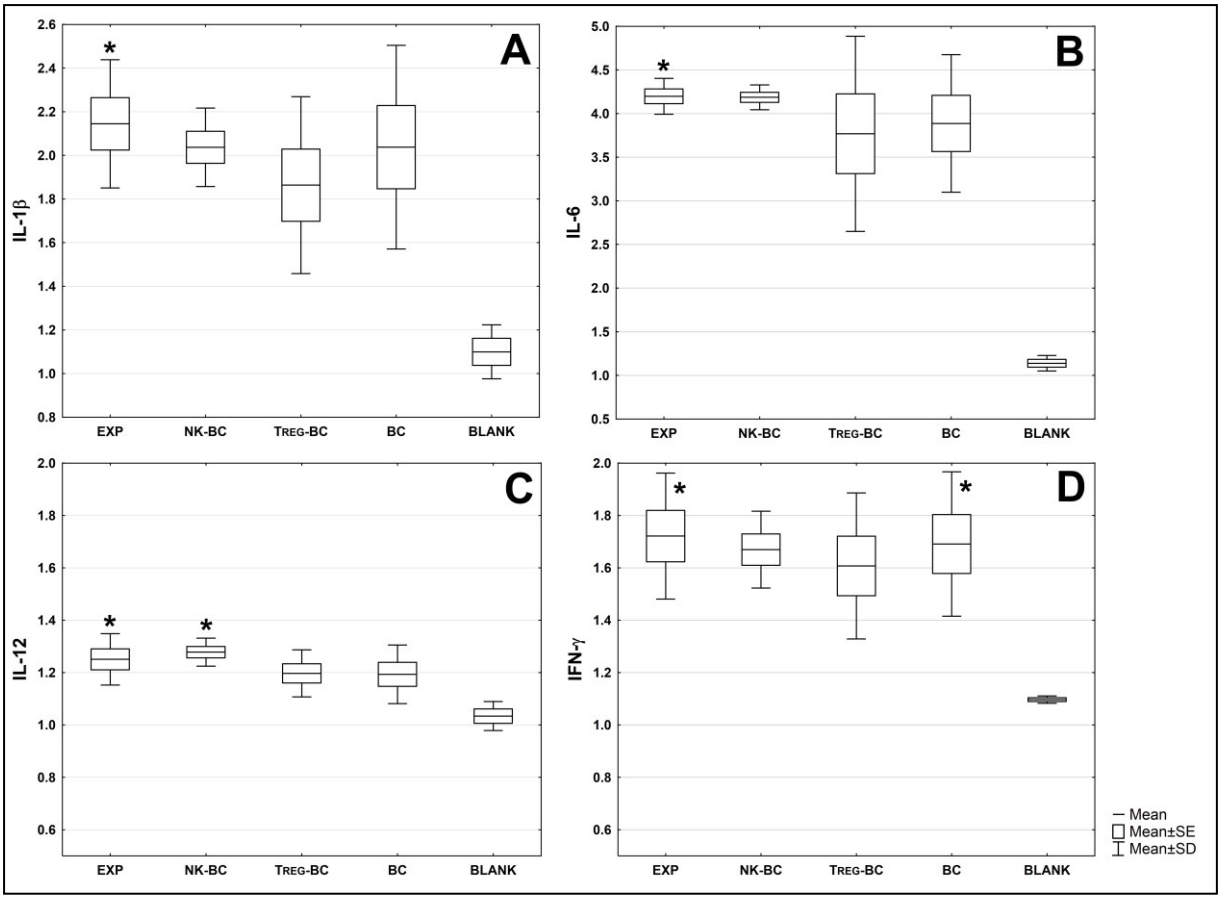

Figure 3.4.1 Box and whisker plots of cytokines determined to be significantly different (p<0.05) within and between multiple culture groups in BPCM.

KEY: X-axis – culture groups; **Y-axis –** log cytokine concentration. **A)** A significant difference in IL-1β expression was found between the EXP culture group and the blank control (*). **B)** The EXP culture group showed less dispersion of the data and differed significantly from the blank control (*) with regard to IL-6 expression. **C**) The EXP culture group and NK-BC control culture group showed a significant difference in the expression of IL-12 compared to the blank control (*). **D)** The EXP culture group and BC control culture group, both exhibiting large spreads of data, were significantly different to the blank control (*) with regard to IFN-γ expression.

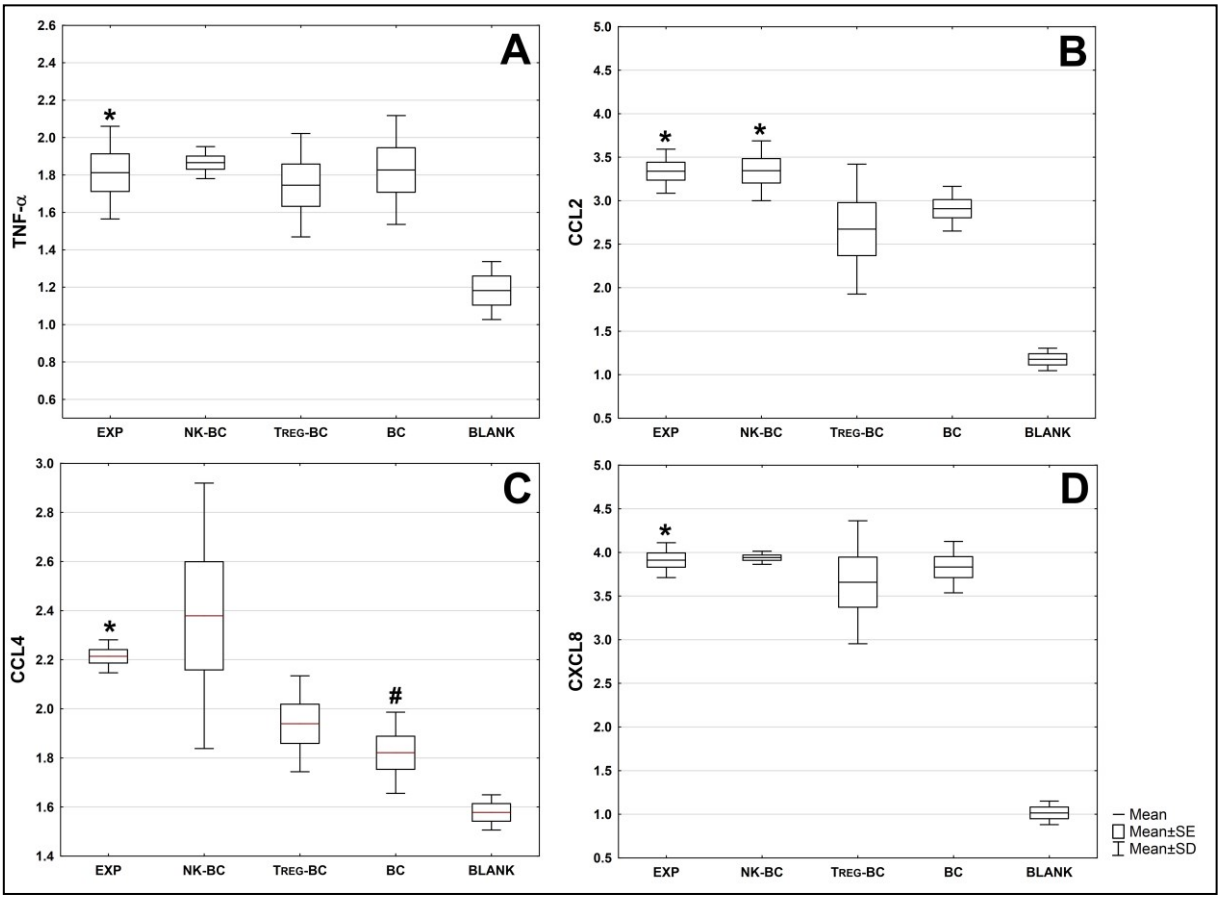

Figure 3.4.2 Box and whisker plots of cytokines determined to be significantly different (p<0.05) within and between multiple culture groups in BPCM.

KEY: X-axis – culture groups; **Y-axis –** log cytokine concentration. **A**) A significant difference in TNF-α expression was found between the EXP culture group and the blank control (*). **B**) The EXP culture group and NK-BC control culture group differed significantly from the blank control (*) with regard to CCL2 expression. **C)** CCL4 expression in the EXP culture group exhibited a tight cluster of data points and was significantly different to the blank control (*) and BC control culture group (#). **D)** The EXP culture group was significantly different to the blank control (*) with regard to CXCL8 expression.

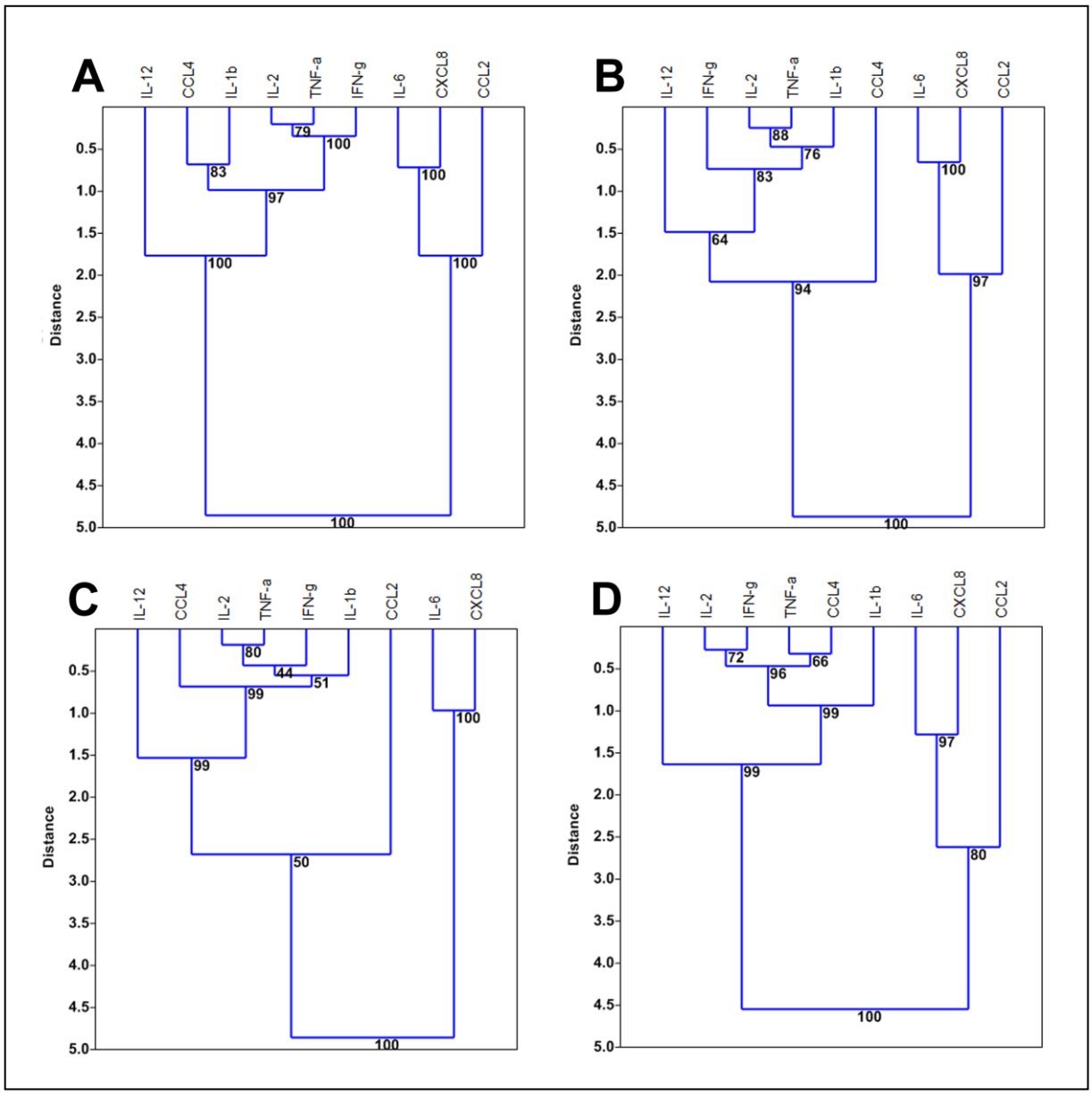

Figure 3.5 Dendrograms indicating cluster analysis of cytokines in each culture group in BPCM.

Culture groups are as follows: **A)** EXP; **B**) NK-BC control; **C)** T_{REG}-BC control; **D)** BC control. Branching points show robustness of bootstrapping in maintaining associations during iterations. The following cophenetic correlation coefficients indicate the high efficiency of the clustering method per culture group: **A)** 0.9129, **B)** 0.906, **C)** 0.8912, **D)** 0.8897

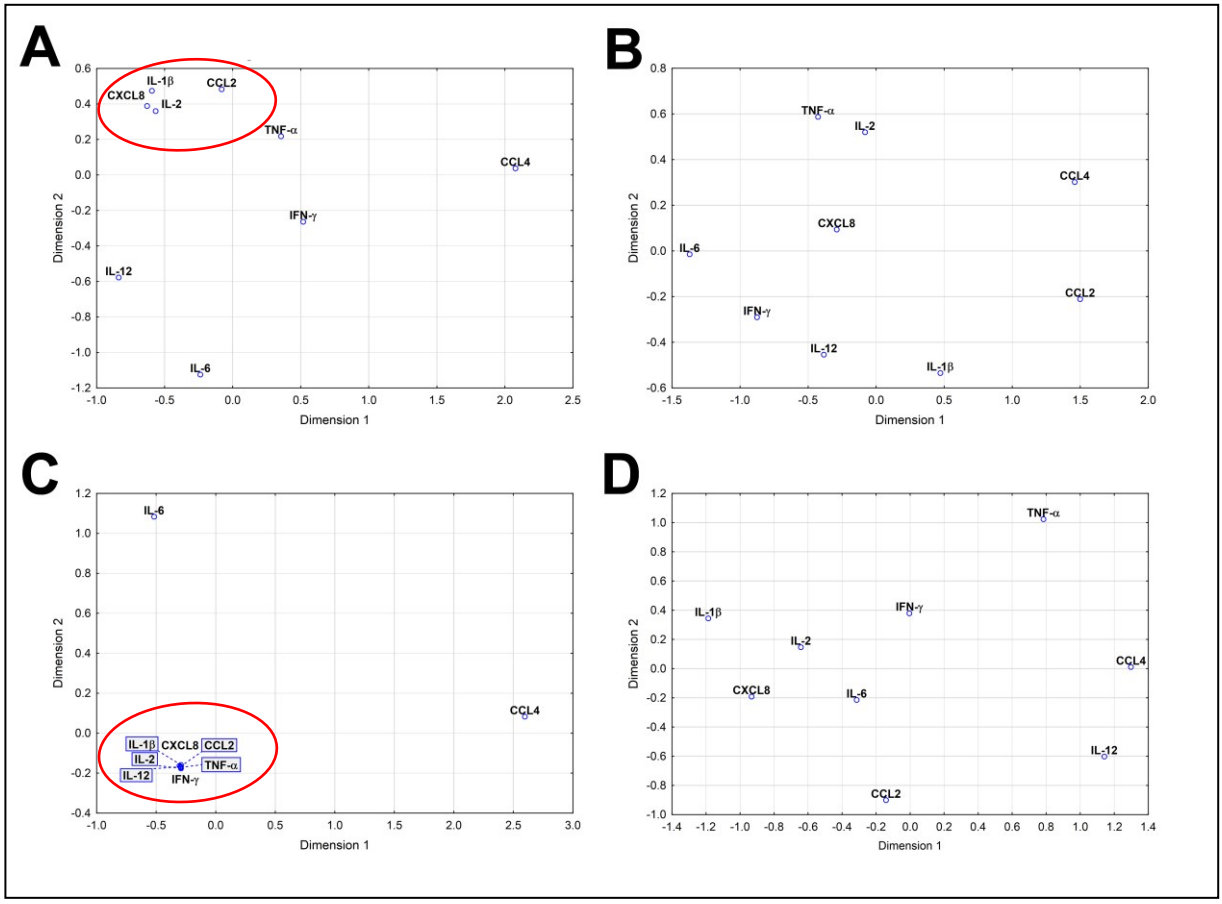

Figure 3.6 Scatterplots illustrating non-metric MDS of cytokines in each culture group in BPCM.

Culture groups are as follows: **A)** EXP; **B)** NK-BC control; **C)** T_{REG}-BC control; **D)** BC control. **A)** In the EXP culture group CCL2, CXCL, IL-1β and IL-2 cluster tightly across both dimensions. **B)** In the NK-BC control culture group, the effects of NK cells alone results in a spread of cytokines. **C**. In the T_{REG}-BC control culture group, under the influence of T_{REG} cells, a clear grouping of all cytokines bar IL-6 and CCL4 is present. **D)** In the BC control culture group *sans* the mediation of immune cells, no distinct groupings are noted.

3.3.3 The effects of T_{REG} and NK cells on cytokine secretion: eliminating the effects of hormone status

To further investigate the effects of T_{REG} and NK cells on cytokine secretion, clustering procedures as previously described were conducted on complete groupings of the EXP, NK-BC and T_{REG}-BC culture groups eliminating the influence of the cell lines themselves (Fig. 3.7, Row 1). The resulting clusters were thereafter supplemented with the clustering of cases based on their association with either the MCF-7 cell line or MDA-MB-231 cell line (Fig. 3.7, Row 2). In the EXP and NK-BC culture groups, notably those under NK cell influence, CCL2 and CXCL8 are closely associated forming an agglomerative cluster with IL-6 and CCL4 (Fig. 3.7, EXP and NK-BC, Row 1). This combination is not maintained in those cultures in which T_{REG} cells were cultured with breast cancer cell lines alone (T_{REG}-BC control culture group), with IL-6 clustering with CXCL8 followed by CCL2 (Fig. 3.7, T_{REG}-BC, Row 1). In the EXP and NK-BC cultures, IL-2 and TNF-α associate with contributions from IFN-γ and IL-1β and culminate in a cluster with IL-12. In the T_{REG}-BC culture, CCL4 joins the aforementioned cluster.

The maintenance of clusters indicates an inter-relatedness of cytokine secretion and points to associated function. The cytokine profile of culture groups further allowed for discrimination of hormone-dependency in each culture group (Fig. 3.7, Row 2). Immune mediation assisted in defining cases associated with either the MCF-7 hormone-dependent cell line or the MDA-MB231 hormone-independent cell line. Notably in the BC control culture group without the influence of NK and T_{REG} cells, clustering cases according to cell line status was inefficient with the cophenetic correlation coefficient indicating a poor fit (Fig 3.7, BC, Row 2).

Non-metric MDS was conducted on complete groupings of EXP, NK-BC and T_{REG}-BC cultures disregarding the influence of the cell lines themselves to determine associated cytokines (Fig.3.8.1). Thereafter, analysis of cases was conducted to allow discrimination based on associated cell lines (Fig. 3.8.2). It was noted that those culture groups under NK cell influence (EXP and NK-BC culture groups), exhibited grouping of cytokines distinct to those in the T_{REG} and BC culture groups (Fig. 3.8.1). In the EXP culture group, all cytokines with the exception of IL-12, CCL2 and CCL4, clustered together. In the NK-BC

culture group, IL-6 was found closely associated with TNF-α and CXCL8. The cytokine profiles in the EXP and NK-BC culture groups, both under NK cell-mediation, were excellent in discriminating between the MCF-7 cell line and the MDA-MB-231 cell line (Fig. 3.8.1A and Fig. 3.8.2B). Poor discrimination between cell lines in the T_{REG}-BC culture group was evident with considerable overlap present, reminiscent of the BC control culture group (Fig. 3.8.1C, D and Fig. 3.8.2C, D).

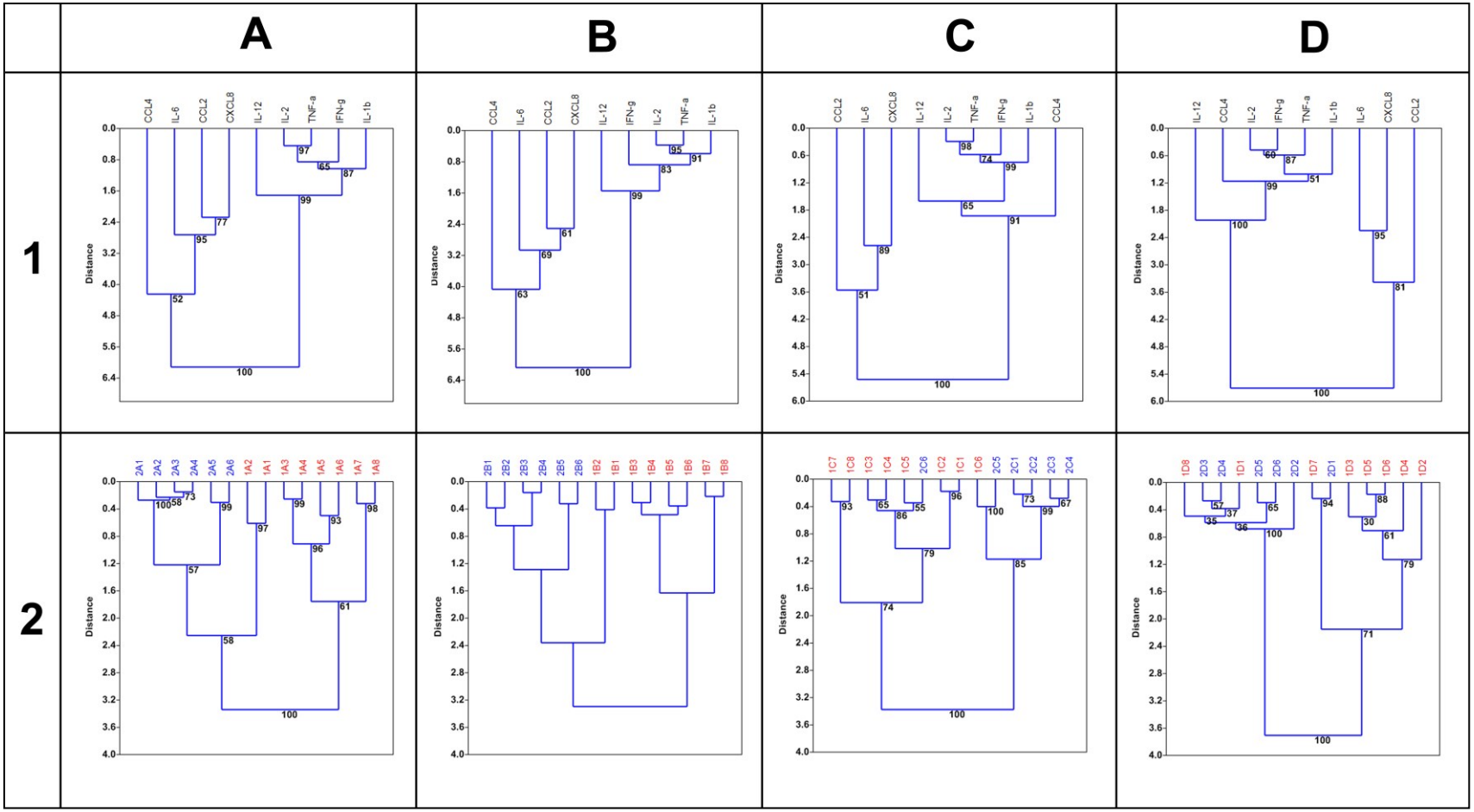

Figure 3.7 Cluster analysis showing the effects of T_{REG} lymphocytes and NK cells on cytokine secretion eliminating the effects of hormone status

Row1: Cytokine (x-axis) cluster analysis in each culture group (regardless of cell line). **Row 2:** Corresponding dendrograms illustrating the clustering of cases (x-axis) in each culture group (Red – MCF-7 cell line, Blue – MDA-MB-231 cell line). Branching points show robusticity of bootstrapping in maintaining associations during iterations. The following cophenetic correlation coefficients indicate efficiency of the clustering methods per aforementioned culture group: **Row 1**: EXP) 0.9047, NK-BC) 0.9096; T_{REG}-BC) 0.877 BC) 0.8934, **Row 2**: EXP) 0.8748, NK-BC) 0.8957, T_{REG}-BC) 0.9191, BC) 0.7226

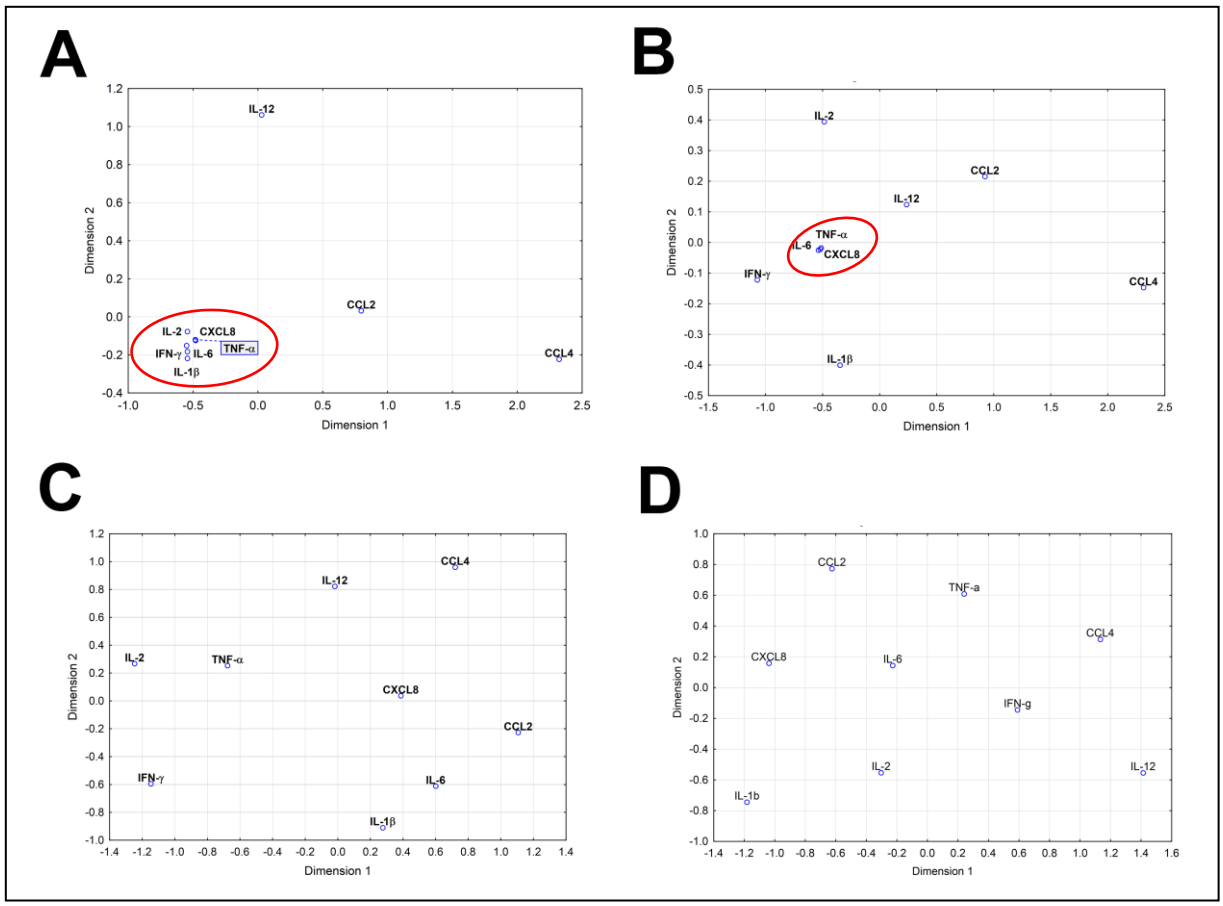

Figure 3.8.1 Scatterplots illustrating non-metric MDS of cytokine associations in each culture group (LPCM and BPCM)

Culture groups are as follows: **A)** EXP; **B)** NK-BC control; **C)** T_{REG}-BC control; **D)** BC control. **A**) EXP culture group A shows a distinct grouping of IL-1β, IL-2, IL-6, CXCL8, TNF-α and IFN-γ. **B)** In the NK-BC control culture, NK cell influence is noted in the tight clustering of IL-4, TNF-α and CXCL8. **C)** and **D)** exhibit no distinct clustering of cytokines.

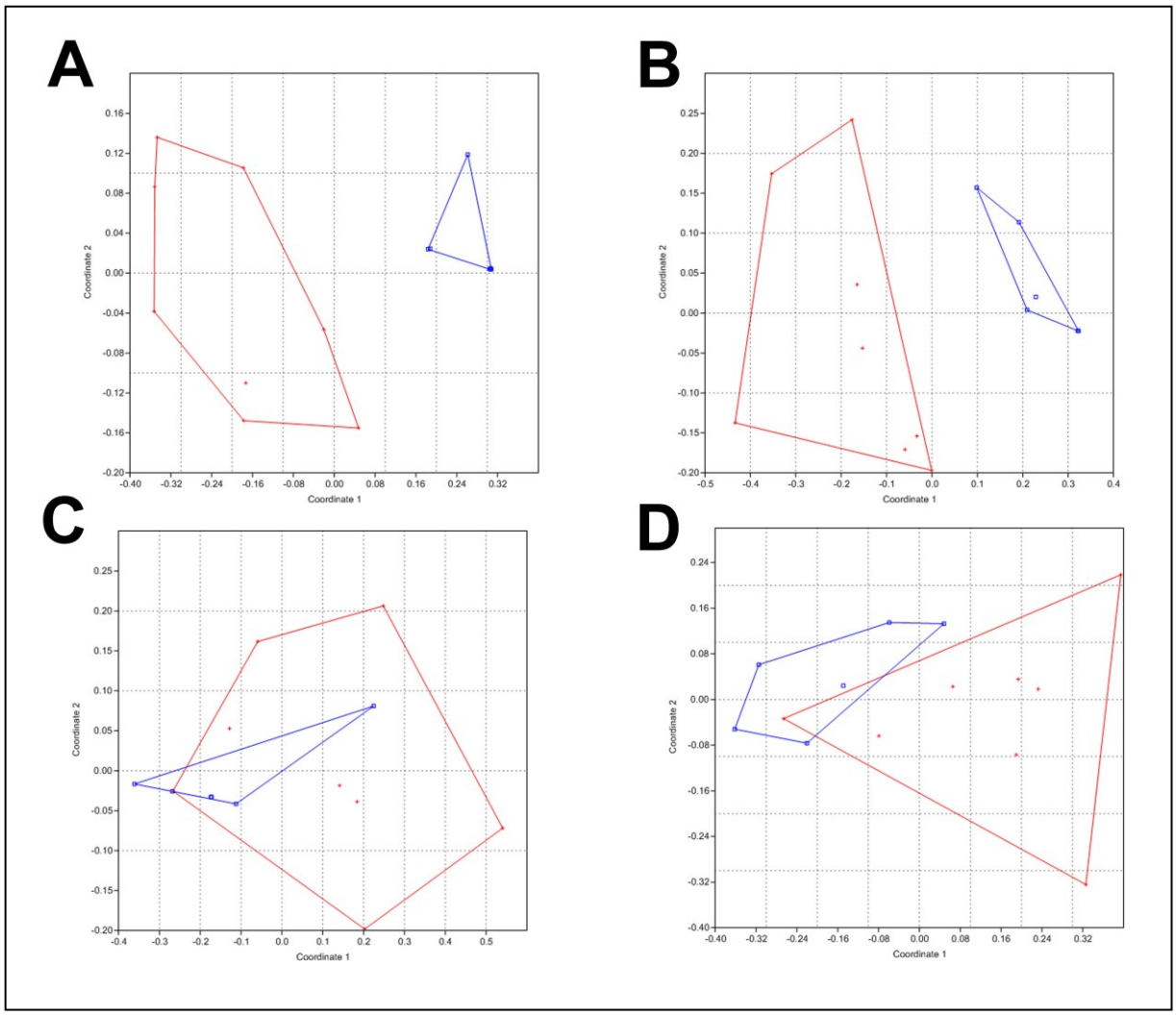

Figure 3.8.2 Corresponding scatterplots (Figure 3.8.1) illustrating differentiation of cases based on cell lines (Red: MCF-7, Blue: MDA-MB-231).

Culture groups are as follows: **A)** EXP; **B)** NK-BC control; **C)** T_{REG}-BC control; **D)** BC control. Cell lines could be clearly differentiated in **A)** EXP culture group and **B)** NK-BC control culture group. However, considerable overlap between cases indicates that cell lines in **C)** T_{REG} control culture group and **D)** BC control culture group were not as easily separated based on the cytokine profiles as seen in Fig. 3.8.1.

3.3.4 Principal components analysis: the effects of hormone-status on cell line discrimination

The first two principal components (PC) are discussed here as they cumulatively explain 97.7% of the observed variance (Fig. 3.9). PC1 positively loaded for all cytokines and presents with high loadings for IL-6, CXCL8 and CCL2 (Table 3.2). Notably PC2 is negatively loaded for CXCL8 and CCL2, and presents with positive and relatively high loadings of IL-1β, IL-6, IFN-γ and IL-2 (Table 3.2). While PC3 was not used in the plots (as it explained only 1.2% of observed variance), of particular interest was the very high value for CCL2 (Table 3.2). The MDA-MB-231 cell line, while falling within the bounds of the MCF-7 cell line appears largely dependent on PC1 (Fig. 3.9). Together however, the PCs obtained cannot differentiate adequately between the two cell lines, echoing the inefficiency of both the clustering procedures and non-metric MDS.

3.3.5 Principal components analysis: Differentiation of culture groups in LPCM and BPCM

The first three principal components from the PCA on culture groups in the LPCM and BPCM cumulatively explained 97.9% of the observed variance (Fig. 3.10.1 and Fig. 3.10.2). PC1 is positively loaded for all variables, with relatively high values of IL-6, CCL2 and CXCL8 (Table 3.3). IL-6, CCL4 and CCL2 contribute highly to PC2, with IL-6 negatively loaded. PC3 is positively loaded for all variables, with IL-2 and CCL4 presenting relatively high loadings. CXCL8 presents a notably high negative loading on PC3 (Table 3.3).

PC2 acts largely to differentiate the EXP and NK-BC culture groups in the LPCM from all other groups (Table 3.3, Fig. 3.10.1). PC1 appears responsible for differentiation between the EXP and NK-BC culture groups in the BPCM, and all other groups. The derived components are able to differentiate culture groups based on cytokine contributions related to tumour phenotype. Since the EXP and NK-BC culture groups in both the LPCM and BPCM overlap, this differentiation highlights the effects of NK mediation, complimenting the results obtained from cluster analysis and non-metric MDS. T_{REG} lymphocyte influence is seen in the overlap of the LPCM and BPCM T_{REG}-BC culture

groups, where PC1 and PC2 are noted to be inadequate in discriminating between tumour phenotype (Fig. 3.10.1); however the plot of PC2 and PC3 indicates that the latter component contributes to discriminating LPCM from BPCM in the T_{REG}-BC culture group (Fig. 3.10.2).

Table 3.2 Principal components loadings for the first three principal components derived for cytokines in BC control culture groups (LPCM and BPCM)

Variable loadings in bold are regarded as relatively high. PC1 is positively loaded for all cytokines with high loadings for IL-6, CXCL8 and CCL2. PC2 is negatively loaded for CXCL8 and CCL2, and presents with positive and relatively high loadings of IL-1β, IL-6, IFN-γ and IL-2. PC3 was not used in the plots (as it explained only 1.2% of observed variance), of particular interest was the very high value for CCL2. PC1 and PC2 cumulatively explained 97.7% of observed variance.

	PC 1	PC 2	PC 3
IL-1β	0.2363	**0.3568**	-0.07128
IL-2	0.156	**0.2506**	0.07558
IL-6	**0.6405**	**0.3667**	-0.1952
IL-12	0.04532	0.1558	-0.00422
IFN-γ	0.1595	**0.2921**	0.06903
TNF-α	0.1625	0.2006	0.1123
CCL2	**0.3918**	**-0.3037**	**0.8543**
CCL4	0.07628	0.2028	0.09131
CXCL8	**0.5444**	**-0.6263**	-0.4422

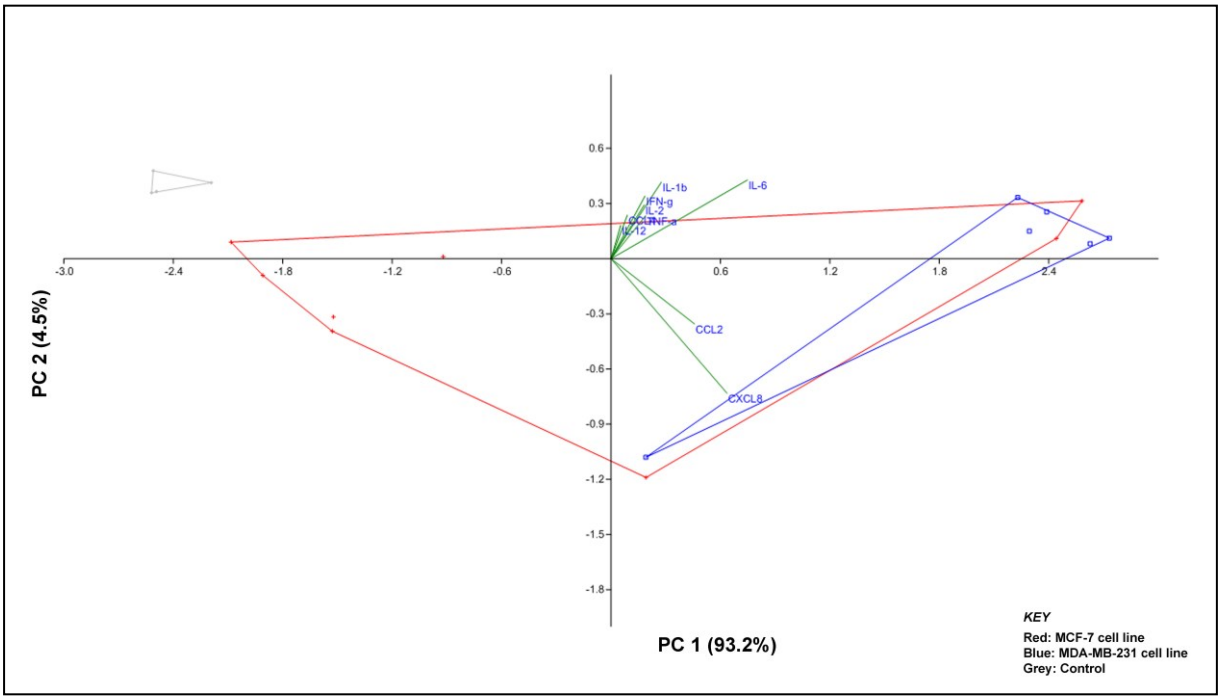

Figure 3.9 Scatterplots for the first two principal components scores derived for cytokines in BC control culture groups (LPCM and BPCM)

PC1 and PC2 cumulatively account for 97.7% of the observed variance. Considerable overlap between the groups was noted, indicating that the derived principal components cannot adequately differentiate between the MCF-7 cell line and MDA-MB-231 cell line.

Table 3.3 Principal components loadings for the first three principal components derived for cytokines in the EXP, NK-BC and T_{REG}-BC culture groups (LPCM and BPCM)

Variable loadings in bold are regarded as relatively high. PC1 is positively loaded for all cytokines with high loadings for IL-6, CXCL8 and CCL2. PC2 presents with positive and relatively high loadings of CCL2 and CCL4, with a negative loading noted for IL-6. PC3 is positively loaded for all cytokines, bar the high negative loading of CXCL8. IL-2 and CCL4 also have relatively high loadings on PC3.

	PC 1	PC 2	PC 3
IL-1β	0.2288	-0.223	0.2329
IL-2	0.1665	-0.156	**0.2837**
IL-6	**0.6385**	**-0.4543**	0.08184
IL-12	0.05633	0.02458	0.09583
IFN-γ	0.1424	-0.1922	0.1931
TNF-α	0.1591	-0.1106	0.227
CCL2	**0.459**	**0.5337**	0.2211
CCL4	0.1497	**0.5999**	**0.3301**
CXCL8	**0.48**	0.1581	**-0.7764**

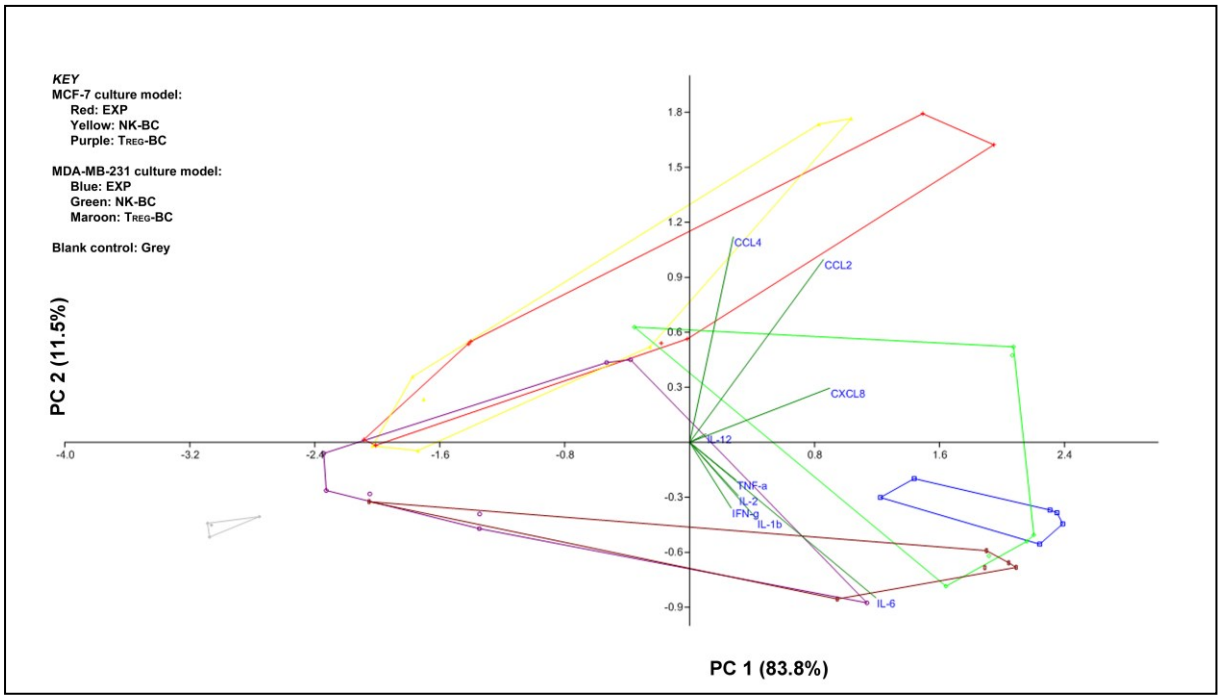

Figure 3.10.1 Scatterplots for principal component 1 and principal component 2 scores derived for cytokines in the EXP, NK-BC and T_{REG}-BC culture groups (LPCM and BPCM)

PC1 and PC2 are largely responsible for differentiation of the EXP and NK-BC culture group, based on the MDA-MB-231 and MCF-7 cell lines respectively. Overlap of the aforementioned culture groups in both culture models is noted reflecting NK cell mediation.

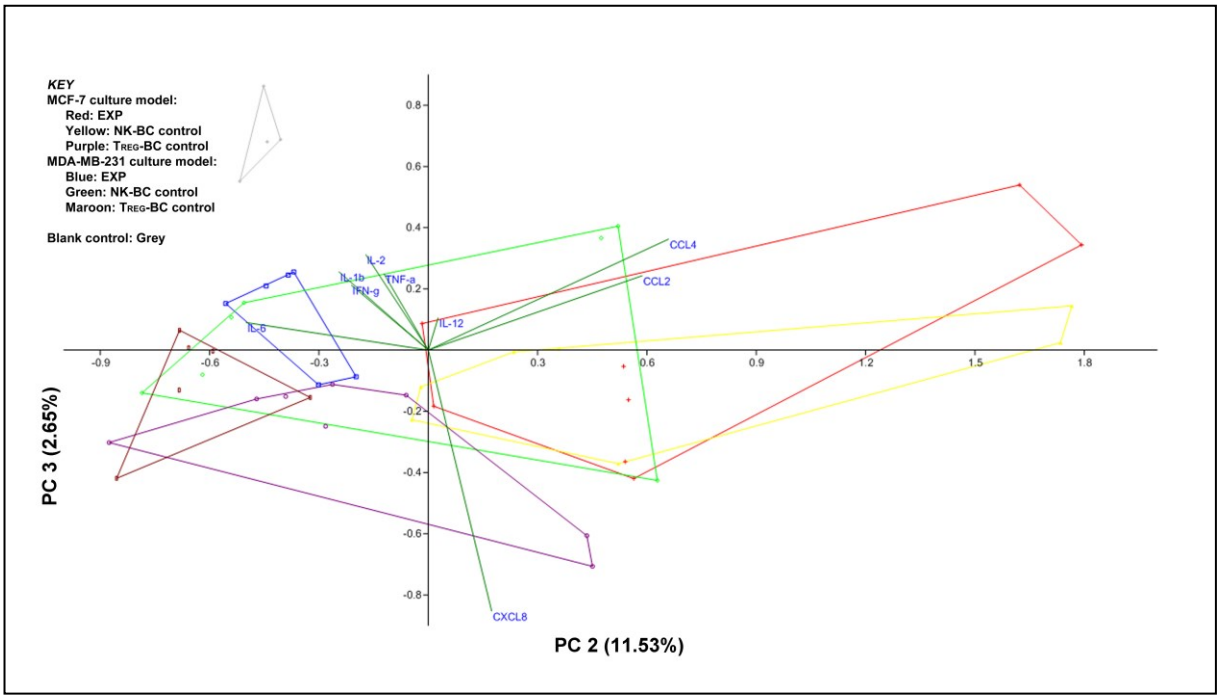

Figure 3.10.2 Scatterplots for principal component 2 and principal component 3 scores derived for cytokines in the EXP, NK-BC and T_{REG}-BC culture groups (LPCM and BPCM)

The overall plot indicates that PC2 versus PC3 presents with considerable overlap of most culture groups. However, PC3 contributes to the discrimination of control culture group T_{REG}-BC based on the MCF-7 and MDA-MB-231 cell lines.

3.4 Discussion

The role of cytokines in tumour progression is being given increasing attention in unravelling the interplay between inflammatory cells and tumour cells. Cytokines may elicit anti-tumourigenic or pro-tumourigenic functions (Balkwill and Mantovani, 2001; Nicolini *et al.,* 2006), with the downstream effects being dependent on a number of factors including concentration and co-stimuli. Three-dimensional culture systems are more effective in reproducing the tumour microenvironment than 2D systems (Baker and Chen, 2012), with distinct morphological alterations indicating crosstalk between mechanical forces within matrices and secreted factors. In 3D cultures, tumour cells have been noted to create necrotic areas, which *in vivo* are associated with hypoxia and noted for inducing the recruitment of leukocytes to tumour sites, initiating an inflammatory response that tumours then subvert to allow for progression. Under the influence of 3D circumstances, tumour cells have further been shown to suppress the functionality of leukocyte populations (Feder-Mengus *et al.,* 2008). It is thus proposed that the 3D model developed in this study is more reflective of the tumour environment, allowing more appropriate inferences regarding cytokine-cell interactions to be made (See summary Fig. 3.11).

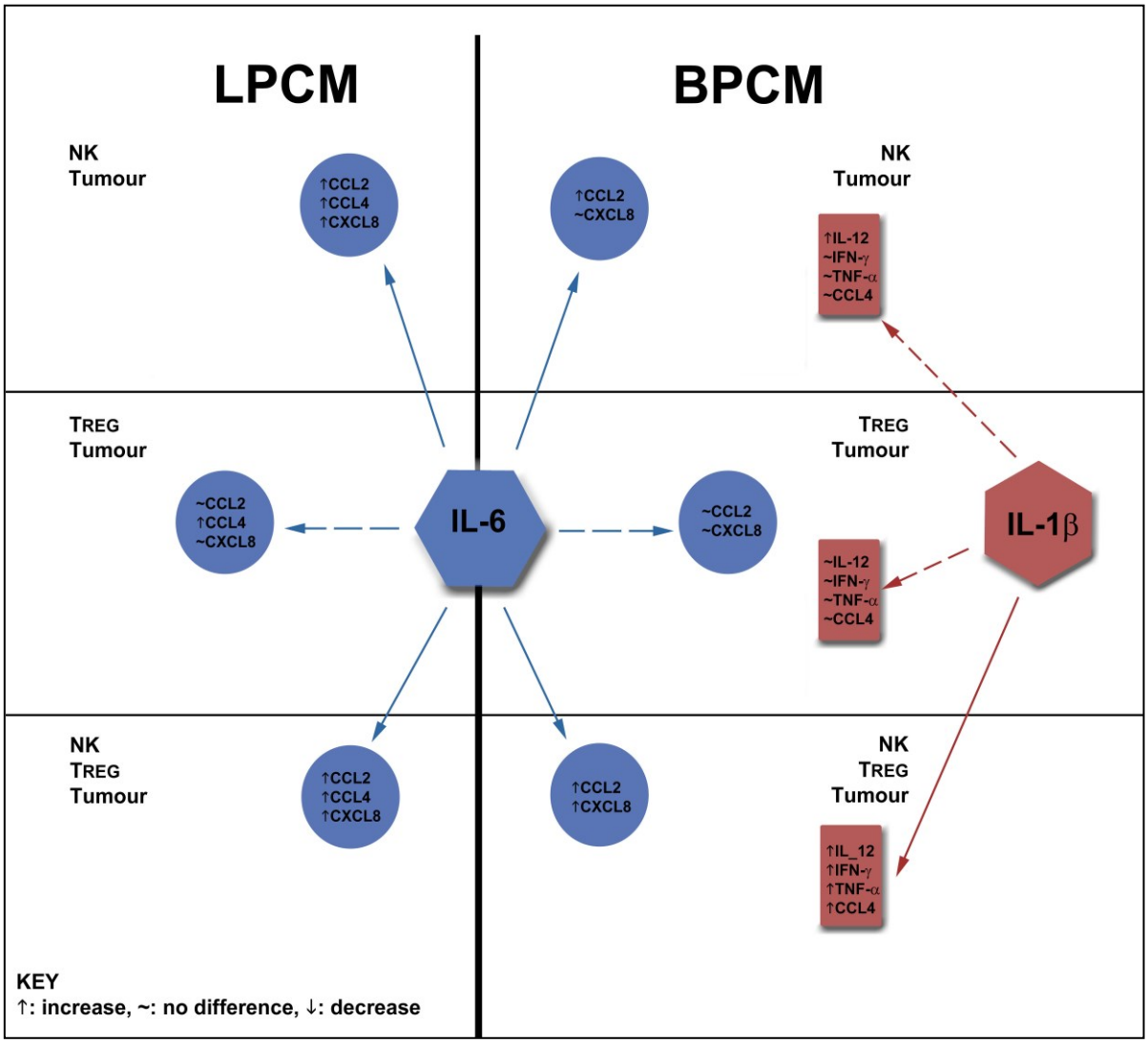

Figure 3.11 Summary of alterations in cytokine expression in culture groups in the LPCM and BPCM

Cytokine secretions in a 3D simulated breast tumour environment are associated with the hormone dependency of tumours. The effects of NK cell-mediation induced a significant increase in CCL2, CCL4 and CXCL8 secretion in the MCF-7 culture model. In the MDA-MB-231 culture model NK cells alone induced a significant increase in IL-12 and CCL2 inferring the dominance of T_{REG} cell-mediation of cytokine secretion. IL-6 plays a significant role in the induction of a chemokine cascade in both culture models, with IL-1β implicated in the induction of proinflammatory environment in the MDA-MB-231 culture model. The results indicate subversion of recruited leukocytes for the promotion of immune evasion and tissue invasion.

3.4.1 Cytokines in hormone-dependent and hormone-independent breast cancers

The hormone status of breast tumours has been shown, by a number of studies, to be linked to the cytokine profile presented (Nicolini *et al.,* 2006; Chavey *et al.,* 2007; Geng *et al.,* 2013). Triple-negative cancers are associated with a cytokine profile linked to metastatic potential (Levano *et al.,* 2011). Our results showed that the basal phenotype culture model is associated with increased expression of proinflammatory cytokines and chemokines, echoing clinical assessments in which IL-6, CCL2, CCL4, CXCL8, IFN-γ and TNF-α are significantly overexpressed in ER-negative tumours, with the addition of IL-1β and IL-12 in PR-negative tumours (Chavey *et al.,* 2007). While this study and others have shown that luminal and basal phenotypes of breast cancer differ considerably with regard to cytokine expression, cytokines do not function in isolation and thus analyses that involve clustering methodology infer linked function or feedback loops associated with tumourigenesis.

Both the MCF-7 and MDA-MB-231 cell lines present with clustering of IL-6 and the chemokines CCL2 and CXCL8. The rest of the pro-inflammatory cytokines cluster independently, with a contribution from CCL4. Furthermore, cluster analysis, non-metric MDS and PCA, had a high degree of efficiency in accurately separating the MCF-7 cell line from the MDA-MB-231 cell line when under the influence of immune mediation only. This indicates that both cell lines, while having a baseline cytokine profile that may allow for discrimination, alter their cytokine secretions in the presence of immune mediation. Furthermore, the influence of T_{REG} lymphocytes scarcely altered the cytokine profile of MCF-7 cells and MDA-MB-231 cells. This indicates that tumour cell-secreted factors influence T_{REG} cells to maintain their cytokine profile and may reflect the induction of tumour escape mechanisms in response to the insult of NK presence.

3.4.2 The effects of T_{REG} and NK cells on cytokine profiles in hormone-dependent and hormone-independent breast cancers

Various mechanisms in hypoxic environments induce the production of IL-1 and TNF-α, leading to a positive feedback loop in which proinflammatory cytokine expression is increased (Le Bitoux and Stamenkovic, 2008). In this study the combined interactions of T_{REG} and NK cells resulted in significant increases in IL-1β, TNF-α, IFN-γ, IL-6, CCL4 and CXCL8 in the basal phenotype culture model; and IL-6, CCL2, CCL4 and CXCL8 in the luminal phenotype model. A definitive association was noted between TNF-α, IFN-γ and IL-12 under the influence of NK cells in the luminal-phenotype culture model. IL-12 is a potent inducer of NK cell proliferation and cytotoxicity, and in a positive feedback loop induces IFN-γ and TNF-α production, cytokines associated with the inhibition of angiogenesis and apoptosis (Nicolini *et al.,* 2006). However, in the luminal phenotype model significant levels of chemokines CCL2 and CXCL8, regarded as pro-angiogenic factors (Ben-Baruch, 2003; Rollins, 2006), infer a struggle for dominance between pro-tumourigenic and anti-tumourigenic processes. Moreover, sustained IFN-γ expression has also been linked with tumour cell resistance to NK cell cytotoxic function (Wang *et al.,* 2012), and by upregulating MHC I presentation on tumour cells (Saha *et al.,* 2010), may reflect tumour cell-induced evasion of NK-mediated cytoxicity. The clustering of IL-6 with these chemokines highlights the role of the proinflammatory cytokine in initiating leukocyte infiltration (Chavey *et al.,* 2007). Results from both non-metric MDA and PCA indicate that this recruitment is based on the phenotype of the tumour cells. Tumour cells are thus proposed to define the immune infiltrate, consequently subverting immune function and thus allowing for tumour progression.

3.4.3 Implications for tumour progression

Interleukin-6, IL-1 and TNF may act together amplifying proinflammatory processes (Ben-Baruch, 2003). Breast cancer cell lines and lymphocytes are sources of IL-6. Notably the pro-tumourigenic function of IL-6, mediated by (gp)-130 activation of signalling pathways, results

not only in the induction of survival mechanisms but also in the increase of oestradiol-17β hydroxysteroid dehydrogenase type I, necessary for the conversion of oestrone to oestradiol (Purohit *et al.,* 2002). While elevated levels of IL-6 have progressive implications for hormone-dependent cancers, in association with TNF-α, IL-6 is implicated in facilitating adhesion of hormone-independent MDA-MB-231 cells during extravasation into the vascular supply (Geng *et al.,* 2013).

Metastatic processes are associated with immune mediation, and with remodelling of tumour microenvironment necessary for proliferation and invasion (DeNardo *et al.,* 2008). Members of the IL-1 family induce MMP function as well as the secretion of chemokines to recruit other leukocytes that would assist in tissue remodelling (Le Bitoux and Stamenkovic, 2008). Our data suggests that the interaction of MCF-7 cells with immune cells elicits a cytokine profile that may enhance the invasive potential of this weakly metastatic cell line. Moreover, IL-6 and CCL2 have been linked to cancer stem cell-driven tumour progression (Chin and Wang, 2013; Jiang and Shapiro, 2013). Cancer stem cell populations have been identified in both the MCF-7 and the MDA-MB-231 cell lines (Engelmann *et al.,* 2008; Hiraga *et al.,* 2011) and thus the secretion of IL-6 and its associated chemokine cluster may indeed not only infer attainment of increased metastatic potential but clonal evolution of stem cell populations.

3.4.4 Implications for cancer immunotherapy

Cancer immunotherapy of solid tumours includes non-specific immunomodulation using the administration of high-dose IL-2, mAb treatment, cancer vaccines, and ACT (Rosenberg *et al.,* 2008). ACT involves the re-establishment of tumour-directed immunity by the transfusion of autologous or allogeneic cytotoxic $CD8^+$ T lymphocytes, lymphokine activated PBMC cells or NK cells (June, 2007; Rosenberg *et al.,* 2008). Since T_{REG} lymphocytes are linked to the induction of tolerance mechanisms in the tumour microenvironment (DeNardo *et al.,* 2008), the removal of this subset is purported essential to the efficacy of ACT. Our results indicate that T_{REG} lymphocytes may not influence the cytokine profile of MCF-7 and MDA-MB-231

cells. However, while this may be indicative of the induction of tumour tolerance, other studies have found conflicting reports regarding their suppressive capacity (Chikileva *et al.,* 2010). Together with the low efficacy of ACT, coupled with non-specific immunomodulation mechanisms (Riker *et al.,* 2005; Rosenberg *et al.,* 2008), T_{REG} lymphocyte elimination may not be sufficient or necessary for the induction of anti-tumour responses. Furthermore, targeted depletion of T_{REG} lymphocytes remains problematic given the lack of defined T_{REG} lymphocyte-specific markers (see Chapter II). Monoclonal antibody therapies that target the IL-2 receptor, upregulated on T_{REG} cells, have produced conflicting results, possibly due to the collateral damage on effector T lymphocytes and NK cells (Chikileva *et al.,* 2010; Lesterhuis *et al.,* 2011).

The cell surface marker CD16 mediates NK cell cytotoxicity toward antibody-coated tumour targets (Sanchez *et al.,* 2010). This ADCC mechanism of function has been linked with the efficacy of Trastuzumab, a mAb treatment for HER2/neu^{+} breast tumours that restricts the HER2/neu oncogenic signalling pathway (Slamon *et al.,* 2001; Beano *et al.,* 2008; Roberti *et al.,* 2012). *In vitro* studies have indicated that ADCC mediated by peripheral blood NK cells from breast cancer patients are effective against Trastuzumab-treated SK-BR-3 breast cancer cells. However, functional response is dependent on CD16 expression, which was notably downregulated in peripheral blood NK cells of patients presenting with invasive metastatic breast cancer (Mamessier *et al.,* 2011). It was further noted that tumour-infiltrating NK cells presented with decreased ADCC potential (Mamessier *et al.,* 2011).

The aforementioned thus have implications for the isolation of NK cells for subsequent ACT, with a proposed derivation from peripheral blood, autologous or allogeneic, not only capable of yielding higher numbers for initial propagation but further as being more amenable to manipulation without the direct influence of the tumour environment. Other studies which propose the use of allogeneic NK cells have had limited success in ACT for breast cancer. The use of irradiation and IL-2 therapy followed by NK cell transfer has proved ineffective, with a failure of lymphopaenia-induced homeostatic expansion of the transfused cells and the reconstitution of the T_{REG} lymphocyte compartment attributed to IL-2 itself

(Geller *et al.,* 2011). Our results further indicate that while NK cell-mediation induces cytokines that may be associated with an anti-tumour response, this may well be subverted by downstream events to encourage invasive behaviour.

Our results indicate that the cytokine profile induced in a 3D culture replica of the tumour microenvironment is primarily directed by the tumour cells themselves in responding to an immune infiltrate. The cytokine profile of hormone-dependent and hormone-independent breast tumours differ considerably despite similarities in the IL-6-chemokine feedback loop. This suggests that non-specific immunomodulation using infused cytokines to enhance the immune response may also concurrently be subverted by tumour cells or tumour stem cells for tumour progression. Such therapies have primarily been conducted in patients presenting with advanced stage cancers. It is thus proposed that tumours at this stage have acquired considerable immunogenicity and increased their capacity to evade immune mechanisms. Ablative adjuvants to ACT, by causing diffuse tissue damage, also notably induce an inflammatory response. This inflammatory response, involving leukocyte recruitment and thus cytokine/chemokine release can then further be manipulated by existing tumour cells. The results presented reflect this concept, with induced tumour cell cytokine secretion in response to NK cell insult, both under the influence of T_{REG} lymphocytes or not, eliciting a chemokine cascade. These factors may contribute to the intransigence of tumours in responding favourably to aspects of immunotherapy.

3.5 Conclusion

The results of this study indicate that both the type and amount of tumour-secreted cytokines are associated with hormone dependency and may be modified by immune mediation. However, their pro-tumourigenic or anti-tumourigenic function remains to be verified without exception. The cytokine network is intricate and these results suggest that while one aspect of cytokine production may promote an anti-tumour response, downstream events may show otherwise. The question thus remains, where in fact is this signalling network modified to allow for tumour tolerance? Our results indicate that tumour cells themselves are the primary forces behind the induction of cytokine profiles, and thus that the roles of T_{REG} lymphocytes and NK cells should not be assessed independently of the tumour phenotype.

CHAPTER IV: Analysis of Biomarkers Associated with Immune Evasion and Tumour Progression

4.1 Introduction

Neoadjuvant or adjuvant targeted therapy has become an integral part of treatment strategies for hormone-dependent tumours. However, despite their increasing use, the median overall survival rate of patients presenting with such tumours remains low (Nicolini and Carpi, 2008). Hormone-independent or triple negative breast cancers are more difficult to treat, with molecular and proteomic sequencing underway to discover targets that have yet to be defined. Breast tumours are heterogeneous, and while subgroups have been identified, tumour cells alter their phenotype dependent on the microenvironmental milieu, be this acquired resistance to therapeutic drugs, or for immune evasion (Renoir *et al.,* 2013).

Cognisance must be taken that therapeutic intervention induces not a singular event, but rather a complex interaction of signalling events that may be sublimated by tumour cells to allow for immune evasion, the induction of immune tolerance and thus tumour progression. T_{REG} lymphocytes, implicated in the induction of tumour tolerance and the suppression of cytotoxic lymphocyte function, are found in elevated numbers in the TIL population and peripheral blood of breast cancer patients (Bates *et al.,* 2006; Pooi *et al.,* 2006; Bohling and Allison, 2008; Decker *et al.,* 2012). Furthermore, NK cells are considerably reduced in such populations (Georgiannos *et al*., 2003; Macchetti *et al*., 2006). This may reflect tumour evasion strategies or the dominance of adaptive immune mechanisms in advanced breast cancer. Investigating whether biomarkers associated with hormone-dependent and hormone-independent breast tumours alter under immune cell-mediation is thus essential in establishing why targeted therapies do not prove as efficacious as hoped. This chapter thus presents a qualitative immunocytochemical analysis of biomarker expression associated with luminal phenotype MCF-7 cells (ER-α and MUC-1) and MDA-MDA-231 cells (EGFR) as well as TGF-β; under immune mediation.

4.1.1 Tumour biomarkers in luminal phenotype breast cancer – ER-α and MUC-1

The oestrogen receptor is a nuclear receptor that mediates the effects of steroid hormones. Two different isoforms of the ER are noted, ER-α and ER-β which share similar structure. The N-terminal domain of the ER is involved in the activation of gene transcription while the DNA binding domain allows ER to associate with specific oestrogen response elements. The hinge domain binds to heat shock chaperone proteins (Hsp) that modulate translocation of the receptor, while the C terminal domain and F domain modulate gene transcription and transcription of ER itself (Acconcia *et al.,* 2006).

Of particular interest to this study is ER-α, which is overexpressed in ER^+ luminal phenotype breast tumours and modulates their response as hormone-dependent tumours, to oestradiol thereby inducing cell proliferation and pro-survival processes (Renoir *et al.,* 2013). ER-α is maintained in its inactive state in the cytoplasm where it remains bound to Hsp's. Functioning via the traditional genomic or classical method, following ligand-binding ER dissociates from its chaperone proteins and translocates to the nucleus where it acts as a transcription factor for a host of genes (Acconcia *et al.,* 2006). However, extranuclear actions of ER have also been documented. ER accumulation in the cytoplasm or plasma membrane, a common trend in tumour cells, functions in a non-genomic or non-classical manner where, upon activation, they may induce a number of signalling events considerably different to that of nuclear ER (Acconcia *et al.,* 2006; Kampa *et al.,* 2013).

A number of targeted therapies exist for ER^+ luminal phenotype breast tumours. These include the SERM and SERD treatment, which function as receptor antagonists or agonists; and AI therapy, which reduce the pool of available oestradiol for tumour progression (Gil *et al.,* 2013; Renoir *et al.,* 2013). Despite such targeted therapy, it remains that these treatments are not successful in all cases with some tumours developing resistance (Renoir *et al.,* 2013). Moreover, circulating tumour cells derived from ER^+ metastatic cancers have been shown to downregulate their ER profile (Aktas *et al.,* 2011), possible as a selective advantage in the face of oestrogen targeted therapies. Furthermore, ER-α expression has

been correlated with MUC-1 expression in the luminal phenotype MCF-7 cell line, with said correlation diverging following treatment with an aromatase inhibitor (Gil *et al.,* 2013).

MUC-1, a transmembrane glycoprotein, is normally expressed on the apical membrane surface of secretory epithelial cells where it plays a protective role as part of the glycocalyx (Gil *et al.,* 2013). Composed of two subunits, the MUC-1 N terminal subunit is large, extending beyond the glycocalyx, with the MUC-1 C terminal subunit tethering the MUC-1 N subunit to the cytoskeleton (Wei *et al.,* 2006). MUC-1 is considered an oncoprotein, presenting aberrant glycosylation and overexpression in luminal phenotype breast cancers as well as other epithelial tumours, localizing to the cell membrane, nucleus and cytoplasm (Lacunza *et al.,* 2010; Nath and Mukherjee, 2014).

In tumour progression, MUC-1 mediates the secretion of a number of growth factors inducing pro-survival and proliferation mechanisms. Moreover, MUC-1 is implicated in the induction and maintenance of epithelial-mesenchymal transitions, via nuclear translocation of the cytoplasmic domain of MUC-1C where its action results in the upregulation of transcription factors *Snail*, *Slug*, *Vimentin* and *Twist*, known inducers of invasive phenotypes (Nath and Mukherjee, 2014). MUC-1 functions in the inhibition of apoptotic mechanisms via the downregulation of pro-apoptotic and upregulation of anti-apoptotic members of the Bcl-2 family (Nath and Mukherjee, 2014). Furthermore, MUC-1 activates both ER-α function and transcription (Wei *et al.,* 2006). This laboratory had previously showed that MUC-1 expression correlates with ER-α expression in MCF-7 cells cultured in monolayer (Gil *et al.,* 2013). However, this correlation was not maintained following short-term treatment with the third generation aromatase inhibitor, Anastrozole (Gil *et al.,* 2013).

In metastasis, MUC-1 is proposed to prevent cell-cell adhesion via the extension of its MUC-1 N terminal subunit, while simultaneously acting as a ligand via the presentation of sialyl Lewis carbohydrates to ICAMs on endothelial cells (Gendler, 2001). The shedding of tumour associated MUC-1 by gamma-secretase into the extracellular milieu, has been associated with immune evasion processes including the active inhibition of lymphocyte migration to the tumour site, inhibition of cytotoxic T lymphocyte and NK cell function (Gendler, 2001;

Suzuki *et al.,* 2012; Villalba *et al.,* 2013). Notably, MUC-1 is also expressed on Foxp3$^+$ T_{REG} lymphocytes, where the glycoprotein is capable of either co-inhibition or co-stimulation of T_{REG} lymphocyte function and proliferation dependent on accessory cell cues (Konowalchuk and Agrawal, 2012). Thus, MUC-1 may facilitate T_{REG} lymphocyte suppression of NK cell function in breast tumours.

Given the heightened expression of MUC-1 in a multitude of tumour types, a number of targeted therapies, including vaccination and immunotherapy strategies are currently being investigated; however their efficacy has yet to be determined (Mukhopadhyay *et al.,* 2011; Nath and Mukherjee, 2014). Of particular interest regarding mAb therapy is the proposed concomitant use of NK cell activating cytokines that may facilitate NK cell homing mechanisms and ADCC (Moreno *et al.,* 2007). Low NK cell numbers in breast tumours may not only be linked to active evasive mechanisms, but also to inadequate homing function as a result of tumour-induced systemic mechanisms (Albertsson *et al.,* 2003).

4.1.2 Tumour biomarker EGFR in basal phenotype breast cancer

EGFR is a transmembrane glycoprotein also known as ErbB1/Her1 belonging to the ErbB family of receptor tyrosine kinases, playing a fundamental role in regulation of cell proliferation, survival and differentiation processes (Lin *et al.,* 2001; Bazley *et al.,* 2005; Foley *et al.,* 2010). EGFR consists of an extracellular binding domain, a single-pass transmembrane domain, and a cytoplasmic domain containing the tyrosine kinase function (Bazley *et al.,* 2005). EGFR ligands include epidermal growth factor and transforming growth factor alpha, among others (Foley *et al.,* 2010; Yewale *et al.,* 2013). The binding of these ligands to the EGFR is dependent on their cleavage by MMPs (Foley *et al.,* 2010).

In tumour progression, EGFR is not only aberrantly expressed, but may also be activated by ligand-independent mechanisms, with its activation allowing for paracrine and autocrine mechanisms of interaction, necessarily important for tumour progression (Yewale *et al.,* 2013). Most basal phenotype breast tumours, of which the MDA-MB-231 cell line is

representative, do not express ER, HER2/neu or PR and are thus known as triple-negative cancers. However, these tumours commonly overexpress EGFR, which is linked with increased invasiveness and overall poor prognosis. EGFR signalling is also associated with the development of breast cancer stem-like cell pools that contribute to the maintenance and progression of tumours (Foley *et al.,* 2010).

Given that basal phenotype tumours are negative for the common treatment targets (ER, PR, Her2/neu), the overexpressed EGFR has become the focus of targeted therapy. These include primarily, the use of mAb therapy, tyrosine kinase inhibitors and antisense oligodeoxynucleotides. However, tumours have exhibited an acquired resistance to EGFR targeted therapy, reducing its efficacy (Yewale *et al.,* 2013).

4.1.3 Transforming Growth Factor-β in cancer

TGF-β is the prototypic member of the TGF-β superfamily with three identified human isoforms (TGF-β1, TGF-β2 and TGF-β3) sharing between 60% and 80% amino acid homology in their mature states (Naber *et al.,* 2008). TGF-β is synthesized as a latent complex, dependent on activation in the extracellular matrix by proteolytic cleavage, integrin interaction or microenvironmental pH changes (Buck and Knabbe 2006; Kubiczkova *et al.,* 2012). Following activation, ligand binding is facilitated by three receptor types, TβRI, TβRII and TβRIII (Elliot and Blobe, 2005; Kubiczkova *et al.,* 2012). TGF-β signalling is mediated primarily by the Smad-dependent pathway. However, signalling may also be mediated by extracellular regulated kinase, Jun kinase, p38 and Rho GTPase mechanisms, which in turn may converge on the Smad pathway (Naber *et al.,* 2008; Korpal and Kang, 2010). As a pleiotrophic growth factor, TGF-β plays a fundamental role in developmental processes, including growth, cellular motility, differentiation and immune system regulation (Gomis and Massague 2006; Naber *et al.,* 2008).

In early epithelial cell neoplasia TGF-β functions as a tumour suppressor, controlling proliferation and differentiation processes via cyclin-dependent kinase inhibition, the

induction of cytostatic gene expression and the inhibition of cytokine and chemokine production (Gomis and Massague 2006; Barcellos-Hoff and Akhurst, 2009; Yang et al., 2010). Conversely, in advanced stage tumours, TGF-β is associated with tumour progression and invasion processes by inducing dysregulation of the cell cycle, angiogenesis and immune escape (Yang et al., 2010). In breast tumours increased TGF-β expression is associated with epithelial-mesenchymal transitions, essentially conversion to a more malignant phenotype with heightened migration and invasive capacity (Barcellos-Hoff and Akhurst, 2009; Korpal and Kang, 2010).

Tumour cells and surrounding stromal components secrete large amounts of TGF-β, implicated in directly suppressing the function of cytotoxic T lymphocytes and NK cells, as well as in recruiting and subverting T_{REG} lymphocytes (Park et al., 2009). Moreover, the inhibition of NK cell function by T_{REG} lymphocytes is proposed to be conducted in a TGF-β-mediated manner (Ghiringhelli et al., 2005; Chikileva et al., 2010). Investigations into therapeutic mechanisms to abrogate TGF-β signalling include the use of TGF-β neutralising mAbs and small molecule TGF-β receptor kinases inhibitors, whose efficacy is associated with their immunostimulatory side effects that include NK cell-ADCC dependent mechanisms and $CD8^+$ T cell cytotoxic mechanisms (Korpal and Kang, 2010).

This chapter thus determined the immune cell-mediated expression of the tumour biomarkers ER-α, MUC-1 and TGF-β in the LPCM, and EGFR and TGF-β in the BPCM using immunocytochemical techniques.

4.2 Materials and Methodology

Samples from culture groups in the LPCM and BPCM were harvested, processed and embedded in paraffin wax, as previously described (Chapter II).

Table 4.1 Culture groups in the Luminal Phenotype Culture Model (LPCM) and the Basal Phenotype Culture Model (BPCM)

Heterotypic 3D co-culture models based on the MCF-7 (luminal phenotype, hormone-dependent) and MDA-MB-231 (basal phenotype, hormone-independent) breast cancer cell lines were developed. The experimental culture groups consisted of T_{REG} lymphocytes and NK cells, co-cultured with either MCF-7 cells or MDA-MB-231 cells at a 1:1:2 ratio in growth factor reduced Matrigel. The control groups included NK cells cultured with either MCF-7 or MDA-MB-231 cells (NK-BC); T_{REG} lymphocytes cultured with either MCF-7 or MDA-MB-231 cells (T_{REG}-BC) and MCF-7 or MDA-MB-231 cell cultured alone (BC).

Culture Group	Luminal Phenotype Culture Model (LPCM)	Basal Phenotype Culture Model (BPCM)
	MCF-7 cell line	***MDA-MB-231 cell line***
Experimental (EXP)	T_{REG} and NK	T_{REG} and NK
NK-breast cancer cells control (NK-BC)	NK alone	NK alone
T_{REG}-breast cancer cells control (T_{REG}-BC)	T_{REG} alone	T_{REG} alone
Breast cancer cells control (BC)	Control – no lymphocytes	Control – no lymphocytes

Serial sections of paraffin wax-embedded cultures were cut at a thickness of 3μm. Sections were collected on glass slides, dried at 60°C on a hot-plate and thereafter stored at 4°C until use. Sections were dewaxed in 2 X 5 min changes of xylene, followed by rehydration in a decreasing series of ethanol (2 X absolute ethanol, 3 min; 95% ethanol, 2 min; 70% ethanol, 1.5 min, 50% ethanol, 1 min) to distilled water. Sections underwent antigen retrieval in freshly prepared 0.1 M Tris, 5% urea buffer (pH9.5) at 95°C for 10 min in an oven, followed by 3 X 5 min washes in distilled water. Thereafter, sections were incubated in 1% BSA in PBS-Tween for 30 min at room temperature for concurrent blocking of non-specific binding sites

and permeabilisation. Subsequently, sections were incubated with relevant first and second sequence primary antibodies (where applicable) in PBS-Tween at 4°C overnight.

For double-labelling of the biomarkers MUC-1 and ER-α in the LPCM, a monoclonal mouse anti-MUC1 antibody (Abcam, Pretoria, South Africa, AB28081) and a polyclonal rabbit anti-ER-α antibody (Abcam, AB31315) at a concentration of 1:1000 was used. EGFR in the BPCM was localised using a polyclonal rabbit anti-EGFR antibody (Abcam, AB2430) at a concentration of 1:50. TGF-β was localised in samples from both the LPCM and BPCM using a polyclonal rabbit anti-TGF-β antibody (detecting all TGF-β isoforms (Abcam, Ab66043) at a concentration of 1:500.

Following overnight incubation with primary antibodies, sections were washed in PBS (3X 5 min). Sections were incubated for 2 h at room temperature with either Alexa Fluor 488 Anti-rabbit (Life Technologies, Johannesburg, South Africa, A11008) and/or Alexa Fluor 594 Anti-goat (Life Technologies, A11005) secondary antibodies diluted to a concentration of 1:1000 in 1% BSA in PBS. Subsequently sections were washed in PBS (3X 5 min). Nuclei were thereafter counterstained with DAPI diluted to 1: 50 000 in PBS for 5 min followed by two washes in PBS (5 min/wash). Sections were mounted in Fluoromount (Sigma-Aldrich, F4680) and stored at 4°C until viewing.

Controls were conducted to ascertain antibody specificity, and identify background and non-specific fluorescence. For negative controls, firstly, primary antibodies were omitted and replaced with PBS followed by incubation with the secondary antibody/antibodies; and secondly, both primary and secondary antibodies were omitted and replaced with PBS. Isotype controls were also conducted, in which each antibody was replaced with the same concentration of its matched isotype control (Mouse IgG3 (Abcam AB18392) for MUC1, and Rabbit IgG (Abcam, AB27478) for ER-α, EGFR and TGF-β), followed by incubation with the secondary antibody/antibodies.

Images were obtained using an Olympus iX51 Inverted Fluorescent Microscope with CellSens Software. The following filters were used U-MWIB2 (Alexa Fluor 488), U-MIY2 (Alexa Fluor

594) and U-MNU2 (DAPI). Exposure time was set at 200ms for all images. All images were obtained at 20 X magnification and enlarged if need be using the software application, with scale bars automatically adjusting. Plates were generated using Adobe Photoshop Elements.

4.3 Results

4.3.1 Remodelling of the ECM

Remodelling of the GFRM was observed in culture groups where cell lines were under the influence of both T_{REG} lymphocytes and NK cells (EXP culture groups), and NK cell-mediation alone, and to a lesser extent T_{REG} cell-mediation alone, in both LPCM and BPCM. These culture groups exhibited a less gel-like consistency with reduced viscosity when compared to the other culture groups, which caused difficulty in harvesting samples from microwells. Using light microscopy, it was evident that GFRM underwent remodelling exhibiting a more filamentous appearance in those culture groups containing lymphocytes as opposed to the relatively homogenous appearance in BC control groups (Fig. 4.1).

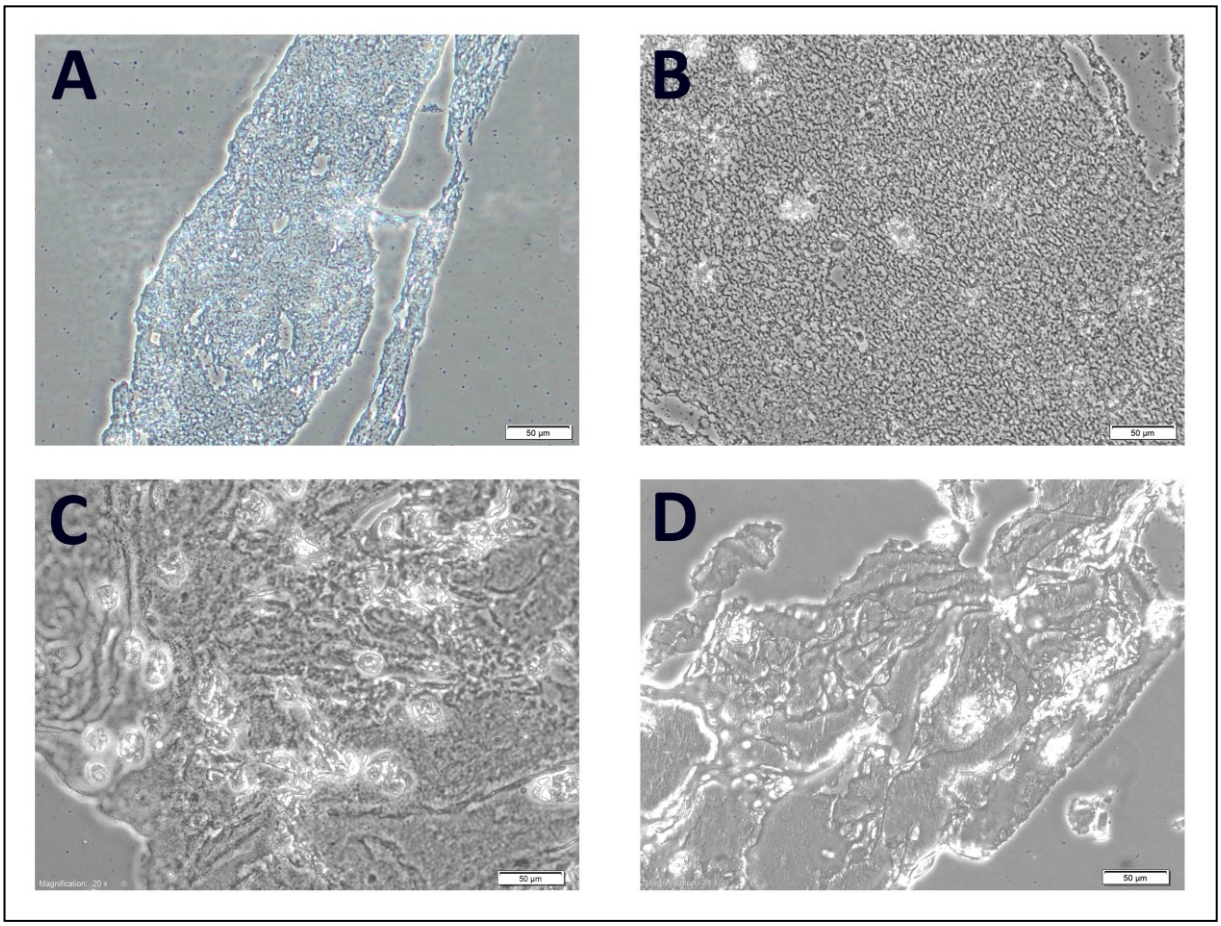

Figure 4.1 Representative light microscopy photomicrographs of GFRM alterations in culture groups

Immune cell-mediated alteration of GFRM structure with notable cavities and filamentous meshwork in culture groups in **A)** EXP culture groups, **B)** NK-BC control culture group and **C)** T_{REG}-BC control culture group. GFRM exhibits a more homogenous appearance in **D)** BC control culture group

4.3.2 Immunolocalisation of tumour biomarkers in the LPCM and BPCM

The data obtained from this study affirms previous findings that MCF-7 cells constitutively express MUC1, ER-α and TGF-β (Engelmann *et al.,* 2008; Klinge *et al.,* 2011; Gomes *et al.,* 2012, Gil *et al.,* 2013). MDA-MB-231 cells were found to express low levels of MUC-1 (data not shown), were negative for ER-α (data not shown) and positive for TGF-β (Walsh *et al.,* 2000; Mitchell *et al.,* 2002; Perrot *et al.,* 2012; Ye *et al.,* 2013). Negative controls including primary and secondary antibody omission, as well as isotype controls exhibited no immunofluorescence, indicating the specificity of the antibodies and the efficacy of the technique (see Appendix G). In some instances, sections were affixed to the filter paper used in sample processing. These sections could not be analysed accurately due to autofluorescence of the filter paper and were excluded from consideration.

In the LPCM ER-α expression (green fluorescence) was noted in all culture groups (Fig. 4.2). Nuclear localisation in the overlays is a dominant light blue fluorescence due to overlap with blue nuclear stain, DAPI. ER-α cytoplasmic localization (primarily yellow due to overlap with red fluorescence denoting MUC-1) was greatest in the NK-BC control culture group, with the EXP and T_{REG}-BC culture groups exhibiting some perinuclear and cytoplasmic localisation (Fig. 4.2). In the NK-BC and EXP culture groups MUC-1 expression was more diffuse, and of intermediate intensity. However, in the T_{REG}-BC and BC culture groups MUC-1 displayed high intensity cytoplasmic localization. Both NK-BC and EXP culture groups demonstrated some MUC-1 nuclear localization (dark red fluorescence) (Fig. 4.2).

In the BPCM, EGFR expression was found predominantly in the cytoplasmic compartment (green fluorescence) in all culture groups (Fig. 4.2). The intensity and patterning of cytoplasmic EGFR was similar in the T_{REG}-BC and BC control culture groups. Areas of high intensity nuclear (light blue) EGFR expression was noted primarily in the EXP, NK-BC and T_{REG}-BC culture groups. Distinct regions of extracellular EGFR expression, indicating secreted EGFR, was noted primarily in the EXP and NK-BC culture groups. These regions appeared diffuse or as clusters. In the T_{REG}-BC and BC culture groups, few regions of secreted EGFR were noted. However, these regions could not be accurately distinguished from the

cytoplasm since cell boundaries could not be resolved. Furthermore, overlay of fluorescence data with light microscopy photomicrographs proved inadequate in distinguishing cell boundaries within the filamentous GFRM.

4.3.3 Localisation of TGF-β in the LPCM and BPCM

TGF-β expression (green fluorescence) was noted in all culture groups in both the LPCM and BPCM (Fig. 4.3). In the LPCM, diffuse TGF-β expression of intermediate intensity was found predominantly in the cytoplasmic compartment and perinuclear regions, exhibiting low to intermediate intensity in the NK-BC, T_{REG}-BC and BC control culture groups. Diffuse TGF-β expression with a speckled appearance was noted extending into the ECM particularly in the NK-BC culture group. TGF-β expression was notably attenuated in the EXP culture group, reduced to perinuclear and ECM expression. In the BPCM, diffuse TGF-β expression of intermediate intensity was found primarily in the cytoplasmic compartment, with many cells exhibiting high intensity perinuclear expression as compared to the LPCM. In the EXP group, cytoplasmic TGF-β appeared reduced with high intensity perinuclear expression noted. TGF-β expression appeared to extend into the ECM in the NK-BC, T_{REG}-BC and BC control culture groups. However, the caveat regarding the discrimination between cell borders and the surrounding GFRM as previously mentioned, must be given due consideration.

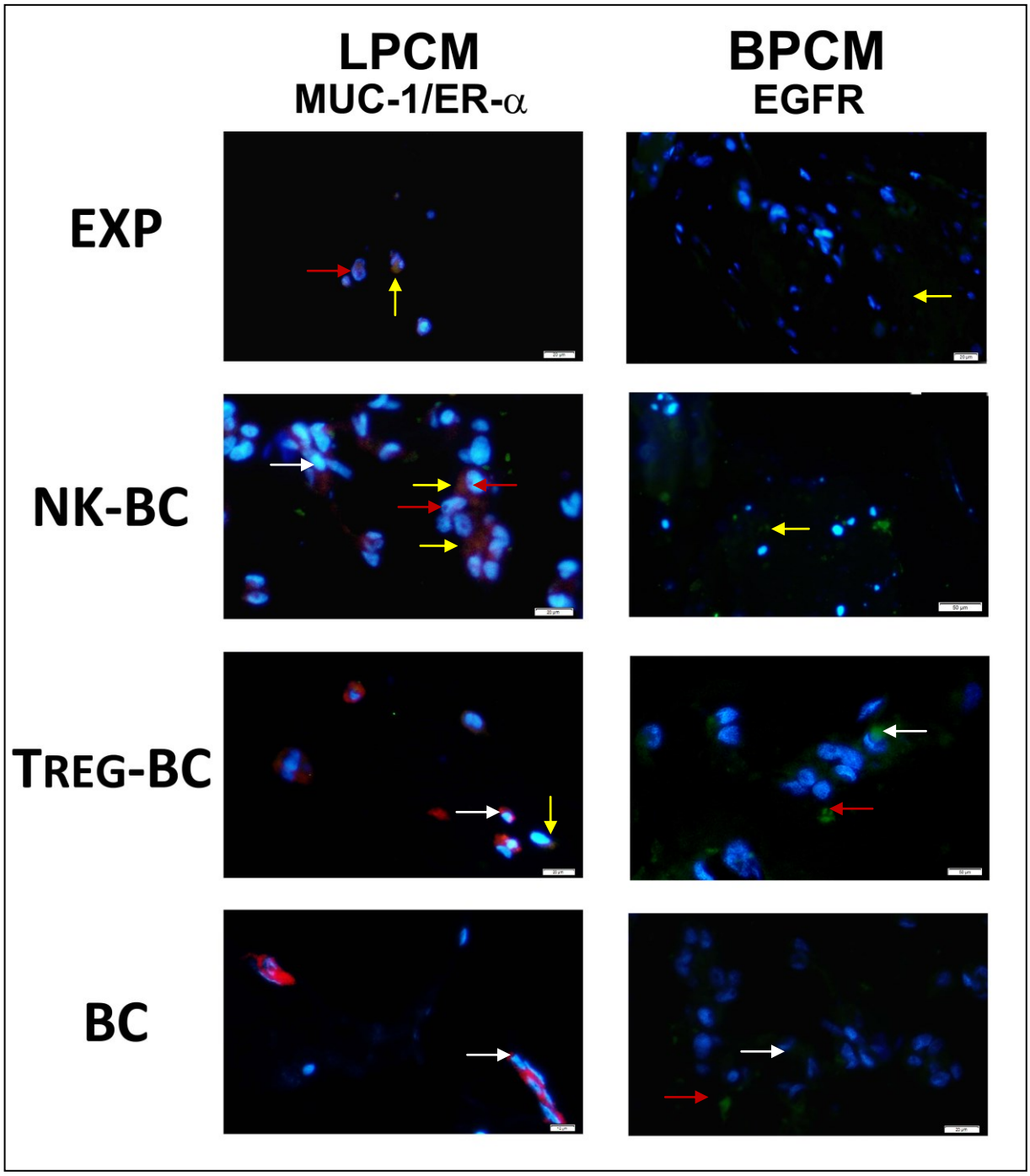

Figure 4.2 Representative photomicrographs of immunolocalisation of tumour biomarkers in LPCM and BPCM

ROWS: Indicate culture groups. **COLUMNS**: **LPCM, MUC-1/ER-α** Immunolocalisation of ER-α (green), MUC-1 (red) with nuclear stain DAPI (blue). Areas of high intensity nuclear ER-α expression (white arrows, light blue) were noted. ER-α cytoplasmic localisation displayed considerable overlap with MUC-1 (yellow arrows, yellow) primarily in the NK-BC group and noted in the T_{REG}-BC and EXP culture groups. MUC1 displayed some nuclear localization (red arrows, red), with diffuse cytoplasmic expression primarily in the NK-BC and EXP culture groups. High intensity cytoplasmic MUC-1 localisation noted in the T_{REG}-BC and BC culture groups. **BPCM, EGFR** Immunolocalisation of EGFR (green) with nuclear stain, DAPI (blue). EGFR expression was primarily cytoplasmic (white arrows). Areas of high intensity nuclear EGFR expression were noted in the EXP, NK-BC and T_{REG}-BC culture groups. ECM EGFR expression (yellow arrows distinct expression, red arrows putative expression) were noted primarily in the EXP, NK-BC and T_{REG}-BC culture groups.

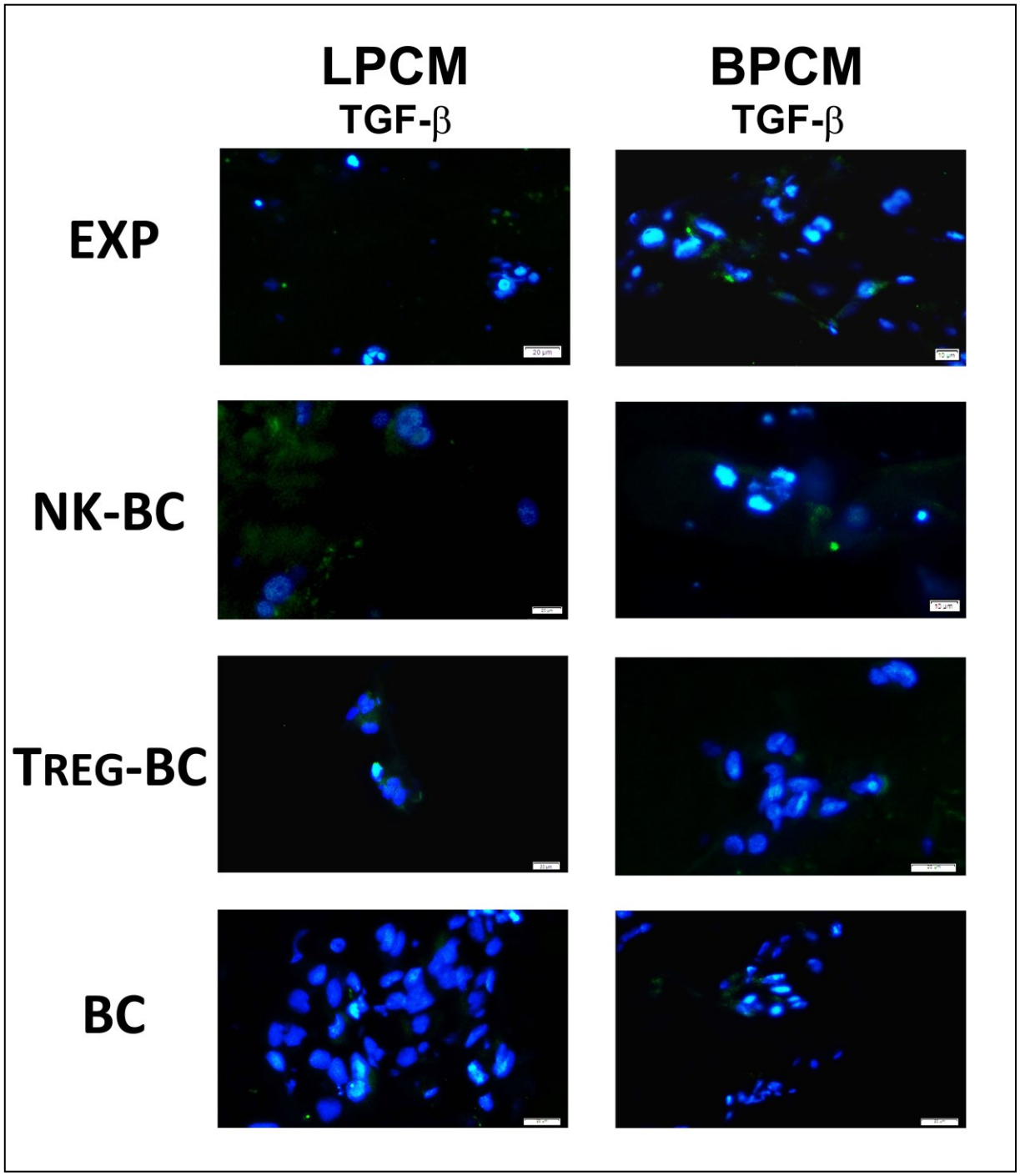

Figure 4.3 Representative photomicrographs of immunolocalisation of TGF-β in LPCM and BPCM

ROWS: Indicate culture groups. **COLUMNS**: **LPCM,** TGF-β expression (green) of intermediate intensity localised primarily to the cytoplasm (white arrows), with some areas of high intensity perinuclear expression noted (DAPI, blue nuclear stain). The NK-BC culture groups exhibit higher intensity TGF-β expression in the ECM (yellow arrows). TGF-β expression in the EXP culture group was considerably attenuated, with primarily perinuclear and ECM expression. **BPCM,** diffuse TGF-β expression of intermediate intensity localised primarily to the cytoplasm, with some cells exhibiting high intensity perinuclear expression. TGF-β expression was noted to extend into the ECM primarily in the BC, T_{REG}-BC and NK-BC culture groups.

4.4 Discussion

4.4.1 Alterations of GFRM structure

The observed alterations of the GFRM structure, from a more homogenous appearance to a filamentous meshwork with numerous cavities is directly linked to the presence of NK cells and/or T_{REG} lymphocytes. These results reflect studies in which IL-2 activated NK cells in 3D cultures induced such modifications to GFRM structure within 24 h (Albertsson *et al.,* 2007). This phenomenon is attributable to migration processes that rely on remodelling of the ECM. Lymphocyte migration is a multifactorial process involving expression of homing molecules in response to specific signals including chemokines, growth factors and ECM molecules, as well as numerous adhesive events allowing extravasation through blood vessels. Degradation of surrounding ECM, including basement membrane, is dependent on the secretion and activation of cathepsins, serine proteases and MMPs (Albertsson *et al.,* 2007; Wolf and Friedl, 2011). Mechanisms of ECM degradation include diffuse proteolysis that results in space for growth; contact-dependent proteolysis that is primarily involved in ECM remodelling for migration; and intracellular proteolysis that allows for targeted intracellular degradation of ECM components associated with translocation into newly acquired space during proliferation (Wolf and Friedl, 2011).

4.4.2 TGF-β in invasion processes and immune evasion

TGF-β is implicated in breast tumour cell migration, upregulating the expression of ECM-degrading enzymes thereby increasing proteolytic capacity and consequently, motility (Elliot and Blobe, 2005). The results obtained in this study affirm the constitutive expression of TGF-β in MCF-7 and MDA-MB-231 cell lines as shown by other studies (Walsh *et al.,* 2000, Mitchell *et al.,* 2002, Gomes *et al.,* 2012). Analysis of TGF-β isoform mRNA expression indicates that while MCF-7 and MDA-MB-231 cells exhibit similar levels of TGF-β1, TGF-β2 expression is notably higher in MDA-MB-231 cells, and TGF-β3 expression higher in MCF7-

cells (Gomes *et al.,* 2012). In this study, a pan TGF-β antibody was used to ascertain overall TGF-β expression (See Fig. 4.4 for a summary of results).

In the LPCM and BPCM, cytoplasmic TGF-β expression was predominantly of intermediate intensity in most culture groups. Cytoplasmic localisation of TGF-β reflects its production as a latent protein and storage in the cytoplasmic compartment (Gomes *et al.,* 2012). While a number of cells in each culture group in the LPCM, exhibited both cytoplasmic and perinuclear TGF-β expression, cells in the EXP culture group demonstrated attenuated cytoplasmic expression with the restriction of TGF-β to the perinuclear region. The EXP group in the BPCM exhibited a similar pattern of expression albeit to a lesser extent. Perinuclear TGF-β expression is associated with a higher rate of biosynthesis (Mizoi *et al.,* 1993; Gomes *et al.,* 2012), and may thus reflect an increase in invasive potential. The LPCM EXP culture group also displayed extracellular TGF-β expression that was not readily discernable in the BPCM EXP culture group. TGF-β is implicated in mediating T_{REG} lymphocyte suppression of NK cell function (Ghiringhelli et al., 2005; Chikileva et al., 2010). In this context, the results indicate that different mechanisms of such suppression may be used by different breast tumour phenotypes, with luminal phenotype tumours primarily employing a soluble form of TGF-β.

TGF-β stored in the cytoplasmic compartment is released into the extracellular matrix where it can be activated by proteases including MMP-9 and MMP-2. Lymphocytes themselves express multiple MMPs for migratory purposes. Short-term IL-2 activation has been shown to increase NK and T cell MMP-9 and migratory ability as opposed to long-term activation (Edsparr *et al.,* 2010). In this study, NK cells and T_{REG} lymphocytes were activated for a total of 72 h (see Chapter II), well within the range for short-term activation. That the GFRM exhibited a filamentous meshwork with numerous cavities in the presence of NK cells and/or T_{REG} lymphocytes in both the LPCM and BPCM is proposed to be associated with an increase in MMP production facilitated by TGF-β.

TGF-β in turn induces increased MMP expression, resulting in a positive feedback loop necessary for migration and invasion (Gomes *et al.,* 2012; Kubiczkova *et al.,* 2012). Extracellular TGF-β expression dominated the LPCM NK-BC culture group. While the BPCM NK-BC culture group did demonstrate secreted TGF-β, such expression was more evident in the T_{REG}-BC culture group. Sustained autocrine and paracrine TGF-β is essential for maintenance of epithelial-mesenchymal transitions and the generation of clonal stem cell populations in breast tumours (Moustakas and Heldin, 2014). Implicated in the invasiveness of basal phenotype breast tumours is the heightened expression of specifically, TGF-β1 and TGF-β2 (Gomes *et al.,* 2012). Luminal phenotype tumours, represented in this study by MCF-7 cells, are traditionally, weakly metastatic. These results may thus reflect the induction of tumour mechanisms aimed not only at evading NK cell insult, but also at increasing the invasive potential of the tumour cells themselves. Notably, an increase in TGF-β signalling capacity is linked with loss of ER-α expression in such tumours which exhibit increased invasive potential (Buck and Knabbe, 2006; Saitoh, 2011).

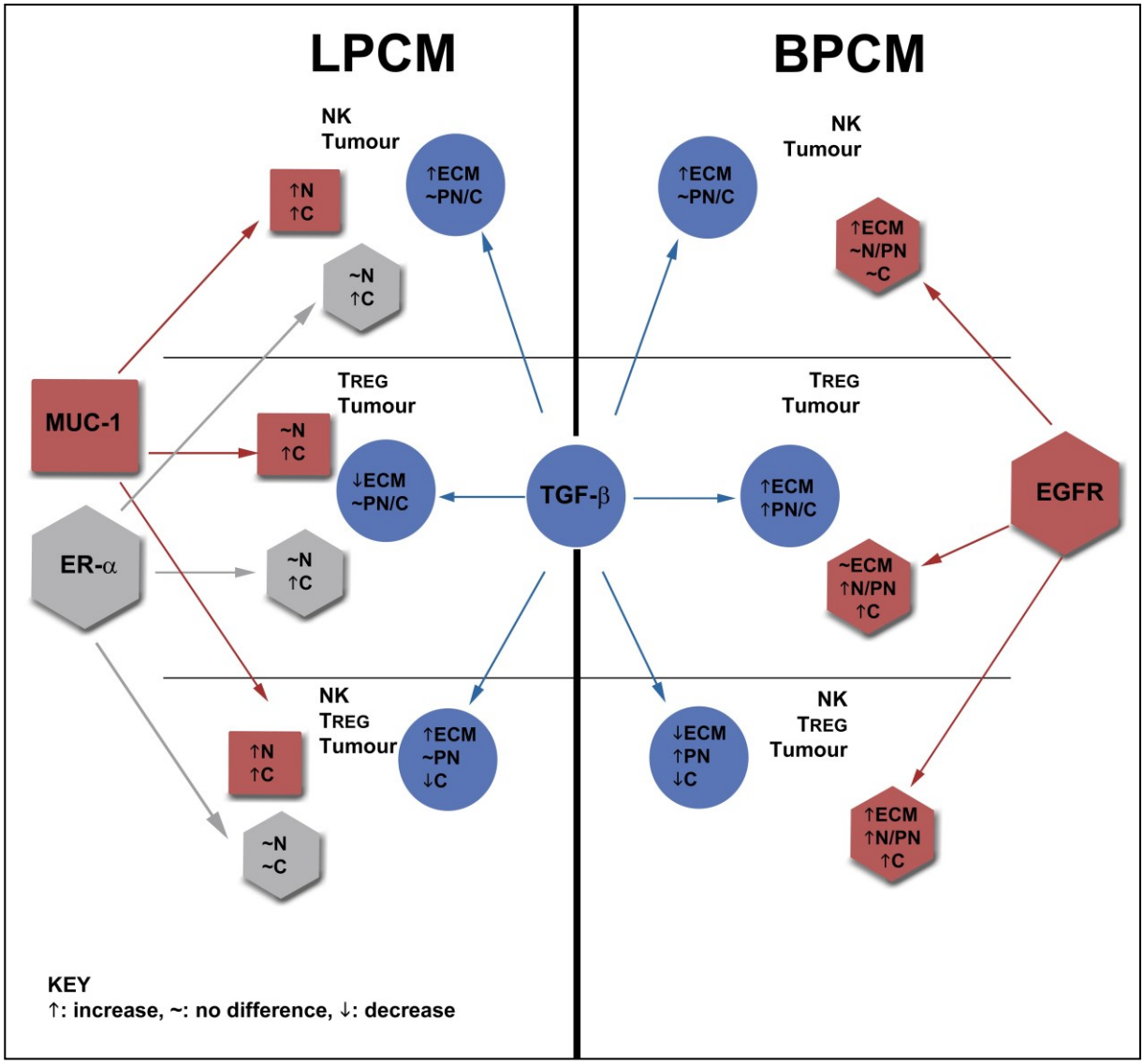

Figure 4.4 Summary of alterations in biomarker expression in culture groups in the LPCM and BPCM

Biomarker expression in a 3D simulated breast tumour environment alter under immune mediation, with shifts between cytoplasmic compartments, and the ECM linked to biological function. In the LPCM, MCF-7 cell subversion of immune mediation for a heightened invasive profile was indicated, with a dominant secreted form of TGF-β and increased cytoplasmic ER-α and MUC-1 expression noted. In the BPCM, extracellular TGF-β and EGFR expression are proposed to be associated with tumour-derived exosomes implicated in immune suppression and cellular communication necessary for tumour progression, and possibly linked to the maintenance of the innate invasive phenotype.

4.4.3 ER-α in invasion processes

Clinically, downregulation of ER-α expression is associated with increased recurrence and metastasis (Dhasarathy *et al.,* 2007). In this study, since MCF-7 cells were cultured in 3D, ER-α expression in the LPCM was of intermediate intensity, appearing reduced, as compared with other studies of MCF-7 cells in monolayer (Gil *et al.,* 2013, Sharan *et al.,* 2013). While ER-α expression localised to the nucleus in all culture groups, expression dominated the cytoplasm in the NK-BC group, with reduced cytoplasmic expression noted in the T_{REG}-BC culture group, and attenuated expression in the EXP culture group (See Fig. 4.4 for a summary of results). In the classical or genomic model of ER activation, cytoplasmic ERs are bound to Hsp's rendering them inactive until ligand binding induces dissociation, dimerisation and translocation to the nucleus, where they can interact with oestrogen response elements in the promoter region of target genes or with transcription factors, including Sp-1 and Ap-1, to initiate gene transcription (Acconcia and Kumar, 2006). Metastatic tumour antigen 1 (MTA1) has been shown to interact with cytoplasmic ER-α sequestering it to the cytoplasmic compartment and preventing nuclear translocation (Kumar *et al.,* 2002). MTA1 is upregulated in breast cancers, including the MCF-7 cell line, and is associated with an increase in invasive potential via its activation of non-classical or non-genomic ER-α function (Kumar *et al.,* 2002). Non-classical cytoplasmic ER function has been demonstrated where upon 17β-oestradiol stimulation, cytoplasmic ERs activate transcription factor Ap-1, while under the same conditions nuclear ERs repress Ap-1 (Björnström and Sjöberg, 2004). Ap-1 is regarded as an essential regulator of the tumour cell invasive profile, inducing the expression of a number of tumour invasion promoters including proteases MMP-3 and MMP-9, and inhibiting tumour invasion suppressors including bone morphogenetic protein 4 (Ozanne *et al.,* 2007).

It is thus proposed that the heightened cytoplasmic ER-α expression in the NK-BC culture group, and to a lesser extent in the T_{REG}-BC culture group, reflects tumour-induced subversion of lymphocyte function and secreted factors to allow for an increase in the MCF-7 invasive profile. That cytoplasmic ER-α expression was attenuated in the EXP culture group

is also of particular interest and may imply a conflict between the induction of pro-tumourigenic and anti-tumourigenic function. However, the heightened expression of TGF-β in the LPCM EXP culture group ECM may indicate the dominance of pro-tumourigenic processes.

4.4.4 MUC-1 in immune evasion processes

MUC-1, a transmembrane glycoprotein, is normally expressed on the apical membrane surface of secretory epithelial cells (Gil *et al.,* 2013). However, in luminal phenotype breast cancers MUC-1 is overexpressed, localizing predominantly to the cytoplasmic compartment (Nath and Mukherjee, 2014). The results of our study bear out these observations with MUC-1 displaying high intensity cytoplasmic localization in the LPCM T_{REG}-BC and BC culture groups (See Fig. 4.4 for a summary of results). The constitutive expression of MUC-1 in both these culture groups may thus be linked to the induction of pro-survival and anti-apoptotic mechanisms, as well as playing an important role in epithelial-mesenchymal transitions and the maintenance thereof (Nath and Mukherjee, 2014).

In the NK-BC and EXP culture groups MUC-1 expression was more diffuse, and of intermediate intensity; however, in these culture groups, a clear overlap with cytoplasmic ER-α localisation was noted. Under oestradiol stimulation, MUC-1 interacts with the DNA binding domain of ER-α, stabilising and activating the receptor (Wei *et al.,* 2006). As previously mentioned, cytoplasmic sequestered ER-α would function in a non-genomic context (Kumar *et al.,* 2002; Björnström and Sjöberg, 2004). Both NK-BC and EXP culture groups also demonstrated some MUC-1 nuclear localisation. As previously mentioned, the cytoplasmic domain of MUC-1 is capable of nuclear translocation where it in turn, may induce ER-α transcription and may interact with the transcription factors β-catenin, p120 catenin, STAT1 (Signal Transducer and Activator of Transcription 1) and p53 (Wei *et al.,* 2006; Khodarev *et al.,* 2009). These transcription factors are implicated in the induction of gene signatures associated with tumour metastasis processes and poor clinical outcome (Wei *et al.,* 2006; Khodarev *et al.,* 2009).

4.4.5 EGFR in tumour progression

The results of the this study confirm the overexpression of EGFR in the MDA-MB-231 cell line as indicated by numerous other studies (Foley *et al.,* 2010; Gumuskaya *et al.,* 2010; Ye *et al.,* 2013). In the BPCM, EGFR expression was found predominantly in the cytoplasmic compartment in all culture groups, but was of a higher intensity in the T_{REG}-BC and NK-BC culture groups (See Fig. 4.4 for a summary of results). EGFR localisation to the cytoplasm has been noted in breast tumours, with a correlation between such staining and increased invasiveness established in pancreatic adenocarcinomas (Ueda *et al.,* 2004). Cytoplasmic staining of EGFR reflects internalization of the receptor following ligand activation and thus may indicate the activation of signalling pathways (Ueda *et al.,* 2004).

Areas of high intensity nuclear and perinuclear EGFR expression were noted primarily in the EXP, NK-BC and T_{REG}-BC culture groups. Nuclear translocation of the EGFR has been linked to its role as a co-transcription factor, particularly of cyclin D1 and c-Myc, which have notable roles in cell growth and proliferation (Li *et al.,* 2001; Nyga *et al.,* 2011; Brand *et al.,* 2013). Nuclear EGFR is also a co-regulator of induced nitrox oxide synthase (iNOS), which is highly expressed in breast tumours, playing a dichotomous role (Brand *et al.,* 2013). iNOS may act as a tumour promoter by inducing DNA strand breaks, increasing MMP activation for invasion and preventing the lymphocyte infiltration into tumour sites; conversely NK cell-derived iNOS is implicated in the induction of cytotoxic processes (Lechner *et al.,* 2005; Brand *et al.,* 2013). However, iNOS is notably suppressed by tumour-derived TGF-β.

Extracellular EGFR, diffuse or in clusters, was noted primarily in the EXP and NK-BC culture groups; however, since cell boundaries could not be resolved with a high degree of accuracy, further investigation with the inclusion of a cytoskeletal marker is required. It is proposed that the extracellular EGFR observed is not soluble but is rather sequestered in exosomes trapped within the GFRM, since the antibody employed recognises the 170kDA EGFR isoform via western blot (Adamczyk *et al.,* 2011). Exosomes are small, biologically active microvesicles released into the extracellular space subsequent to the fusion of intracellular multivesicular bodies with the plasma membrane (Keller *et al.,* 2006; Sanderson *et al.,* 2008).

Tumour-derived exosomes may express variable amounts of EGFR as well as TGF-β, and are implicated in immune suppression and cellular communication necessary for tumour progression (Zhang and Grizzle, 2011). Their function in breast tumour progression specifically, however, remains to be delineated.

4.4.6 Implications for tumour progression

Migration and remodelling of the extracellular matrix are hallmarks of tumour progression. Alterations of the GFRM in this study are proposed to be a result of migratory and invasive processes, linked to an increase in the production of MMPs, and facilitated by TGF-β in basal and luminal phenotype breast cancer cells under NK cell and/or T_{REG} lymphocyte mediation. Notably in the LPCM, TGF-β expression was linked to diminished ER-α expression, as compared with MCF-7 cells cultured alone in monolayer, possibly reflecting increased invasive capacity as a result of spatial considerations in 3D cultures. Clinically a reduction in tumour ER expression is related to an increase in the invasive profile; however, pathological assessment of ER presentation is limited to the nucleus (Welsh *et al.,* 2013). The results obtained from this study indicate that under immune mediation, ER-α may be sequestered in the cytoplasm where it has functions distinct to that of nuclear ER. As such, it is proposed that cytoplasmic ER expression should undergo further assessment regarding its diagnostic capacity, given its association with immune cell infiltration.

It is proposed that the putative association of MUC-1, which is itself implicated in immune evasion and tumour progression, with ER-α may be dependent on the phenotype of the immune infiltrate. This is of particular interest in the MCF-7 cell line, which as a traditionally weakly metastatic line may redirect processes targeting lymphocyte migration to that of tumour cell invasion. This concept was further highlighted by the overall expression of TGF-β, which in advanced tumours is implicated in immune evasion and tumour invasion strategies.

In breast tumours increased TGF-β expression is associated with epithelial-mesenchymal transitions, conversion to a more malignant phenotype with heightened migration and invasive capacity (Barcellos-Hoff and Akhurst, 2009; Korpal and Kang, 2010). This is characteristic of basal phenotype tumours, together with a heightened expression of EGFR (Yewale *et al.,* 2013). The results of this study indicate that immune mediation affects TGF-β and EGFR localisation to cytoplasmic compartments and the extracellular matrix, reflecting the processes of biosynthesis, storage or activation. Tumour-derived exosomes may express variable amounts of EGFR as well as TGF-β, and are implicated in immune suppression and cellular communication (Zhang and Grizzle, 2011). The results of this study implicate the sublimation of immune mediation by both luminal and basal phenotype breast tumour cells to aid in the remodelling of the tumour microenvironment necessary for proliferation and invasion (DeNardo *et al.,* 2008).

4.4.7 Implications for therapeutic strategies

In addition to surgery, radiotherapy and chemotherapy, intervention strategies for luminal phenotype breast carcinomas includes the use of SERM, SERD and AI as either a neo-adjuvant therapy or adjuvant therapy (Howell *et al.,* 2004). Such targeted therapy aims to either reduce the action of the ER by acting as an ER antagonist or agonist, or reduce the available oestrogenic milieu. While targeted therapy for hormone-independent or triple-negative breast cancers have yet to be fully developed, promising results have been obtained using EGFR directed monoclonal antibody therapy, tyrosine kinase inhibitors and antisense oligodeoxynucleotides (Yewale *et al.,* 2013). However, while some clinical success has been reported, the median overall survival rate remains low (Nicolini and Carpi, 2008). As the results of this study indicate, immune infiltration alters the expression of biomarkers associated with both luminal and basal phenotype tumours, which in turn may alter disease progression and response to treatment.

The use of mAb therapy against MUC-1, EGFR and TGF-β for example, theoretically should elicit NK cell ADCC (Moreno *et al.,* 2007; Korpal and Kang, 2010; Yewale *et al.,* 2013), as documented by others studies regarding the Her2/neu antibody, Trastuzumab (Mozaffari *et al.,* 2007). However, firstly breast tumours commonly acquire resistance to targeted therapies (Yewale *et al.,* 2013), and secondly surgical intervention, radiotherapy and chemotherapy have been shown to reduce both the number of activated NK cells as well as their cytotoxic potential (Mozaffari *et al.,* 2007). Thus while the integration of different modalities is encouraged, the complexity of the interactions between tumour cells and the immune system may negate such therapeutic intervention.

4.4.8 Limitations of the study

The first limiting factor to this study was the reduced viscosity of the GFRM in cultures containing lymphocytes. The more liquid-like nature of the samples resulted in active loss during harvesting after the culture period. Moreover, sections that were affixed to filter paper were either lost during the immunocytochemistry protocol or could not be analysed due to autofluorescence of the filter paper. Since a large number of either samples or sample sections were lost, and given the funding and time limitations, more co-cultures could not be generated, thus a qualitative approach was applied to this part of the study instead of the quantitative approach intended.

4.5 Conclusion

The results of this study indicate that immune cells are able to mediate the expression of biomarkers associated with tumour progression. While the pro-tumourigenic or anti-tumourigenic functions of the altered levels of biomarker expression remain to be verified without exception, both luminal and basal phenotype tumours appeared to induce immune evasion strategies and subvert immune function to increase the tumour cell invasive profile. These results were further borne out by observations indicating immune mediated alteration of the GFRM. It will be necessary to further elucidate the relationship between the investigated biomarkers and immune cells to understand their interactions and potentially provide more information for therapeutic intervention.

Chapter V: Concluding Discussion – A Synthesis

5.1 Introduction

The incidence of breast cancer in developing countries is increasing (Youlden *et al*., 2012). Given that advances in surgical procedures and adjuvant treatments have not significantly reduced the median overall survival rate of patients presenting with metastatic breast cancer (Nicolini and Carpi, 2008), intimates a greater level of complexity inherent to this disease. The reductionist approach of 2D culture systems fails to recapitulate the complexity of the *in vivo* environment with regard to the spatial interaction of multiple cell types (Pinto *et al.,* 2011). Three-dimensional studies of breast tumour progression have concentrated on metastatic processes, primarily using homotypic cultures to investigate breast cancer cell invasion (Poincloux *et al.,* 2011; Chandrasekaran *et al.,* 2012; Yu and Machesky, 2012) or heterotypic cultures investigating breast tumour cell and fibroblast interaction (Olsen *et al.,* 2010). To date, assessment of scientific literature has yielded no studies investigating the heterotypic interactions between immune cells and breast cancer cells in such a system. The latter is of especial concern since it has long been known that the immune system may function in a Machiavellian manner, both suppressing tumour formation and promoting tumour progression (Sakaguchi *et al.,* 1995; Balkwill and Mantovani 2001; Ichim, 2005; Visser, 2008; Mougiakakos *et al.,* 2010).

Tumour infiltrating populations in breast tumours demonstrate a distinct paucity of NK cells (Georgiannos *et al.,* 2003; Macchetti *et al.,* 2006) which may reflect inadequate NK cell-homing mechanisms and tumour-induced evasion strategies dependent on secreted factors including cytokines and other signalling molecules (Albertsson *et al.,* 2003). Furthermore, the accumulation of T_{REG} lymphocytes, both in TIL populations and in peripheral blood of patients presenting with advanced breast tumours, are implicated in the induction of tumour tolerance and the suppression of NK cell function (Bates *et al.,* 2006; Pooi *et al.,* 2006; Bohling and Allison, 2008; Decker *et al.,* 2012). Such clinical evidence for dysregulated immune function in breast tumours thus provided the impetus for this study, in which 3D

culture systems were established to investigate the interaction between NK cells and T_{REG} lymphocytes and breast cancer.

5.2 Findings

In early tumour formation, TGF-β acts as a tumour suppressor; however, in established breast tumours, including the luminal phenotype MCF-7 cells and basal phenotype MDA-MB-231 cells, TGF-β acts as potent promoter of tumour progression (Korpal and Kang, 2010). TGF-β is a multifunctional growth factor, capable of inducing pro-angiogenic factors and of particular importance for this study, capable of inducing ECM remodelling and suppressing the immune system, either directly or indirectly (Korpan and Kang, 2010). ECM remodelling in this study is evidenced by the changes of the GFRM, from a more homogenous appearance to a filamentous network in the culture groups primarily under NK cell-mediation; as well as by the significant increase in chemokine expression. Chemokines are essential for the directional migration of lymphocytes as well as tumour cell invasion (Vicari and Caux, 2002).

In the LPCM, the chemokines CCL2, CCL4 and CXCL8 grouped together consistently. CXCL8 is an established promoter of tumour growth and is fundamental to ECM remodelling via the induction of MMP function, specifically MMP2 and MMP9 (Vicari and Caux, 2002). In the LPCM, in which CXCL8 was significantly increased in the NK-BC and EXP culture groups, qualitative analysis showed, particularly in the former group, heightened expression of both cytoplasmic MUC-1 and ER-α (Fig. 5.1). Cytoplasmic ER-α is implicated in the induction of the transcription factor Ap-1 which itself induces the expression of MMPs, thereby promoting tumour invasion (Björnström and Sjöberg, 2004). Furthermore, MUC-1 has been shown to stabilise and activate ER directly (Wei *et al.,* 2006), implicating a complex pathway directed at promoting tumour invasion (see Fig. 5.1 for a summary of results).

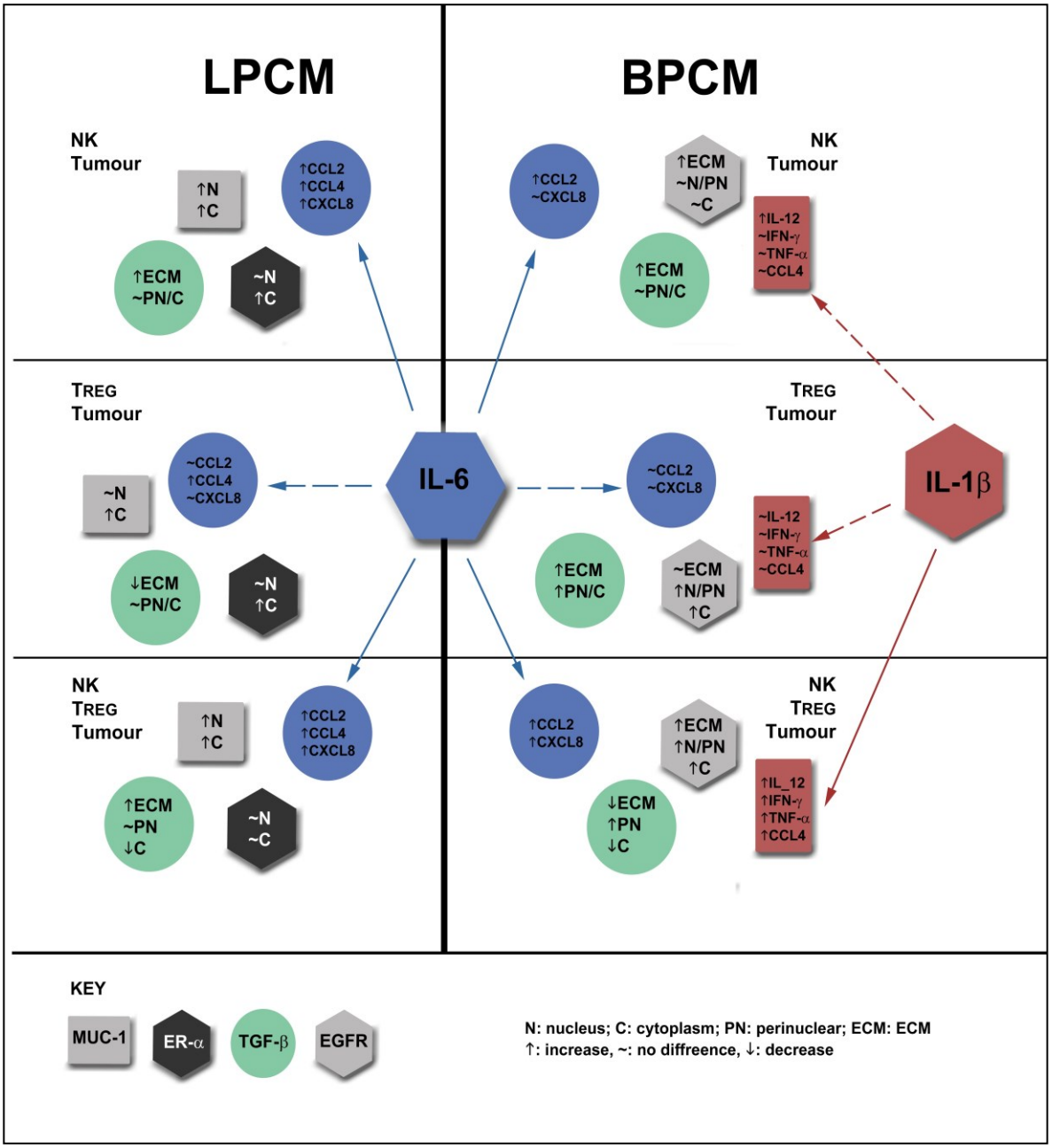

Figure 5.1 Summary of alterations in cytokine and biomarker expression in culture groups in LPCM and BPCM

Biomarker expression and cytokine secretions in a 3D simulated breast tumour environment are associated with the hormone dependency of tumours and alter under immune mediation. The results indicate the subversion of secreted factors for the creation of a tumour-promoting microenvironment. In the NK-BC and EXP culture groups in the LPCM, IL-6 and associated chemokines, together with the secreted form of TGF-β and increased cytoplasmic ER-α and MUC-1 expression are proposed to induce a more invasive phenotype. In the BPCM under NK cell mediation, extracellular TGF-β and EGFR expression are linked to the maintenance of an invasive phenotype. Within the EXP culture group there was a notable increase in the proinflammatory cytokine cohort, with a proposed association with immune evasion processes.

The CCL2, CCL4, CXCL8 grouping that presented consistently in the LPCM was not maintained in the BPCM, where grouping of CCL2 and CXCL8 were rather prevalent. This may reflect another pathway by which CCL4 may be activated, with results indicating that such activation may be dependent on IL-1β in the BPCM (Fig. 5.1). CCL2 is implicated as a major recruiter of macrophages, which play a pro-tumourigenic role in breast cancer. Moreover, high concentrations of CCL2 are linked to more aggressive tumours (Vicari and Caux, 2002). While CCL2 was significantly increased in the culture groups under NK cell-mediation in both the LPCM and BPCM; CCL2 was relatively higher in the LPCM. MCF-7 cells are weakly metastatic, thus the increase in CCL2 may be linked to the generation of a more invasive profile by subversion of NK cell-mediated cytokine secretions.

Importantly in the T_{REG}-BC culture group in both LPCM and BPCM, CCL2 and CCXL8 expression was low; moreover, TGF-β, the sustained expression of which is essential to tumour maintenance (Moustakas and Heldin, 2014) was of a similar level to that seen in the BC control group. Furthermore, no significant increases in any other proinflammatory cytokine was noted in this culture group compared to the BC control group (Fig. 5.1). It is proposed that these results reflect the induction of tumour tolerance mechanisms as opposed to immune activation. T_{REG} lymphocytes in the tumour microenvironment not only suppress cytotoxic cell function but also mediate the growth and progression of the tumour itself.

The results obtained from this study indicate that IL-6 is a major promoter of chemokine function when tumour cells are under NK cell-mediation, regardless of the presence of T_{REG} lymphocytes. Importantly, CCL2 and CXCL8 induction are highlighted in both basal and luminal phenotype culture models and as such, these chemokines may be a common pathway used in tumour progression regardless of breast cancer phenotype. IL-6, which was significantly increased in the EXP group in both the BPCM and LPCM, has been shown to abrogate the effects of TGF-β suppression on canine derived-tumour infiltrating LAK cells (Hsiao *et al.,* 2004). However, IL-6 as previously mentioned is a pleiotrophic cytokine. At concentrations of below 5ng/ml, detected in this study, IL-6 has been shown to be unable to

restore LAK function as influenced by tumour cells, whereas at high concentrations IL-6 has been shown to actively suppress NK function (Hsiao *et al,* 2004). Moreover, IL-6 and CCL2 have been linked to cancer stem cell-driven tumour progression (Chin and Wang, 2013; Jiang and Shapiro, 2013). Cancer stem-cell populations have been identified in both the MCF-7 cell line and the MDA-MB-231 cell line (Engelmann *et al.,* 2008; Hiraga *et al.,* 2011) and thus the secretion of IL-6 and its associated chemokine cluster may indeed not only infer attainment of increased metastatic potential but clonal evolution of stem cell populations.

An increase in proinflammatory cytokines was noted particularly in the BPCM EXP culture group (Fig. 5.1). Basal phenotype breast tumours constitutively express more proinflammatory cytokines during tumour progression; however, the significant increases in IL-12, IFN-γ and TNF-α, notably clustering with IL-1β, indicates the generation of a chronic inflammatory environment implicated in increasing tumour cell invasiveness in the BPCM EXP culture group (Baumgarten and Fraser, 2012). Exogenous IL-12 and TNF-α have been shown to act in a synergistic manner presenting with anti-tumourigenic function (Sabel *et al.,* 2010). TNF-α, which is produced by NK cells, is associated with an upregulation of endothelial cell surface receptors and a loss of intercellular adhesion molecules, necessary for the extravasation of lymphocytes to tumour sites (Sabel *et al.,* 2010). However, tumour cells may equally subvert the functions of TNF-α, which are further associated with an increase in MMP function, to allow for tumour cell migration and invasion (Nath and Mukerjee, 2014).

The grouping of IL-12 and TNF-α with IFN-γ, an interferon necessary for immune system activation against transformed cells, in the BPCM EXP culture group, can be further linked with the cytotoxic function of NK cells (Saha *et al.,* 2010). Furthermore, the upregulation of IFN-γ secretion by NK cells has been shown to be linked with inhibition of endogenous TGF-β (Meadows *et al.,* 2006), reflecting the results of this study in which the BPCM EXP culture group exhibited reduced cytoplasmic and ECM endogenous TGF-β, with expression limited to the perinuclear region (Fig. 5.1). However, sustained IFN-γ expression has also been linked with tumour cell resistance to NK cell cytotoxic function (Wang *et al.,* 2012), and by

upregulating MHC I presentation on tumour cells (Saha *et al.,* 2010), may be linked with tumour cell evasion of NK cells. Thus, although these results may be interpreted as activation of NK cell cytotoxic function, even under T_{REG} lymphocyte mediation, that the BPCM NK-BC control group only showed a significant increase in IL-12, of the aforementioned cytokines, may reflect sublimation of NK cell function in the EXP culture group. Supporting this assertion is the expression of EGFR, which was notably higher in the cytoplasmic, nuclear and extracellular matrix of the BPCM EXP culture group. Nuclear EGFR can act as a co-transcription factor, notably of cyclin D1 and c-Myc which have fundamental roles in cell growth and proliferation (Li *et al.,* 2001; Nyga *et al.,* 2011; Brand *et al.,* 2013) as well as co-regulating iNOS expression in breast tumours (Brand *et al.,* 2013). Moreover, extracellular EGFR, contained within tumour-derived exosomes, are implicated in immune suppression and cellular communication necessary for tumour progression (Zhang and Grizzle, 2011).

5.3 Implications of this study and future directions

Advances in traditional cancer treatment modalities for patients presenting with advanced breast cancer has not significantly improved the median overall survival rate (Nicolini and Carpi, 2008). Furthermore, cancer immunotherapy including non-specific immunomodulation, mAb therapy, cancer vaccines and ACT, have yet to prove clinically efficacious (Rosenberg *et al.,* 2008). That cancer remains incurable implicates a more complex tumour microenvironment that requires multiple treatment modalities to elicit a beneficial outcome. However, such treatment strategy is in effect, a double-edged sword, with a combination of traditional regimens prone to reducing the efficacy of NK cell mediated cytotoxic effects; yet alone, being incapable of inducing even limited benefits (Mozaffari *et al.,* 2007; Kirkwood *et al*., 2012; Tiwari and Roy, 2012).

Given the complexity of the *in vivo* tumour microenvironment, this study developed a novel 3D culture system in which to investigate the heterotypic interactions of tumour cells and immune cells. This culture system has proven suitable for exploring alterations in gene profiles, as evidenced by the successful optimisation of RNA extraction and for examining

cytokine profiles in which innovative multivariate exploratory techniques were used to deduce functional associations.

A limiting factor to any study involving T_{REG} lymphocytes is the phenotypic characterisation thereof. It would thus be of interest to isolate T_{REG} lymphocytes using additional markers to ascertain whether derived subgroups have any significant impact on the results obtained in this study. A further restriction noted was the yield of NK cells and T_{REG} lymphocytes constrained by the volume of blood we were permitted to obtain per volunteer (Human Ethics Clearance M081036 and M140155). It would be advisable to increase the volume of blood obtained for isolation of lymphocytes, ethical issues permitting, to allow for the establishment of additional cultures and flow cytometric characterisation of isolated lymphocyte populations per volunteer.

Furthermore, while limitations were noted regarding the efficacy of immunocytochemistry on harvested samples, these limitations themselves were closely related with immune mediation of migration processes and thus provided additional, albeit unforeseen, insight into the interaction of immune cells with tumour cells. To resolve the problems encountered during sample harvesting, immunolocalisation of biomarkers within cultures could rather be conducted *in situ* followed by confocal microscopy. As was intended for this study, quantitative analysis using CellProfiler software would then allow for a less subjective view of alterations in biomarker expression.

Collectively, the results of this study point to the sublimation of NK cell and/or T_{REG} lymphocyte function by tumour cells, with an emphasis on the generation of an inflammatory microenvironment for tumour progression. The roles of T_{REG} lymphocytes and NK cells should not be assessed independently of the tumour phenotype, given that luminal phenotype and basal phenotype tumours differ in their response to immune mediation, be it by the alteration of biomarker or cytokine expression. However, the mechanisms by which they elicit responses result in a similar outcome – that of enhanced evasive and invasive capacity.

Cancer is akin to the Lernaean Hydra, possessing many mechanisms with which to evade anti-tumourigenic processes; and when balked, possessing the ability to develop novel methods to ensure its survival. The question thus remains: where in fact is the signalling network modified to allow for tumour tolerance and progression under immune mediation? Subsequent studies based on this methodology, currently underway, will assess the induction of pro-apoptotic markers, as well as investigate major players in selected signal transduction pathways. It is necessary to further elucidate the relationship between the investigated cytokines, biomarkers and immune cells, to understand their interactions and potentially provide more information for therapeutic intervention, given that these factors may contribute to the intransigence of tumours in responding favourably to combined modalities of therapy.

References

Acconcia F and Kumar R (2006) Signaling regulation of genomic and nongenomic functions of estrogen receptors. *Cancer Letters* 238: 1–14.

Adamczyk KA, Klein-Scory S, Moradian M, Warnken U, Schmiegel W, Schnölzer M and Schwarte-waldhoff I (2011) Characterization of soluble and exosomal forms of the EGFR released from pancreatic cancer cells. *Life Sciences* 89(9-10): 304–312.

Aktas B, Müller V, Tewes M, Zeitz J, Kasimir-bauer S, Loehberg CR, Rack B, Schneeweiss A and Fehm T (2011) Comparison of estrogen and progesterone receptor status of circulating tumor cells and the primary tumor in metastatic breast cancer patients. *Gynecologic Oncology* 122(2): 356–360.

Albertsson PA, Basse PH, Hokland M, Goldfarb RH, Nagelkerke JF, Nannmark U and Kuppen PJK (2003) NK cells and the tumour microenvironment: implications for NK-cell function and anti-tumour activity. *Trends in Immunology* 24(11): 603–609.

Albertsson PA, Basse PH, Edsparr K, Kim MH, Golfarb RH, Kitson RP, Lennernäs B, Nannmark U and Johansson BR (2007) Differential locomotion of long- and short-term IL-2-activated murine natural killer cells in a model matrix environment. *Scandinavian Journal of Immunology* 66: 402–409.

Ampuja M, Jokimäki R, Juuti-Uusitalo K, Rodriguez-Martinez A, Alarmo EL and Kallioniemi A (2013) BMP4 inhibits the proliferation of breast cancer cells and induces an MMP-dependent migratory phenotype in MDA-MB-231 cells in 3D environment. *BMC Cancer* 13: 429–542.

Andrianifahanana M, Moniaux N and Batra SK (2006) Regulation of mucin expression: Mechanistic aspects and implications for cancer and inflammatory diseases. *Cancer* 1765: 189–222.

Arnon TI, Markel G and Mandelboim O (2006) Tumor and viral recognition by natural killer cells receptors. *Seminars in Cancer Biology* 16: 348–358.

Ascierto ML, Idowu MO, Zhao Y, Khalak H, Payne KK, Wang X, Dumur CI, Bedognetti D, Tomei S, Ascierto PA, Shanker A, Bear HD, Wang E, Marincola FM, Maria A De and Manjili MH (2013) Molecular signatures mostly associated with NK cells are predictive of relapse free survival in breast cancer patients. *Journal of Translational Medicine* 11(1): 145–156.

Bacchetta R, Gregori S and Roncarolo M (2005) CD4+ regulatory T cells: Mechanisms of induction and effector function. *Autoimmunity Reviews* 4: 491–496.

Baker BM and Chen CS (2012) Deconstructing the third dimension – how 3D culture microenvironments alter cellular cues. *Journal of Cell Science* 125: 1–10.

Balkwill F and Mantovani A (2001) Inflammation and cancer: back to Virchow? *Lancet* 357: 539–45.

Barcellos-Hoff MH and Akhurst RJ (2009) Transforming growth factor-β in breast cancer: too much, too late. *Breast Cancer Research* 11:202 (doi: 10.1186/bcr2224).

Bates GJ, Fox SB, Han C, Leek RD, Garcia JF, Harris AL and Banham AH (2008) Quantification of regulatory T cells enables the identification of high-risk breast cancer patients and those at risk of late relapse. *Journal of Clinical Oncology* 24(34): 5373–5380.

Baumgarten SC and Frasor J (2012) Inflammation: an instigator of more aggressive estrogen receptor (ER) positive breast cancers. *Molecular Endocrinology* 26(3): 360–71.

Bazley LA and Gullick WJ (2005) The epidermal growth factor receptor family. *Endocrine-Related Cancer* 12(Conference Paper): 17–28.

Beano A, Signorino E, Evangelista A, Brusa D, Mistrangelo M, Polimeni MA, Spadi R, Donadio M, Ciuffreda L and Matera L (2008) Correlation between NK function and response to trastuzumab in metastatic breast cancer patients. *Journal of Translational Medicine* 6: 25 (doi: 10.1186/1479-5876-6-25).

Ben-Baruch A (2003) Inflammatory cells, cytokines and chemokines in breast cancer progression: reciprocal tumor–microenvironment interactions. *Breast Cancer Research* 5: 31–36.

Beyer M and Schultze JL (2006) Regulatory T cells in cancer. *Blood* 108: 804–811.

Billingham RE, Brent L and Medawar PB (1953) 'Actively Acquired Tolerance' of Foreign Cells. *Nature* 172: 603-606.

Björnström L and Sjöberg M (2004) Estrogen receptor-dependent activation of AP-1 via non-genomic signalling. *Nuclear Receptor* 2: 3–14.

Bohling SD and Allison KH (2008) Immunosuppressive regulatory T cells are associated with aggressive breast cancer phenotypes: a potential therapeutic target. *Modern Pathology* 21(12): 1527–32.

Bottino C, Biassoni R, Millo R, Moretta L and Moretta A (2000) The human natural cytotoxicity receptors (NCR) that induce HLA class I-independent NK cell triggering. *Human Immunology* 61: 1–6.

Brand TM, Iida M, Luthar N, Starr MM, Huppert EJ and Wheeler DL (2013) Nuclear EGFR as a molecular target in cancer. *Radiotherapy and Oncology* 108(3): 370–377.

Buck MB and Knabbe C (2006) TGF-beta signaling in breast cancer. *Annals of the New York Academy of Sciences* 126: 119–126.

Bustin SA, Benes V, Garson JA, Hellemans J, Huggett J, Kubista M, Mueller R, Nolan T, Pfaffl MW, Shipley GL, Vandesompele J and Wittwer CT (2009) The MIQE Guidelines: *M*inimum *I*nformation for publication of *Q*uantitative real-time PCR *E*xperiments. *Clinical Chemistry* 55(4): 611–622.

Chambers BJ (2010) NK cell–T cell interactions. In (Ed. Lotze MT and Thomson AW) *Natural Killer Cells, Basic Science and Clinical Application.* Academic Press Elsevier Ltd. London. Pp297–308.

Chandrasekaran S, Geng Y, DeLouise L and King MR (2012) Effect of homotypic and heterotypic interaction in 3D on the E-selectin mediated adhesive properties of breast cancer cell lines. *Biomaterials* 33(35): 9037–48.

Chavey C, Bibeau F, Gourgou-Bourgade S, Burlinchon S, Boissière F, Laune D, Roques S and Lazennec G (2007) Oestrogen receptor negative breast cancers exhibit high cytokine content. *Breast Cancer Research* 9(1): R15 (doi: 10.1186/bcr1648).

Chen L, Xiao Z, Meng Y, Zhao Y, Han J, Su G, Chen B and Dai J (2012) The enhancement of cancer stem cell properties of MCF-7 cells in 3D collagen scaffolds for modeling of cancer and anti-cancer drugs. *Biomaterials* 33(5): 1437–1444.

Cheng G, Aixin Y and Malek TR (2011) T-cell tolerance and the multi-functional role of IL-2R signaling in T-regulatory cells. *Immunological Reviews* 241: 63–76.

Chikileva IO, Shubina IZ, Baronzio G and Kiselevsky M V (2010) Is it necessary to deplete the lymphokine activated killers' populations of CD4+CD25+ lymphocytes? Regulatory Foxp3-positive T cells within lymphokine activated killers. *Biomedicine et Pharmacotherapy* 64: 379–385.

Chin AR and Wang SE (2013) Cytokines driving breast cancer stemness. *Molecular and Cellular Endocrinology* Article in press (doi: 10.1016/j.mce.2013.03.024).

Cimino-Mathews A, Ye X, Meeker A, Argani P and Emens L (2013) Metastatic triple-negative breast cancers at first relapse have fewer tumor-infiltrating lymphocytes than their matched primary breast tumors: a pilot study. *Human Pathology* 44(10): 2055–63.

Coley WB (1931) Some thoughts on the problem of cancer control. *American Journal of Surgery* 14(3): 605–619.

Conti I and Rollins BJ (2004) CCL2 (monocyte chemoattractant protein-1) and cancer. *Seminars in Cancer Biology* 14: 149–154.

Cooper MA, Fehniger TA and Caligiuri MA (2001) The biology of human natural killer-cell subsets. *Trends in Immunology* 22(11): 633–640.

Coughlin SS and Ekwueme DU (2009) Breast cancer as a global health concern. *Cancer Epidemiology* 33: 315–318.

Decker T, Fischer G, Bücke W, Bücke P, Stotz F, Grüneberger A, Gropp-Meier M, Wiedemann G, Pfeiffer C, Peschel C and Götze K (2012) Increased number of regulatory T cells (T-regs) in the peripheral blood of patients with Her-2/neu-positive early breast cancer. *Journal of Cancer Research and Clinical Oncology* 138(11): 1945–50.

DeNardo DG, Johansson M and Coussens LM (2008) Immune cells as mediators of solid tumor metastasis. *Cancer Metastasis Reviews* 27(1): 11–8.

de Visser K and Coussens L (2005) The interplay between innate and adaptive immunity regulates cancer development. *Cancer Immunology, Immunotherapy* 25: 1143–1152.

Dewan Z, Takada M, Terunuma H, Deng X, Ahmed S, Yamamoto N and Toi M (2009) Natural killer activity of peripheral-blood mononuclear cells in breast cancer patients. *Biomedicine & Pharmacotherapy* 63(9): 703–706.

Dhasarathy A, Kajita M and Wade PA (2007). The transcription factor Snail mediates epithelial to mesenchymal transitions by repression of estrogen receptor alpha. *Molecular Endocrinology* 21(12): 2907–2918.

Dinarello CA (2008) Interleukin-1 family of ligands and receptors. In (Ed. Paul WE) *Fundamental Immunology 6th Ed.* Lippincott Williams and Wilkins. Philadelphia, USA. Pp750–803.

do Amaral JB, Rezende-Teixeira P, Freitas VM and Machado-Santelli GM (2011) MCF-7 Cells as a three-dimensional model for the study of human breast cancer. *Tissue Engineering: Part C* 17(11): 1097–1107.

Drescher KM and Lynch HT (2005) Tumor infiltrating lymphocytes (TILs): Lessons learned in 30 years of study. *Clinical and Applied Immunology Reviews* 5: 149–166.

Droeser R, Obermann EC, Wolf AM, Wallner S, Wolf D and Tzankov A (2013) Negligible nuclear FOXP3 expression in breast cancer epithelial cells compared with FOXP3-positive T cells. *Clinical Breast Cancer* 13(4): 264–270.

Dunn GP, Bruce AT, Ikeda H, Old LJ and Schreiber RD (2002) Cancer immunoediting: from immunosurveillance to tumor escape. *Nature Immunology* 3(11): 991–998.

Dunn GP, Old LJ and Schreiber RD (2004) The immunobiology of cancer immunosurveillance and immunoediting. *Immunity* 21: 137–148.

Edsparr K, Speetjens FM, Mulder-Stapel A, Goldfarb RH, Basse PH, Lennernäs B, Kuppen PJK, and Albertsson P (2010) Effects of IL-2 on MMP expression in freshly isolated human NK cells and the IL-2-independent NK cell line YT1. *Journal of Immunotherapy* 33(5): 475–481.

Edsparr K, Basse PH, Goldfarb RH and Albertsson P (2011) Matrix metalloproteinases in cytotoxic lymphocytes impact on tumour infiltration and immunomodulation. *Cancer Microenvironment* (4): 351–360.

Elliott RL and Blobe GC (2005) Role of transforming growth factor beta in human cancer. *Journal of Clinical Oncology* 23(9): 2078–2093.

Elstner E, Muller C, Koshizuka K, Wimmilianson EA, Park D, Asou H, Shintaku P, Said JW, Heber D and Koeffler HP (1998) Ligands for peroxisome proliferator-activated receptor y and retinoic acid receptor inhibit growth and induce apoptosis of human breast cancer cells in vitro and in BNX mice. *Proceedings of the National Academy of Sciences of the United States of America* 95(July): 8806–8811.

Emens LA, Silverstein SC, Khleif S, Marincola FM and Galon J (2012) Toward integrative cancer immunotherapy: targeting the tumor microenvironment. *Journal of Translational Medicine* 10(1): 70 (doi: 10.1186/1479-5876-10-70)

Engelmann K, Shen H and Finn OJ (2008) MCF7 side population cells with characteristics of cancer stem/progenitor cells express the tumor antigen MUC1. *Cancer Research* 68: 2419–2426.

Farag SS and Caligiuri MA (2006) Human natural killer cell development and biology. *Blood Reviews* 20: 123–137.

Fauriat C, Long EO, Ljunggren HG, Bryceson YT (2010) Regulation of human NK-cell cytokine and chemokine production by target cell recognition. *Blood* 115(11): 2167–2176.

Feder-Mengus C, Ghosh S, Reschner A, Martin I, Spagnoli GC (2008) New dimensions in tumor immunology: what does 3D culture reveal? *Trends in Molecular Medicine* 14(8): 333–340.

Fiore E, Fusco C, Romero P and Stamenkovic I (2002) Matrix metalloproteinase 9 (MMP-9/gelatinase B) proteolytically cleaves ICAM-1 and participates in tumor cell resistance to natural killer cell-mediated cytotoxicity. *Oncogene* 21: 5213–5223.

Foley J, Nickerson NK, Nam S, Tan K, Gilmore JL, Nephew KP and Riese II DJ (2010) EGFR signaling in breast cancer: Bad to the bone. *Seminars in Cell and Developmental Biology* 21(9): 951–960.

Fox BP and Kadpal RP (2004) Invasiveness of breast carcinoma cells and transcript profile: Eph receptors and ephrin ligands as molecular markers of potential diagnostic and prognostic application. *Biochemical and Biophysical Research Communications* 318: 882–892.

Ganapathy V, Ge R, Grazioli A, Xie W, Banach-Petrosky W, Kang Y, Lonning S, McPherson J, Yingling JM, Biswas S, Mundy GR and Reiss M (2010) Targeting the transforming growth factor-β pathway inhibits human basal-like breast cancer metastasis. *Molecular Cancer* 9: 122–138.

Geller M, Cooley S, Judson PL, Ghebre R, Carson LF, Argenta P, Jonson AL, Panoskaltsis-Mortari A, Curtsinger J, McKenna D, Dusenbery K, Bliss R, Downs LS and Miller JS (2011) A phase II study of allogeneic natural killer cell therapy to treat patients with recurrent ovarian and breast cancer. *Cytotherapy* 13(1): 98–107.

Gendler SJ (2001) MUC1, the renaissance molecule. *Journal of Mammary Gland Biology and Neoplasia* 6(3): 339–353.

Geng Y, Chandrasekaran S, Hsu J, Gidwani M, Hughes AD and King MR (2013) Phenotypic switch in blood: effects of pro-inflammatory cytokines on breast cancer cell aggregation and adhesion. *PloS ONE* 8(1): 1–10.

Georgiannos SN, Renaut A, Goode AW and Sheaff M (2003) The immunophenotype and activation status of the lymphocytic infiltrate in human breast cancers, the role of the major histocompatibility complex in cell-mediated immune mechanisms, and their association with prognostic indicators. *Surgery* 134: 827–834.

Ghiringhelli F, Ménard C, Terme M, Flament C, Taieb J, Chaput N, Puig PE, Novault S, Escudier B, Vivier E, Lecesne A, Robert C, Blay J, Bernard J, Caillat-Zucman S, Freitas A, Tursz T, Wagner-Ballon O, Capron C, Vainchencker W, Martin F and Zitvogel L (2005) CD4 CD25 regulatory T cells inhibit natural killer cell functions in a transforming growth factor-β-dependent manner. *The Journal of Experimental Medicine* 202(8): 1075–1085.

Gil JF, Augustine TN and Hosie MJ. (2013) Anastrozole and RU486: Effects on estrogen receptor α and Mucin 1 expression and correlation in the MCF-7 breast cancer cell line. *Acta Histochemica* 115: 851–857.

Giricz O, Calvo V, Pero SC, Krag DN, Sparano JA and Kenny PA (2012) GRB7 is required for triple-negative breast cancer cell invasion and survival. *Breast Cancer Research and Treatment* 133: 607–615.

Gisterek I, Frydecka I, Świątoniowski G, Fidler S and Kornafel J (2008) Tumour-infiltrating CD4 and CD8 T lymphocytes in breast cancer. *Reports of Practical Oncology and Radiotherapy* 13(4): 205–208.

Gomes LR, Terra LF, Wailemann RAM, Labriola L and Sogayar MC (2012) TGF-b1 modulates the homeostasis between MMPs and MMP inhibitors through p38 MAPK and ERK1/2 in highly invasive breast cancer cells. *BMC Cancer* 12:26 (doi: 10.1186/1471-2407-12-26).

Gomis RR and Massague J (2006) The logic of TGFb signaling. *FEBS Letters* 580: 2811–2820.

Graham JD, Mote PA, Salagame U, Balleine RL, Huschtscha LI and Clarke CL (2009) Hormone-responsive model of primary human breast epithelium. *Journal of Mammary Gland Biology and Neoplasia* 14: 367–379.

Gumuskaya B, Alper M, Hucumenoglu S, Altundag K, Uner A and Guler G (2010) EGFR expression and gene copy number in triple-negative breast carcinoma. *Cancer Genetics and Cytogenetics*. 203(2): 222–229.

Han J, Chang H, Giricz O, Lee GY, Baehner FL, Gray JW, Bissell MJ, Kenny PA and Parvin B (2010) Molecular predictors of 3D morphogenesis by breast cancer cell lines in 3D culture. *PLoS Computational Biology* 6(2): e1000684 (doi: 10.1371/journal.pcbi.1000684).

Howell S, Johnston SRD and Howell A (2004) The use of selective estrogen receptor modulators and selective estrogen receptor down-regulators in breast cancer. *Best Practice & Research Clinical Endocrinology & Metabolism* 18(1): 47 –66.

Herrera MB, Bruno S, Buttiglieri S, Tetta C, Gatti S, Deregibus MC, Bussolati B and Camussi G (2006) Isolation and characterization of a stem cell population from adult human liver. *Stem Cells* 24: 2840–2850.

Hiraga T, Ito S and Nakamura H (2011) Side population in MDA-MB-231 human breast cancer cells exhibits cancer stem cell-like properties without higher bone-metastatic potential. *Oncology Reports* 25(1): 289–296.

Honma S, Shimodaira K, Shimizu Y, Tsuchiya N, Saito H, Yanaihara T, Okai T (2002) The influence of inflammatory cytokines on estrogen production and cell proliferation in human breast cancer cells. *Endocrine Journal* 49:371–7.

Hoover RG, Gullickson G and Kornbluth J (2012) Natural killer lytic-associated molecule plays a role in controlling tumor dissemination and metastasis. *Frontiers in Immunology* 3:393 (doi: 10.3389/fimmu.2012.0039).

Hsiao Y, Liao K, Hung S and Chu R (2004) Tumor-infiltrating lymphocyte secretion of IL-6 antagonizes tumor-derived TGF-β1 and restores the lymphokine-activated killing activity 1. *The Journal of Immunology* 172: 1508–1514.

Ichim C V (2005) Revisiting immunosurveillance and immunostimulation: Implications for cancer immunotherapy. *Journal of Translational Medicine* 3(13): 8–21.

Jiang X and Shapiro DJ (2013) The immune system and inflammation in breast cancer. *Molecular and Cellular Endocrinology* Article in press (doi: 10.1016/j.mce.2013.06.003).

Jin Q, Yuan LX, Boulbes D, Baek JM, Wang YN, Gomez-cabello D, Hawke DH, Yeung SC, Lee MH, Hortobagyi GN, Hung MC and Esteva FJ (2010) Fatty acid synthase phosphorylation : a novel therapeutic target in HER2-overexpressing breast cancer cells. *Breast Cancer Research* 12(6): R96 (doi: 10.1186/bcr2777).

Jonuleit H and Schmitt E (2003) The regulatory T cell family: distinct subsets and their interrelations. *The Journal of Immunology* 171: 6323–6327.

June CH (2007) Principles of adoptive T cell cancer therapy. *The Journal of Clinical Investigation* 117: 1204–1212.

Kao J, Salari K, Bocanegra M, Choi YL, Girard L, Gandhi J, Kwei KA, Hernandez-Boussard T, Wang P, Gazdar AF, Minna JD and Pollack JR (2009) Molecular profiling of breast cancer cell lines defines relevant tumor models and provides a resource for cancer gene discovery. *PLoS ONE* 4(7): e6146 (doi: 10.1371/journal.pone.0006146).

Kampa M, Pelekanou V, Notas G, Stathopoulos EN and Castanas E (2013) The estrogen receptor: two or more molecules, multiple variants, diverse localizations, signaling and functions. Are we undergoing a paradigm-shift as regards their significance in breast cancer? *Hormones* 12(1): 69–85.

Keller S, Sanderson MP, Stoeck A and Altevogt P (2006) Exosomes: From biogenesis and secretion to biological function. *Immunology Letters* 107: 102–108.

Kenny PA, Lee GY Myers CA, Neve RM, Semeiks JR, Spellman PT, Lorenz K and Lee EH (2007) The morphologies of breast cancer cell lines in three-dimensional assays correlate with their profiles of gene expression. *Molecular Oncology* 1(1): 84–96.

Kim J B (2005) Three-dimensional tissue culture models in cancer biology. *Seminars in Cancer Biology* 15(5): 365–77.

Kim SS, Ruiz VE, Carroll JD and Moss SF (2011) Helicobacter pylori in the pathogenesis of gastric cancer and gastric lymphoma. *Cancer Letters* 305: 228–238.

Khodarev NN, Pitroda SP, Beckett MA, Macdermed DM, Huang L, Kufe DW and Weichselbaum RR (2009) MUC1-induced transcriptional programs associated with tumorigenesis predict outcome in breast and lung cancer. *Cancer Research* 69(7): 2833–2837.

Kirkwood JM, Butterfield LH, Tarhini AA, Zarour H, Kalinski P and Ferrone S (2012) Immunotherapy of cancer in 2012. *CA: A Cancer Journal for Clinicians* 62: 309–335.

Kleinman HK and Martin GR (2005) Matrigel: Basement membrane matrix with biological activity. *Seminars in Cancer Biology* 15: 378–386.

Klinge CM, Radde BN, Imbert-Fernandez Y, Teng Y, Ivanova MM, Abner SM and Martin A L (2011) Targeting the intracellular MUC1 C-terminal domain inhibits proliferation and estrogen receptor transcriptional activity in lung adenocarcinoma cells. *Molecular Cancer Therapeutics* 10(11): 2062–2071.

Koch J, Steinle A, Watzl C and Mandelboim O (2013) Activating natural cytotoxicity receptors of natural killer cells in cancer and infection. *Trends in Immunology* 34(4): 182–91.

Kon J, Ooe H, Oshima H, Kikkawa Y and Mitaka T (2006) Expression of CD44 in rat hepatic progenitor cells. *Journal of Hepatology* 45: 90–98.

Konowalchuk JD and Agrawal B (2012) MUC1 mucin is expressed on human T-regulatory cells: Function in both co-stimulation and co-inhibition. *Cellular Immunology* 272(2): 193–199.

Korpal M and Kang Y (2010) Targeting the transforming growth factor-b signalling pathway in metastatic cancer *European Journal of Cancer* 46: 1232–1240.

Krause S, Maffini M V, Soto AM and Sonnenschein C (2010) The microenvironment determines the breast cancer cells' phenotype: organization of MCF7 cells in 3D cultures. *BMC Cancer* (10): 263–276.

Kruger W and Apffelstaedt J (2007) Young breast cancer patients in the developing world: incidence, choice of surgical treatment and genetic factors. *SA Family Practice* 49(9): 18–24.

Kubiczkova L, Sedlarikova L, Hajek R and Sevcikova S (2012) TGF-β – an excellent servant but a bad master. *Journal of Translational Medicine* 10: 1183–1207.

Kumar R, Wang R, Mazumdar A, Talukder AH, Mandal M, Yang Z, Bagheri-Yarmand R, Sahin A, Hortobagyi GN, Adam L, Barnes CJ and Vadlamudi RK (2002) A naturally occurring MTA1 variant sequesters oestrogen receptor-a in the cytoplasm. *Nature* 418(August): 256–260.

Le Bitoux M-A and Stamenkovic I (2008) Tumor-host interactions: the role of inflammation. *Histochemistry and Cell Biology* 130: 1079–1090.

Lacunza E, Baudis M, Colussi AG, Segal-Eiras A, Croce M V and Abba MC (2010) MUC1 oncogene amplification correlates with protein overexpression in invasive breast carcinoma cells. *Cancer Genetics and Cytogenetics* 201(2): 102–110.

Lee GY, Kenny PA, Lee EH and Bissell MJ (2007) 3D culture models of normal and malignant breast epithelial cells. *Nature Methods* 4(4): 359–365.

Lee SK, Kim JY, Jang BW, Hur SE, Na BJ, Lee M, Fukui A, Gilman-Sachs A and Kwak-Kim J (2011) Foxp3(high) and Foxp3(low) Treg cells differentially correlate with T helper 1 and natural killer cells in peripheral blood. *Human immunology* 72(8): 621–6.

Lechner M, Lirk P and Rieder J (2005) Inducible nitric oxide synthase (iNOS) in tumor biology: The two sides of the same coin. *Seminars in Cancer Biology* 15: 277–289.

Leonard WJ (2008) Type I cytokines and interferons and their receptors. In (Ed. Paul WE) *Fundamental Immunology 6th Ed.* Lippincott Williams and Wilkins. Philadelphia, USA. Pp706–749.

Lester SC. (2010). The Breast. In (Ed. Kumar V, Abbas AK, Fausto N and Aster JC) *Robbins and Cotran Pathologic Basis of Disease 8th Ed.* Saunders Elsevier. Philadelphia, USA. Pp1066–1095.

Lesterhuis WJ, Haanen JBAG and Punt CJA (2011) Cancer immunotherapy – revisited. *Nature Reviews Drug Discovery* 10: 591–600.

Levano KS, Jung EH and Kenny PA (2011) Breast cancer subtypes express distinct receptor repertoires for tumor-associated macrophage derived cytokines. *Biochemical and Biophysical Research Communications* 411: 107–110.

Levitzki A and Klein S (2010) Signal transduction therapy of cancer. *Molecular Aspects of Medicine* 31(4): 287–329.

Li L and Lu Y (2011) Optimizing a 3D culture system to study the interaction between epithelial breast cancer and its surrounding fibroblasts. *Journal of Cancer* 2: 458–466.

Lin S, Makino K, Xia W, Matin A, Wen Y, Kwong KY, Bourguignon L and Hung M (2001) Nuclear localization of EGF receptor and its potential new role as a transcription factor. *Nature Cell Biology* 3(September): 802–808.

Lorusso G and Rüegg C (2008) The tumor microenvironment and its contribution to tumor evolution toward metastasis. *Histochemistry and Cell Biology* 130: 1091–1103.

Macchetti AH, Marana HRC, Silva JS, De Andrade JM, Ribeiro-Silva A and Bighetti S (2006) Tumor-infiltrating CD4+ T lymphocytes in early breast cancer reflect lymph node involvement. *Clinics* 61(3): 203–208.

Malmberg K-J and Ljunggren H (2006) Escape from immune- and nonimmune-mediated tumor surveillance. *Seminars in Cancer Biology* 16(1): 16–31.

Mamessier E, Sylvain A, Thibult M, Houvenaeghel G, Jacquemier J, Castellano R, Gonçalves A, André P, Romagné F, Thibault G, Viens P, Birnbaum D, Bertucci F, Moretta A and Olive D (2011) Human breast cancer cells enhance self tolerance by promoting evasion from NK cell antitumor immunity. *The Journal of Clinical Investigation* 121(9): 3609–3622.

Mamessier E, Pradel LC, Thibult M-L, Drevet C, Zouine A, Jacquemier J, Houvenaeghel G, Bertucci F, Birnbaum D and Olive D (2013) Peripheral blood NK cells from breast cancer patients are tumor-induced composite subsets. *The Journal of Immunology* 190(5): 2424–36.

Mandapathil M, Lang S, Gorelik E and Whiteside TL (2009) Isolation of functional human regulatory T cells (Treg) from the peripheral blood based on the CD39 expression. *Journal of Immunological Methods* 346(1-2): 55–63.

Mantovani A, Savino B, Locati M, Zammataro L, Allavena P and Bonecchi R (2010) The chemokine system in cancer biology and therapy. *Cytokine and Growth Factor Reviews* 21(1): 27–39.

Meadows SK, Eriksson M, Barber A and Sentman CL (2006) Human NK cell IFN-gamma production is regulated by endogenous TGF-b. *International Immunopharmacology* 6: 1020–1028.

Miller JS (2001) The biology of natural killer cells in cancer, infection, and pregnancy. *Experimental Hematology* 29: 1157–1168.

Mitchell S, Abel P, Madaan S, Jeffs J, Chaudhary K, Stamp G and Lalani EN (2002) Androgen-dependent regulation of human MUC1 mucin expression. *Neoplasia* 4(1): 9–18.

Mizoi T, Ohtani H, Miyazono K, Miyazawa M, Matsuno S and Nagura H (1993) Immunoelectron microscopic localization of transforming growth factor β1 and latent transforming growth factor β1 binding protein in human gastrointestinal carcinomas: qualitative difference between cancer cells and stromal cells. *Cancer Research* 53: 183–190.

Moreno M, Bontkes HJ, Scheper RJ, Kenemans P, Verheijen R and von Mensdirff-Pouilly S (2007) High level of MUC1 in serum of ovarian and breast cancer patients

inhibits huHMFG-1 dependent cell-mediated cytotoxicity (ADCC). *Cancer Letters* 257: 47–55.

Moretta L (2010) Dissecting CD56^{dim} NK cells. *Blood* 116: 3689–3691.

Mougiakakos D, Choudhury A, Lladser A, Kiessling R and Johansson CC (2010) Regulatory T cells in cancer. *Advances in Cancer Research* 107:57–117.

Moustakas A and Heldin P (2014) TGFβ and matrix-regulated epithelial to mesenchymal transition. *Biochemica et Biophysica Acta* 1840(8): 2621–2634.

Mozaffari F, Lindemalm C, Choudhury A, Granstam-Björneklett H, Helander I, Lekander M, Mikaelsson E, Nilsso B, Ojutkangas M-L, Osterborg A, Bergkvist L and Mellstedt H (2007) NK-cell and T-cell functions in patients with breast cancer: effects of surgery and adjuvant chemo- and radiotherapy. *British Journal of Cancer* 97: 105–111.

Mukhopadhyay P, Chakraborty S, Ponnusamy MP, Lakshmanan I, Jain M and Batra SK (2011) Mucins in the pathogenesis of breast cancer: Implications in diagnosis, prognosis and therapy. *Biochemica et Biophysica Acta* 1815(2): 224–240.

Muranski P, Boni A, Wrzesinski C, Citrin DE, Rosenberg SA, Childs R and Restifo NP (2006) Increased intensity lymphodepletion and adoptive immunotherapy – how far can we go? *Nature Clinical Practice Oncology* 3(12)**:** 668–681.

Muul LM, Spiess PJ, Director EP and Rosenberg SA (1987) Identification of specific cytolytic immune responses against autologous tumor in humans bearing malignant melanoma. *The Journal of Immunology* 138(3): 989–995.

Naber HPH, ten Dijke P, Pardali E (2008) Role of TGF-β in the tumor stroma. *Current Cancer Drug Targets* 8:466–7.

Nath S and Mukherjee P (2014) MUC1: a multifaceted oncoprotein with a key role in cancer progression. *Trends in Molecular Medicine* 20(6):332–342.

Neve RM, Chin K, Fridlyand J, Yeh J, Baehner FL, Fevr T, Clark L, Bayani N, Coppe J, Tong F, Speed T, Spellman PT, Devries S, Lapuk A, Wang NJ, Kuo W, Stilwell JL, Pinkel D, Albertson DG, Waldman FM, Mccormick F, Dickson RB, Johnson MD, Lippman M, Ethier S, Gazdar A and Gray JW (2006) A collection of breast cancer cell lines for the study of functionally distinct cancer subtypes. *Cancer Cell* 10(December): 515–527.

Nicolini A, Carpi A and Rossi G (2006) Cytokines in breast cancer. *Cytokine & Growth Factor Reviews* 17: 325–337.

Nicolini A and Carpi A (2008) Immune manipulation of advanced breast cancer: an interpretative model of the relationship between immune system and tumor cell biology. *Medicinal Research Reviews* 29(3): 436–471.

Nyga A, Cheema U and Loizidou M (2011) 3D tumour models: novel in vitro approaches to cancer studies. *Journal of Cell Communication and Signalling* 5: 239–248.

Olsen CJ, Moreira J, Lukanidin EM and Ambartsumian NS (2010) Human mammary fibroblasts stimulate invasion of breast cancer cells in a three-dimensional culture and increase stroma development in mouse xenografts. *BMC Cancer* (10): 444–470.

Ozanne BW, Spence HJ, McGarry LC and Hennigan RF (2007) Transcription factors control invasion: AP-1 the first among equals. *Oncogene* 26: 1–10.

Pahwa R, Jaggaiahgari S, Pahwa S, Inverardi L, Tzakis A and Ricordi C (2010) Isolation and expansion of human natural T regulatory cells for cellular therapy. *Journal of Immunological Methods* 363: 67–79.

Parish CR (2003) Cancer immunotherapy: The past, the present and the future. *Immunology and Cell Biology* 81: 106–113.

Park H, Wakefield LM and Mamura M (2009) Regulation of tumor immune surveillance and tumor immune subversion by TGF-β. *Immune Network* 9(4): 8–12.

Pegram M and Ngo D (2006) Application and potential limitations of animal models utilized in the development of trastuzumab (Herceptin®): A case study. *Advanced Drug Delivery Reviews* 58: 723–734.

Perrot CY, Javelaud D and Mauviel A (2013) Overlapping activities of TGF-β and Hedgehog signaling in cancer: Therapeutic targets for cancer treatment. *Pharmacology and Therapeutics* 137(2): 183–199.

Piersma SJ, Welters MJP and Burg SH Van Der (2008) Tumor-specific regulatory T cells in cancer patients. *Human Immunology* 69: 241–249.

Pinto M, Jacobsen BM and Horwitz KB (2011) An immunohistochemical method to study breast cancer cell subpopulations and their growth regulation by hormones in three-dimensional cultures. *Cell* 2(June): 1–6.

Poincloux R, Collin O, Lizárraga F, Romao M, Debray M, Piel M and Chavrier P (2011) Contractility of the cell rear drives invasion of breast tumor cells in 3D Matrigel. *Proceedings of the National Academy of Sciences of the United States of America* 108(5): 1943–1948.

Pollard JW, Iyengar P, Combs TP, Shah SJ, Albanese C, Flanagan L, Tenniswood MP, Guha C, Lisanti MP, Pestell RG and Scherer PE (2003) Adipocyte-secreted factors synergistically promote mammary tumorigenesis through induction of anti-apoptotic transcriptional programs and proto-oncogene stabilization. *Oncogene* 22: 6408–6423.

Pooi P, Mohammad R, Ibrahim N, Ithnin H, Abdullah M, Davis WC and Seow HF (2006) Phenotyping of lymphocytes expressing regulatory and effector markers in infiltrating ductal carcinoma of the breast. *Immunology Letters* 102: 229–236.

Prat A and Perou CM (2010) Deconstructing the molecular portraits of breast cancer. *Molecular Oncology* 5(1): 1–19.

Prehn RT (1972) The immune reaction as a stimulator of tumor growth. *Science* 176(April): 170–171.

Prestwich RJ, Errington F, Hatfieldy P, Merrick AE, Ilett EJ, Selby PJ and Melcher AA (2008) The immune system - is it relevant to cancer development, progression and treatment? *Clinical Oncology* 20: 101–112.

Purohit A, Newman SP and Reed MJ (2002) The role of cytokines in regulating estrogen synthesis: implications for the etiology of breast cancer. *Breast Cancer Research* 4: 65–9.

Ralainirina N, Poli A, Michel T, Poos L, Emmanuel A, Hentges F and Zimmer J (2007) Control of NK cell functions by CD4+CD25+ regulatory T cells. *Journal of Leukocyte Biology* 81: 144–153.

Renoir J-M, Marsaud V and Lazennec G (2013) Estrogen receptor signaling as a target for novel breast cancer therapeutics. *Biochemical Pharmacology* 85: 449–465.

Riker AI, Sondak VK, Fishman M, Daud A and Pilon-Thomas S (2005) Current immunotherapy of melanoma. *Clinical and Applied Immunology Reviews* 5: 111–132.

Roberti MP, Mordoh J and Levy EM (2012) Biological role of NK cells and immunotherapeutic approaches in breast cancer. *Frontiers in Immunology* 3:375–382.

Rollins BJ (2006) Inflammatory chemokines in cancer growth and progression. *European Journal of Cancer* 42: 760–767.

Rosenberg SA, Packard BS, Aebersold PM, Soloman D, Topalian SL, Toy ST, Simon P, Lotze MT, Yang JC, Seipp CA, Simpson C, Carter C, Bock S, Schwartzentrubber D, Wei JP and White DE (1988) Use of tumor infiltrating lymphocytes and interleukin-2 in the immunotherapy of patients with metastatic melanoma. Preliminary report. *New England Journal of Medicine* 319: 1676–1680.

Rosenberg SA, Restifo NP, Yang JC, Morgan RA and Dudley ME (2008) Adoptive cell transfer: a clinical path to effective cancer immunotherapy. *Nature Reviews Cancer* 8: 229–308.

Rosenberg SA, Spiess P. and Lafreniere R (1986) A new approach to the adoptive immunotherapy of cancer with tumor-infiltrating lymphocytes. *Science* 233: 1318–1321.

Saitoh M (2011) Transforming growth factor β signaling and epithelial mesenchymal transition in cancer progression. *Journal of Oral Biosciences* 53(1): 57–64.

Sabel MS, Su G, Griffith KA and Chang AE (2010) Intratumoral delivery of encapsulated IL-12, IL-18 and TNF-a in a model of metastatic breast cancer. *Breast Cancer Research and Treatment* 122: 325–336.

Saha B, Jyothi Prasanna S, Chandrasekar B and Nandi D (2010) Gene modulation and immunoregulatory roles of interferon gamma. *Cytokine* 50(1): 1–14.

Sakaguchi S, Sakaguchi N, Asano M, Itoh M and Toda M (1995) Immunologic self-tolerance maintained by activated T cells expressing IL-2 receptor α-chains (CD25). Breakdown of a single mechanism of self-tolerance causes various autoimmune diseases. *The Journal of Immunology* 155: 1151–1164.

Salagianni M, Lekka E, Moustaki A, Iliopoulou EG, Baxevanis CN, Papamichail M and Perez S a (2011) NK cell adoptive transfer combined with Ontak-mediated regulatory T cell elimination induces effective adaptive antitumor immune responses. *Journal of Immunology* 186(6): 3327–3335.

Sanchez C, Le Treut T, Boehrer A, Knoblauch B, Imbert J, Olive D and Costello R (2010) Natural killer cells and malignant haemopathies: a model for the interaction of cancer with innate immunity. *Cancer Immunology, Immunotherapy* 60(1): 1–13.

Sanderson MP, Keller S, Alonso A, Riedle S, Dempsey PJ and Altevogt P (2008) Generation of novel, secreted epidermal growth factor receptor (EGFR/ErbB1) isoforms via metalloprotease-dependent ectodomain shedding and exosome secretion. *Journal of Cellular Biochemistry* 103: 1783–1797.

Selander KS, Li L, Watson L, Merrell M, Dahmen H, Heinrich PC and Harris KW (2004) Inhibition of gp130 signaling in breast cancer blocks constitutive activation of Stat3 and inhibits in vivo malignancy. *Cancer Research* 64: 6924–6933.

Sharan S, Nikhil K and Roy P (2013) Effects of low dose treatment of tributyltin on the regulation of estrogen receptor functions in MCF-7 cells. *Toxicology and Applied Pharmacology* 269: 176–186.

Shyyan R, Masood S, Badwe RA, Errico KM, Liberman L, Ozmen V, Stalsberg H, Vargas H and Vass L (2006) Breast cancer in limited-resource countries: diagnosis and pathology. *The Breast Journal* 12(Supplement 1): S26–S37.

Slamon DJ, Leyland-Jones B, Shak S, Fuchs H, Paton V, Bajamonde A, Fleming T, Eiermann W, Wolter J, Pegram M, Balselga J and Norton L (2001) Use of chemotherapy plus a monoclonal antibody against HER2 for metastatic breast cancer that overexpresses HER2. *New England Journal of Medicine* 344: 783–792.

Smyth MJ, Cretney E, Kelly JM, Westwood JA, Street SEA, Yagita H, Takeda K, van Dommelen, Serani L H Degli-Esposti MA and Hayakawa Y (2005) Activation of NK cell cytotoxicity. *Molecular Immunology* 42: 501–510.

Sung KE, Su X, Berthier E, Pehlke C, Friedl A and Beeb DJ (2013) Understanding the impact of 2D and 3D fibroblast cultures on in vitro breast cancer models. *PLoS ONE* 8(10): 1–13.

Suzuki Y, Sutoh M, Hatakeyama S, Mori K, Yamamoto H, Koie T, Saitoh H, Yamaya K, Funyu T, Habuchi T, Arai Y, Fukuda M, Ohyma C and Tsuboi S (2012) MUC1 carrying core 2 O-glycans as a molecular shield against NK cell attack, promoting bladder tumor metastasis. *International Journal of Oncology* 40(6): 1831–1838.

Swamydas M, Eddy JM, Burg KJL and Dréau D (2010) Matrix compositions and the development of breast acini and ducts in 3D cultures. *In Vitro Cellular and Developmental Biology - Animal* 46: 673–684.

Tate CR, Rhodes LV, Segar HC, Driver JL, Pounder FN, Burow ME and Collins-Burow BM (2012) Targeting triple-negative breast cancer cells with the histone deacetylase inhibitor panobinostat. *Breast Cancer Research* 14(3): R79 (doi: 10.1186/bcr3192).

Tiwari AK and Roy HK (2012) Progress against cancer (1971 – 2011): how far have we come? *Journal of Internal Medicine* 271: 392–399.

Trzonkowski P, Szmit E, Myśliwska J, Dobyszuk A and Myśliwska A (2004) CD4+CD25+ T regulatory cells inhibit cytotoxic activity of T CD8+ and NK lymphocytes in the direct cell-to-cell interaction. *Clinical Immunology* 112: 258–267.

Ueda S, Ogata S, Tsuda H, Kawarabayashi N, Kimura M, Sugiura Y, Tamai S, Matsubara O, Hatsuse K and Mochizuki H (2004) The correlation between cytoplasmic overexpression of epidermal growth factor receptor and tumor aggressiveness. *Pancreas* 29(1): 1–8.

Vaillant F, Lindeman GJ and Visvader JE (2011) Jekyll or Hyde: does Matrigel provide a more or less physiological environment in mammary repopulating assays? *Breast Cancer Research* 13: 108–112.

Vicari AP and Caux C (2002) Chemokines in cancer. *Cytokine & Growth Factor Reviews* 13: 143–154.

Villalba M, Rathore MG, Lopez-royuela N, Krzywinska E, Garaude J and Allende-Vega N (2013) From tumor cell metabolism to tumor immune escape. *The International Journal of Biochemistry & Cell Biology* 45(1): 106–13.

Vitiello PF, Shainheit MG, Allison EM, Adler EP and Kurt RA (2004) Impact of tumor-derived CCL2 on T cell effector function. *Immunology Letters* 91: 239–245.

Walker RA (2009) The Breast. In (Ed. Underwood JCE and Cross SS) *General and Systematic Pathology 5Th Ed*. Elsevier Limited. London, UK. Pp468–495.

Walsh MD, Luckie SM, Cummings MC, Antalis TM and Mcguckin A (2000) Heterogeneity of MUC1 expression by human breast carcinoma cell lines in vivo and in vitro. *Breast Cancer Research and Treatment* 58: 255–266.

Wang RF (2006) Functional control of regulatory T cells and cancer immunotherapy. *Seminars in Cancer Biology* 16: 106–114.

Wang R, Jaw JJ, Stutzman NC, Zou Z and Sun PD (2012) Natural killer cell-produced IFN-γ and TNF-α induce target cell cytolysis through up-regulation of ICAM-1. *Journal of Leukocyte Biology* 91(2): 299–309.

Wei X, Xu H and Kufe D (2006) MUC1 oncoprotein stabilizes and activates estrogen receptor α. *Molecular Cell* 21: 295–305.

Weigelt B and Bissell MJ (2014) The need for complex 3D culture models to unravel novel pathways and identify accurate biomarkers in breast cancer. *Advanced Drug Delivery Reviews*. 2013: 1–10.

Welsh AW, Lannin DR, Young GS, Sherman ME, Figueroa JD, Henry NL, Ryden L, Kim C, Love RR, Schiff R and Rimm DL (2013) Cytoplasmic estrogen receptor in breast cancer. *Clinical Cancer Research* 18(1): 118–126.

West NR, Kost SE, Martin SD, Milne K, Deleeuw RJ, Nelson BH and Watson PH (2013) Tumour-infiltrating FOXP3(+) lymphocytes are associated with cytotoxic immune responses and good clinical outcome in oestrogen receptor-negative breast cancer. *British Journal of Cancer* 108(1): 155–62.

Whiteside TL (2012) What are regulatory T cells (Treg) regulating in cancer and why? *Seminars in Cancer Biology* 22: 327–334.

Whiteside TL, Jost LM and Herberman B (1992) Tumor-infiltrating lymphocytes: potential and limitations to their use for cancer therapy. *Critical Reviews in Oncology/Hematology* 12: 25–47.

Wiemann B and Starnes CO (1994). Coley's toxins, tumor necrosis factor and cancer research: a historical perspective. *Pharmacology and Therapeutics* 64: 529–564.

Wilk E, Kalippke K, Buyny S, Schmidt RE and Jacobs R (2008) New aspects of NK cell subset identification and inference of NK cells' regulatory capacity by assessing functional and genomic profiles. *Immunobiology* 213: 271–283.

Wolf K and Friedl P (2011) Extracellular matrix determinants of proteolytic and non-proteolytic cell migration. *Trends in Cell Biology* 21(12): 736–744.

Wood KJ, Bushell AR and Jones ND (2010). The discovery of immunological tolerance: now more than just a laboratory solution. *The Journal of Immunology* 184(1): 3–4.

Yang L, Pang Y and Moses HL (2010) TGF-beta and immune cells: an important regulatory axis in the tumor microenvironment and progression. *Trends in Immunology* 31(6): 220–227.

Ye Q, Kantonen S and Gomez-Cambronero J (2013) Serum deprivation confers the MDA-MB-231 breast cancer line with an EGFR/JAK3/PLD2 system that maximizes cancer cell invasion. *Journal of Molecular Biology* 425: 755–766.

Yewale C, Baradia D, Vhora I, Patil S and Misra A (2013) Epidermal growth factor receptor targeting in cancer: A review of trends and strategies. *Biomaterials*. 34(34): 8690–8707.

Youlden DR, Cramb SM, Dunn NAM, Muller JM, Pyke CM and Baade PD (2012) The descriptive epidemiology of female breast cancer: An international comparison of screening, incidence, survival and mortality. *Cancer Epidemiology* 36: 237–248.

Yu P and Fu Y (2006) Tumor-infiltrating T lymphocytes: friends or foes? *Laboratory Investigation* 86: 231–245.

Yu X and Machesky LM (2012) Cells assemble invadopodia-like structures and invade into matrigel in a matrix metalloprotease dependent manner in the circular invasion assay. *PLoS ONE* 7(2): e30605 (doi: 10.1371/journal.pone.0030605).

Zhang H and Grizzle WE (2011) Exosomes and cancer: a newly described pathway of immune suppression. *Clinical Cancer Research* 17: 959–964.

Zhou J and Zhong Y (2004) Breast cancer immunotherapy. *Cellular & Molecular Immunology* 1(4): 247–255.

Zuo L, Li W and You S (2010) Progesterone reverses the mesenchymal phenotypes of basal phenotype breast cancer cells via a membrane progesterone receptor mediated pathway. *Breast Cancer Research* 12: R34 (doi: 10.1186/bcr2588).

APPENDIX A

Activation media A

RPMI 1640

0.1% P/S

10% FBS

1µg/ml PHA

0.8ng/ml IL-2

Activation media B

RPMI 1640

0.1% P/S

10% FBS

0.8ng/ml IL-2

Cryopreservation medium

10% DMSO

90% FBS

Sorting buffer (Miltenyi Biotec Magnetic sorting buffer)

1M PBS pH 7.2

0.5% BSA

2mM EDTA

Phosphate buffered saline (PBS)

8.5g NaCl

1.07g Disodium hydrogen orthophosphate

0.39g Sodium dihydrogen orthophosphate dehydrate

1L dH_2O

1M, pH to 7.4. Autoclave to sterilise

PBT

1M PBS

0.1% Tween-20

APPENDIX B

Figure illustrating techniques used for optimization of RNA extraction. All techniques were followed by analysis of RNA yield and integrity.

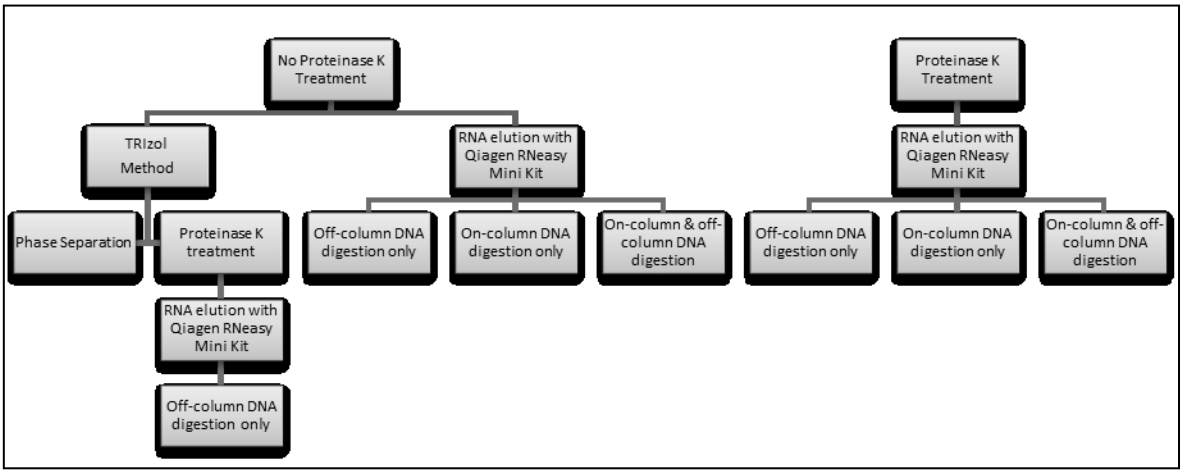

TRIzol technique

Samples were incubated with 150µl TRIzol followed by homogenization using a 21 gauge needle. Samples were centrifuged at 12 000 X *g* for 10 min. The supernatants were then harvested, flash-frozen in liquid nitrogen and stored at -80°C until use. Prior to phase separation, samples were defrosted and incubated at room temperature for 5 min. For phase separation, 30µl chloroform was added to each sample and vigorously shaken for 15 sec, followed by incubation at room temperature for 2 min. Samples were centrifuged at 12 000 X *g* for 15 min at 4°C. This yielded a lower phenol red-chloroform phase, an interphase and an upper aqueous clear phase. The latter was aspirated into a new tube for subsequent RNA precipitation. Each sample was incubated with 75µl 100% isopropanol at room temperature for 10 min, following which samples were centrifuged at 12 000 X *g* for 10 min at 4°C. The resulting supernatant was discarded and the RNA pellet washed in 150µl 75% ethanol. The samples were briefly vortexed and subsequently centrifuged at 7500 X *g* for 5 min at 4°C. The pellet was air-dried followed by resuspension in 30µl RNase-free water. The suspension was thereafter placed on a 60°C dry block heater for 15 min and subsequently stored at -70°C for RNA quality control.

Combined TRIzol-Qiagen RNeasy RNA Purification technique

Samples were defrosted on ice. For disruption of residual Matrigel, 295µl RNAse-free water and 5µl proteinase K were added to samples. Following centrifugation at 8 000 X *g* for 3 min, the supernatant was removed and placed in a 1.5ml eppendorf to which 300µl 70% ethanol was added and mixed by pipetting. Each sample was applied to an RNeasy spin column within a 2ml collection tube and centrifuged at 8 000 X *g* for 15 sec. The flow-through was discarded and 350µl Buffer RW added to the column. The column was centrifuged at 8 000 X *g* for 15 sec and the flow-through discarded.

To elute the RNA, 500µl Buffer RPE was added to the column, centrifuged at 8 000 X *g* for 15sec and the flow-through discarded. A further 500µl Buffer RPE was added to the RNeasy spin column and centrifuged at 8 000 X *g* for 2 min. The column was removed from the collection tube, placed on to a new 2ml collection tube and centrifuged for a further 1 min at 8 000 X *g*. The column was then removed from the collection tube, placed in a new 1.5ml collection tube and 30µl RNAse-free water added to the membrane. The column was centrifuged at 8 000 X *g* for 1min.

For off-column DNA-digestion, 20µl of each RNA elution was incubated with 10µl NEB Buffer, 68µl Sabex water and 2µl NEB DNAse at 37°C on a dry block heater for 10 min. A further 1µl 0.5M EDTA was added to each elution followed by heat-inactivation at 75°C on a dry block heater for 10 min. For RNA clean-up, each sample was adjusted to 100µl with RNase-free water followed by the addition of 350µl Buffer RLT and 250µl ethanol. The sample was mixed by pipetting and up to 750µl placed on to a column in a 2ml collection tube. The column was centrifuged at 8 000 X *g* for 15 sec and the flow-through discarded. A further 500µl Buffer RPE was added to the column, centrifuged at 8 000 X *g* for 15 sec and the flow-through discarded. The column was removed from the collection tube and placed in a new 2ml collection tube, followed by centrifugation at 8 000 X *g* for 1 min. The column was removed from the collection tube and placed into a new 1.5ml collection tube with 30µl RNAse-free water added to the column membrane. The column was centrifuged at 8 000 X *g* for 1 min and the flow-through discarded. The column was centrifuged again at 8 000 X *g* for 1 min. The resulting elutes were stored at -80°C until RNA quality control.

APPENDIX C1

Compensation controls for flow cytometric analysis on the LSR Fortessa.

Rows: **A)** unstained compensation beads; **B)** APC stained beads; **C)** PE stained beads; **D)** PE-Cy.7 stained beads. **Columns**: **1)** scatterplots of SSC vs FSC; **2)** scatterplots gated (black circle) on column 1; **3)** histograms with unstained samples indicated in light blue.

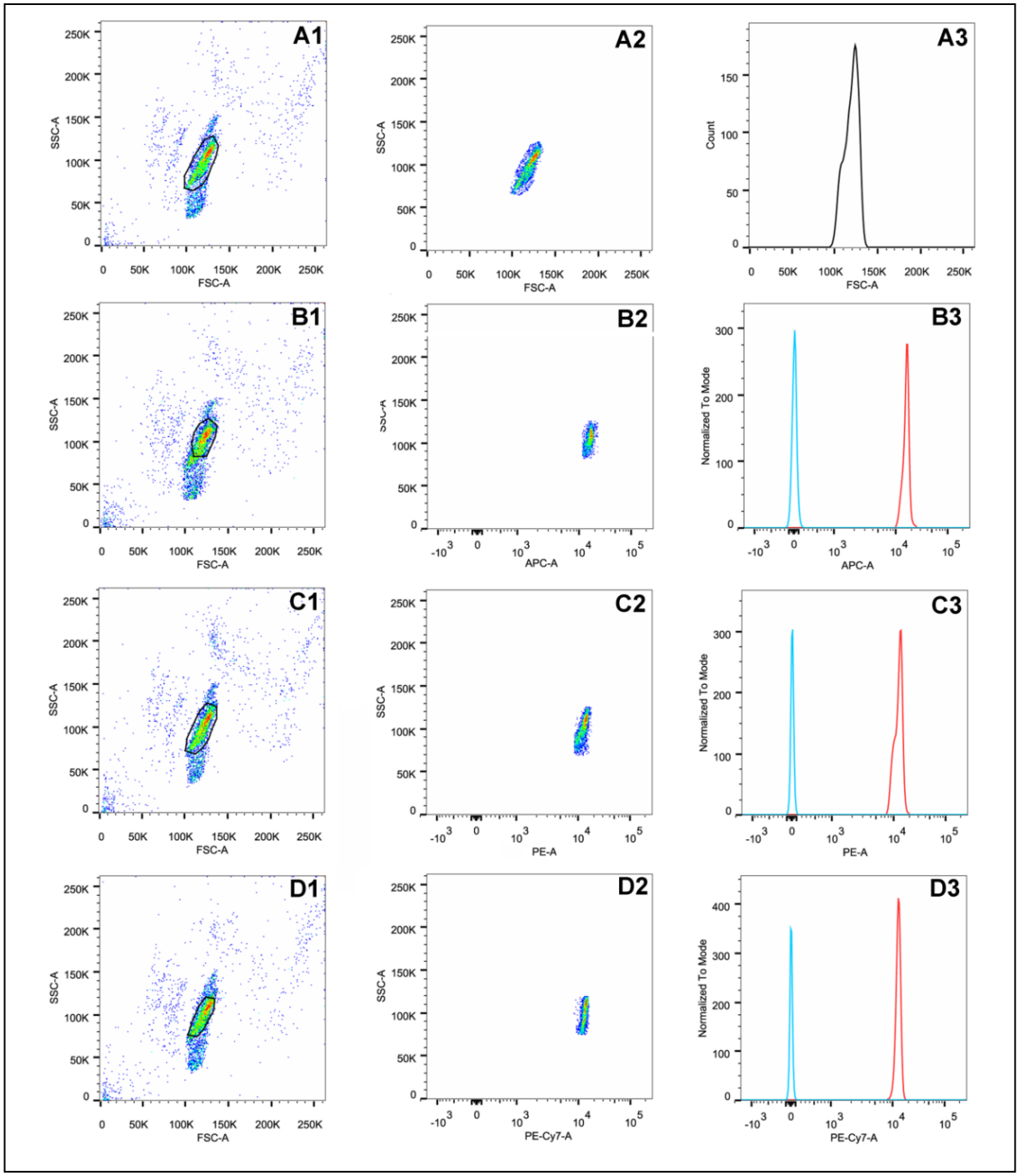

APPENDIX C2

Representative flow cytometric analysis results (FACSCalibur) of **A)** $CD4^{+}CD25^{+}$ T_{REG} lymphocytes and **B)** $NKp46^{+}$ NK cells isolated from PBMCs obtained from density gradient centrifugation using Ficoll-Hypaque.

A

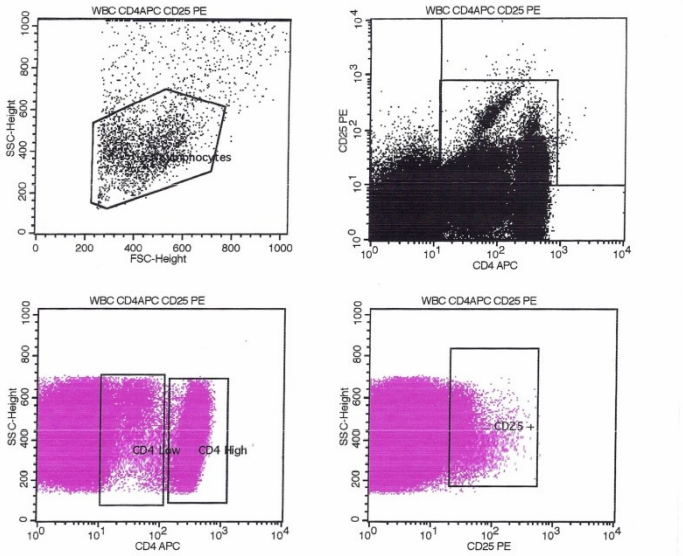

Region Statistics

File: WBC CD4APC CD25 PE
Sample ID: WBC CD4APC CD25 PE
Tube: Untitled
Acquisition Date: 15-Jul-11
Gated Events: 236802
X Parameter: CD4 APC (Log)
Log Data Units: Linear Values
Patient ID: 002
Panel: Untitled Acquisition Tube List
Gate: G1
Total Events: 359700
Y Parameter: SSC-Height (Linear)

Region	Events	% Gated	% Total	X Mean	X Geo Mean	Y Mean	Y Geo Mean	PxPy
Lymphocytes	236802	100.00	65.83	91.36	13.08	412.31	398.52	1, 2
CD4 High	56661	23.93	15.75	360.20	350.48	398.73	383.22	7, 2
CD4 Low	15137	6.39	4.21	25.88	19.88	459.78	441.87	7, 2
CD25 +	9819	4.15	2.73	310.41	158.42	437.79	426.31	4, 2
CD4+CD25+	19286	8.14	5.36	374.80	338.77	438.62	427.54	7, 4

B

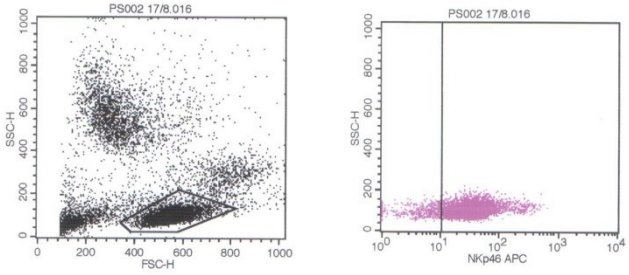

Region Statistics

Region	Events	% Gated	% Total	X Mean	X Geo Mean	Y Mean	Y Geo Mean	PxPy
R2	1174	11.74	11.74	606.15	603.08	200.08	155.80	1, 7
R1	4804	48.04	48.04	557.82	554.13	100.57	97.34	1, 2

Region Statistics

Region	Events	% Gated	% Total	X Mean	X Geo Mean	Y Mean	Y Geo Mean	PxPy
R2	878	18.28	8.78	108.50	89.50	114.34	112.12	1, 7
R1	4804	100.00	48.04	42.79	29.34	100.57	97.34	1, 2

APPENDIX D

Results from Spearman Rank Order Correlations.

Variable	Spearman Rank Order Correlations (Spreadsheet in Sorting Analysis) MD pairwise deleted Marked correlations are significant at p <.05000 PBMC L	CD4+ L	STreg L	SNK L	A1 Treg L	A1 NK L	A2 Treg L	A2 NK L
PBMC L	1.000000	-0.393939	-0.309091	-0.109091	0.683333	0.376572	0.116667	-0.016667
CD4+ L	-0.393939	1.000000	0.866667	0.006061	0.233333	-0.443519	0.666667	-0.357143
STreg L	-0.309091	0.866667	1.000000	0.081818	0.283333	-0.158997	0.733333	0.033333
SNK L	-0.109091	0.006061	0.081818	1.000000	0.083333	0.125524	-0.016667	0.466667
A1 Treg L	0.683333	0.233333	0.283333	0.083333	1.000000	0.284521	0.738095	0.285714
A1 NK L	0.376572	-0.443519	-0.158997	0.125524	0.284521	1.000000	-0.335335	0.598813
A2 Treg L	0.116667	0.666667	0.733333	-0.016667	0.738095	-0.335335	1.000000	-0.033333
A2 NK L	-0.016667	-0.357143	0.033333	0.466667	0.285714	0.598813	-0.033333	1.000000

APPENDIX E1

Results of Kruskal-Wallis ANOVA by Ranks tests followed by Multiple Comparisons Post Hoc tests. Grouping variable: GRFM-conditioned media and Media alone control groups

Kruskal-Wallis ANOVA by Ranks; IL - 1b (Controls in IL Workbook)
Independent (grouping) variable: Culture group
Kruskal-Wallis test: H (1, N= 4) =.6000000 p =.4386

Depend.: IL - 1b	Code	Valid N	Sum of Ranks	Mean Rank
GFRM	101	2	6.000000	3.000000
Media	102	2	4.000000	2.000000

Kruskal-Wallis ANOVA by Ranks; IL-2 (Controls in IL Workbook)
Independent (grouping) variable: Culture group
Kruskal-Wallis test: H (1, N= 4) =0.000000 p =1.000

Depend.: IL-2	Code	Valid N	Sum of Ranks	Mean Rank
GFRM	101	2	5.000000	2.500000
Media	102	2	5.000000	2.500000

Kruskal-Wallis ANOVA by Ranks; IL-6 (Controls in IL Workbook)
Independent (grouping) variable: Culture group
Kruskal-Wallis test: H (1, N= 4) =.1666667 p =.6831

Depend.: IL-6	Code	Valid N	Sum of Ranks	Mean Rank
GFRM	101	2	5.500000	2.750000
Media	102	2	4.500000	2.250000

Kruskal-Wallis ANOVA by Ranks; IL-12 (Controls in IL Workbook)
Independent (grouping) variable: Culture group
Kruskal-Wallis test: H (1, N= 4) =2.400000 p =.1213

Depend.: IL-12	Code	Valid N	Sum of Ranks	Mean Rank
GFRM	101	2	7.000000	3.500000
Media	102	2	3.000000	1.500000

Kruskal-Wallis ANOVA by Ranks; IL-12 (Controls in IL Workbook)
Independent (grouping) variable: Culture group
Kruskal-Wallis test: H (1, N= 4) =2.400000 p =.1213

Depend.: IL-12	Code	Valid N	Sum of Ranks	Mean Rank
GFRM	101	2	7.000000	3.500000
Media	102	2	3.000000	1.500000

Kruskal-Wallis ANOVA by Ranks; IFN-g (Controls in IL Workbook)
Independent (grouping) variable: Culture group
Kruskal-Wallis test: H (1, N= 4) =1.500000 p =.2207

Depend.: IFN-g	Code	Valid N	Sum of Ranks	Mean Rank
GFRM	101	2	6.500000	3.250000
Media	102	2	3.500000	1.750000

Kruskal-Wallis ANOVA by Ranks; TNF-a (Controls in IL Workbook)
Independent (grouping) variable: Culture group
Kruskal-Wallis test: H (1, N= 4) =.6000000 p =.4386

Depend.: TNF-a	Code	Valid N	Sum of Ranks	Mean Rank
GFRM	101	2	6.000000	3.000000
Media	102	2	4.000000	2.000000

Kruskal-Wallis ANOVA by Ranks; CCL2 (Controls in IL Workbook)
Independent (grouping) variable: Culture group
Kruskal-Wallis test: H (1, N= 4) =2.400000 p =.1213

Depend.: CCL2	Code	Valid N	Sum of Ranks	Mean Rank
GFRM	101	2	7.000000	3.500000
Media	102	2	3.000000	1.500000

Kruskal-Wallis ANOVA by Ranks; CCL4 (Controls in IL Workbook)
Independent (grouping) variable: Culture group
Kruskal-Wallis test: H (1, N= 4) =0.000000 p =1.000

Depend.: CCL4	Code	Valid N	Sum of Ranks	Mean Rank
GFRM	101	2	5.000000	2.500000
Media	102	2	5.000000	2.500000

Kruskal-Wallis ANOVA by Ranks; CXCL8 (Controls in IL Workbook)
Independent (grouping) variable: Culture group
Kruskal-Wallis test: H (1, N= 4) =0.000000 p =1.000

Depend.: CXCL8	Code	Valid N	Sum of Ranks	Mean Rank
GFRM	101	2	5.000000	2.500000
Media	102	2	5.000000	2.500000

Multiple Comparisons p values (2-tailed); IL - 1b (Controls in IL Workbook)
Independent (grouping) variable: Culture group
Kruskal-Wallis test: H (1, N= 4) =.6000000 p =.4386

Depend.: IL - 1b	GFRM R:3.0000	Media R:2.0000
GFRM		0.438578
Media	0.438578	

Multiple Comparisons p values (2-tailed); IL-2 (Controls in IL Workbook)
Independent (grouping) variable: Culture group
Kruskal-Wallis test: H (1, N= 4) =0.000000 p =1.000

Depend.: IL-2	GFRM R:2.5000	Media R:2.5000
GFRM		1.000000
Media	1.000000	

Multiple Comparisons p values (2-tailed); IL-6 (Controls in IL Workbook)
Independent (grouping) variable: Culture group
Kruskal-Wallis test: H (1, N= 4) =.1666667 p =.6831

Depend.: IL-6	GFRM R:2.7500	Media R:2.2500
GFRM		0.698535
Media	0.698535	

Multiple Comparisons p values (2-tailed); IL-12 (Controls in IL Workbook)
Independent (grouping) variable: Culture group
Kruskal-Wallis test: H (1, N= 4) =2.400000 p =.1213

Depend.: IL-12	GFRM R:3.5000	Media R:1.5000
GFRM		0.121335
Media	0.121335	

Multiple Comparisons p values (2-tailed); IFN-g (Controls in IL Workbook)
Independent (grouping) variable: Culture group
Kruskal-Wallis test: H (1, N= 4) =1.500000 p =.2207

Depend.: IFN-g	GFRM R:3.2500	Media R:1.7500
GFRM		0.245278
Media	0.245278	

Multiple Comparisons p values (2-tailed); TNF-a (Controls in IL Workbook)
Independent (grouping) variable: Culture group
Kruskal-Wallis test: H (1, N= 4) =.6000000 p =.4386

Depend.: TNF-a	GFRM R:3.0000	Media R:2.0000
GFRM		0.438578
Media	0.438578	

APPENDIX E2

Results of Kruskal-Wallis ANOVA by Ranks tests followed by Multiple Comparisons Post Hoc tests. Grouping variable: Cell lines

Kruskal-Wallis ANOVA by Ranks; IL-1b
Independent (grouping) variable: Cell line
Kruskal-Wallis test: H (2, N= 61) =33.07705 p =.0000

Depend.: IL-1b	Code	Valid N	Sum of Ranks	Mean Rank
MCF7	101	33	707.500	21.43939
MDA	102	24	1129.000	47.04167
Control	105	4	54.500	13.62500

Kruskal-Wallis ANOVA by Ranks; IL-2
Independent (grouping) variable: Cell line
Kruskal-Wallis test: H (2, N= 61) =25.86803 p =.0000

Depend.: IL-2	Code	Valid N	Sum of Ranks	Mean Rank
MCF7	101	33	731.500	22.16667
MDA	102	24	1087.000	45.29167
Control	105	4	72.500	18.12500

Kruskal-Wallis ANOVA by Ranks; IL-6
Independent (grouping) variable: Cell line
Kruskal-Wallis test: H (2, N= 61) =36.93550 p =.0000

Depend.: IL-6	Code	Valid N	Sum of Ranks	Mean Rank
MCF7	101	33	745.000	22.57576
MDA	102	24	1132.000	47.16667
Control	105	4	14.000	3.50000

Kruskal-Wallis ANOVA by Ranks; IL-12
Independent (grouping) variable: Cell line
Kruskal-Wallis test: H (2, N= 61) =19.07698 p =.0001

Depend.: IL-12	Code	Valid N	Sum of Ranks	Mean Rank
MCF7	101	33	801.000	24.27273
MDA	102	24	1031.000	42.95833
Control	105	4	59.000	14.75000

Kruskal-Wallis ANOVA by Ranks; IFN-g
Independent (grouping) variable: Cell line
Kruskal-Wallis test: H (2, N= 61) =32.12823 p =.0000

Depend.: IFN-g	Code	Valid N	Sum of Ranks	Mean Rank
MCF7	101	33	688.000	20.84848
MDA	102	24	1127.000	46.95833
Control	105	4	76.000	19.00000

Kruskal-Wallis ANOVA by Ranks; TNF-a
Independent (grouping) variable: Cell line
Kruskal-Wallis test: H (2, N= 61) =30.51030 p =.0000

Depend.: TNF-a	Code	Valid N	Sum of Ranks	Mean Rank
MCF7	101	33	709.500	21.50000
MDA	102	24	1116.000	46.50000
Control	105	4	65.500	16.37500

Kruskal-Wallis ANOVA by Ranks; CCL2
Independent (grouping) variable: Cell line
Kruskal-Wallis test: H (2, N= 61) =21.04893 p =.0000

Depend.: CCL2	Code	Valid N	Sum of Ranks	Mean Rank
MCF7	101	33	867.000	26.27273
MDA	102	24	1009.000	42.04167
Control	105	4	15.000	3.75000

Kruskal-Wallis ANOVA by Ranks; CCL4
Independent (grouping) variable: Cell line
Kruskal-Wallis test: H (2, N= 61) =7.056693 p =.0294

Depend.: CCL4	Code	Valid N	Sum of Ranks	Mean Rank
MCF7	101	33	1028.000	31.15152
MDA	102	24	827.000	34.45833
Control	105	4	36.000	9.00000

Kruskal-Wallis ANOVA by Ranks; CXCL8
Independent (grouping) variable: Cell line
Kruskal-Wallis test: H (2, N= 61) =34.56212 p =.0000

Depend.: CXCL8	Code	Valid N	Sum of Ranks	Mean Rank
MCF7	101	33	768.000	23.27273
MDA	102	24	1113.000	46.37500
Control	105	4	10.000	2.50000

Multiple Comparisons p values (2-tailed); IL-1b
Independent (grouping) variable: Cell line
Kruskal-Wallis test: H (2, N= 61) =33.07705 p =.0000

Depend.: IL-1b	MCF7 R:21.439	MDA R:47.042	Control R:13.625
MCF7		0.000000	1.000000
MDA	0.000000		0.001474
Control	1.000000	0.001474	

Multiple Comparisons p values (2-tailed); IL-2
Independent (grouping) variable: Cell line
Kruskal-Wallis test: H (2, N= 61) =25.86803 p =.0000

Depend.: IL-2	MCF7 R:22.167	MDA R:45.292	Control R:18.125
MCF7		0.000004	1.000000
MDA	0.000004		0.013813
Control	1.000000	0.013813	

Multiple Comparisons p values (2-tailed); IL-6
Independent (grouping) variable: Cell line
Kruskal-Wallis test: H (2, N= 61) =36.93550 p =.0000

Depend.: IL-6	MCF7 R:22.576	MDA R:47.167	Control R:3.5000
MCF7		0.000001	0.127210
MDA	0.000001		0.000016
Control	0.127210	0.000016	

Multiple Comparisons p values (2-tailed); IL-12
Independent (grouping) variable: Cell line
Kruskal-Wallis test: H (2, N= 61) =19.07698 p =.0001

Depend.: IL-12	MCF7 R:24.273	MDA R:42.958	Control R:14.750
MCF7		0.000262	0.932954
MDA	0.000262		0.009778
Control	0.932954	0.009778	

Multiple Comparisons p values (2-tailed); IFN-g
Independent (grouping) variable: Cell line
Kruskal-Wallis test: H (2, N= 61) =32.12823 p =.0000

Depend.: IFN-g	MCF7 R:20.848	MDA R:46.958	Control R:19.000
MCF7		0.000000	1.000000
MDA	0.000000		0.010634
Control	1.000000	0.010634	

Multiple Comparisons p values (2-tailed); TNF-a
Independent (grouping) variable: Cell line
Kruskal-Wallis test: H (2, N= 61) =30.51030 p =.0000

Depend.: TNF-a	MCF7 R:21.500	MDA R:46.500	Control R:16.375
MCF7		0.000000	1.000000
MDA	0.000000		0.005033
Control	1.000000	0.005033	

Multiple Comparisons p values (2-tailed); CCL2
Independent (grouping) variable: Cell line
Kruskal-Wallis test: H (2, N= 61) =21.04893 p =.0000

Depend.: CCL2	MCF7 R:26.273	MDA R:42.042	Control R:3.7500
MCF7		0.002789	0.049688
MDA	0.002789		0.000195
Control	0.049688	0.000195	

Multiple Comparisons p values (2-tailed); CCL4
Independent (grouping) variable: Cell line
Kruskal-Wallis test: H (2, N= 61) =7.056693 p =.0294

Depend.: CCL4	MCF7 R:31.152	MDA R:34.458	Control R:9.0000
MCF7		1.000000	0.055302
MDA	1.000000		0.023770
Control	0.055302	0.023770	

Multiple Comparisons p values (2-tailed); CXCL8
Independent (grouping) variable: Cell line
Kruskal-Wallis test: H (2, N= 61) =34.56212 p =.0000

Depend.: CXCL8	MCF7 R:23.273	MDA R:46.375	Control R:2.5000
MCF7		0.000004	0.081297
MDA	0.000004		0.000014
Control	0.081297	0.000014	

APPENDIX E3

Results of Kruskal-Wallis ANOVA by Ranks tests and Multiple Comparisons Post Hoc tests. Grouping variable: Culture groups where **A**: EXP; **B**: NK-BC; **C**: T_{REG}-BC; **D**: BC and where **MCF7**: MCF-7 cells, LPCM; **MDA:** MDA-MB-231 cells, BPCM

Kruskal-Wallis ANOVA by Ranks; IL-1b
Independent (grouping) variable: Culture Groups
Kruskal-Wallis test: H (8, N= 61) =34.68124 p =.0000

Depend.: IL-1b	Code	Valid N	Sum of Ranks	Mean Rank
MCF7A	101	9	219.5000	24.38889
MDAA	102	6	305.0000	50.83333
MCF7B	103	8	173.5000	21.68750
MDAB	104	6	283.5000	47.25000
MCF7C	105	8	133.5000	16.68750
MDAC	106	6	253.0000	42.16667
MCF7D	107	8	181.0000	22.62500
MDAD	108	6	287.5000	47.91667
Control	111	4	54.5000	13.62500

Kruskal-Wallis ANOVA by Ranks; IL-2
Independent (grouping) variable: Culture Groups
Kruskal-Wallis test: H (8, N= 61) =29.49710 p =.0003

Depend.: IL-2	Code	Valid N	Sum of Ranks	Mean Rank
MCF7A	101	9	226.5000	25.16667
MDAA	102	6	297.0000	49.50000
MCF7B	103	8	129.5000	16.18750
MDAB	104	6	299.5000	49.91667
MCF7C	105	8	155.0000	19.37500
MDAC	106	6	251.0000	41.83333
MCF7D	107	8	220.5000	27.56250
MDAD	108	6	239.5000	39.91667
Control	111	4	72.5000	18.12500

Kruskal-Wallis ANOVA by Ranks; IL-6
Independent (grouping) variable: Culture Groups
Kruskal-Wallis test: H (8, N= 61) =37.97358 p =.0000

Depend.: IL-6	Code	Valid N	Sum of Ranks	Mean Rank
MCF7A	101	9	220.5000	24.50000
MDAA	102	6	311.0000	51.83333
MCF7B	103	8	175.5000	21.93750
MDAB	104	6	291.0000	48.50000
MCF7C	105	8	168.0000	21.00000
MDAC	106	6	273.0000	45.50000
MCF7D	107	8	181.0000	22.62500
MDAD	108	6	257.0000	42.83333
Control	111	4	14.0000	3.50000

Kruskal-Wallis ANOVA by Ranks; IL-12
Independent (grouping) variable: Culture Groups
Kruskal-Wallis test: H (8, N= 61) =25.20474 p =.0014

Depend.: IL-12	Code	Valid N	Sum of Ranks	Mean Rank
MCF7A	101	9	292.5000	32.50000
MDAA	102	6	273.5000	45.58333
MCF7B	103	8	204.0000	25.50000
MDAB	104	6	298.5000	49.75000
MCF7C	105	8	119.0000	14.87500
MDAC	106	6	230.0000	38.33333
MCF7D	107	8	185.5000	23.18750
MDAD	108	6	229.0000	38.16667
Control	111	4	59.0000	14.75000

Kruskal-Wallis ANOVA by Ranks; IFN-g
Independent (grouping) variable: Culture Groups
Kruskal-Wallis test: H (8, N= 61) =33.04489 p =.0001

Depend.: IFN-g	Code	Valid N	Sum of Ranks	Mean Rank
MCF7A	101	9	174.0000	19.33333
MDAA	102	6	300.0000	50.00000
MCF7B	103	8	155.5000	19.43750
MDAB	104	6	275.5000	45.91667
MCF7C	105	8	158.0000	19.75000
MDAC	106	6	267.0000	44.50000
MCF7D	107	8	200.5000	25.06250
MDAD	108	6	284.5000	47.41667
Control	111	4	76.0000	19.00000

Kruskal-Wallis ANOVA by Ranks; CCL2
Independent (grouping) variable: Culture Groups
Kruskal-Wallis test: H (8, N= 61) =29.42240 p =.0003

Depend.: CCL2	Code	Valid N	Sum of Ranks	Mean Rank
MCF7A	101	9	319.0000	35.44444
MDAA	102	6	289.0000	48.16667
MCF7B	103	8	243.0000	30.37500
MDAB	104	6	289.0000	48.16667
MCF7C	105	8	154.5000	19.31250
MDAC	106	6	209.0000	34.83333
MCF7D	107	8	150.5000	18.81250
MDAD	108	6	222.0000	37.00000
Control	111	4	15.0000	3.75000

Kruskal-Wallis ANOVA by Ranks; TNF-a
Independent (grouping) variable: Culture Groups
Kruskal-Wallis test: H (8, N= 61) =32.61584 p =.0001

Depend.: TNF-a	Code	Valid N	Sum of Ranks	Mean Rank
MCF7A	101	9	216.0000	24.00000
MDAA	102	6	292.5000	48.75000
MCF7B	103	8	156.5000	19.56250
MDAB	104	6	287.0000	47.83333
MCF7C	105	8	127.0000	15.87500
MDAC	106	6	254.5000	42.41667
MCF7D	107	8	210.0000	26.25000
MDAD	108	6	282.0000	47.00000
Control	111	4	65.5000	16.37500

Kruskal-Wallis ANOVA by Ranks; CCL4
Independent (grouping) variable: Culture Groups
Kruskal-Wallis test: H (8, N= 61) =41.45248 p =.0000

Depend.: CCL4	Code	Valid N	Sum of Ranks	Mean Rank
MCF7A	101	9	440.5000	48.94444
MDAA	102	6	273.5000	45.58333
MCF7B	103	8	352.0000	44.00000
MDAB	104	6	249.0000	41.50000
MCF7C	105	8	137.5000	17.18750
MDAC	106	6	178.0000	29.66667
MCF7D	107	8	98.0000	12.25000
MDAD	108	6	126.5000	21.08333
Control	111	4	36.0000	9.00000

Kruskal-Wallis ANOVA by Ranks; CXCL8
Independent (grouping) variable: Culture Groups
Kruskal-Wallis test: H (8, N= 61) =36.39648 p =.0000

Depend.: CXCL8	Code	Valid N	Sum of Ranks	Mean Rank
MCF7A	101	9	255.0000	28.33333
MDAA	102	6	296.0000	49.33333
MCF7B	103	8	194.0000	24.25000
MDAB	104	6	288.0000	48.00000
MCF7C	105	8	158.0000	19.75000
MDAC	106	6	255.0000	42.50000
MCF7D	107	8	161.0000	20.12500
MDAD	108	6	274.0000	45.66667
Control	111	4	10.0000	2.50000

Multiple Comparisons p values (2-tailed); IL-1b
Independent (grouping) variable: Culture Groups
Kruskal-Wallis test: H (8, N= 61) =34.68124 p =.0000

Depend.: IL-1b	MCF7A R:24.389	MDAA R:50.833	MCF7B R:21.688	MDAB R:47.250	MCF7C R:16.688	MDAC R:42.167	MCF7D R:22.625	MDAD R:47.917	Control R:13.625
MCF7A		0.169530	1.000000	0.523917	1.000000	1.000000	1.000000	0.429052	1.000000
MDAA	0.169530		0.085189	1.000000	0.013278	1.000000	0.117341	1.000000	0.041993
MCF7B	1.000000	0.085189		0.276185	1.000000	1.000000	1.000000	0.224081	1.000000
MDAB	0.523917	1.000000	0.276185		0.051630	1.000000	0.367809	1.000000	0.120366
MCF7C	1.000000	0.013278	1.000000	0.051630		0.283410	1.000000	0.040504	1.000000
MDAC	1.000000	1.000000	1.000000	1.000000	0.283410		1.000000	1.000000	0.459019
MCF7D	1.000000	0.117341	1.000000	0.367809	1.000000	1.000000		0.300286	1.000000
MDAD	0.429052	1.000000	0.224081	1.000000	0.040504	1.000000	0.300286		0.099636
Control	1.000000	0.041993	1.000000	0.120366	1.000000	0.459019	1.000000	0.099636	

Multiple Comparisons p values (2-tailed); IL-2
Independent (grouping) variable: Culture Groups
Kruskal-Wallis test: H (8, N= 61) =29.49710 p =.0003

Depend.: IL-2	MCF7A R:25.167	MDAA R:49.500	MCF7B R:16.188	MDAB R:49.917	MCF7C R:19.375	MDAC R:41.833	MCF7D R:27.563	MDAD R:39.917	Control R:18.125
MCF7A		0.334966	1.000000	0.293925	1.000000	1.000000	1.000000	1.000000	1.000000
MDAA	0.334966		0.018424	1.000000	0.060396	1.000000	0.796757	1.000000	0.222591
MCF7B	1.000000	0.018424		0.015655	1.000000	0.269127	1.000000	0.479698	1.000000
MDAB	0.293925	1.000000	0.015655		0.052019	1.000000	0.710075	1.000000	0.199172
MCF7C	1.000000	0.060396	1.000000	0.052019		0.689737	1.000000	1.000000	1.000000
MDAC	1.000000	1.000000	0.269127	1.000000	0.689737		1.000000	1.000000	1.000000
MCF7D	1.000000	0.796757	1.000000	0.710075	1.000000	1.000000		1.000000	1.000000
MDAD	1.000000	1.000000	0.479698	1.000000	1.000000	1.000000	1.000000		1.000000
Control	1.000000	0.222591	1.000000	0.199172	1.000000	1.000000	1.000000	1.000000	

Multiple Comparisons p values (2-tailed); IL-12
Independent (grouping) variable: Culture Groups
Kruskal-Wallis test: H (8, N= 61) =25.20474 p =.0014

Depend.: IL-12	MCF7A R:32.500	MDAA R:45.583	MCF7B R:25.500	MDAB R:49.750	MCF7C R:14.875	MDAC R:38.333	MCF7D R:23.188	MDAD R:38.167	Control R:14.750
MCF7A		1.000000	1.000000	1.000000	1.000000	1.000000	1.000000	1.000000	1.000000
MDAA	1.000000		1.000000	1.000000	0.048979	1.000000	0.701878	1.000000	0.256733
MCF7B	1.000000	1.000000		0.411460	1.000000	1.000000	1.000000	1.000000	1.000000
MDAB	1.000000	1.000000	0.411460		0.009911	1.000000	0.201504	1.000000	0.081227
MCF7C	1.000000	0.048979	1.000000	0.009911		0.518991	1.000000	0.544559	1.000000
MDAC	1.000000	1.000000	1.000000	1.000000	0.518991		1.000000	1.000000	1.000000
MCF7D	1.000000	0.701878	1.000000	0.201504	1.000000	1.000000		1.000000	1.000000
MDAD	1.000000	1.000000	1.000000	1.000000	0.544559	1.000000	1.000000		1.000000
Control	1.000000	0.256733	1.000000	0.081227	1.000000	1.000000	1.000000	1.000000	

Multiple Comparisons p values (2-tailed); TNF-a
Independent (grouping) variable: Culture Groups
Kruskal-Wallis test: H (8, N= 61) =32.61584 p =.0001

Depend.: TNF-a	MCF7A R:24.000	MDAA R:48.750	MCF7B R:19.563	MDAB R:47.833	MCF7C R:15.875	MDAC R:42.417	MCF7D R:26.250	MDAD R:47.000	Control R:16.375
MCF7A		0.293925	1.000000	0.390909	1.000000	1.000000	1.000000	0.502753	1.000000
MDAA	0.293925		0.083968	1.000000	0.021819	1.000000	0.681745	1.000000	0.170118
MCF7B	1.000000	0.083968		0.114895	1.000000	0.617022	1.000000	0.151673	1.000000
MDAB	0.390909	1.000000	0.114895		0.030899	1.000000	0.877531	1.000000	0.217718
MCF7C	1.000000	0.021819	1.000000	0.030899		0.202852	1.000000	0.042082	1.000000
MDAC	1.000000	1.000000	0.617022	1.000000	0.202852		1.000000	1.000000	0.830024
MCF7D	1.000000	0.681745	1.000000	0.877531	1.000000	1.000000		1.000000	1.000000
MDAD	0.502753	1.000000	0.151673	1.000000	0.042082	1.000000	1.000000		0.271069
Control	1.000000	0.170118	1.000000	0.217718	1.000000	0.830024	1.000000	0.271069	

Multiple Comparisons p values (2-tailed); IFN-g
Independent (grouping) variable: Culture Groups
Kruskal-Wallis test: H (8, N= 61) =33.04489 p =.0001

Depend.: IFN-g	MCF7A R:19.333	MDAA R:50.000	MCF7B R:19.438	MDAB R:45.917	MCF7C R:19.750	MDAC R:44.500	MCF7D R:25.063	MDAD R:47.417	Control R:19.000
MCF7A		0.037698	1.000000	0.161836	1.000000	0.257444	1.000000	0.096734	1.000000
MDAA	0.037698		0.051630	1.000000	0.057761	1.000000	0.334635	1.000000	0.245758
MCF7B	1.000000	0.051630		0.206947	1.000000	0.322131	1.000000	0.126724	1.000000
MDAB	0.161836	1.000000	0.206947		0.228560	1.000000	1.000000	1.000000	0.677919
MCF7C	1.000000	0.057761	1.000000	0.228560		0.354203	1.000000	0.140619	1.000000
MDAC	0.257444	1.000000	0.322131	1.000000	0.354203		1.000000	1.000000	0.938360
MCF7D	1.000000	0.334635	1.000000	1.000000	1.000000	1.000000		0.710075	1.000000
MDAD	0.096734	1.000000	0.126724	1.000000	0.140619	1.000000	0.710075		0.473303
Control	1.000000	0.245758	1.000000	0.677919	1.000000	0.938360	1.000000	0.473303	

Multiple Comparisons p values (2-tailed); CCL2
Independent (grouping) variable: Culture Groups
Kruskal-Wallis test: H (8, N= 61) =29.42240 p =.0003

Depend.: CCL2	MCF7A R:35.444	MDAA R:48.167	MCF7B R:30.375	MDAB R:48.167	MCF7C R:19.313	MDAC R:34.833	MCF7D R:18.813	MDAD R:37.000	Control R:3.7500
MCF7A		1.000000	1.000000	1.000000	1.000000	1.000000	1.000000	1.000000	0.106883
MDAA	1.000000		1.000000	1.000000	0.094203	1.000000	0.079242	1.000000	0.003823
MCF7B	1.000000	1.000000		1.000000	1.000000	1.000000	1.000000	1.000000	0.515591
MDAB	1.000000	1.000000	1.000000		0.094203	1.000000	0.079242	1.000000	0.003823
MCF7C	1.000000	0.094203	1.000000	0.094203		1.000000	1.000000	1.000000	1.000000
MDAC	1.000000	1.000000	1.000000	1.000000	1.000000		1.000000	1.000000	0.240430
MCF7D	1.000000	0.079242	1.000000	0.079242	1.000000	1.000000		1.000000	1.000000
MDAD	1.000000	1.000000	1.000000	1.000000	1.000000	1.000000	1.000000		0.133684
Control	0.106883	0.003823	0.515591	0.003823	1.000000	0.240430	1.000000	0.133684	

Multiple Comparisons p values (2-tailed); CCL4
Independent (grouping) variable: Culture Groups
Kruskal-Wallis test: H (8, N= 61) =41.45248 p =.0000

Depend.: CCL4	MCF7A R:48.944	MDAA R:45.583	MCF7B R:44.000	MDAB R:41.500	MCF7C R:17.188	MDAC R:29.667	MCF7D R:12.250	MDAD R:21.083	Control R:9.0000
MCF7A		1.000000	1.000000	1.000000	0.008351	1.000000	0.000757	0.104555	0.006513
MDAA	1.000000		1.000000	1.000000	0.110140	1.000000	0.018276	0.606008	0.050793
MCF7B	1.000000	1.000000		1.000000	0.090811	1.000000	0.012518	0.606178	0.046237
MDAB	1.000000	1.000000	1.000000		0.403880	1.000000	0.082166	1.000000	0.164414
MCF7C	0.008351	0.110140	0.090811	0.403880		1.000000	1.000000	1.000000	1.000000
MDAC	1.000000	1.000000	1.000000	1.000000	1.000000		1.000000	1.000000	1.000000
MCF7D	0.000757	0.018276	0.012518	0.082166	1.000000	1.000000		1.000000	1.000000
MDAD	0.104555	0.606008	0.606178	1.000000	1.000000	1.000000	1.000000		1.000000
Control	0.006513	0.050793	0.046237	0.164414	1.000000	1.000000	1.000000	1.000000	

Multiple Comparisons p values (2-tailed); CXCL8
Independent (grouping) variable: Culture Groups
Kruskal-Wallis test: H (8, N= 61) =36.39648 p =.0000

Depend.: CXCL8	MCF7A R:28.333	MDAA R:49.333	MCF7B R:24.250	MDAB R:48.000	MCF7C R:19.750	MDAC R:42.500	MCF7D R:20.125	MDAD R:45.667	Control R:2.5000
MCF7A		0.893039	1.000000	1.000000	1.000000	1.000000	1.000000	1.000000	0.556391
MDAA	0.893039		0.320088	1.000000	0.073142	1.000000	0.083364	1.000000	0.001574
MCF7B	1.000000	0.320088		0.476787	1.000000	1.000000	1.000000	0.917937	1.000000
MDAB	1.000000	1.000000	0.476787		0.115705	1.000000	0.131211	1.000000	0.002582
MCF7C	1.000000	0.073142	1.000000	0.115705		0.635474	1.000000	0.247290	1.000000
MDAC	1.000000	1.000000	1.000000	1.000000	0.635474		0.705966	1.000000	0.017352
MCF7D	1.000000	0.083364	1.000000	0.131211	1.000000	0.705966		0.277976	1.000000
MDAD	1.000000	1.000000	0.917937	1.000000	0.247290	1.000000	0.277976		0.005950
Control	0.556391	0.001574	1.000000	0.002582	1.000000	0.017352	1.000000	0.005950	

APPENDIX E4

Results of Kruskal-Wallis ANOVA by Ranks tests followed by Multiple Comparisons Post Hoc tests. Grouping variable: Groups (LPCM and BPCM) **A**: EXP; **B**: NK-BC; **C**: T_{REG}-BC; **D**: BC

Kruskal-Wallis ANOVA by Ranks; IL-1b (Spreadsheet in IL Workbook)
Independent (grouping) variable: Groups
Kruskal-Wallis test: H (4, N= 61) =5.494440 p =.2402

Depend.: IL-1b	Code	Valid N	Sum of Ranks	Mean Rank
A	101	15	524.5000	34.96667
B	102	14	457.0000	32.64286
C	103	14	386.5000	27.60714
D	105	14	468.5000	33.46429
Control	107	4	54.5000	13.62500

Kruskal-Wallis ANOVA by Ranks; IL-2 (Spreadsheet in IL Workbook)
Independent (grouping) variable: Groups
Kruskal-Wallis test: H (4, N= 61) =3.169251 p =.5299

Depend.: IL-2	Code	Valid N	Sum of Ranks	Mean Rank
A	101	15	523.5000	34.90000
B	102	14	429.0000	30.64286
C	103	14	406.0000	29.00000
D	105	14	460.0000	32.85714
Control	107	4	72.5000	18.12500

Kruskal-Wallis ANOVA by Ranks; IL-6 (Spreadsheet in IL Workbook)
Independent (grouping) variable: Groups
Kruskal-Wallis test: H (4, N= 61) =10.78879 p =.0290

Depend.: IL-6	Code	Valid N	Sum of Ranks	Mean Rank
A	101	15	531.5000	35.43333
B	102	14	466.5000	33.32143
C	103	14	441.0000	31.50000
D	105	14	438.0000	31.28571
Control	107	4	14.0000	3.50000

Kruskal-Wallis ANOVA by Ranks; IL-12 (Spreadsheet in IL Workbook)
Independent (grouping) variable: Groups
Kruskal-Wallis test: H (4, N= 61) =8.338830 p =.0799

Depend.: IL-12	Code	Valid N	Sum of Ranks	Mean Rank
A	101	15	566.0000	37.73333
B	102	14	502.5000	35.89286
C	103	14	349.0000	24.92857
D	105	14	414.5000	29.60714
Control	107	4	59.0000	14.75000

Kruskal-Wallis ANOVA by Ranks; IFN-g (Spreadsheet in IL Workbook)
Independent (grouping) variable: Groups
Kruskal-Wallis test: H (4, N= 61) =2.463609 p =.6512

Depend.: IFN-g	Code	Valid N	Sum of Ranks	Mean Rank
A	101	15	474.0000	31.60000
B	102	14	431.0000	30.78571
C	103	14	425.0000	30.35714
D	105	14	485.0000	34.64286
Control	107	4	76.0000	19.00000

Kruskal-Wallis ANOVA by Ranks; CCL4 (Spreadsheet in IL Workbook)
Independent (grouping) variable: Groups
Kruskal-Wallis test: H (4, N= 61) =38.71221 p =.0000

Depend.: CCL4	Code	Valid N	Sum of Ranks	Mean Rank
A	101	15	714.0000	47.60000
B	102	14	601.0000	42.92857
C	103	14	315.5000	22.53571
D	105	14	224.5000	16.03571
Control	107	4	36.0000	9.00000

Kruskal-Wallis ANOVA by Ranks; CXCL8 (Spreadsheet in IL Workbook)
Independent (grouping) variable: Groups
Kruskal-Wallis test: H (4, N= 61) =12.49564 p =.0140

Depend.: CXCL8	Code	Valid N	Sum of Ranks	Mean Rank
A	101	15	551.0000	36.73333
B	102	14	482.0000	34.42857
C	103	14	413.0000	29.50000
D	105	14	435.0000	31.07143
Control	107	4	10.0000	2.50000

Multiple Comparisons p values (2-tailed); IL-1b (Spreadsheet in IL Workbook)
Independent (grouping) variable: Groups
Kruskal-Wallis test: H (4, N= 61) =5.494440 p =.2402

Depend.: IL-1b	A R:34.967	B R:32.643	C R:27.607	D R:33.464	Control R:13.625
A		1.000000	1.000000	1.000000	0.326571
B	1.000000		1.000000	1.000000	0.588235
C	1.000000	1.000000		1.000000	1.000000
D	1.000000	1.000000	1.000000		0.487098
Control	0.326571	0.588235	1.000000	0.487098	

Multiple Comparisons p values (2-tailed); IL-2 (Spreadsheet in IL Workbook)
Independent (grouping) variable: Groups
Kruskal-Wallis test: H (4, N= 61) =3.169251 p =.5299

Depend.: IL-2	A R:34.900	B R:30.643	C R:29.000	D R:32.857	Control R:18.125
A		1.000000	1.000000	1.000000	0.931215
B	1.000000		1.000000	1.000000	1.000000
C	1.000000	1.000000		1.000000	1.000000
D	1.000000	1.000000	1.000000		1.000000
Control	0.931215	1.000000	1.000000	1.000000	

Multiple Comparisons p values (2-tailed); IL-6 (Spreadsheet in IL Workbook)
Independent (grouping) variable: Groups
Kruskal-Wallis test: H (4, N= 61) =10.78879 p =.0290

Depend.: IL-6	A R:35.433	B R:33.321	C R:31.500	D R:31.286	Control R:3.5000
A		1.000000	1.000000	1.000000	0.013911
B	1.000000		1.000000	1.000000	0.030476
C	1.000000	1.000000		1.000000	0.054037
D	1.000000	1.000000	1.000000		0.057689
Control	0.013911	0.030476	0.054037	0.057689	

Kruskal-Wallis ANOVA by Ranks; TNF-a (Spreadsheet in IL Workbook)
Independent (grouping) variable: Groups
Kruskal-Wallis test: H (4, N= 61) =4.529977 p =.3390

Depend.: TNF-a	Code	Valid N	Sum of Ranks	Mean Rank
A	101	15	508.5000	33.90000
B	102	14	443.5000	31.67857
C	103	14	381.5000	27.25000
D	105	14	492.0000	35.14286
Control	107	4	65.5000	16.37500

Kruskal-Wallis ANOVA by Ranks; CCL2 (Spreadsheet in IL Workbook)
Independent (grouping) variable: Groups
Kruskal-Wallis test: H (4, N= 61) =17.91066 p =.0013

Depend.: CCL2	Code	Valid N	Sum of Ranks	Mean Rank
A	101	15	608.0000	40.53333
B	102	14	532.0000	38.00000
C	103	14	363.5000	25.96429
D	105	14	372.5000	26.60714
Control	107	4	15.0000	3.75000

Multiple Comparisons p values (2-tailed); IL-12 (Spreadsheet in IL Workbook)
Independent (grouping) variable: Groups
Kruskal-Wallis test: H (4, N= 61) =8.338830 p =.0799

Depend.: IL-12	A R:37.733	B R:35.893	C R:24.929	D R:29.607	Control R:14.750
A		1.000000	0.522656	1.000000	0.214141
B	1.000000		1.000000	1.000000	0.356727
C	0.522656	1.000000		1.000000	1.000000
D	1.000000	1.000000	1.000000		1.000000
Control	0.214141	0.356727	1.000000	1.000000	

Multiple Comparisons p values (2-tailed); IFN-g (Spreadsheet in IL Workbook)
Independent (grouping) variable: Groups
Kruskal-Wallis test: H (4, N= 61) =2.463609 p =.6512

Depend.: IFN-g	A R:31.600	B R:30.786	C R:30.357	D R:34.643	Control R:19.000
A		1.000000	1.000000	1.000000	1.000000
B	1.000000		1.000000	1.000000	1.000000
C	1.000000	1.000000		1.000000	1.000000
D	1.000000	1.000000	1.000000		1.000000
Control	1.000000	1.000000	1.000000	1.000000	

Multiple Comparisons p values (2-tailed); CCL2 (Spreadsheet in IL Workbook)
Independent (grouping) variable: Groups
Kruskal-Wallis test: H (4, N= 61) =17.91066 p =.0013

Depend.: CCL2	A R:40.533	B R:38.000	C R:25.964	D R:26.607	Control R:3.7500
A		1.000000	0.272186	0.347787	0.002314
B	1.000000		0.728604	0.895271	0.006668
C	0.272186	0.728604		1.000000	0.273078
D	0.347787	0.895271	1.000000		0.231494
Control	0.002314	0.006668	0.273078	0.231494	

Multiple Comparisons p values (2-tailed); CCL4 (Spreadsheet in IL Workbook)
Independent (grouping) variable: Groups
Kruskal-Wallis test: H (4, N= 61) =38.71221 p =.0000

Depend.: CCL4	A R:47.600	B R:42.929	C R:22.536	D R:16.036	Control R:9.0000
A		1.000000	0.001451	0.000017	0.001116
B	1.000000		0.023722	0.000613	0.007491
C	0.001451	0.023722		1.000000	1.000000
D	0.000017	0.000613	1.000000		1.000000
Control	0.001116	0.007491	1.000000	1.000000	

Multiple Comparisons p values (2-tailed); CXCL8 (Spreadsheet in IL Workbook)
Independent (grouping) variable: Groups
Kruskal-Wallis test: H (4, N= 61) =12.49564 p =.0140

Depend.: CXCL8	A R:36.733	B R:34.429	C R:29.500	D R:31.071	Control R:2.5000
A		1.000000	1.000000	1.000000	0.006109
B	1.000000		1.000000	1.000000	0.015126
C	1.000000	1.000000		1.000000	0.073058
D	1.000000	1.000000	1.000000		0.045298
Control	0.006109	0.015126	0.073058	0.045298	

APPENDIX E5

Box and whisker plots of cytokines showing no significant difference ($p>0.05$) within and between multiple culture groups in LPCM (A-E); and BPCM (F). **KEY: X-axis** – culture groups; **Y-axis –** log cytokine concentration.

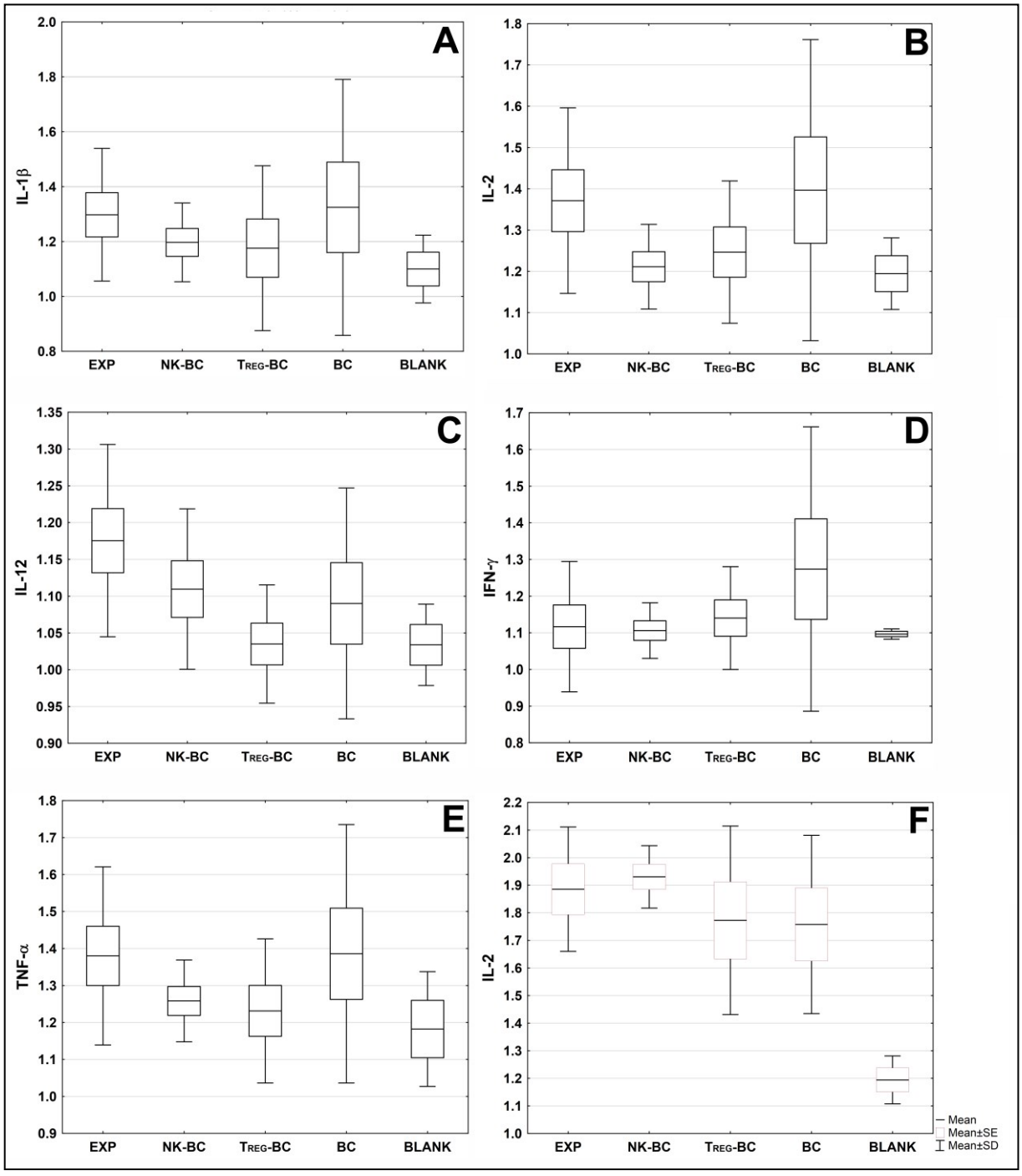

APPENDIX F1

Results from Spearman Rank Order Correlations and subsequent non-metric MDS in each culture group in LPCM.

EXP culture group

Variable	Spearman Rank Order Correlations (MCF-7 A in IL Cluster analysis) MD pairwise deleted Marked correlations are significant at p <.05000 IL-1b	IL-2	IL-6	IL-12	IFN-g	TNF-a	CCL2	CCL4	CXCL8
IL-1b	1.000000	0.452381	0.880952	0.538932	0.694623	0.778457	0.904762	0.476190	0.809524
IL-2	0.452381	1.000000	0.476190	0.610789	0.790433	0.730552	0.595238	0.500000	0.500000
IL-6	0.880952	0.476190	1.000000	0.778457	0.826362	0.898220	0.976190	0.785714	0.976190
IL-12	0.538932	0.610789	0.778457	1.000000	0.716867	0.740964	0.802410	0.970077	0.778457
IFN-g	0.694623	0.790433	0.826362	0.716867	1.000000	0.987952	0.874267	0.694623	0.886243
TNF-a	0.778457	0.730552	0.898220	0.740964	0.987952	1.000000	0.934148	0.718576	0.934148
CCL2	0.904762	0.595238	0.976190	0.802410	0.874267	0.934148	1.000000	0.761905	0.952381
CCL4	0.476190	0.500000	0.785714	0.970077	0.694623	0.718576	0.761905	1.000000	0.809524
CXCL8	0.809524	0.500000	0.976190	0.778457	0.886243	0.934148	0.952381	0.809524	1.000000
Mean	1.280936	1.343868	2.144941	1.170268	1.099569	1.353628	2.609634	2.582365	3.064875
Std. Dev.	0.252811	0.223712	0.752193	0.138677	0.18166	0.243352	1.08922	0.742153	0.699851
No. Cases	8.000000								
Matrix	2.000000								

	Final Configuration (Spearman Rank Order Correlations (MCF-7 A in IL Cluster analysis) in IL Workbook) D-star: Raw stress = .0000000; Alienation = .0000084 D-hat: Raw stress = .0000000; Stress = .0000048 DIM. 1	DIM. 2
IL-1b	-1.13144	-0.679121
IL-2	1.58562	-0.872049
IL-6	-0.56407	0.004165
IL-12	0.36028	1.099520
IFN-g	0.25875	-0.330190
TNF-a	0.25871	-0.330177
CCL2	-0.56405	0.004136
CCL4	0.36025	1.099545
CXCL8	-0.56404	0.004170

	Distances in Final Configuration (Spearman Rank Order Correlations (MCF-7 A in IL Cluster analysis) in IL Workbook) D-star: Raw stress = .0000000; Alienation = .0000084 D-hat: Raw stress = .0000000; Stress = .0000048 IL-1b	IL-2	IL-6	IL-12	IFN-g	TNF-a	CCL2	CCL4	CXCL8
IL-1b	0.000000	2.723904	0.888137	2.321379	1.433316	1.433274	0.888132	2.321377	0.888163
IL-2	2.723904	0.000000	2.321409	2.321324	1.433244	1.433293	2.321373	2.321363	2.321378
IL-6	0.888137	2.321409	0.000000	1.433260	0.888165	0.888117	0.000039	1.433257	0.000035
IL-12	2.321379	2.321324	1.433260	0.000000	1.433311	1.433301	1.433265	0.000042	1.433234
IFN-g	1.433316	1.433244	0.888165	1.433311	0.000000	0.000049	0.888130	1.433333	0.888135
TNF-a	1.433274	1.433293	0.888117	1.433301	0.000049	0.000000	0.888081	1.433324	0.888087
CCL2	0.888132	2.321373	0.000039	1.433265	0.888130	0.888081	0.000000	1.433262	0.000034
CCL4	2.321377	2.321363	1.433257	0.000042	1.433333	1.433324	1.433262	0.000000	1.433231
CXCL8	0.888163	2.321378	0.000035	1.433234	0.888135	0.888087	0.000034	1.433231	0.000000

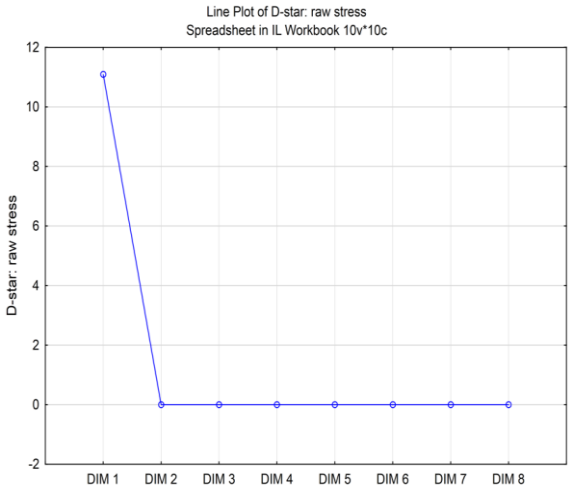
Line Plot of D-star: raw stress
Spreadsheet in IL Workbook 10v*10c
D-star: raw stress
12
10
8
6
4
2
0
-2
DIM 1
DIM 2
DIM 3
DIM 4
DIM 5
DIM 6
DIM 7
DIM 8

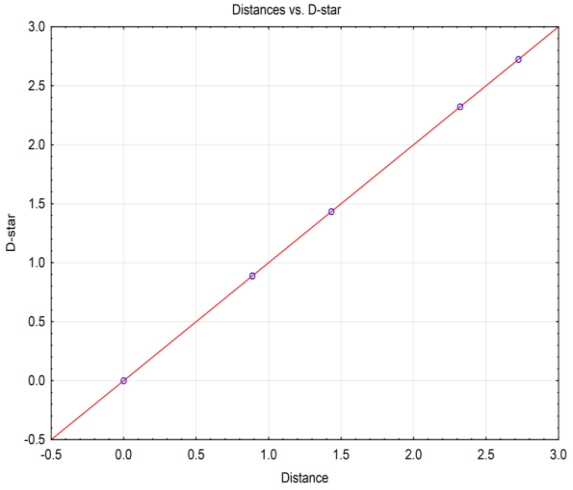
Distances vs. D-star
D-star
3.0
2.5
2.0
1.5
1.0
0.5
0.0
-0.5
-0.5
0.0
0.5
1.0
1.5
2.0
2.5
3.0
Distance

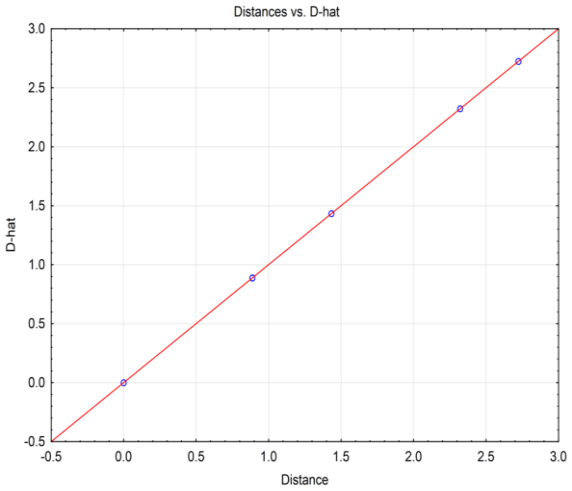
Distances vs. D-hat
D-hat
3.0
2.5
2.0
1.5
1.0
0.5
0.0
-0.5
-0.5
0.0
0.5
1.0
1.5
2.0
2.5
3.0
Distance

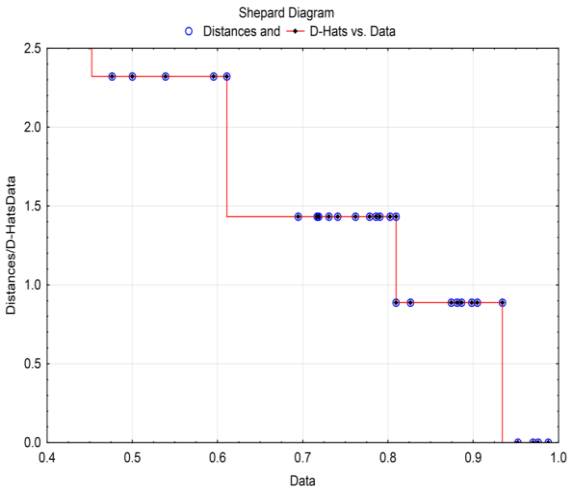
Shepard Diagram
Distances and D-Hats vs. Data
Distances/D-HatsData
2.5
2.0
1.5
1.0
0.5
0.0
0.4
0.5
0.6
0.7
0.8
0.9
1.0
Data

NK-BC culture group

	Spearman Rank Order Correlations (MCF-7 B in IL Workbook) MD pairwise deleted Marked correlations are significant at p <.05000								
Variable	IL - 1b	IL-2	IL-6	IL-12	IFN-g	TNF-a	CCL2	CCL4	CXCL8
IL - 1b	1.000000	0.455098	0.833333	0.675164	0.299407	0.754505	0.738095	0.761905	0.785714
IL-2	0.455098	1.000000	0.646718	0.759491	0.102410	0.596386	0.838338	0.706599	0.586837
IL-6	0.833333	0.646718	1.000000	0.773370	0.431145	0.814386	0.904762	0.904762	0.976190
IL-12	0.675164	0.759491	0.773370	1.000000	-0.030874	0.716268	0.847024	0.908403	0.773370
IFN-g	0.299407	0.102410	0.431145	-0.030874	1.000000	0.451807	0.383240	0.359288	0.503003
TNF-a	0.754505	0.596386	0.814386	0.716268	0.451807	1.000000	0.718576	0.778457	0.850315
CCL2	0.738095	0.838338	0.904762	0.847024	0.383240	0.718576	1.000000	0.952381	0.880952
CCL4	0.761905	0.706599	0.904762	0.908403	0.359288	0.778457	0.952381	1.000000	0.928571
CXCL8	0.785714	0.586837	0.976190	0.773370	0.503003	0.850315	0.880952	0.928571	1.000000
Mean	1.19696543	1.21121345	1.97072346	1.10964606	1.10607274	1.25818347	2.52748615	2.3852571	2.95488843
Std. Dev.	0.14328322	0.10261843	0.50190284	0.108972509	0.075722202	0.11069573	1.06972256	0.52719585	0.6369668
No. Cases	8.000000								
Matrix	2.000000								

	Final Configuration (Spearman Rank Order Correlations (MCF-7 B in IL Workbook) in IL Workbook) D-star: Raw stress = .6270011; Alienation = .0878964 D-hat: Raw stress = .2080727; Stress = .0506833	
	DIM. 1	DIM. 2
IL - 1b	-0.349664	-0.929744
IL-2	-0.374000	1.090842
IL-6	-0.231801	-0.289131
IL-12	-0.839300	0.185335
IFN-g	2.269077	0.137110
TNF-a	0.385669	-0.195560
CCL2	-0.402653	0.215752
CCL4	-0.463463	-0.050905
CXCL8	0.006133	-0.163699

	Distances in Final Configuration (Spearman Rank Order Correlations (MCF-7 B in IL Workbook) in IL Workbook) D-star: Raw stress = .6270011; Alienation = .0878964 D-hat: Raw stress = .2080727; Stress = .0506833								
	IL - 1b	IL-2	IL-6	IL-12	IFN-g	TNF-a	CCL2	CCL4	CXCL8
IL - 1b	0.000000	2.020733	0.651366	1.217844	2.827717	1.039105	1.146721	0.886176	0.844640
IL-2	2.020733	0.000000	1.387280	1.018061	2.809886	1.493964	0.875559	1.145247	1.310869
IL-6	0.651366	1.387280	0.000000	0.770826	2.536942	0.624519	0.533007	0.332293	0.268972
IL-12	1.217844	1.018061	0.770826	0.000000	3.108751	1.282820	0.437705	0.443918	0.914648
IFN-g	2.827717	2.809886	2.536942	3.108751	0.000000	1.912563	2.672887	2.739000	2.282850
TNF-a	1.039105	1.493964	0.624519	1.282820	1.912563	0.000000	0.889173	0.861364	0.380870
CCL2	1.146721	0.875559	0.533007	0.437705	2.672887	0.889173	0.000000	0.273503	0.557754
CCL4	0.886176	1.145247	0.332293	0.443918	2.739000	0.861364	0.273503	0.000000	0.482952
CXCL8	0.844640	1.310869	0.268972	0.914648	2.282850	0.380870	0.557754	0.482952	0.000000

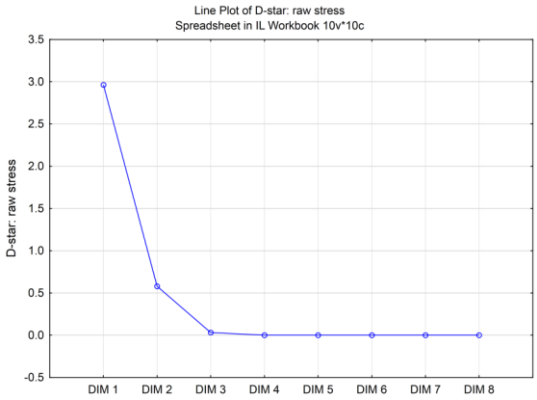
Line Plot of D-star: raw stress
Spreadsheet in IL Workbook 10v*10c
D-star: raw stress
DIM 1
DIM 2
DIM 3
DIM 4
DIM 5
DIM 6
DIM 7
DIM 8

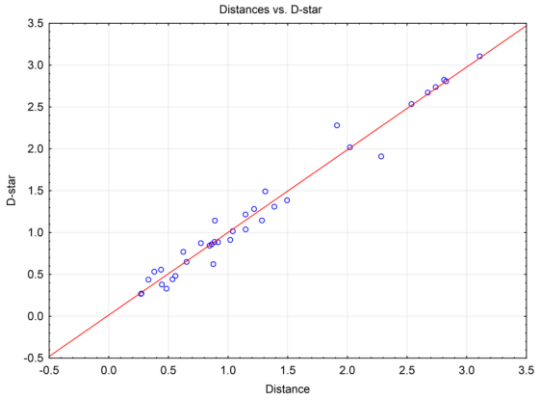
Distances vs. D-star
D-star
Distance

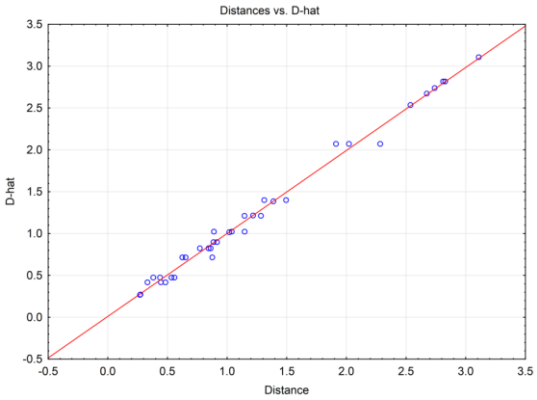
Distances vs. D-hat
D-hat
Distance

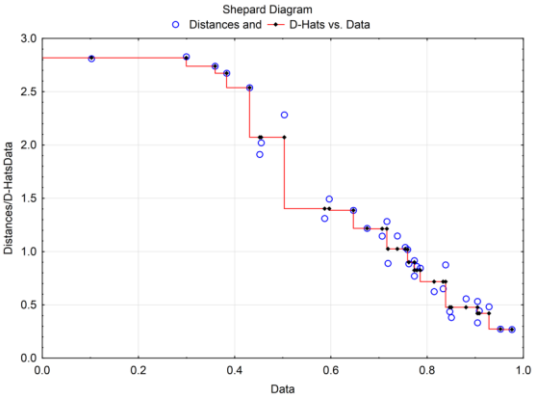
Shepard Diagram
Distances and
D-Hats vs. Data
Distances/D-HatsData
Data

T_{REG}-BC culture group

	Spearman Rank Order Correlations (MCF-7 C in IL Workbook) MD pairwise deleted Marked correlations are significant at p <.05000								
Variable	IL - 1b	IL-2	IL-6	IL-12	IFN-g	TNF-a	CCL2	CCL4	CXCL8
IL - 1b	1.000000	-0.012121	0.614502	0.207317	0.327354	0.111120	0.698846	0.481963	0.843435
IL-2	-0.012121	1.000000	0.155691	0.387886	0.720931	0.748593	-0.131739	0.071858	0.167668
IL-6	0.614502	0.155691	1.000000	0.325325	0.494663	0.463553	0.619048	0.500000	0.761905
IL-12	0.207317	0.387886	0.325325	1.000000	-0.044931	0.679064	0.481963	0.831386	0.566306
IFN-g	0.327354	0.720931	0.494663	-0.044931	1.000000	0.493881	-0.012684	-0.088786	0.279040
TNF-a	0.111120	0.748593	0.463553	0.679064	0.493881	1.000000	0.243975	0.536745	0.463553
CCL2	0.698846	-0.131739	0.619048	0.481963	-0.012684	0.243975	1.000000	0.857143	0.904762
CCL4	0.481963	0.071858	0.500000	0.831386	-0.088786	0.536745	0.857143	1.000000	0.809524
CXCL8	0.843435	0.167668	0.761905	0.566306	0.279040	0.463553	0.904762	0.809524	1.000000
Mean	1.17589003	1.24667652	2.11059379	1.03500824	1.14022723	1.23122797	1.90120542	1.73128466	2.74591737
Std. Dev.	0.300365265	0.172445171	0.89462709	0.080395359	0.140240345	0.19482675	0.582228552	0.124922028	0.66498045
No. Cases	8.000000								
Matrix	2.000000								

	Final Configuration (Spearman Rank Order Correlations (MCF-7 C in IL Workbook) in IL Workbook) D-star: Raw stress = .3371214; Alienation = .0644799 D-hat: Raw stress = .1478784; Stress = .0427277	
	DIM. 1	DIM. 2
IL - 1b	-0.812986	-0.720121
IL-2	1.311112	-0.012177
IL-6	-0.251983	-0.648159
IL-12	0.021436	1.031097
IFN-g	1.052931	-0.802763
TNF-a	0.747540	0.572944
CCL2	-0.898673	-0.009637
CCL4	-0.588010	0.647336
CXCL8	-0.581367	-0.058521

	Distances in Final Configuration (Spearman Rank Order Correlations (MCF-7 C in IL Workbook) in IL Workbook) D-star: Raw stress = .3371214; Alienation = .0644799 D-hat: Raw stress = .1478784; Stress = .0427277								
	IL - 1b	IL-2	IL-6	IL-12	IFN-g	TNF-a	CCL2	CCL4	CXCL8
IL - 1b	0.000000	2.238969	0.565600	1.939852	1.867746	2.026638	0.715632	1.385840	0.700972
IL-2	2.238969	0.000000	1.687525	1.658820	0.831675	0.812392	2.209786	2.010379	1.893047
IL-6	0.565600	1.687525	0.000000	1.701370	1.314041	1.578017	0.908800	1.338365	0.675401
IL-12	1.939852	1.658820	1.701370	0.000000	2.104049	0.858563	1.389147	0.720207	1.245247
IFN-g	1.867746	0.831675	1.314041	2.104049	0.000000	1.409196	2.106609	2.189857	1.795780
TNF-a	2.026638	0.812392	1.578017	0.858563	1.409196	0.000000	1.746258	1.337620	1.471306
CCL2	0.715632	2.209786	0.908800	1.389147	2.106609	1.746258	0.000000	0.726722	0.321049
CCL4	1.385840	2.010379	1.338365	0.720207	2.189857	1.337620	0.726722	0.000000	0.705888
CXCL8	0.700972	1.893047	0.675401	1.245247	1.795780	1.471306	0.321049	0.705888	0.000000

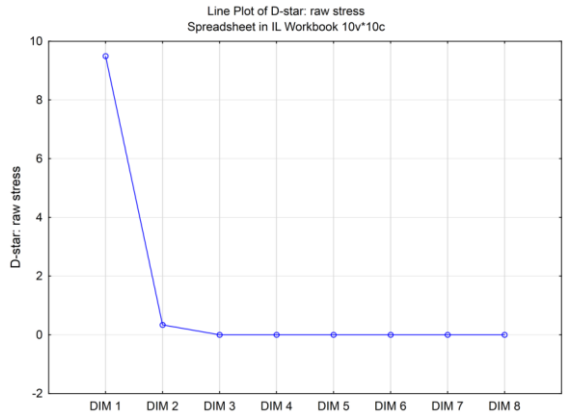
Line Plot of D-star: raw stress
Spreadsheet in IL Workbook 10v*10c
D-star: raw stress
10
8
6
4
2
0
-2
DIM 1
DIM 2
DIM 3
DIM 4
DIM 5
DIM 6
DIM 7
DIM 8

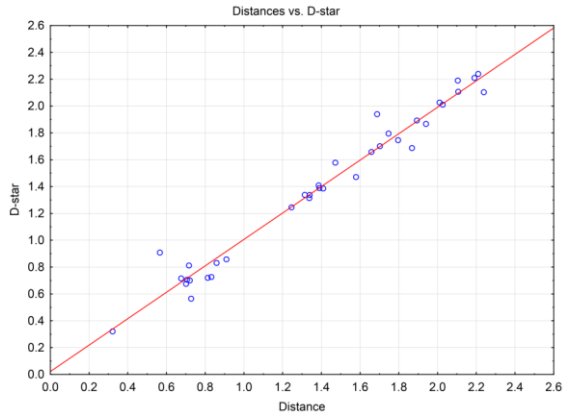
Distances vs. D-star
D-star
Distance
0.0
0.2
0.4
0.6
0.8
1.0
1.2
1.4
1.6
1.8
2.0
2.2
2.4
2.6

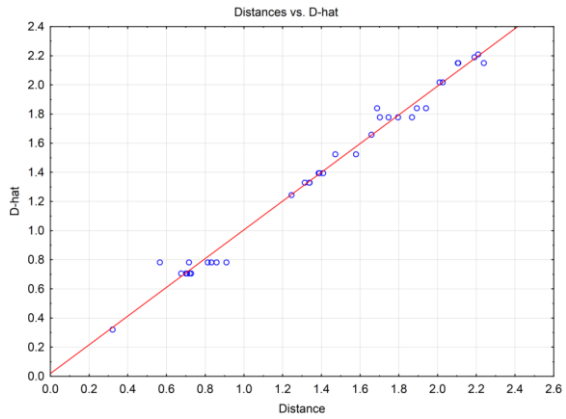
Distances vs. D-hat
D-hat
Distance
0.0
0.2
0.4
0.6
0.8
1.0
1.2
1.4
1.6
1.8
2.0
2.2
2.4
2.6

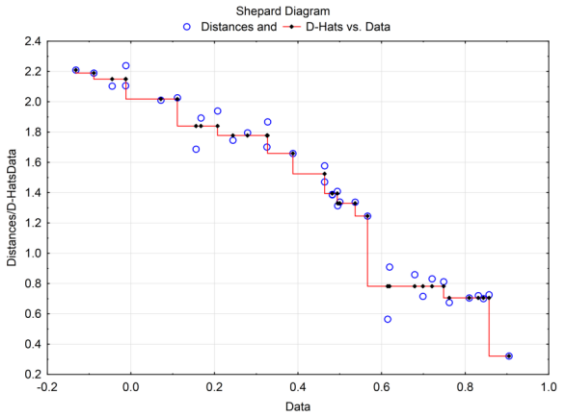
Shepard Diagram
Distances and
D-Hats vs. Data
Distances/D-HatsData
Data
-0.2
0.0
0.2
0.4
0.6
0.8
1.0
1.2
1.4
1.6
1.8
2.0
2.2
2.4

BC culture group

Variable	Spearman Rank Order Correlations (MCF-7 D in IL Workbook) MD pairwise deleted Marked correlations are significant at p <.05000 IL - 1b	IL-2	IL-6	IL-12	IFN-g	TNF-a	CCL2	CCL4	CXCL8
IL - 1b	1.000000	0.830318	0.359288	0.455098	0.351522	0.562884	0.503003	0.335335	0.491027
IL-2	0.830318	1.000000	0.481963	0.409668	0.451220	0.843435	0.734993	0.481963	0.602453
IL-6	0.359288	0.481963	1.000000	0.452381	0.566306	0.785714	0.833333	0.619048	0.928571
IL-12	0.455098	0.409668	0.452381	1.000000	0.963925	0.333333	0.261905	0.928571	0.285714
IFN-g	0.351522	0.451220	0.566306	0.963925	1.000000	0.469914	0.397619	0.988024	0.385570
TNF-a	0.562884	0.843435	0.785714	0.333333	0.469914	1.000000	0.880952	0.547619	0.857143
CCL2	0.503003	0.734993	0.833333	0.261905	0.397619	0.880952	1.000000	0.428571	0.857143
CCL4	0.335335	0.481963	0.619048	0.928571	0.988024	0.547619	0.428571	1.000000	0.452381
CXCL8	0.491027	0.602453	0.928571	0.285714	0.385570	0.857143	0.857143	0.452381	1.000000
Mean	1.32466736	1.39678451	2.30236346	1.09016886	1.27377016	1.38573536	1.90606394	1.63841226	2.67141947
Std. Dev.	0.46643407	0.36465148	1.2703044	0.15687791	0.38773322	0.34933783	0.8808979	0.234545	0.92449674
No. Cases	8.000000								
Matrix	2.000000								

	Final Configuration (Spearman Rank Order Correlations (MCF-7 D in IL Workbook) in IL Workbook) D-star: Raw stress = .2972921; Alienation = .0605550 D-hat: Raw stress = .1285304; Stress = .0398346 DIM. 1	DIM. 2
IL - 1b	-0.200598	-1.20786
IL-2	-0.613642	-0.72652
IL-6	-0.254823	0.76412
IL-12	1.236225	-0.16135
IFN-g	1.087776	0.19728
TNF-a	-0.661804	0.07463
CCL2	-0.907906	0.31765
CCL4	0.999796	0.20036
CXCL8	-0.685024	0.54169

	Distances in Final Configuration (Spearman Rank Order Correlations (MCF-7 D in IL Workbook) in IL Workbook) D-star: Raw stress = .2972921; Alienation = .0605550 D-hat: Raw stress = .1285304; Stress = .0398346 IL - 1b	IL-2	IL-6	IL-12	IFN-g	TNF-a	CCL2	CCL4	CXCL8
IL - 1b	0.000000	0.634266	1.972725	1.777540	1.906394	1.362894	1.681511	1.850412	1.815376
IL-2	0.634266	0.000000	1.533218	1.934277	1.936036	0.802592	1.084847	1.860722	1.270216
IL-6	1.972725	1.533218	0.000000	1.754912	1.457351	0.800647	0.791105	1.375462	0.484302
IL-12	1.777540	1.934277	1.754912	0.000000	0.388143	1.912642	2.196985	0.432123	2.045840
IFN-g	1.906394	1.936036	1.457351	0.388143	0.000000	1.753874	1.999308	0.088033	1.805944
TNF-a	1.362894	0.802592	0.800647	1.912642	1.753874	0.000000	0.345875	1.666350	0.467640
CCL2	1.681511	1.084847	0.791105	2.196985	1.999308	0.345875	0.000000	1.911304	0.316018
CCL4	1.850412	1.860722	1.375462	0.432123	0.088033	1.666350	1.911304	0.000000	1.719048
CXCL8	1.815376	1.270216	0.484302	2.045840	1.805944	0.467640	0.316018	1.719048	0.000000

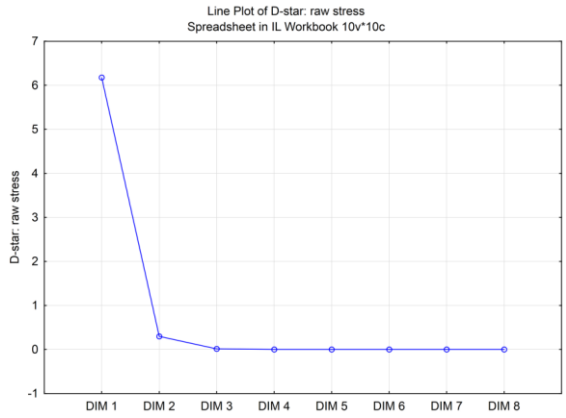
Line Plot of D-star: raw stress
Spreadsheet in IL Workbook 10v*10c
D-star: raw stress
7
6
5
4
3
2
1
0
-1
DIM 1
DIM 2
DIM 3
DIM 4
DIM 5
DIM 6
DIM 7
DIM 8

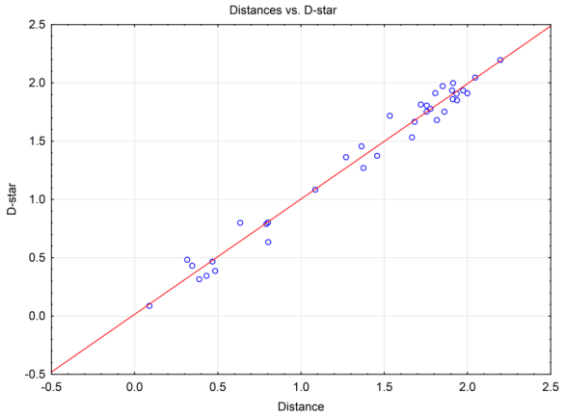
Distances vs. D-star
D-star
2.5
2.0
1.5
1.0
0.5
0.0
-0.5
-0.5
0.0
0.5
1.0
1.5
2.0
2.5
Distance

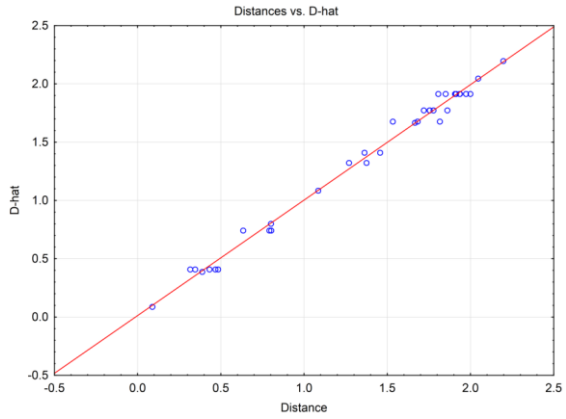
Distances vs. D-hat
D-hat
2.5
2.0
1.5
1.0
0.5
0.0
-0.5
-0.5
0.0
0.5
1.0
1.5
2.0
2.5
Distance

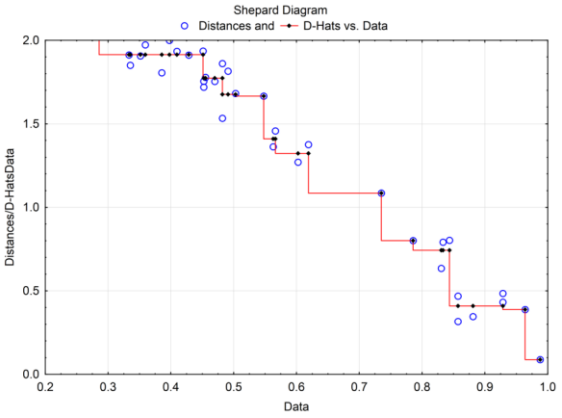
Shepard Diagram
Distances and
D-Hats vs. Data
Distances/D-HatsData
2.0
1.5
1.0
0.5
0.0
0.2
0.3
0.4
0.5
0.6
0.7
0.8
0.9
1.0
Data

APPENDIX F2

Results from Spearman Rank Order Correlations and subsequent non-metric MDS in each culture group in BPCM.

EXP culture group

	Spearman Rank Order Correlations (MDA A in IL Workbook) MD pairwise deleted Marked correlations are significant at p <.05000								
Variable	IL - 1b	IL-2	IL-6	IL-12	IFN-g	TNF-a	CCL2	CCL4	CXCL8
IL - 1b	1.000000	1.000000	0.542857	0.600000	0.600000	0.828571	0.942857	0.085714	1.000000
IL-2	1.000000	1.000000	0.542857	0.600000	0.600000	0.828571	0.942857	0.085714	1.000000
IL-6	0.542857	0.542857	1.000000	0.600000	0.600000	0.600000	0.485714	-0.028571	0.542857
IL-12	0.600000	0.600000	0.600000	1.000000	0.542857	0.428571	0.542857	0.142857	0.600000
IFN-g	0.600000	0.600000	0.600000	0.542857	1.000000	0.885714	0.771429	0.485714	0.600000
TNF-a	0.828571	0.828571	0.600000	0.428571	0.885714	1.000000	0.942857	0.428571	0.828571
CCL2	0.942857	0.942857	0.485714	0.542857	0.771429	0.942857	1.000000	0.371429	0.942857
CCL4	0.085714	0.085714	-0.028571	0.142857	0.485714	0.428571	0.371429	1.000000	0.085714
CXCL8	1.000000	1.000000	0.542857	0.600000	0.600000	0.828571	0.942857	0.085714	1.000000
Mean	2.14452014	1.8854891	4.19734344	1.25039022	1.72131206	1.81248551	3.3388768	2.21376403	3.91145961
Std. Dev.	0.29375473	0.22544132	0.205148261	0.09800619	0.24056589	0.24744005	0.25263442	0.067145184	0.19976032
No. Cases	8.000000								
Matrix	2.000000								

	Final Configuration (Spearman Rank Order Correlations (MDA A in IL Workbook) in IL Workbook) D-star: Raw stress = .5404987; Alienation = .0816192 D-hat: Raw stress = .1744226; Stress = .0464044	
	DIM. 1	DIM. 2
IL - 1b	-0.594716	0.47445
IL-2	-0.566475	0.36067
IL-6	-0.237885	-1.12383
IL-12	-0.837827	-0.57736
IFN-g	0.517367	-0.26273
TNF-a	0.355023	0.21865
CCL2	-0.082095	0.48356
CCL4	2.077060	0.03780
CXCL8	-0.630451	0.38879

	Distances in Final Configuration (Spearman Rank Order Correlations (MDA A in IL Workbook) in IL Workbook) D-star: Raw stress = .5404987; Alienation = .0816192 D-hat: Raw stress = .1744226; Stress = .0464044								
	IL - 1b	IL-2	IL-6	IL-12	IFN-g	TNF-a	CCL2	CCL4	CXCL8
IL - 1b	0.000000	0.117238	1.637635	1.079541	1.334229	0.983586	0.512702	2.707222	0.092817
IL-2	0.117238	0.000000	1.520432	0.976485	1.250335	0.932378	0.499727	2.663178	0.069884
IL-6	1.637635	1.520432	0.000000	0.811521	1.145385	1.467579	1.614926	2.590051	1.562734
IL-12	1.079541	0.976485	0.811521	0.000000	1.391238	1.434054	1.302567	2.979092	0.988153
IFN-g	1.334229	1.250335	1.145385	1.391238	0.000000	0.508013	0.957238	1.588383	1.319834
TNF-a	0.983586	0.932378	1.467579	1.434054	0.508013	0.000000	0.511129	1.731507	1.000054
CCL2	0.512702	0.499727	1.614926	1.302567	0.957238	0.511129	0.000000	2.204688	0.556485
CCL4	2.707222	2.663178	2.590051	2.979092	1.588383	1.731507	2.204688	0.000000	2.730166
CXCL8	0.092817	0.069884	1.562734	0.988153	1.319834	1.000054	0.556485	2.730166	0.000000

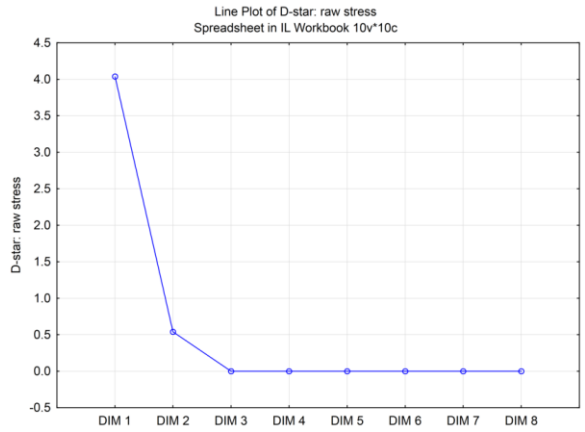
Line Plot of D-star: raw stress
Spreadsheet in IL Workbook 10v*10c
D-star: raw stress
DIM 1
DIM 2
DIM 3
DIM 4
DIM 5
DIM 6
DIM 7
DIM 8

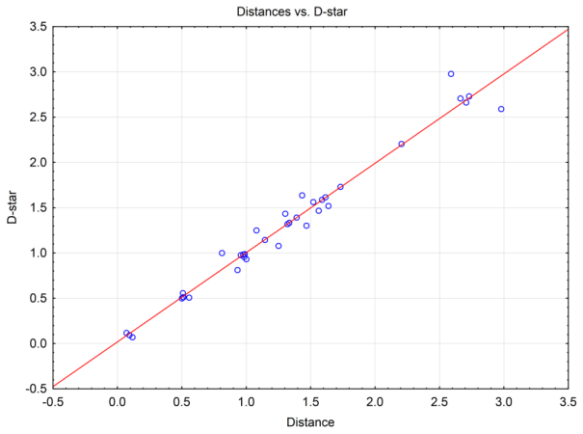
Distances vs. D-star
D-star
Distance

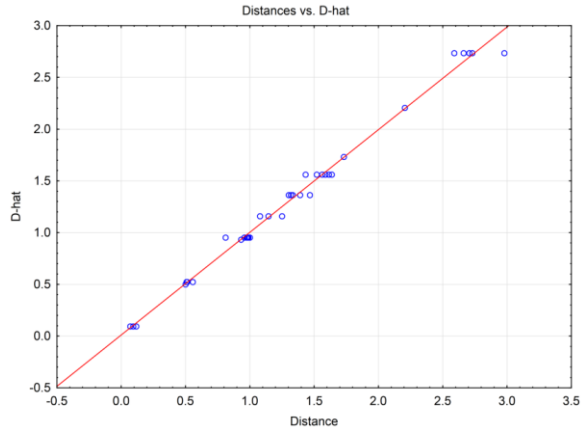
Distances vs. D-hat
D-hat
Distance

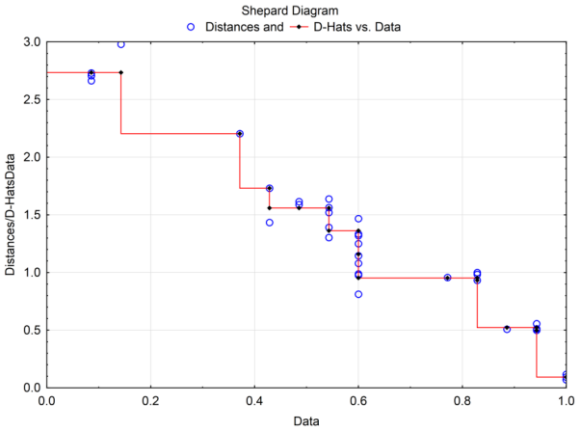
Shepard Diagram
Distances and
D-Hats vs. Data
Distances/D-HatsData
Data

NK-BC culture group

	Spearman Rank Order Correlations (MDA B in IL Workbook) MD pairwise deleted Marked correlations are significant at p <.05000								
Variable	IL - 1b	IL-2	IL-6	IL-12	IFN-g	TNF-a	CCL2	CCL4	CXCL8
IL - 1b	1.000000	0.579771	-0.085714	0.695725	0.428571	0.371429	0.428571	0.428571	0.600000
IL-2	0.579771	1.000000	0.347863	0.529412	0.637748	0.724714	-0.057977	0.115954	0.869657
IL-6	-0.085714	0.347863	1.000000	0.608760	0.828571	0.600000	-0.542857	-0.657143	0.542857
IL-12	0.695725	0.529412	0.608760	1.000000	0.840668	0.695725	-0.028989	-0.115954	0.782691
IFN-g	0.428571	0.637748	0.828571	0.840668	1.000000	0.600000	-0.371429	-0.485714	0.714286
TNF-a	0.371429	0.724714	0.600000	0.695725	0.600000	1.000000	-0.085714	0.085714	0.942857
CCL2	0.428571	-0.057977	-0.542857	-0.028989	-0.371429	-0.085714	1.000000	0.885714	0.028571
CCL4	0.428571	0.115954	-0.657143	-0.115954	-0.485714	0.085714	0.885714	1.000000	0.142857
CXCL8	0.600000	0.869657	0.542857	0.782691	0.714286	0.942857	0.028571	0.142857	1.000000
Mean	2.03671352	1.93034869	4.18551384	1.27790384	1.66973586	1.86612314	3.34350144	2.37879538	3.93951135
Std. Dev.	0.179974576	0.113082261	0.142426253	0.053333679	0.146870379	0.085764184	0.343858598	0.540645019	0.07513159
No. Cases	8.000000								
Matrix	2.000000								

	Final Configuration (Spearman Rank Order Correlations (MDA B in IL Workbook) in IL Workbook) D-star: Raw stress = .3517269; Alienation = .0658604 D-hat: Raw stress = .1244532; Stress = .0391977	
	DIM. 1	DIM. 2
IL - 1b	0.47119	-0.534522
IL-2	-0.08171	0.520053
IL-6	-1.37091	-0.014196
IL-12	-0.38436	-0.453544
IFN-g	-0.87553	-0.289984
TNF-a	-0.42706	0.587173
CCL2	1.49832	-0.211029
CCL4	1.45974	0.302016
CXCL8	-0.28968	0.094033

	Distances in Final Configuration (Spearman Rank Order Correlations (MDA B in IL Workbook) in IL Workbook) D-star: Raw stress = .3517269; Alienation = .0658604 D-hat: Raw stress = .1244532; Stress = .0391977								
	IL - 1b	IL-2	IL-6	IL-12	IFN-g	TNF-a	CCL2	CCL4	CXCL8
IL - 1b	0.000000	1.190726	1.914174	0.859372	1.368741	1.437027	1.076867	1.295005	0.986912
IL-2	1.190726	0.000000	1.395509	1.019552	1.134153	0.351807	1.740972	1.556802	0.474069
IL-6	1.914174	1.395509	0.000000	1.079956	0.566973	1.119151	2.875971	2.848261	1.086637
IL-12	0.859372	1.019552	1.079956	0.000000	0.517688	1.041592	1.898234	1.992885	0.555703
IFN-g	1.368741	1.134153	0.566973	0.517688	0.000000	0.985155	2.375162	2.409143	0.700496
TNF-a	1.437027	0.351807	1.119151	1.041592	0.985155	0.000000	2.084275	1.908229	0.511919
CCL2	1.076867	1.740972	2.875971	1.898234	2.375162	2.084275	0.000000	0.514493	1.813832
CCL4	1.295005	1.556802	2.848261	1.992885	2.409143	1.908229	0.514493	0.000000	1.761740
CXCL8	0.986912	0.474069	1.086637	0.555703	0.700496	0.511919	1.813832	1.761740	0.000000

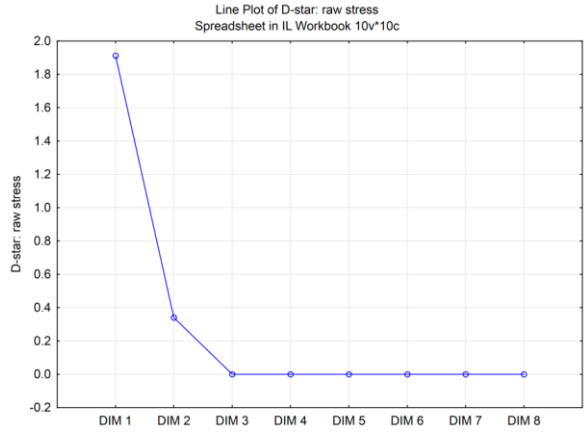
Line Plot of D-star: raw stress
Spreadsheet in IL Workbook 10v*10c
D-star: raw stress
2.0
1.8
1.6
1.4
1.2
1.0
0.8
0.6
0.4
0.2
0.0
-0.2
DIM 1
DIM 2
DIM 3
DIM 4
DIM 5
DIM 6
DIM 7
DIM 8

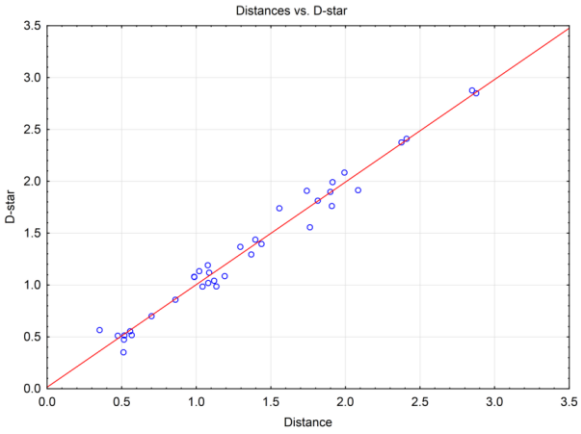
Distances vs. D-star
D-star
3.5
3.0
2.5
2.0
1.5
1.0
0.5
0.0
0.0
0.5
1.0
1.5
2.0
2.5
3.0
3.5
Distance

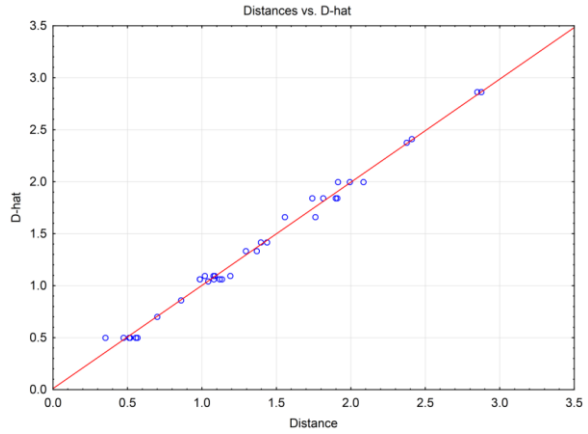
Distances vs. D-hat
D-hat
3.5
3.0
2.5
2.0
1.5
1.0
0.5
0.0
0.0
0.5
1.0
1.5
2.0
2.5
3.0
3.5
Distance

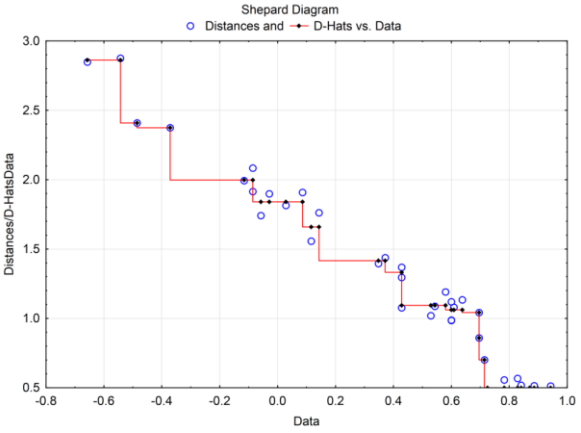
Shepard Diagram
Distances and
D-Hats vs. Data
Distances/D-HatsData
3.0
2.5
2.0
1.5
1.0
0.5
-0.8
-0.6
-0.4
-0.2
0.0
0.2
0.4
0.6
0.8
1.0
Data

T_{REG}-BC culture group

Variable	Spearman Rank Order Correlations (MDA C in IL Workbook) MD pairwise deleted Marked correlations are significant at p <.05000 IL - 1b	IL-2	IL-6	IL-12	IFN-g	TNF-a	CCL2	CCL4	CXCL8
IL - 1b	1.000000	0.828571	0.657143	0.927634	0.885714	0.898645	0.942857	0.371429	0.885714
IL-2	0.828571	1.000000	0.485714	0.927634	0.828571	0.985611	0.942857	0.428571	0.828571
IL-6	0.657143	0.485714	1.000000	0.492805	0.771429	0.550782	0.600000	-0.028571	0.771429
IL-12	0.927634	0.927634	0.492805	1.000000	0.898645	0.970588	0.985611	0.405840	0.898645
IFN-g	0.885714	0.828571	0.771429	0.898645	1.000000	0.898645	0.942857	0.085714	1.000000
TNF-a	0.898645	0.985611	0.550782	0.970588	0.898645	1.000000	0.985611	0.376851	0.898645
CCL2	0.942857	0.942857	0.600000	0.985611	0.942857	0.985611	1.000000	0.314286	0.942857
CCL4	0.371429	0.428571	-0.028571	0.405840	0.085714	0.376851	0.314286	1.000000	0.085714
CXCL8	0.885714	0.828571	0.771429	0.898645	1.000000	0.898645	0.942857	0.085714	1.000000
Mean	1.86343348	1.77276137	3.76807597	1.1967211	1.60711059	1.74541914	2.67345052	1.93904245	3.65825912
Std. Dev.	0.40518602	0.34157447	1.11786754	0.08991582	0.27868115	0.27621471	0.74574599	0.195297538	0.7036814
No. Cases	8.000000								
Matrix	2.000000								

	Final Configuration (Spearman Rank Order Correlations (MDA C in IL Workbook) in IL Workbook) D-star: Raw stress = .0000427; Alienation = .0007259 D-hat: Raw stress = .0000134; Stress = .0004074 DIM. 1	DIM. 2
IL - 1b	-0.292455	-0.158817
IL-2	-0.292673	-0.176179
IL-6	-0.518143	1.083665
IL-12	-0.292153	-0.167718
IFN-g	-0.305089	-0.162824
TNF-a	-0.293591	-0.170857
CCL2	-0.296719	-0.167387
CCL4	2.595912	0.082940
CXCL8	-0.305089	-0.162824

	Distances in Final Configuration (Spearman Rank Order Correlations (MDA C in IL Workbook) in IL Workbook) D-star: Raw stress = .0000427; Alienation = .0007259 D-hat: Raw stress = .0000134; Stress = .0004074 IL - 1b	IL-2	IL-6	IL-12	IFN-g	TNF-a	CCL2	CCL4	CXCL8
IL - 1b	0.000000	0.017364	1.262812	0.008906	0.013254	0.012094	0.009572	2.898467	0.013254
IL-2	0.017364	0.000000	1.279861	0.008477	0.018235	0.005400	0.009678	2.900184	0.018235
IL-6	1.262812	1.279861	0.000000	1.271625	1.264565	1.274460	1.270496	3.270900	1.264565
IL-12	0.008906	0.008477	1.271625	0.000000	0.013831	0.003453	0.004577	2.898922	0.013831
IFN-g	0.013254	0.018235	1.264565	0.013831	0.000000	0.014026	0.009533	2.911392	0.000000
TNF-a	0.012094	0.005400	1.274460	0.003453	0.014026	0.000000	0.004672	2.900627	0.014026
CCL2	0.009572	0.009678	1.270496	0.004577	0.009533	0.004672	0.000000	2.903442	0.009533
CCL4	2.898467	2.900184	3.270900	2.898922	2.911392	2.900627	2.903442	0.000000	2.911392
CXCL8	0.013254	0.018235	1.264565	0.013831	0.000000	0.014026	0.009533	2.911392	0.000000

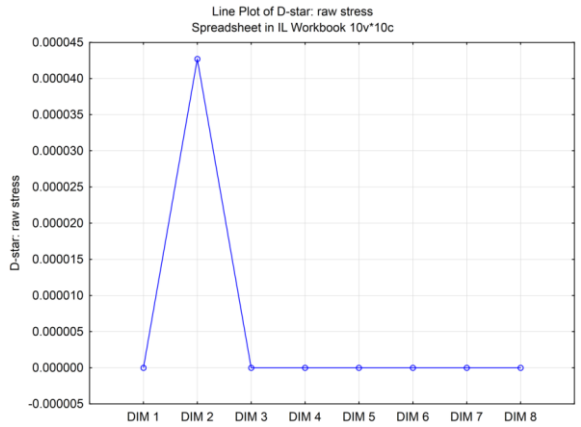
Line Plot of D-star: raw stress
Spreadsheet in IL Workbook 10v*10c
D-star: raw stress
0.000045
0.000040
0.000035
0.000030
0.000025
0.000020
0.000015
0.000010
0.000005
0.000000
-0.000005
DIM 1
DIM 2
DIM 3
DIM 4
DIM 5
DIM 6
DIM 7
DIM 8

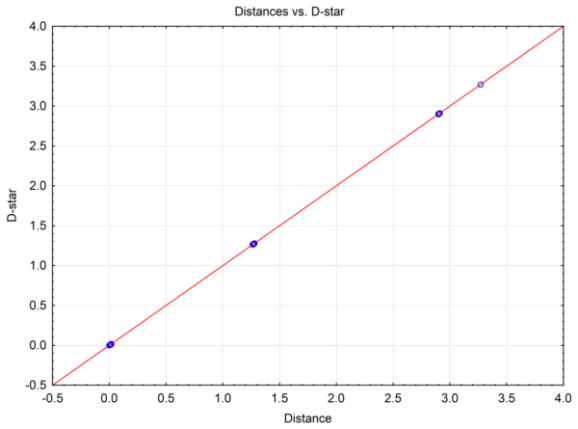
Distances vs. D-star
D-star
Distance
4.0
3.5
3.0
2.5
2.0
1.5
1.0
0.5
0.0
-0.5

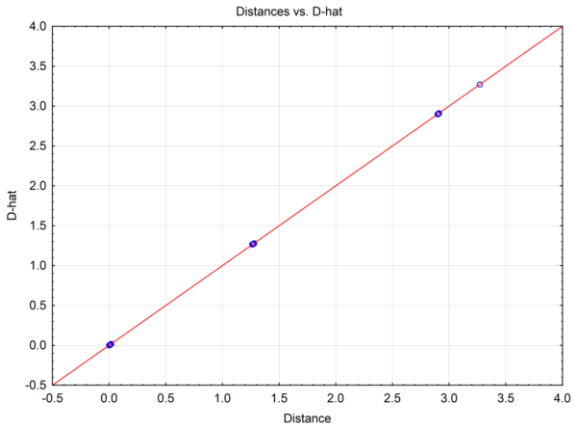
Distances vs. D-hat
D-hat
Distance
4.0
3.5
3.0
2.5
2.0
1.5
1.0
0.5
0.0
-0.5

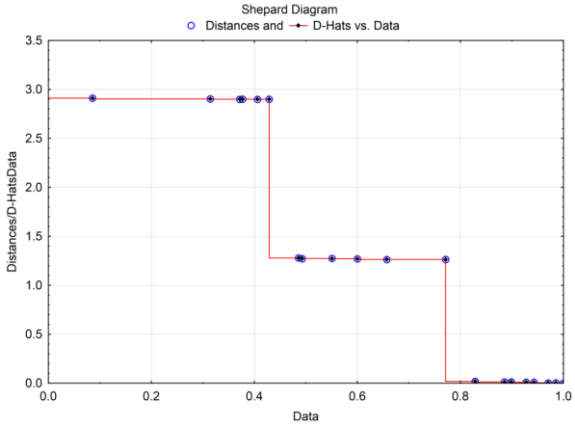
Shepard Diagram
Distances and D-Hats vs. Data
Distances/D-HatsData
Data
3.5
3.0
2.5
2.0
1.5
1.0
0.5
0.0
0.2
0.4
0.6
0.8
1.0

BC culture group

Variable	Spearman Rank Order Correlations (MDA D in IL Workbook) MD pairwise deleted Marked correlations are significant at p <.05000 IL - 1b	IL-2	IL-6	IL-12	IFN-g	TNF-a	CCL2	CCL4	CXCL8
IL - 1b	1.000000	0.771429	0.600000	0.028989	0.405840	0.085714	0.257143	-0.142857	0.828571
IL-2	0.771429	1.000000	0.942857	0.057977	0.811679	0.314286	0.657143	0.085714	0.942857
IL-6	0.600000	0.942857	1.000000	0.231908	0.811679	0.371429	0.828571	0.257143	0.828571
IL-12	0.028989	0.057977	0.231908	1.000000	0.147059	0.376851	0.405840	0.840668	0.115954
IFN-g	0.405840	0.811679	0.811679	0.147059	1.000000	0.753702	0.463817	0.463817	0.666737
TNF-a	0.085714	0.314286	0.371429	0.376851	0.753702	1.000000	0.028571	0.771429	0.142857
CCL2	0.257143	0.657143	0.828571	0.405840	0.463817	0.028571	1.000000	0.257143	0.600000
CCL4	-0.142857	0.085714	0.257143	0.840668	0.463817	0.771429	0.257143	1.000000	0.028571
CXCL8	0.828571	0.942857	0.828571	0.115954	0.666737	0.142857	0.600000	0.028571	1.000000
Mean	2.03775478	1.75787492	3.88651321	1.19333664	1.69096713	1.82675568	2.90801465	1.82110856	3.83181907
Std. Dev.	0.466851294	0.3232205	0.7872498	0.11200676	0.27579542	0.29108901	0.25592401	0.165475128	0.29417231
No. Cases	8.000000								
Matrix	2.000000								

	Final Configuration (Spearman Rank Order Correlations (MDA D in IL Workbook) in IL Workbook) D-star: Raw stress = .5680574; Alienation = .0836705 D-hat: Raw stress = .1902570; Stress = .0484650 DIM. 1	DIM. 2
IL - 1b	-1.18675	0.343807
IL-2	-0.64251	0.147690
IL-6	-0.31485	-0.213726
IL-12	1.14113	-0.602070
IFN-g	-0.00443	0.380014
TNF-a	0.78406	1.023793
CCL2	-0.14238	-0.900475
CCL4	1.29808	0.011879
CXCL8	-0.93234	-0.190911

	Distances in Final Configuration (Spearman Rank Order Correlations (MDA D in IL Workbook) in IL Workbook) D-star: Raw stress = .5680574; Alienation = .0836705 D-hat: Raw stress = .1902570; Stress = .0484650 IL - 1b	IL-2	IL-6	IL-12	IFN-g	TNF-a	CCL2	CCL4	CXCL8
IL - 1b	0.000000	0.578501	1.034919	2.512714	1.182877	2.084822	1.624483	2.506902	0.592158
IL-2	0.578501	0.000000	0.487834	1.934817	0.679058	1.674113	1.161368	1.945332	0.445703
IL-6	1.034919	0.487834	0.000000	1.506883	0.669991	1.655010	0.708074	1.628629	0.617908
IL-12	2.512714	1.934817	1.506883	0.000000	1.508908	1.664612	1.317747	0.633692	2.113841
IFN-g	1.182877	0.679058	0.669991	1.508908	0.000000	1.017923	1.287898	1.353532	1.089480
TNF-a	2.084822	1.674113	1.655010	1.664612	1.017923	0.000000	2.135674	1.134982	2.102742
CCL2	1.624483	1.161368	0.708074	1.317747	1.287898	2.135674	0.000000	1.705084	1.061841
CCL4	2.506902	1.945332	1.628629	0.633692	1.353532	1.134982	1.705084	0.000000	2.239613
CXCL8	0.592158	0.445703	0.617908	2.113841	1.089480	2.102742	1.061841	2.239613	0.000000

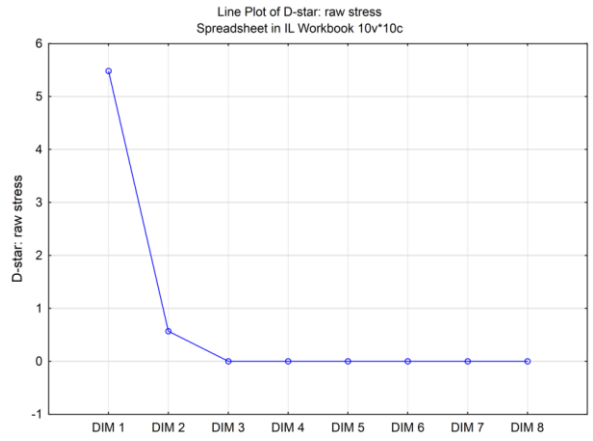
Line Plot of D-star: raw stress
Spreadsheet in IL Workbook 10v*10c
D-star: raw stress
6
5
4
3
2
1
0
-1
DIM 1
DIM 2
DIM 3
DIM 4
DIM 5
DIM 6
DIM 7
DIM 8

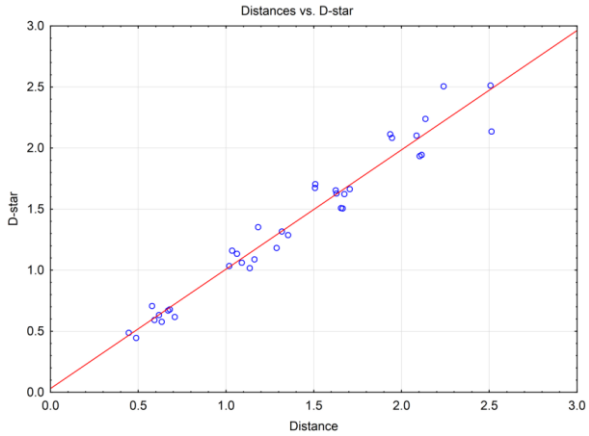
Distances vs. D-star
D-star
3.0
2.5
2.0
1.5
1.0
0.5
0.0
0.0
0.5
1.0
1.5
2.0
2.5
3.0
Distance

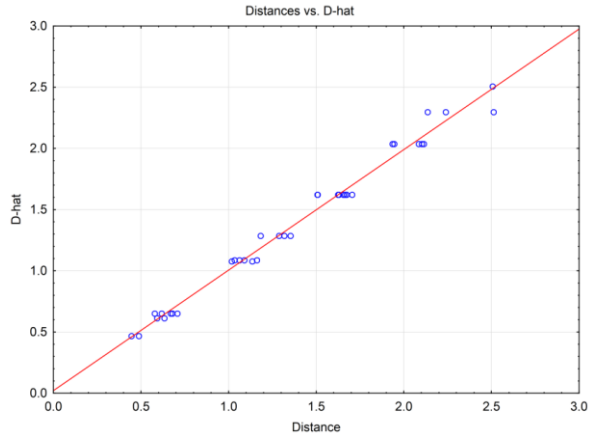
Distances vs. D-hat
D-hat
3.0
2.5
2.0
1.5
1.0
0.5
0.0
0.0
0.5
1.0
1.5
2.0
2.5
3.0
Distance

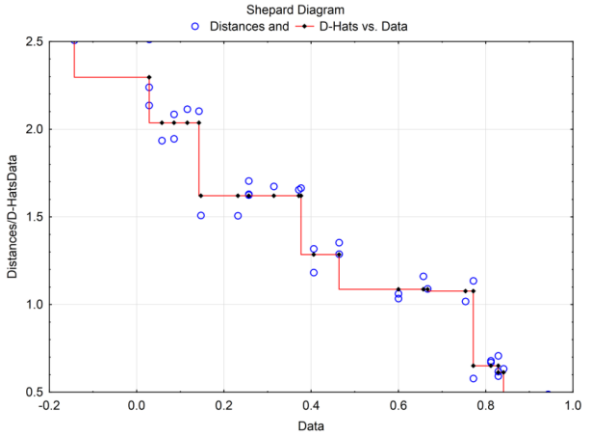
Shepard Diagram
Distances and
D-Hats vs. Data
Distances/D-HatsData
2.5
2.0
1.5
1.0
0.5
-0.2
0.0
0.2
0.4
0.6
0.8
1.0
Data

APPENDIX F3

Results from Spearman Rank Order Correlations and subsequent non-metric MDS in each culture group incorporating both LPCM and BPCM.

EXP culture group

Variable	Groups = A Spearman Rank Order Correlations (Spreadsheet in IL Workbook) MD pairwise deleted Marked correlations are significant at p <.05000 1A1.2	5A1.2	6A1.2	10A1.2	5A2.1	5A2.2	6A2.2	10A2.2
1A1.2	1.000000	0.895405	0.883333	0.933333	0.733333	0.800000	0.733333	0.733333
5A1.2	0.895405	1.000000	0.903774	0.820091	0.577411	0.694567	0.577411	0.652725
6A1.2	0.883333	0.903774	1.000000	0.833333	0.666667	0.750000	0.666667	0.716667
10A1.2	0.933333	0.820091	0.833333	1.000000	0.866667	0.900000	0.866667	0.850000
5A2.1	0.733333	0.577411	0.666667	0.866667	1.000000	0.983333	1.000000	0.966667
5A2.2	0.800000	0.694567	0.750000	0.900000	0.983333	1.000000	0.983333	0.983333
6A2.2	0.733333	0.577411	0.666667	0.866667	1.000000	0.983333	1.000000	0.966667
10A2.2	0.733333	0.652725	0.716667	0.850000	0.966667	0.983333	0.966667	1.000000
Mean	2.60477773	1.60086916	1.43429741	1.88106848	2.58471469	2.61540785	2.64268292	2.21317999
Std. Dev.	1.18991193	0.62613075	0.40602625	0.82460532	1.06376927	1.06066813	1.06784443	1.02616684
No. Cases	9.000000							
Matrix	2.000000							

	Final Configuration (Spearman Rank Order Correlations (Spreadsheet in IL Workbook) D-star: Raw stress = .0000000; Alienation = .0000098 D-hat: Raw stress = .0000000; Stress = .0000049 DIM. 1	DIM. 2
1A1.2	-0.81053	0.587686
5A1.2	-1.45848	-0.126822
6A1.2	-1.02494	-0.609354
10A1.2	-0.17541	0.455752
5A2.1	0.96750	0.039631
5A2.2	0.63573	-0.066171
6A2.2	0.96753	0.039843
10A2.2	0.89861	-0.320565

	Distances in Final Configuration (Spearman Rank Order Correlations (Spreadsheet in IL Workbook) in IL Workbook) D-star: Raw stress = .0000000; Alienation = .0000098 D-hat: Raw stress = .0000000; Stress = .0000049 1A1.2	5A1.2	6A1.2	10A1.2	5A2.1	5A2.2	6A2.2	10A2.2
1A1.2	0.000000	0.964548	1.216090	0.648681	1.860587	1.587200	1.860548	1.935481
5A1.2	0.964548	0.000000	0.648681	1.409130	2.431684	2.095083	2.431724	2.365034
6A1.2	1.216090	0.648681	0.000000	1.362408	2.095478	1.747249	2.095567	1.945110
10A1.2	0.648681	1.409130	1.362408	0.000000	1.216311	0.964547	1.216262	1.325212
5A2.1	1.860587	2.431684	2.095478	1.216311	0.000000	0.348237	0.000214	0.366725
5A2.2	1.587200	2.095083	1.747249	0.964547	0.348237	0.000000	0.348326	0.365817
6A2.2	1.860548	2.431724	2.095567	1.216262	0.000214	0.348326	0.000000	0.366938
10A2.2	1.935481	2.365034	1.945110	1.325212	0.366725	0.365817	0.366938	0.000000

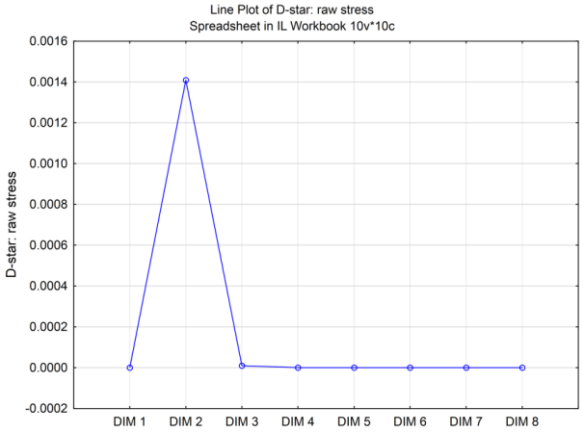
Line Plot of D-star: raw stress
Spreadsheet in IL Workbook 10v*10c
D-star: raw stress
0.0016
0.0014
0.0012
0.0010
0.0008
0.0006
0.0004
0.0002
0.0000
-0.0002
DIM 1
DIM 2
DIM 3
DIM 4
DIM 5
DIM 6
DIM 7
DIM 8

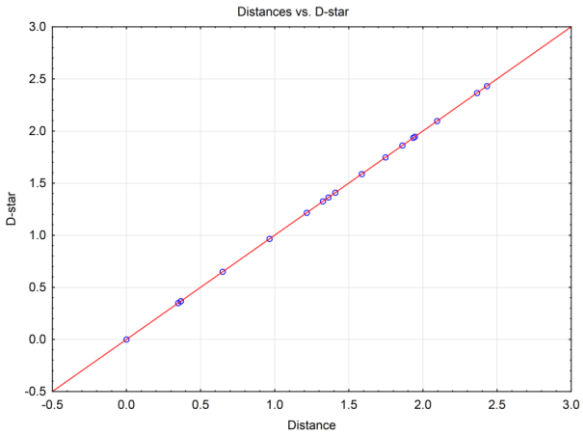
Distances vs. D-star
D-star
Distance
3.0
2.5
2.0
1.5
1.0
0.5
0.0
-0.5

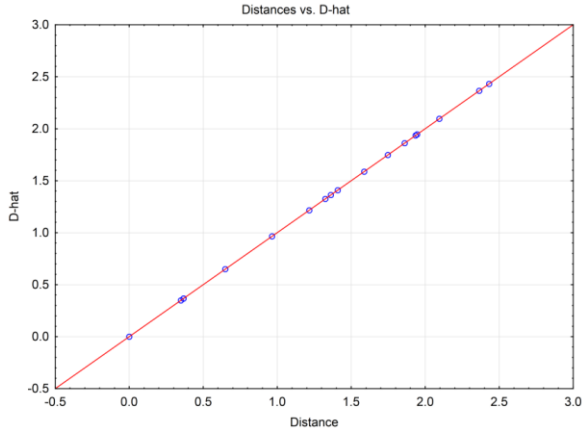
Distances vs. D-hat
D-hat
Distance
3.0
2.5
2.0
1.5
1.0
0.5
0.0
-0.5

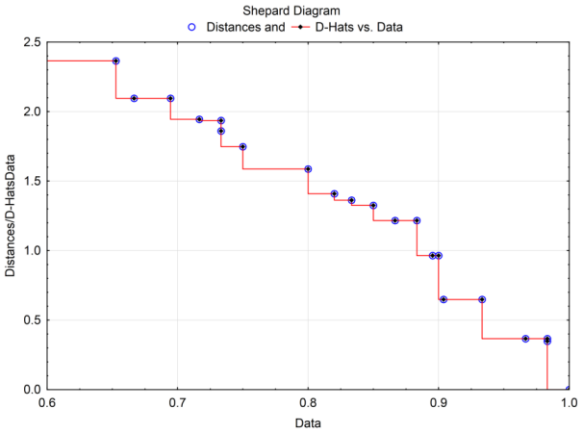
Shepard Diagram
Distances and D-Hats vs. Data
Distances/D-HatsData
Data
2.5
2.0
1.5
1.0
0.5
0.0
0.6
0.7
0.8
0.9
1.0

NK-BC culture group

Variable	Groups=B Spearman Rank Order Correlations (Spreadsheet in IL Workbook) MD pairwise deleted Marked correlations are significant at p <.05000 IL-1b	IL-2	IL-6	IL-12	IFN-g	TNF-a	CCL2	CCL4	CXCL8
IL-1b	1.000000	0.867844	0.885714	0.785416	0.827283	0.906491	0.617582	0.173626	0.929670
IL-2	0.867844	1.000000	0.885465	0.852558	0.808159	0.905182	0.678416	0.129956	0.914099
IL-6	0.885714	0.885465	1.000000	0.831877	0.882289	0.935094	0.652747	0.054945	0.960440
IL-12	0.785416	0.852558	0.831877	1.000000	0.610198	0.826148	0.756654	0.247793	0.854001
IFN-g	0.827283	0.808159	0.882289	0.610198	1.000000	0.868943	0.451045	-0.114412	0.886689
TNF-a	0.906491	0.905182	0.935094	0.826148	0.868943	1.000000	0.640264	0.094610	0.968097
CCL2	0.617582	0.678416	0.652747	0.756654	0.451045	0.640264	1.000000	0.692308	0.692308
CCL4	0.173626	0.129956	0.054945	0.247793	-0.114412	0.094610	0.692308	1.000000	0.164835
CXCL8	0.929670	0.914099	0.960440	0.854001	0.886689	0.968097	0.692308	0.164835	1.000000
Mean	1.556857	1.519414	2.919919	1.181757	1.3476426	1.518729	2.877207	2.3824878	3.37687
Std. Dev.	0.457704	0.383381	1.198811	0.12229	0.3085081	0.326958	0.915018	0.5119478	0.690164
No. Cases	14.0								
Matrix	2.000000								

	Final Configuration (Spearman Rank Order Correlations (Spreadsheet in IL Workbook) in IL Workbook) D-star: Raw stress = .1082561; Alienation = .0365520 D-hat: Raw stress = .0337078; Stress = .0203997 DIM. 1	DIM. 2
IL-1b	-0.34653	-0.400100
IL-2	-0.48551	0.394335
IL-6	-0.52036	-0.021867
IL-12	0.23639	0.123865
IFN-g	-1.07215	-0.122086
TNF-a	-0.51207	-0.017663
CCL2	0.92332	0.215632
CCL4	2.31310	-0.147116
CXCL8	-0.53619	-0.024999

	Distances in Final Configuration (Spearman Rank Order Correlations (Spreadsheet in IL Workbook) in IL Workbook) D-star: Raw stress = .1082561; Alienation = .0365520 D-hat: Raw stress = .0337078; Stress = .0203997 IL-1b	IL-2	IL-6	IL-12	IFN-g	TNF-a	CCL2	CCL4	CXCL8
IL-1b	0.000000	0.806500	0.416265	0.783798	0.777056	0.416730	1.411253	2.671633	0.420323
IL-2	0.806500	0.000000	0.417658	0.770907	0.781561	0.412853	1.420114	2.850503	0.422385
IL-6	0.416265	0.417658	0.000000	0.770656	0.560819	0.009289	1.463080	2.836223	0.016137
IL-12	0.783798	0.770907	0.770656	0.000000	1.331457	0.761732	0.693026	2.094310	0.786793
IFN-g	0.777056	0.781561	0.560819	1.331457	0.000000	0.569726	2.023843	3.385340	0.544684
TNF-a	0.416730	0.412853	0.009289	0.761732	0.569726	0.000000	1.454227	2.828138	0.025205
CCL2	1.411253	1.420114	1.463080	0.693026	2.023843	1.454227	0.000000	1.436342	1.479209
CCL4	2.671633	2.850503	2.836223	2.094310	3.385340	2.828138	1.436342	0.000000	2.851902
CXCL8	0.420323	0.422385	0.016137	0.786793	0.544684	0.025205	1.479209	2.851902	0.000000

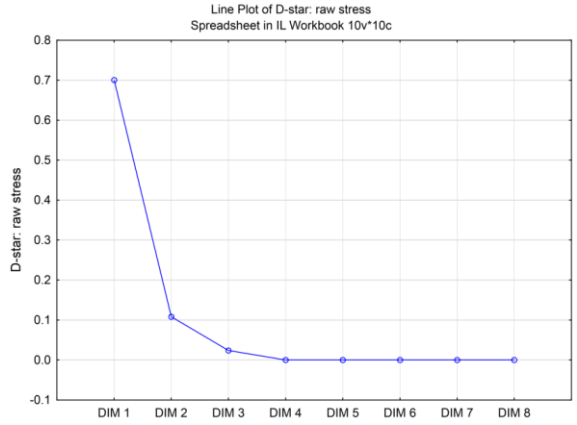
Line Plot of D-star: raw stress
Spreadsheet in IL Workbook 10v*10c
D-star: raw stress
0.8
0.7
0.6
0.5
0.4
0.3
0.2
0.1
0.0
-0.1
DIM 1
DIM 2
DIM 3
DIM 4
DIM 5
DIM 6
DIM 7
DIM 8

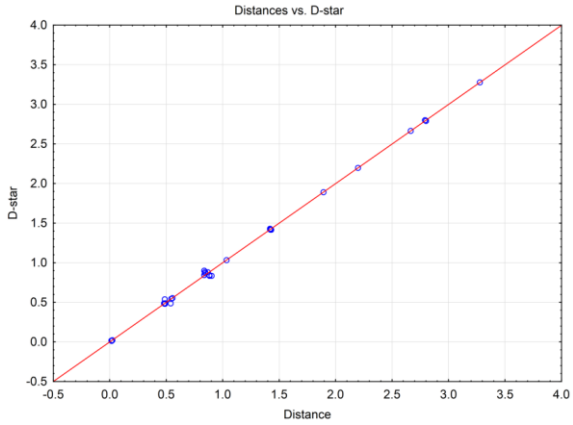
Distances vs. D-star
D-star
4.0
3.5
3.0
2.5
2.0
1.5
1.0
0.5
0.0
-0.5
-0.5
0.0
0.5
1.0
1.5
2.0
2.5
3.0
3.5
4.0
Distance

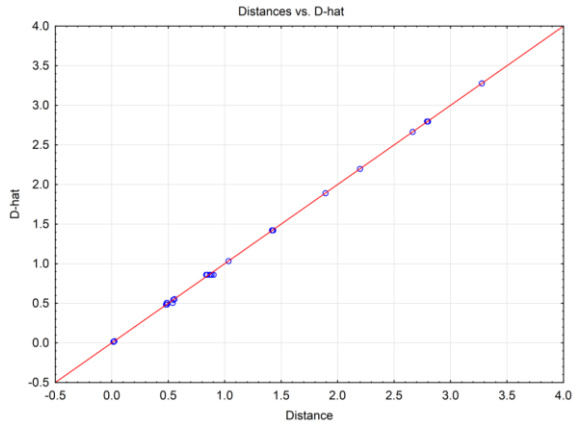
Distances vs. D-hat
D-hat
4.0
3.5
3.0
2.5
2.0
1.5
1.0
0.5
0.0
-0.5
-0.5
0.0
0.5
1.0
1.5
2.0
2.5
3.0
3.5
4.0
Distance

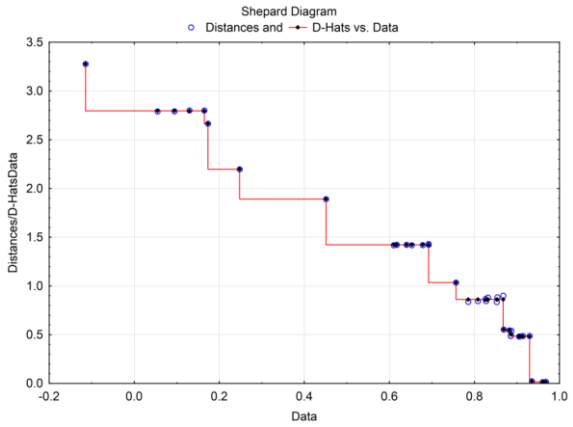
Shepard Diagram
Distances and
D-Hats vs. Data
Distances/D-HatsData
3.5
3.0
2.5
2.0
1.5
1.0
0.5
0.0
-0.2
0.0
0.2
0.4
0.6
0.8
1.0
Data

T_{REG}-BC culture group

Variable	Groups=C Spearman Rank Order Correlations (Spreadsheet in IL Workbook) MD pairwise deleted Marked correlations are significant at p <.05000 IL-1b	IL-2	IL-6	IL-12	IFN-g	TNF-a	CCL2	CCL4	CXCL8
IL-1b	1.000000	0.703868	0.853367	0.781358	0.822768	0.773838	0.862188	0.738703	0.917315
IL-2	0.703868	1.000000	0.740090	0.824842	0.868631	0.903659	0.680618	0.744495	0.770927
IL-6	0.853367	0.740090	1.000000	0.761079	0.800049	0.806642	0.859341	0.784615	0.934066
IL-12	0.781358	0.824842	0.761079	1.000000	0.721484	0.894328	0.800903	0.876125	0.854001
IFN-g	0.822768	0.868631	0.800049	0.721484	1.000000	0.867053	0.653374	0.591148	0.771159
TNF-a	0.773838	0.903659	0.806642	0.894328	0.867053	1.000000	0.751393	0.766863	0.833162
CCL2	0.862188	0.680618	0.859341	0.800903	0.653374	0.751393	1.000000	0.832967	0.951648
CCL4	0.738703	0.744495	0.784615	0.876125	0.591148	0.766863	0.832967	1.000000	0.872527
CXCL8	0.917315	0.770927	0.934066	0.854001	0.771159	0.833162	0.951648	0.872527	1.000000
Mean	1.470552	1.472141	2.820943	1.104314	1.34032	1.451596	2.232168	1.820324	3.136921
Std. Dev.	0.486206	0.365896	1.279116	0.116133	0.312969	0.345706	0.74412	0.185624	0.805035
No. Cases	14.000								

	Final Configuration (Spearman Rank Order Correlations (Spreadsheet in IL Workbook) in IL Workbook) D-star: Raw stress = 1.147027; Alienation = .1187884 D-hat: Raw stress = .4938339; Stress = .0780815 DIM. 1	DIM. 2
IL-1b	0.27567	-0.909802
IL-2	-1.24692	0.267715
IL-6	0.60023	-0.611400
IL-12	-0.01842	0.823175
IFN-g	-1.14692	-0.594891
TNF-a	-0.67638	0.253195
CCL2	1.10616	-0.226329
CCL4	0.71984	0.960641
CXCL8	0.38675	0.037695

	Distances in Final Configuration (Spearman Rank Order Correlations (Spreadsheet in IL Workbook) in IL Workbook) D-star: Raw stress = 1.147027; Alienation = .1187884 D-hat: Raw stress = .4938339; Stress = .0780815 IL-1b	IL-2	IL-6	IL-12	IFN-g	TNF-a	CCL2	CCL4	CXCL8
IL-1b	0.000000	1.924794	0.440889	1.757753	1.457024	1.502985	1.075575	1.922459	0.953986
IL-2	1.924794	0.000000	2.045680	1.348243	0.868384	0.570725	2.404392	2.085258	1.649788
IL-6	0.440889	2.045680	0.000000	1.562282	1.747223	1.541835	0.635809	1.576585	0.683298
IL-12	1.757753	1.348243	1.562282	0.000000	1.812298	0.870514	1.538228	0.750946	0.883822
IFN-g	1.457024	0.868384	1.747223	1.812298	0.000000	0.969873	2.283029	2.429910	1.659007
TNF-a	1.502985	0.570725	1.541835	0.870514	0.969873	0.000000	1.845919	1.565221	1.084755
CCL2	1.075575	2.404392	0.635809	1.538228	2.283029	1.845919	0.000000	1.248257	0.766332
CCL4	1.922459	2.085258	1.576585	0.750946	2.429910	1.565221	1.248257	0.000000	0.981213
CXCL8	0.953986	1.649788	0.683298	0.883822	1.659007	1.084755	0.766332	0.981213	0.000000

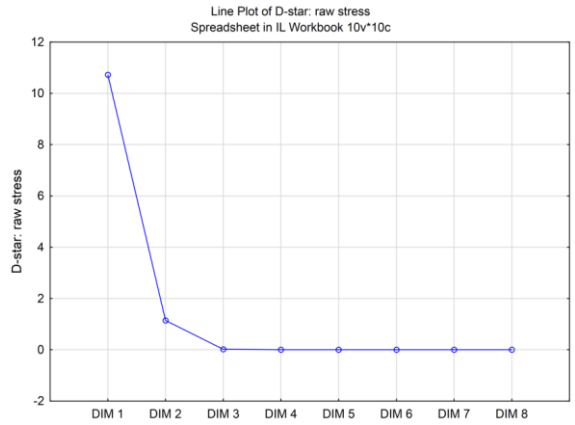
Line Plot of D-star: raw stress
Spreadsheet in IL Workbook 10v*10c
D-star: raw stress
DIM 1
DIM 2
DIM 3
DIM 4
DIM 5
DIM 6
DIM 7
DIM 8

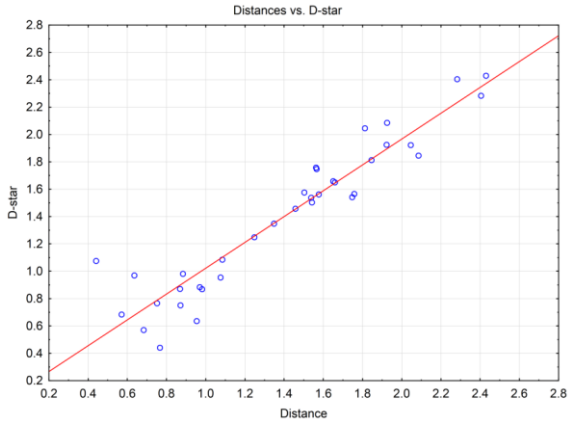
Distances vs. D-star
D-star
Distance

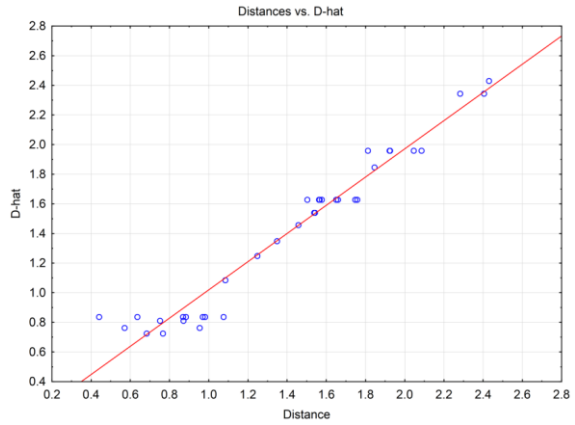
Distances vs. D-hat
D-hat
Distance

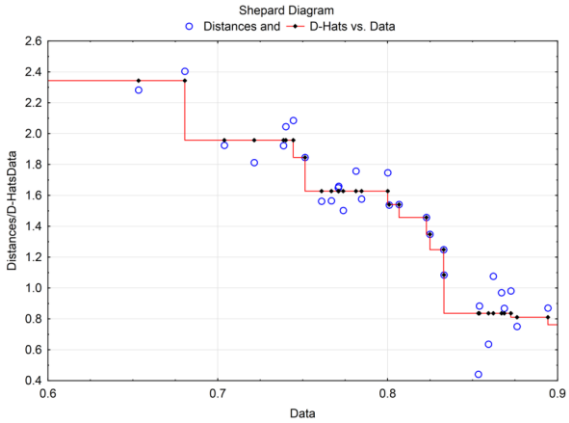
Shepard Diagram
Distances and D-Hats vs. Data
Distances/D-HatsData
Data

BC culture group

Variable	Groups=D Spearman Rank Order Correlations (Spreadsheet in IL Workbook) MD pairwise deleted Marked correlations are significant at p <.05000 IL-1b	IL-2	IL-6	IL-12	IFN-g	TNF-a	CCL2	CCL4	CXCL8
IL-1b	1.000000	0.790287	0.753306	0.634555	0.727072	0.728777	0.713658	0.601323	0.876654
IL-2	0.790287	1.000000	0.801764	0.730901	0.766851	0.760750	0.788548	0.733482	0.773130
IL-6	0.753306	0.801764	1.000000	0.693933	0.846752	0.796480	0.912088	0.758242	0.907692
IL-12	0.634555	0.730901	0.693933	1.000000	0.831488	0.661511	0.634264	0.954711	0.574594
IFN-g	0.727072	0.766851	0.846752	0.831488	1.000000	0.850995	0.765164	0.906289	0.727678
TNF-a	0.728777	0.760750	0.796480	0.661511	0.850995	1.000000	0.770077	0.798680	0.792080
CCL2	0.713658	0.788548	0.912088	0.634264	0.765164	0.770077	1.000000	0.692308	0.832967
CCL4	0.601323	0.733482	0.758242	0.954711	0.906289	0.798680	0.692308	1.000000	0.635165
CXCL8	0.876654	0.773130	0.907692	0.574594	0.727678	0.792080	0.832967	0.635165	1.000000
Mean	1.630276	1.551538	2.981285	1.134384	1.452569	1.574744	2.335471	1.716711	3.168734
Std. Dev.	0.578864	0.38232	1.330085	0.144514	0.395107	0.386779	0.841305	0.22126	0.921212
No. Cases	14.00								

	Final Configuration (Spearman Rank Order Correlations (Spreadsheet in IL Workbook) in IL Workbook) D-star: Raw stress = 1.214577; Alienation = .1222235 D-hat: Raw stress = .4974440; Stress = .0783663 DIM. 1	DIM. 2
IL-1b	-1.18208	-0.744586
IL-2	-0.30361	-0.553948
IL-6	-0.22757	0.143313
IL-12	1.41349	-0.554276
IFN-g	0.59014	-0.145031
TNF-a	0.24069	0.608799
CCL2	-0.62530	0.773512
CCL4	1.13262	0.313588
CXCL8	-1.03838	0.158629

	Distances in Final Configuration (Spearman Rank Order Correlations (Spreadsheet in IL Workbook) in IL Workbook) D-star: Raw stress = 1.214577; Alienation = .1222235 D-hat: Raw stress = .4974440; Stress = .0783663 IL-1b	IL-2	IL-6	IL-12	IFN-g	TNF-a	CCL2	CCL4	CXCL8
IL-1b	0.000000	0.898922	1.303633	2.602536	1.870890	1.963653	1.616981	2.545112	0.914575
IL-2	0.898922	0.000000	0.701395	1.717094	0.982849	1.283839	1.365883	1.677909	1.023549
IL-6	1.303633	0.701395	0.000000	1.783170	0.867056	0.660261	0.745210	1.370810	0.810952
IL-12	2.602536	1.717094	1.783170	0.000000	0.919449	1.651724	2.433035	0.912180	2.553403
IFN-g	1.870890	0.982849	0.867056	0.919449	0.000000	0.830886	1.523484	0.710368	1.656583
TNF-a	1.963653	1.283839	0.660261	1.651724	0.830886	0.000000	0.881514	0.939517	1.355975
CCL2	1.616981	1.365883	0.745210	2.433035	1.523484	0.881514	0.000000	1.817091	0.740753
CCL4	2.545112	1.677909	1.370810	0.912180	0.710368	0.939517	1.817091	0.000000	2.176524
CXCL8	0.914575	1.023549	0.810952	2.553403	1.656583	1.355975	0.740753	2.176524	0.000000

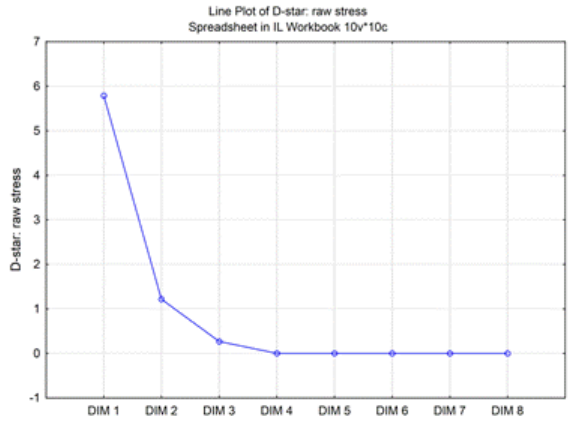
Line Plot of D-star: raw stress
Spreadsheet in IL Workbook 10v*10c
D-star: raw stress
DIM 1
DIM 2
DIM 3
DIM 4
DIM 5
DIM 6
DIM 7
DIM 8

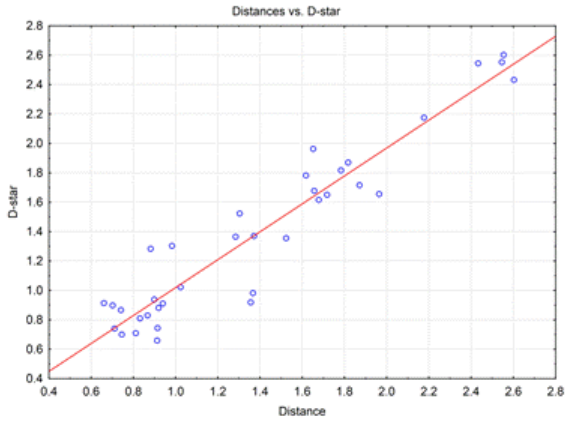
Distances vs. D-star
D-star
Distance

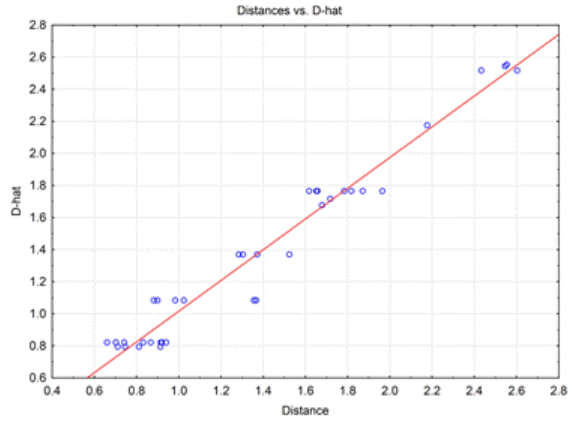
Distances vs. D-hat
D-hat
Distance

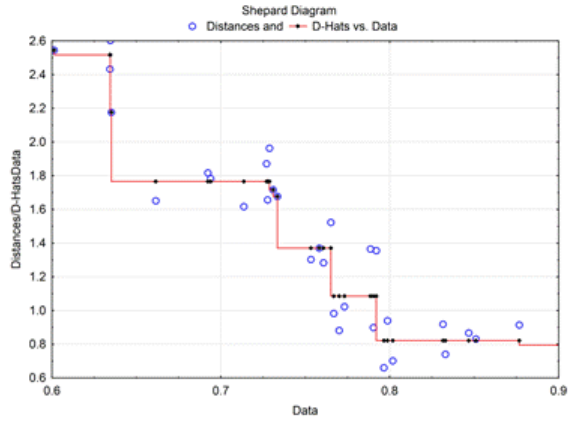
Shepard Diagram
Distances and
D-Hats vs. Data
Distances/D-HatsData
Data

APPENDIX G

Representative photomicrographs showing efficacy of negative control and isotype controls for ICC. **A)** primary antibody omission; **B)** primary and secondary antibody omission; **C)** isotype IgG3 control; **D)** isotype IgG control. Only blue DAPI nuclear stain is present, with no immunofluorescence indicating the specificity of the antibodies and the efficacy of the technique.